

**Metabolomic and Metabolomic Flux Studies  
of the Effects of Sphingosine kinase  
Inhibitors on Prostate Cancer Cells Using  
High-Resolution Mass Spectrometry as an  
analytical technique**

A Thesis Submitted in Fulfilment of the Requirements for the Degree  
of Doctor of Philosophy in the Strathclyde Institute of Pharmacy and  
Biomedical Sciences at the University of Strathclyde

Presented by

Mohammad Abdullah Alrofaidi

2020

## Declaration

‘I declare that, except where specifically indicated, all the work presented in this report is my own and I am the sole author of all parts.’

The copyright of this thesis belongs to the author under the terms of the United Kingdom Copyright Acts as qualified by University of Strathclyde Regulation 3.50. Due acknowledgement must always be made of the use of any material contained in, or derived from, this thesis.’

Signed: \_\_\_\_\_

Date: \_\_\_\_\_

## **Acknowledgements**

First and foremost, I would like to express my sincerest gratitude to Allah (God) for providing me the blessings to complete this work. I would like also to express my sincere appreciation and immense gratitude to my supervisor, Dr. David G Watson and Prof. Nigel Pyne for their continued support, patience, advices and guidance throughout this study. My thanks also extend to Prof. Susan Pyne, for her support in the laboratory and her kind words of encouragement during the various phases of developing this work. I would like also to thank my academic assessor, Dr. Edmond Chan. Also, I would like to thank all my friends in the labs and SIPBS, especially Mohammad Alwashih, Ahmed Alshihiri, Adel Alghamdi, Abdulwahab Alamri, Abdulmalak Al-Quarni.

I would like to express the deepest appreciation to my father, who supported me to complete my degree, wife Fatimah and my daughter Lamia. Lastly, I would like to express my thanks for my brothers and sisters for their support during my educational journey.

Finally, I wish to thank the Al-Baha University and Saudi Government for sponsoring my PhD study.

## **Abstract**

There is evidence of the involvement of sphingosine kinases (two isoforms termed SK1 and SK2), which catalyse the formation of the bioactive lipid, sphingosine 1-phosphate (S1P), in various diseases including cancer. Over the last few years, metabolomics has become an increasingly critical part in many fields of research. Therefore, metabolomic and lipidomic analysis was performed to investigate the effect of different sphingosine kinase inhibitors in prostate cancer cells in order to establish the role of SK1 and SK2 in this cancer. Previous studies have shown that the SK1/2 inhibitor, SKi (2-(p-hydroxyanilino)-4-(pchlorophenyl)thiazole) inhibits aerobic glycolysis (Warburg effect) and this might contribute to the anti-cancer activity of this compound. This was further investigated in the current study, where  $^{13}\text{C}_6$ -glucose was employed to determine the flux through different metabolic and lipid pathways, including the glycolysis in androgen-independent LNCaP-AI prostate cancer cells. The LNCaP-AI cell line was treated with SKi in the presence of  $^{13}\text{C}_6$ -glucose for 24 hours before extraction and global metabolite analysis of cell lysate by LC-MS. The levels of glycolytic metabolites, pentose phosphate pathway, glutathione disulfide (GSSG) and *sn*-G3P were increased in response to the SKi. On the other hand, NADPH, some metabolites in TCA, nucleotides were found to be lower in the SKi-treated cells. These findings suggest that SKi reprograms cellular metabolism of LNCaP-AI cells, which results in reduced flux through glycolytic and TCA cycles and re-diversion of glucose to produce, *sn*-G3P, which is capable of increasing ROS production, and which might programme senescent death in these cells. The flux in the

<sup>13</sup>C experiment suggests that much of glucose is metabolized through the pentose glucuronate interconversion pathway in LNCaP-AI cells.

In order to recapitulate a more aggressive phenotype in prostate cancer cells, SK1b was stably expressed in androgen-sensitive LNCaP cells. These LNCaP-SK1b cells were then treated with SKi and compared with LNCaP cells. The treatment of LNCaP-SK1b cells with SKi increased the levels of sphingomyelins, ceramides, lysoPC and PC and these changes were more substantial than in LNCaP cells. It is proposed that the over-expression of SK1b increases flux through sphingolipid and phospholipid pathways such that inhibition of SK1b with SKi results in a more profound increase in lipid metabolites compared with LNCaP cells. Part of this effect is in blockade of the sphingolipid rheostat and inhibition of phospholipid turnover that is limited by the availability of S1P. The use of the SK2 inhibitor, ROME in LNCaP-SK1b cells suggests that both SK1 and SK2 regulate the sphingolipid rheostat, but inhibition of these enzymes with SKi results in differential effects on ceramide and phospholipid metabolism. Indeed, the effect of ROME tends to be more robust in LNCaP cells compared with LNCaP-SK1b cells, with linkage of SK2 with sphinganine and sphinganine-1-phosphate metabolism. Several highly potent selective SK1 and SK2 inhibitors (PLR24, ST55 and ST81) were also used in LNCaP-AI cells and LNCaP-SK1b cells, and shown to disrupt the sphingolipid rheostat and modulate phospholipid turnover. The major conclusion of this thesis is that SK1 and SK2 regulate the metabolome (Warburg effect) and the lipidome to protect prostate cancer cells from apoptosis/senescence and this might contribute to certain hallmarks of cancer including replicative immortality and increased cell survival.

## **Table of Contents**

<b>1</b>	<b>Introduction.....</b>	<b>2</b>
<b>1.1</b>	<b>Mammalian cells and cancer .....</b>	<b>2</b>
1.1.1	Cell culture analysis .....	2
1.1.2	Cancer cell metabolism.....	3
1.1.3	Lipid metabolism and cancer .....	8
1.1.4	Reactive oxygen species (ROS).....	14
<b>1.2</b>	<b>Introduction to metabolomics .....</b>	<b>15</b>
1.2.1	Metabolomics.....	15
1.2.2	Metabolomics flux .....	17
<b>1.3</b>	<b>Metabolomics in prostate Cancer .....</b>	<b>19</b>
1.3.1	Prostate cancer .....	19
<b>1.4</b>	<b>Prostate cancer treatment.....</b>	<b>21</b>
1.4.1	Current chemotherapy.....	21
1.4.2	Sphingosine kinase inhibitors .....	21
1.4.3	Study on LNCaP cell lines using SKi .....	23
<b>1.5</b>	<b>Techniques used in Metabolomics Studies.....</b>	<b>24</b>
1.5.1	Principles of chromatographic separation.....	24
1.5.2	Mobile phase.....	25
1.5.3	Stationary phases.....	26
1.5.4	Mass spectrometry MS.....	28
<b>1.6</b>	<b>Data Extraction and Processing.....</b>	<b>36</b>
1.6.1	Mz-Mine.....	36
1.6.2	Multivariate analysis .....	37
<b>1.7</b>	<b>Aims .....</b>	<b>41</b>
<b>2</b>	<b>Materials and methods .....</b>	<b>44</b>
<b>2.1</b>	<b>Chemicals and solvents .....</b>	<b>44</b>
2.1.1	Solvents and chemicals .....	44

2.1.2	Materials used in cell culture: .....	44
<b>2.2</b>	<b>Method: .....</b>	<b>45</b>
2.2.1	Preparation of LNCaP, LNCaP-SK1b and LNCaP-AI .....	45
2.2.2	Cell Extraction .....	46
2.2.3	Cell extraction for flux-analysis.....	46
2.2.4	Cell extraction for pulse-chase analysis.....	47
2.2.5	ROS Assay .....	47
2.2.6	LC-MS conditions.....	47
2.2.7	Standards preparation.....	49
2.2.8	LC-MS conditions.....	56
2.2.9	Data extraction, processing and analysis .....	57
2.2.10	Data bases used for identification of metabolites .....	58
2.2.11	Xcalibur.....	59
<b>3</b>	<b>Metabolomics profiling of the effect of sphingosine kinase inhibitor SKi on the metabolome of LNCaP-AI cells using PHILIC column and flux analysis using <sup>13</sup>C<sub>6</sub> glucose .....</b>	<b>61</b>
<b>3.1</b>	<b>Introduction .....</b>	<b>61</b>
<b>3.2</b>	<b>Materials and methods.....</b>	<b>64</b>
3.2.1	Cell lines chemical and culture .....	64
3.2.2	Cell Extraction .....	64
3.2.3	Cell extraction for flux-analysis and pulse-chase experiment .....	64
3.2.4	ROS measurement.....	64
<b>3.3</b>	<b>Results.....</b>	<b>65</b>
3.3.1	Metabolomic profile of the effect of SKi on LNCaP-AI .....	65
3.3.2	Effect of SKi on LNCaP-AI cells using <sup>13</sup> C <sub>6</sub> -glucose (pulse-chase analysis) 73	
3.3.3	ROS measurement.....	100
<b>3.4</b>	<b>Discussion .....</b>	<b>102</b>
3.4.1	Metabolomic profile of the effect of SKi on LNCaP-AI cells.....	102
3.4.2	Effect of SKi on LNCaP-AI cells using <sup>13</sup> C <sub>6</sub> -glucose.....	104

3.4.3	Reactive oxygen species (ROS).....	109
<b>3.5</b>	<b>Summary .....</b>	<b>110</b>
<b>4</b>	<b>Lipidomics analysis of the effects of the sphingosine kinase inhibitors SKi and ROME on LNCaP and LNCaP-SK1b prostate cancer cells using Mass spectrometry</b>	<b>113</b>
<b>4.1</b>	<b>Introduction .....</b>	<b>113</b>
<b>4.2</b>	<b>Materials and Methods .....</b>	<b>117</b>
4.2.1	Cell lines and cultures .....	117
4.2.2	Chromatographic conditions for columns.....	117
4.2.3	Data extraction and analysis .....	117
<b>4.3</b>	<b>Results.....</b>	<b>118</b>
4.3.1	Effect of SKi on the lipidome of LNCaP and LNCaP-SK1b cell lines ...	118
4.3.2	Effect of ROME on LNCaP and LNCaP-SK1b cell lines .....	127
<b>4.4</b>	<b>Discussion .....</b>	<b>133</b>
4.4.1	Effect of SKi on the lipidome of LNCaP and LNCaP-SK1b cells .....	133
4.4.2	Effect of ROME on LNCaP and LNCaP-SK1b cell lines .....	139
<b>4.5</b>	<b>Summary .....</b>	<b>140</b>
<b>5</b>	<b>Metabolomic Profiling of the Effects of Different SK Inhibitors on LNCaP-AI and LNCaP-SK1b Prostate Cancer Cells Using Mass Spectrometry. ....</b>	<b>143</b>
<b>5.1</b>	<b>Introduction .....</b>	<b>143</b>
<b>5.2</b>	<b>Materials and Methods .....</b>	<b>147</b>
5.2.1	Cell lines and cultures .....	147
5.2.2	Chromatographic conditions for columns.....	147
5.2.3	Data extraction and analysis .....	147
<b>5.3</b>	<b>Results.....</b>	<b>147</b>
5.3.1	Effect of new sphingosine kinase inhibitors (SKIs) on LNCaP-SK1b cells. 147	
5.3.2	Effect of SKIs; namely, PLR24, ST55 and ST81 inhibitors on LNCaP-AI cell lines 152	
<b>5.4</b>	<b>Discussion .....</b>	<b>158</b>



5.4.1	The effect of SK inhibitors (SKIs) on lipids metabolism on a LNCaP-SK1b cell line. ....	159
5.4.2	The effect of SK inhibitors (SKIs) on lipids metabolism on LNCaP-AI cell line. ....	161
<b>5.5</b>	<b>Conclusion.....</b>	<b>163</b>
<b>6</b>	<b>Summary .....</b>	<b>166</b>
<b>6.1</b>	<b>The effect of SKi on the metabolome of LNCaP-AI cells using <sup>13</sup>C<sub>6</sub> glucose</b> Error! Bookmark not defined.	
<b>6.2</b>	<b>Proposed future work .....</b>	<b>171</b>
	<b>References .....</b>	<b>172</b>

## List of Tables

Table 1-1 Some examples for SK inhibitors and a summary of their activity [27] -----	22
Table 1-2 examples of zwitterionic phases and their functional groups. -----	28
Table 1-3 The predicatability of ROC model -----	41
Table 2-1: The gradient system used in the LCMS experiment. -----	48
Table 2-2 The distribution of metabolite standards into seven mixed standard solutions. Where S.N= standard number. -----	50
Table 2-3 Online databases used in the in-house macro -----	59
Table 3-1 Summary of the alteration in unlabelled and labelled metabolites in LNCaP- AI cells in the pulse-chase experiments.-----	75
Table 4-1 table shows cell population of untreated and treated LNCaP and LNCaP-SK1b with SKi in two different experiments -----	123
Table 4-2 Alterations in lipids metabolites of LNCaP and LNCaP-SK1b cells treated with SKi. Where: (T/C)= treated cells /untreated cells, (C-1b/C)= peak intensity of untreated of (LNCaP-SK1b / LNCaP). (T-1b/T) = peak intensity of treated of (LNCaP- SK1b / LNCaP).-----	<b>Error! Bookmark not defined.</b>
Table 4-3 cells count in LNCaP and LNCaP-SK1b cells with and without ROME. ---	128
Table 4-4 show the changes in sphingolipids occurred in response to the treatment of LNCaP and LNCaP-SK1b with ROME, where T/C= the ratio of the average amount of a given metabolites in samples from treated cells compared with the average amount of a given metabolite in samples from control cells (n=3), -----	181
Table 4-5 shows the changes in PC, PE, PG, PS and PI occurred in LNCaP and LNCaP- SK1b in response to ROME -----	182
Table 5-1 information of inhibitors used in this experiment-----	146
Table 5-2 show the effect of different inhibitors, non-selective (PLR24), and SK II selective (ST55 and ST81) on LNCaP-SK1b cells using Silica gel conjugated with high resolution mass spectroscopy -----	150
Table 5-3 show the effect of different inhibitors, non-selective (PLR24), SK I selective (ST55) and SK II selective (ST81) on LNCaP-SK1b cells using Silica gel conjugated with high resolution mass spectroscopy -----	<b>Error! Bookmark not defined.</b>
Table 5-4 shows the effect of different inhibitors, non-selective (PLR24), SK I selective (ST55) and SK II selective (ST81) on LNCaP-AI cells using Silica gel conjugated with high resolution mass spectroscopy. -----	190

Table 5-5 shows the effect of different inhibitors, non-selective (PLR24) and SK2 selective inhibitors (ST55 and ST81) on LNCaP-AI cells using silica gel conjugated with high resolution mass spectroscopy. Where: T/C= treated cells/ untreated cells. - 156

## List of Figures

Figure 1.1-1 The glycolysis pathway -----	5
Figure 1.1-2 Oxidative and non-oxidative phases of the pentose phosphate pathway. ----	7
Figure 1.1-3 Ceramide synthesis from the degradation of sphingomyelin -----	10
Figure 1.1-4 De novo ceramide synthesis pathway. -----	11
Figure 1.1-5 Ceramide salvage pathway occurs in lysosomes[37]. Where, SMS: sphingomyelin synthase, SMase; sphingomyelinase, CK; ceramide kinase, C1PP; ceramide-1-phosphatase, GRS; glucocerebrosidase and GCS; glycosyl ceramide synthase.-----	12
Figure 1.1-6 Rheostat model, the correlation between ceramide and S1P. -----	13
Figure 1.4-1 Chemical structures of FTY720 [64] and ROME [75]. -----	24
Figure 1-1.5-1 different types of silanol in a silica gel column. -----	27
Figure 1.5-2 Schematic diagram of the main components of a mass spectrometer. ----	29
Figure 1.5-3 Schematic of the ESI process [90]. -----	30
Figure 1.5-4 Ion generator in an electron impact source. where: M=molecule; e=electron. modified from. [78] -----	32
Figure 1.5-5 Separation of ions using a quadrupole mass analyser. Resonant ions with specific m/z values pass into the detector. Obtained and modified from [93].-----	33
Figure 1.5-6 schematic diagram representing the Orbitrap Mass Spectrometer. Obtain and modified from [92].-----	35
Figure 1.6-1 schematic diagram of data processing using MzMine 2.10. -----	37
Figure 1.6-2 Orthogonal Partial Least Discrimination Analysis (OPLS-DA) score plot.	39
Figure 1.6-3 permutations test. It shows the vertical axis gives the R <sup>2</sup> Y and Q <sup>2</sup> Y -values of each model. The horizontal axis represents the correlation coefficient between the original Y, which has correlation 1.0 with itself, and the permuted Y. -----	40
Figure 1.6-4 the ROC curve shows sensitivity (true positive rate (TPR)) on the y-axis versus (false positive rate (FPR = 1 - Specificity)) on the x-axis, the value of both normalised to 1 which represents the value of AUC for a group. (A) excellent AUC accuracy= 1; (B) fail model AUC= 0.5, which is the worst model. Where; TPR= true positive rate. FPR=false a positive rate. -----	41
Figure 2.2-2 MZMine 2.10 procedure and settings -----	58
Figure 3.3-1 The bar graph is a comparison of the changes in some metabolites in the pentose phosphate pathway (linked with oxidative stress) in response to the treatment of	

LNCaP-AI cells with SKi, where T/C = the ratio of the average amount of a given metabolites in samples from treated cells compared with the average amount of a given metabolites in samples from control cells (n=3), numbers above bars represent ratios.- 66

Figure 3.3-2 The bar graph is a comparison of the changes in some metabolites in the pentose phosphate pathway (linked with oxidative stress) in response to the treatment of LNCaP-AI cells with SKi, where T/C = the ratio of the average amount of a given metabolites in samples from treated cells compared with the average amount of a given metabolite in samples from control cells (n=3), numbers represent the ratio for each metabolite. ----- 67

Figure 3.3-3 Bar graph is a comparison of changes in some metabolites in the Nucleotide pathways in response to treatment of LNCAP-AI cells with SKi, where T/C = the ratio of the average amount of a given metabolites in samples from treated cells compared with the average amount of a given metabolites in samples from control cells (n=3), numbers above bars represent the ratio for each metabolite.\* significant. ----- 67

Figure 3.3-4 Bar graph is a comparison of the changes in ribose, NADPH and TCA metabolites, citrate, malate, fumarate in response to the treatment of LNCaP-AI with SKi, where T/C = the ratio of the average amount of a given metabolites in samples from treated cells compared with the average amount of a given metabolites in samples from control cells (n=3), numbers represent the ratio for each metabolite. ----- 68

Figure 3.3-5 Bar graph is a comparison of changes occurring in some metabolites in the amino acid pathways in response to treatment of LNCAP-AI cells with SKi, where T/C = the ratio of the average amount of a given metabolites in samples from treated cells compared with the average amount of a given metabolites in samples from control cells (n=3), numbers above bars represent ratios of each metabolite. ----- 69

Figure 3.3-6 Bar graph is a comparison of changes occurring in some metabolites in the amino acid pathways in response to treatment of LNCAP-AI cells with SKi, where T/C = the ratio of the average amount of a given metabolites in samples from treated cells compared with the average amount of a given metabolites in samples from control cells (n=3), numbers above bars represent the ratio of each metabolite. ----- 69

Figure 3.3-7 Bar graph is a comparison of changes occurring in some energy metabolites in response to treat LNCAP-AI cells with SKi, where T/C = the ratio of the average amount of a given metabolites in samples from treated cells compared with the average amount of a given metabolites in samples from treated cells compared with the average amount of a given metabolites in samples from control cells (n=3), numbers above bars represent the ratio of each metabolite. \*significant. ----- 70

Figure 3.3-8 Bar graph is a comparison of changes occurring in some metabolites in the fatty acid (carnitines) in response to treat LNCAP-AI cells with SKi, where T/C = the ratio of the average amount of a given metabolites in samples from treated cells

compared with the average amount of a given metabolites in samples from control cells (n=3), numbers above bars represent the ratio of each metabolite. -----	71
Figure 3.3-9 Bar graph is a comparison of changes in some metabolites in lipid metabolism in response to treat LNCAP-AI cells with SKi, where T/C = the ratio of the average amount of a given metabolites in samples from treated cells compared with the average amount of a given metabolites in samples from control cells (n=3), numbers above bars represent ratio of each metabolite. * p-value < 0.05 -----	72
Figure 3.3-10 <i>sn</i> -glycerol 3-phosphate chromatograms in untreated and treated samples with the mass spectra. -----	72
Figure 3.3-11 summary of <sup>13</sup> C incorporation from <sup>13</sup> C <sub>6</sub> -glucose into pathways in LNCaP-AI cells -----	74
Figure 3.3-12 Bar graph is a comparison of the changes in GSSG in the pulse-chase experiments, where T/C = the ratio of the average amount of a given metabolites in samples from treated cells compared with the amount of a given metabolites in samples from control cells (n=3), numbers above bars represent ratio of each metabolite. -----	80
Figure 3.3-13 Chromatograms of NADPH of untreated and treated LNCaP-AI cells with SKi (24 hours). -----	81
Figure 3.3-14 (A) Bar chart is a comparison of the changes occurring in certain metabolites in the glycolysis and PPP and (B) their isotopes. Where T/C = the ratio of the average amount of a given metabolites in samples from treated cells compared with the amount of a given metabolites in samples from control cells (n=3), the numbers above bars represent the ratio of each metabolite at time point 24 hours. -----	83
Figure 3.3-15 Bar graphs represent absolute levels of (A) F-1,6,P2, (B) <sup>13</sup> C <sub>6</sub> -F-1,6 P2, (C) GAP, (D) <sup>13</sup> C <sub>3</sub> -GAP, (E) phosphoglycerate and (F) <sup>13</sup> C <sub>3</sub> -phosphoglycerate in the pulse experiment. -----	84
Figure 3.3-16 Bar graphs represent absolute levels of (A) phosphogluconate, (B) <sup>13</sup> C <sub>6</sub> -phosphogluconate, (C) R5P and (D) <sup>13</sup> C <sub>5</sub> -R5P in the pulse experiment. (E) R5P and (F) <sup>13</sup> C <sub>5</sub> -R5P in the chase experiment. -----	85
Figure 3.3-17 Extracted chromatograms of peak intensities of R5P and its isotopically labelled equivalent in the control and SKi-treated cells in the pulse-chase experiments. -----	86
Figure 3.3-18 intensity levels of GIP (left) and its isotope (right) over time in the pulse-chase experiment. Number above bars represent ratios (Treated/Control) of each time point. -----	88
Figure 3.3-19 Bar graphs show absolute levels of (A) GDP-glucose, (B) <sup>13</sup> C <sub>6</sub> - GDP-glucose, (C) UDP-galacturonate and (D) <sup>13</sup> C <sub>6</sub> - UDP-galacturonate; (E) UDP-N-acetyl-glucosamine and (F) <sup>13</sup> C <sub>6</sub> - UDP-N-acetyl-glucosamine. -----	89

Figure 3.3-20 Bar graphs show absolute levels of (A) ATP; (B) $^{13}\text{C}_5$ - ATP; (C) ADP; (D) $^{13}\text{C}_5$ - ADP; (E) NAD; (F) $^{13}\text{C}_5$ - NAD -----	91
Figure 3.3-21 GTP and GDP and their isotopes levels in the pulse-chase experiment. -	92
Figure 3.3-22 Bar graphs show a comparison of the changes in levels of acetyl-CoA and acetyl-carnitine and the intensities of $^{13}\text{C}$ -labelled isotopologues in untreated and SKi-treated cells over time in the pulse-chase experiment, where bars represent the average amount of a given metabolites in samples from untreated (blue) or treated (red) LNCaP-AI cells with SKi, (n=3) -----	94
Figure 3.3-23 bar graphs is a comparison of the changes in levels of citrate, oxoglutarate and the intensities of $^{13}\text{C}$ -labelled isotopologues untreated and SKi-treated cells over time in the pulse-chase experiment, where bars represent the average amount of a given metabolites in samples from untreated (blue) or treated (red) LNCaP-AI cells with SKi, (n=3). -----	95
Figure 3.3-24 Extracted chromatograms of acetyl-CoA, acetylcarnitine, citrate and their isotopologues from 12 hours untreated cells in the chase experiment.-----	96
Figure 3.3-25 Extracted chromatograms of acetyl-CoA, acetylcarnitine, citrate and their isotopologues from 12 hours treated cells in the chase experiment.-----	96
Figure 3.3-26 reaction between $^{13}\text{C}_2$ -sn-G3P and DHAP in the cytosol and mitochondrial membrane. -----	97
Figure 3.3-27 bar graphs show the changes of sn-G3P and acetyl-carnitine and the intensities of $^{13}\text{C}$ -labelled isotopologues in untreated and SKi-treated cells over time at 24 hours in the pulse experiment and 1, 4, 12 and 24 hours in the chase experiment. * significant. -----	98
Figure 3.3-28 bar graphs show the changes of GPCm GPE, LPA and the intensities of $^{13}\text{C}$ -labelled isotopologues in untreated and SKi-treated cells over time 0-24 hours in the pulse experiment and 1, 4, 12 and 24 hours in the chase experiment. -----	99
Figure 3.3-29 Extracted ion chromatograms showing sn-glycerol 3-phosphate and its isotope detected in negative ion mode and eluted at the same retention time (15.10). The accurate mass spectra of sn-glycerol 3-phosphate and its isotope, 171.0057 and 174.0159, in untreated and treated LNCaP-AI cells. -----	100
Figure 3.3-30 The effect of 10 $\mu\text{M}$ SKi (24 hours) on ROS production in LNCaP-Ai cells using <i>dihydroethidium (DHE)</i> as a detector and angiotensin II (100nM) as a positive control for 1 hour. (n=4 and P.value <0.05). error bars represent the standard error of the mean (SEM). -----	101
Figure 3.4-1 Flux map of $^{13}\text{C}_6$ -glucose in LNCaP-AI cells that have been treated with SKi,. Several pathways include glycolysis, pentose phosphate pathway (PPP), nucleotides, nucleotide-sugar and glycerolipids biosynthesis. -----	105

Figure 4.3-1 Bar chart illustrates cell numbers in untreated and treated LNCaP and LNCaP-SK1b cells with 10 $\mu$ M SKi for 24 hours in two different experiments. ----- 123

Figure 4.3-2 (A) PCA score plot of LNCaP and LNCaP-SK1b cell lines before and after treatment with SKi with pooled samples (P). (B) OPLS-DA score plot of LNCaP and LNCaP-SK1b before and after treatment with SKi. The groups: As-C= untreated LNCaP cells; As-T= LNCaP treated cells; SK1b-C= untreated LNCaP-SK1b cells; SK1b-T= LNCaP-SK1b treated cells. (C)= Permutation analysis of OPLS-DA model derived from model-B; (D) Receiver Operating Characteristics (ROC) curve shows the sensitivity (true positive rate (TPR)) on the y-axis versus (false positive rate (FPR)) on the X-axis. The area under ROC curve (AUROCC)=1 for MS and C groups. ----- 126

Figure 4.3-3 (A) PCA and (B) OPLS-DA show the separation between LNCaP and LNCaP-SK1b treated with ROME inhibitor. The groups: Pooled (green); As-control (dark blue); As-ROME (red); LNCaP-SK1b control (yellow); LNCaP-SK1b-ROME (bright blue). ----- 131

Figure 4.3-4 (A)= Permutation analysis of OPLS-DA model derived from model-B; (B) Receiver Operating Characteristics (ROC) curve shows the sensitivity (true positive rate (TPR)) on the y-axis versus (false positive rate (FPR)) on the X-axis. The area under ROC curve shows the sensitivity (true positive rate (TPR)) on the y-axis versus (false positive rate (FPR)) on the X-axis. The area under ROC curve (AUROCC)=1 for MS and C groups. ----- 132

Figure 4.4-1 summaries of the changes occurred on sphingo-bases in the LNCaP cells due to the over expression of SK1b gene then the treatment of LNCaP-SK1b cells with SKi. Where: CerS: ceramide synthase; SMS: sphingomyelin synthase; DMS: dimethylsphingosine. ----- 135

Figure 5.3-1 (A) OPLS-DA model for SK1b cells and (B) permutation test ----- 149

Figure 5.3-2 HCA analysis of 16 prostate cancer LNCaP-SK1b samples. It shows two main groups and four sub-groups. The groups: Group 1 (green), control of LNCaP-SK1b cells; Group 2 (blue): ST-55-treated LNCaP-SK1b cells; Group3 (red): PLR24-treated LNCaP-SK1b cells; Group 4 (yellow): ST-81-treated LNCaP-SK1b cells. ----- 150

Figure 5.3-3 OPLS-DA model of androgen independent (LNCaP-AI) prostate cancer cells treated with SKIs, PLR24 (red); ST55 (yellow) and ST81 (bright blue). ----- 154

Figure 5.3-4 Hierarchical clustering analysis (HCA) of 16 prostate cancer LNCaP-AI cell samples, four replicates of each condition. It shows two main groups and four subgroups. The groups; group 1 (green): LNCaP-AI treated cells with PLR; group 2 (blue): LNCaP-AI untreated cells; group 3 (red); LNCaP-AI treated cells with ST55 and group 4 (yellow): LNCaP-AI treated cells with ST81. ----- 155

Figure 5.3-5 (A) Permutation analysis of OPLS-DA model derived from LNCaP-AI cells treated with SKi inhibitors and untreated cells. Statistical validation of the OPLS-



DA model by permutation analysis using 20 different model permutations. The goodness of fit (R2) and predictive capability (Q2) of the original model are indicated on the far right and remain higher than those of the 100 permuted models to the left. OPLS-DA, orthogonal partial least squares discriminant analysis. (B) Receiver Operating Characteristics (ROC) curve shows sensitivity (true positive rate (TPR)) on the y-axis versus (false positive rate (FPR = 1 - Specificity)) on the x-axis. The area under ROC curve (AUROCC) =1 for SOR and CR groups. ----- 155

Figure 5.3-6 Extracted chromatogram of (dimethylsphingosine) DMS from control and PLR and ST55-treated LNCaP-AI cells. ----- 158

## Abbreviations

ACER2: Ceramidase 2

AR: Androgen receptor

ATP: Adenosine triphosphate

AUC: Area Under the Curve

CPT1: Carnitine palmitoyltransferase I

DAG: Diacylglycerol

DHAP: Dihydroxy acetone phosphate

DHcer: Dihydroceramide

DMS: Dimethylsphingosine

DMSO: Dimethyl Sulfoxide

DNA: Deoxyribonucleic acid

EI: Electron impact

ERK: Extracellular signal-regulated kinase

ESI: Electrospray ionisation

ETC: Electron transport chain

FADH<sub>2</sub>: Flavin Adenine Dinucleotide (reduced)

FTIR: Fourier transform Infrared

GAP: Glyceraldehyde phosphate

GC-MS: Gas chromatography- mass spectrometry

GHS: Glutathione

GMP: Guanosine monophosphate

GPCRs: G protein-coupled receptors

GS: Gas chromatography

GSSG: Glutathione disulfide

H<sub>2</sub>O<sub>2</sub>: Hydrogen Peroxide

HDAC: Histone deacetylase

HPLC: High performance liquid chromatography

KDa: Kilo Dalton

KEGG: Kyoto Encyclopedia of Genes and Genomes

LC: Liquid chromatography

LC-MS: Liquid chromatography- mass spectrometry

LTQ: Linear ion trap quadrupole

LysoPC: Lysophosphatidylcholine

MAPK: Mitogen-activated protein kinases

MVA: Multivariate analysis

NAD<sup>+</sup>: Nicotinamide Adenine Dinucleotide (oxidized)

NADH: Nicotinamide Adenine Dinucleotide (reduced)

NADP<sup>+</sup>: Nicotinamide Adenine Dinucleotide Phosphate (oxidized)

NADPH: Nicotinamide Adenine Dinucleotide Phosphate (reduced)

NMR: Nuclear magnetic resonance.

OPLS-DA: Orthogonal partial least squares

PC: Phosphatidylcholine

PCA: Principle component analysis

PCR: Polymerase chain reaction

PE: Phosphatidylethanolamine

PG: Phosphatidylglycerol

PI: Phosphatidylinositols

PLA2: Phospholipase 2

PPP: Pentose Phosphate Pathway

PPP: The pentose phosphate pathway.

PS: Phosphatidylserine

PSA: Prostate-specific antigen

R5P: Ribulose-5-phosphate

RNA: Ribonucleic acid

ROC: Receiver Operating Characteristic

ROMe: (R)-FTY720 methyl ether

ROS: Reactive Oxygen Species

RT: Retention Time

SKi: 2-(p-Hydroxyanilino)-4-(p-chlorophenyl)thiazole

SMS: Sphingomyelin synthesis

SMS: sphingomyelin(s)

*Sn*-G3P: *sn*-Glycerol-3-phosphate

TCA cycle: Tricarboxylic acid or Krebs cycle

UPLC: Ultra-high Performance Liquid Chromatography

UTP: Uridine triphosphate

# **Chapter I**

---

## **General introduction**

---

# 1 Introduction

## 1.1 Mammalian cells and cancer

### 1.1.1 Cell culture analysis

The field of cell culture analysis requires combined techniques to provide meaningful information about the complexity of mammalian life in health and disease. Cell culture analysis typically utilizes a cell line cultured *in vitro* that has been firstly isolated from a tissue or organ of interest; known as a primary cell source [1]. Cell culture is a fabricated environment which can provide researchers with the ability to study alterations in living cells when they are exposed to any stress or grown under different conditions [1]. For example, botanical sourced drugs such as gossypol were tested in cancer cells and this enabled identification that it promotes oxidative stress and cell death [2]. Therefore, cell culture bypasses the strict ethics requirement needed for metabolomics in animals [3]. Prostate cancer cells have also been used to identify distinct metabolic biomarkers that are altered during prostate tumorigenesis [4]. Metabolomics and cell culture are also robust applications for cell line testing and discovery of novel signaling pathways. There are several previous studies in which cells have been employed to identify metabolic differences under various conditions and treatment with drugs. For example, the metabolic effects of sphingosine kinase inhibitors have been studied in prostate cell lines [5]. Also, androgen effects in activating amino acid metabolism and the stimulation of methylation have been studied using cultured prostate cancer cells [6]. Overall, these studies demonstrated that cell culture could provide insights for testing and dissecting metabolic mechanisms during early drug development.

The techniques applied to explore the effects of new potential treatments are varied and span a range of disciplines. Traditionally, optical and fluorescence microscopy has been widely employed to image cells which are usually pre-stained with dyes to identify sub-cellular compartments [7]. Other well reported techniques include electron microscopy, x-ray microscopy, confocal optical microscopy, scanning probe microscopy, such as atomic force microscopy, and more recently spectroscopy (Fourier transform Infrared (FTIR) and Raman) and mass spectrometry. Mass spectrometers offer an extra dimension of chemical specificity that has not been provided by earlier techniques [8]. However, additional techniques are required to support interpretation of results obtained by mass spectrometry. For instance, molecular biological techniques, such as polymerase chain reaction (PCR) or western blotting with specific antibodies, aim to monitor gene and protein expression profiles that can contextualize metabolic changes [9]. These data can be integrated to provide better understanding to the key biochemical changes associated with drug treatments in healthy and diseased cells.

### 1.1.2 Cancer cell metabolism

In the last few decades, the revolution in experimental technology and tool development has enabled characterization of the complex biology underlying heterogeneous diseases such as cancer [10]. One of the hallmarks of cancer cells, compared with healthy cells, is an altered metabolism that supports rapid division, proliferation and invasion [11]. A metabolic pathway is a chain of biochemical reactions (catabolic or anabolic) that is regulated by nutrients, hormones and growth factors [12]. Many enzymatic pathways are involved in cancer and these are orchestrated to increase macromolecule biosynthesis to support malignant cell proliferation, replicative immortality, cell survival, immune evasion and metastasis [13].



The current study investigated the role of sphingosine kinase, the enzyme that catalyses the synthesis of the bioactive lipid, sphingosine 1-phosphate (S1P), with specific focus on how it regulates aberrant metabolism in cancer cells. This has identified functional interaction with aerobic glycolysis, the pentose phosphate pathway (PPP), phospholipid biosynthesis and *sn*-glycerol-3-phosphate (*sn*-G3P) metabolism

#### *1.1.2.1 Glycolysis*

Generally, mammalian cells obtain energy as ATP *via* two major routes, one of which is glycolysis that involves the conversion of glucose to pyruvate. This pathway provides two moles of adenosine triphosphate (ATP) per mole of glucose. Where glucose is converted to lactate in the absence of oxygen, this process is known as an anaerobic glycolysis **Figure 1.1-1** [14]. In the presence of oxygen, pyruvate is converted into acetyl-CoA, which is the intermediate between the citric acid cycle and pyruvate. Acetyl CoA then enters a chain of reactions in the citric acid cycle, known as the TCA or Krebs cycle. The TCA cycle largely generates NADH which enters the electron transport chain process to produce 34 moles of ATP. High glycolysis rates in the presence of oxygen, is known as the Warburg effect and this is a distinctive feature of malignant cells. Typically, cancer cells consume glucose at a higher rate in comparison with normal cells; at least 10 times more, and producing more lactic acid causing an acidic environment [14],[15].

Glucose metabolism plays an important role in cancer cell survival and growth [16]. Cancer cells rely on the glycolysis to generate ATP and used some intermediates as precursors for macromolecule biosynthesis such as RNA, DNA, nucleotides and lipids[17]. Furthermore, glucose is diverted into the pentose phosphate pathway to produce sufficient NADPH in order to counter the effect of ROS, which are generated during the rapid growth [17].

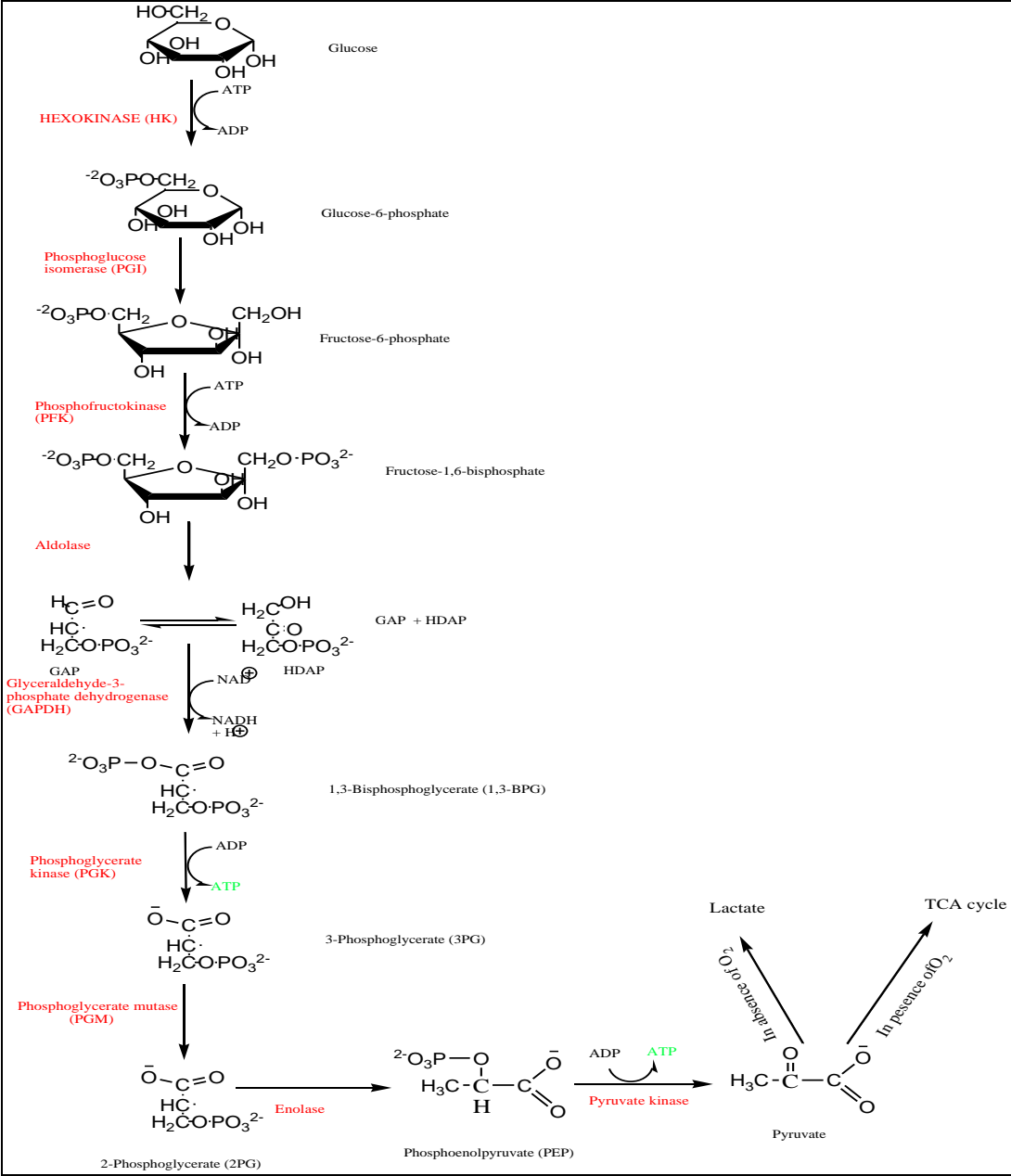


Figure 1.1-1 The glycolysis pathway

### *1.1.2.2 The Pentose phosphate pathway (PPP)*

The pentose phosphate shunt (PPP) also known as the phosphogluconate pathway is connected to the glycolysis pathway by glucose-6-phosphate (G6P), which is formed by hexokinase [18],[19]. Indeed, there are two phases in this pathway, which are the oxidative and non-oxidative as shown in **Figure 1.1-2**. The oxidative phase gains importance since it yields two moles of NADPH. One molecule of NADPH is formed when G6P is converted into 6-phosphogluconolactone by glucose-6-phosphate dehydrogenase. Another NADPH molecule is formed when 6-phosphogluconate is converted into ribulose-5-phosphate by 6-phosphogluconate dehydrogenase [18]. NADPH is involved in fatty acid biosynthesis and in the scavenging of reactive oxygen species (ROS), which endows this pathway with a pivotal role in cancer [20]. In malignant cells, several metabolites in this pathway are used as intermediates in DNA synthesis during the S phase of the cell cycle [21]. From flux analysis using  $^{13}\text{C}$  carbon, it was found that the non-oxidative phase was responsible for producing approximately 80% of the ribonucleotides required for the synthesis of RNA and DNA [22].

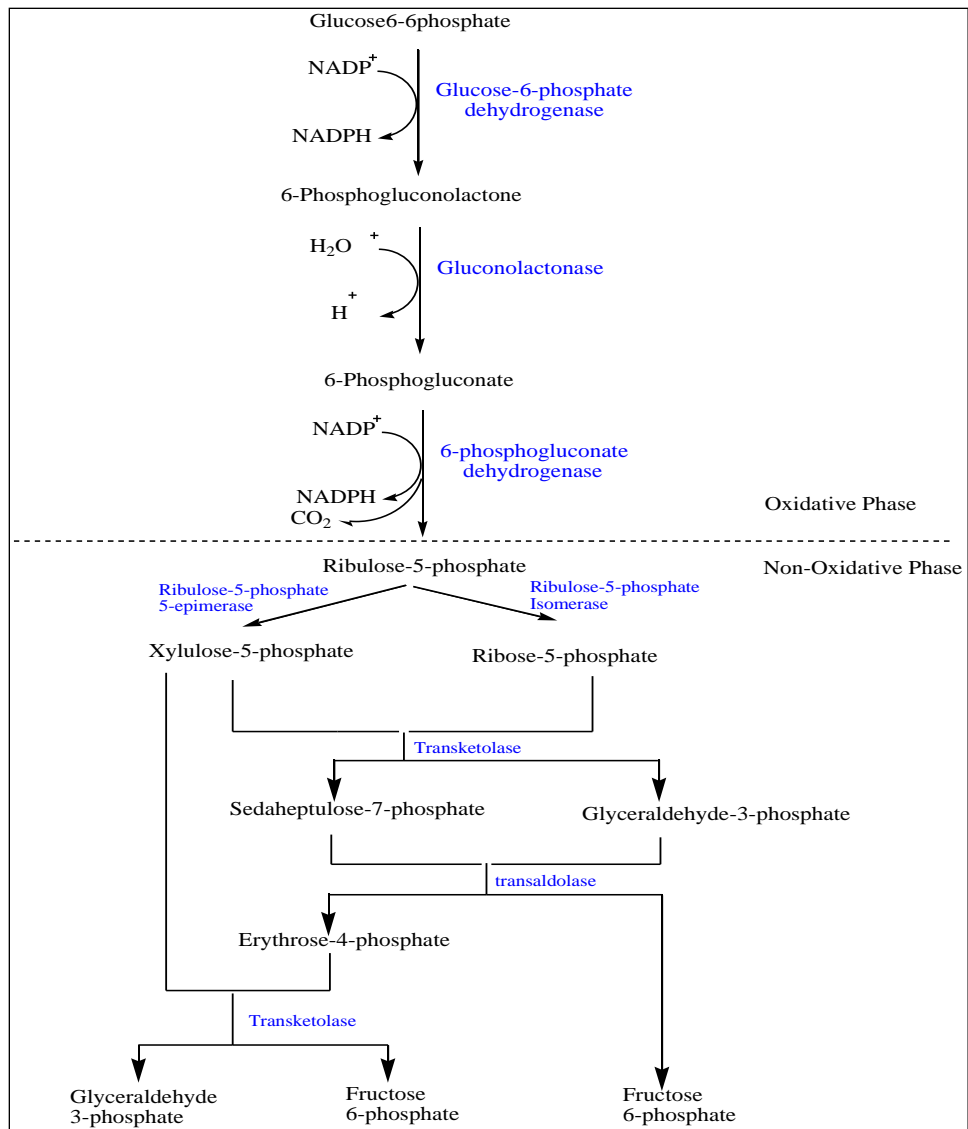


Figure 1.1-2 Oxidative and non-oxidative phases of the pentose phosphate pathway.

### 1.1.3 Lipid metabolism and cancer

In general, there are three main classes of lipids including fats and waxes; complex lipids, including phospholipids and glycolipids; and precursors and derived lipids. However, sphingosine is both a simple lipid and a component of many more complex lipids [23]. Sphingosine provides a backbone of sphingolipids (for example sphingomyelin) and glycolipids (for example galactosylceramide). Both examples contain a fatty acid and sphingosine, which is an alcohol [23]. In addition, phospholipids contain a phosphoric acid residue while glycolipids contain carbohydrate [23].

In normal cells, lipid metabolism plays essential roles in biological processes, cell membrane integrity, cell signaling and energy status [24]. Membrane phospholipids and glycolipids interact with key proteins in lipid rafts involved in cell signaling. Moreover, the composition of lipid vesicles involved in membrane trafficking has been discovered to be a crucial factor for protein targeting. Some lower abundance but highly important lipids fulfill roles as precursors of second messengers or have specialised functions [25]. Alteration in lipid metabolism is a remarkable hallmark of cancer cells, which supports their survival and proliferation [26]. Indeed, genes, enzymes, regulatory factors and transporters involved in lipid transport, lipid synthesis and lipid degradation are dysregulated in cancer cells. Therefore, lipids are of great interest and can yield specific information on physiological functions within cells.

There is evidence of the involvement of sphingosine kinase, the enzyme that catalyses the formation of the bioactive lipid, sphingosine 1-phosphate (S1P) in various human cancer cells [27]. S1P levels are also controlled by its dephosphorylation by S1P phosphatase and by irreversibly cleavage of S1P catalysed by S1P lyase. There are two isoforms of sphingosine kinase termed SK1

and SK2 [27]. SK1a is a 42.5 kDa protein while SK1b is a 51 kDa protein. SK1b similar to SK1a but has an 86 amino acid N-terminal extension and is more stable than SK1a [28]. SK2 is a 69.2 kDa protein and contains 654 amino acids, which is much larger than SK1 isoform [29].

These enzymes are involved in the so-called “sphingolipid rheostat” involving the enzymatic interconversion of ceramide sphingosine and S1P and that the position of the rheostat determines cell fate as generally ceramide promote apoptosis while S1P promotes survival [30],[27].

#### *1.1.3.1 Ceramide*

Many studies have focused on understanding the link between ceramides and apoptosis [31]. There are numerous mechanisms that lead to an increased cellular levels of ceramide including sphingomyelin degradation, the *de novo* ceramide synthesis pathway and the salvage pathway [32]. These pathways are discussed below.

**Sphingomyelin degradation:** sphingomyelin is cleaved into ceramide and phosphorylcholine by lysosomal acidic sphingomyelinase [33] **Figure 1.1-3.**

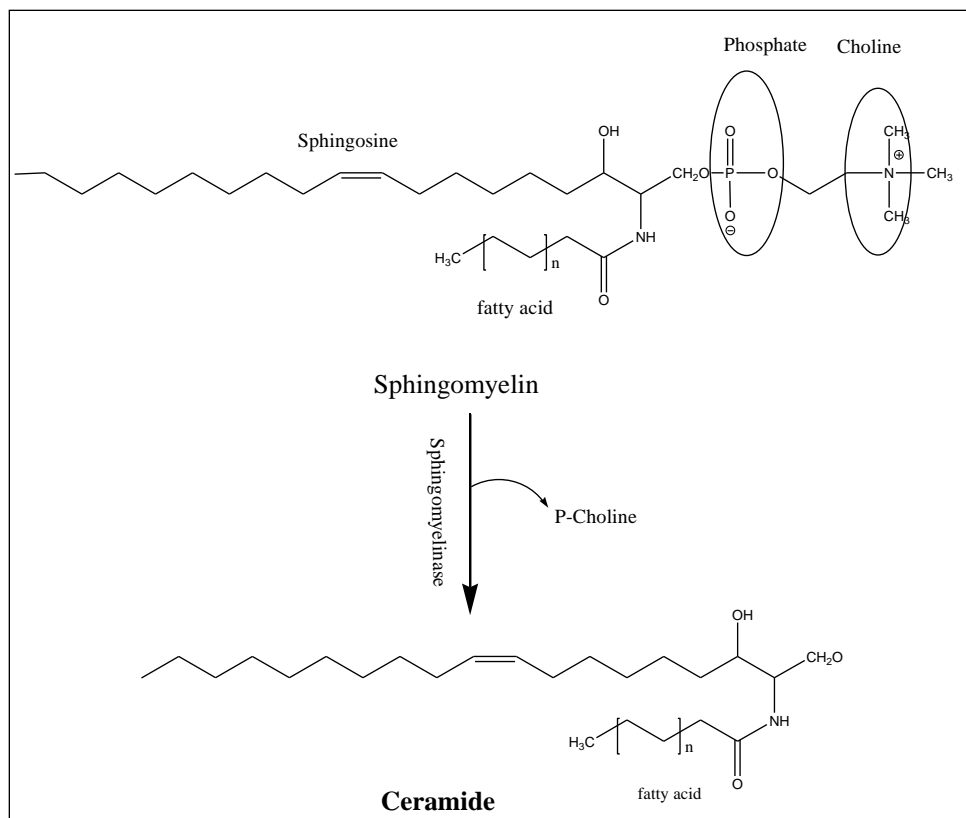


Figure 1.1-3 Ceramide synthesis from the degradation of sphingomyelin

Sphingomyelinase enzymes are classified according to the pH at which their enzymatic activity is optimal. Neutral sphingomyelinase can be activated by TNF binding to the TNF receptor and this can lead to apoptotic cell death, differentiation and inflammation [34].

**De novo ceramide synthesis pathway:** Intriguingly, previous research stated that high cellular concentrations of ceramide produced through stimulating the ceramide pathway might induce apoptosis while S1P promotes cell survival [35],[36]. Ceramide synthesis is initiated **Figure 1.1-4** by the condensation of palmitoyl CoA and serine and catalyzed by serine palmitoyltransferase to produce 3-ketosphinganine. 3-ketosphinganine is reduced by 3-ketosphinganine reductase to form dihydrosphingosine (sphinganine). Acyl CoA is then condensed with dihydrosphingosine by ceramide synthase to produce dihydroceramide, which is then converted to ceramide by

dihydroceramide desaturase [23].

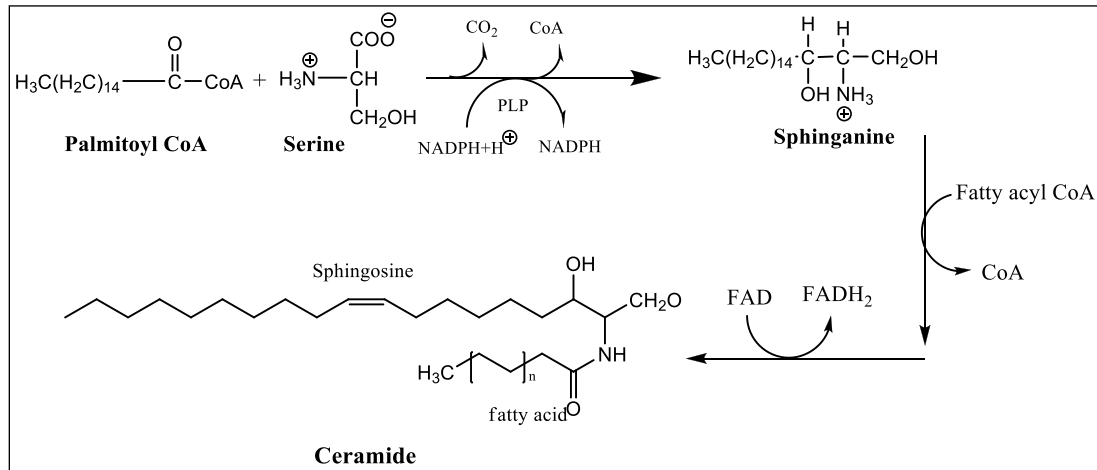


Figure 1.1-4 De novo ceramide synthesis pathway.

**The salvage pathway:** The ceramide salvage pathway occurs in late endosomes and the lysosomes and involves the regeneration of ceramide as a result of the catabolism of complex sphingolipids [32]. **Figure 1.1-5** shows that the formation of ceramide occurs through a number of lysosomal enzymes involved in the metabolism of complex sphingolipids. For instance; ceramide-1-phosphate, glucosylceramide, galactosyl-ceramide and sphingomyelin. In addition, ceramide can be converted into sphingosine via deacylation of ceramide catalyzed by ceramidase (CDase) while it is synthesised by acylation of sphingosine by ceramide synthase (CS) in the endoplasmic reticulum (ER).



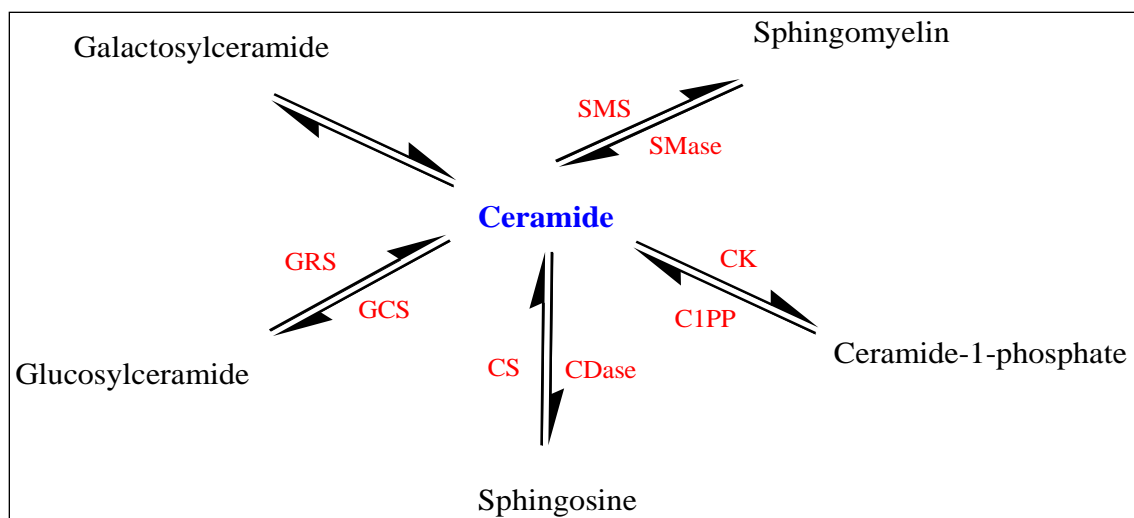


Figure 1.1-5 Ceramide salvage pathway occurs in lysosomes[37]. Where, SMS: sphingomyelin synthase, SMase; sphingomyelinase, CK; ceramide kinase, C1PP; ceramide-1-phosphatase, GRS; glucocerebrosidase and GCS; glycosyl ceramide synthase.

### 1.1.3.2 Sphingosine 1-phosphate (S1P)

S1P is a hydrophilic sphingolipid metabolite, which plays a significant role in regulating growth, survival, migration and the inhibition of apoptosis [30]. S1P is formed by the phosphorylation of sphingosine catalyzed by the enzyme sphingosine kinase. S1P is dephosphorylated by the sphingosine-1-phosphatase enzyme (S1Pase). Alternatively, it can irreversibly cleaved to hexadecenal and phosphoethanolamine catalyzed by sphingosine-1-phosphate lyase (S1P lyase) [27] as shown in **Figure 1.1-6**. S1P appears to play a deleterious role in cancers and other diseases, such as atherosclerosis and inflammation [30]. **Figure 1.1-6** summaries the correlation between ceramide, sphingosine and S1P and its relation to cell fate.



two identified isoforms of SK, known as SK1 and SK2, which differ in their biochemical characteristics and physiological roles [38]. For example, SK1 found in cytosol where it can couple to TARF2 and translocate SK1 from cytosol to plasma membrane [45]. Unlike SK1, SK2 is enriched in mitochondria where it produces mitochondrial S1P required for mitochondrial function [44]. SK2 is also responsible for the synthesis of S1P regulating hTERT in the nucleus [43].

#### 1.1.4 Reactive oxygen species (ROS)

ROS production is a normal physiological consequence of cellular processes. However, ROS serves as an important factor during tumorigenesis. ROS have multiple roles in cancer where it could be a causal factor. For example, the genetic targeting of p53 has been shown to elevate ROS production [46]. Similarly, mutations in breast cancer 1 (*Brcal*) also results in the elevation of ROS [47]. These findings suggest that ROS accumulation observed in cancer cells is due to complications arising during cancer development. On the other hand, elevated ROS further promotes tumorigenesis as a result of direct induction of genomic instability and mutagenesis of DNA [48]. Similarly, ROS also plays critical roles in the development of hallmarks of cancer such as promoting cell migration, angiogenesis and tumor metastasis. At the signaling level, elevated ROS stimulated by hydrogen peroxide activates pathways such as MAPK/ERK and Akt/mTOR, both of which promote cellular growth and survival and are therefore targets for cancer treatment [49],[50]. In contrast, the excessive elevation of ROS has been shown to promote cancer cell death due to increased oxidative stress, hence ROS increase is also considered a strategy for cancer therapy [51]. These studies, therefore, indicate that the interplay of ROS and cancer is context-specific.

## 1.2 Introduction to metabolomics

It has become widely accepted that it is not possible to fully understand biological systems, from microbial or plant species to higher organisms, simply by studying a small and isolated part of this system. Instead, the emerging ‘systems biology’ approach is being widely adopted. Recent efforts are focused on merging all branches of ‘-omics’, such as metabolomics, lipidomics, genomics and proteomics and combining this with a key understanding of the biological pathways affected by a particular disease or treatment in order to make a valuable contribution to improved understanding of human physiology and pathophysiology.

### 1.2.1 Metabolomics

The evolution of metabolomics has been a focus of many studies over the last two decades. Indeed, the term “metabolome” in a biological system refers to metabolites below 1,500 Daltons [52]. In addition, the metabolic composition of the cell is an outcome of its regulation of gene expression, protein abundance, genetic characteristics and environmental influences [52]. The first appearance of the term “metabolomics” was in the late 1990s. However, urine vapour and breath were analysed and quantified using gas-liquid partition chromatography by Pauling in the 1970s. This was identified as the first theoretical, analytical and technological [53] system for quantifying metabolites in biological samples. Over the years, the developments made in analysis technology have had a positive impact on metabolomics studies especially since separation methods and resolution have been significantly improved. For instance, reliable metabolomic analysis techniques including liquid chromatography (LC), high-performance liquid chromatography (HPLC), ultra-high performance (UPLC), gas chromatography (GC), multidimensional gas chromatography (GC-GC) and many types of mass spectrometry have either emerged or have been

improved. Indeed, there is no specific technique used for a metabolomics study but liquid chromatography interfaced to a mass spectrometer (LC-MS) and nuclear magnetic resonance (NMR) are the most commonly used metabolomics techniques [54]. Besides this, there are two strategies used for analysing cells, one of which is non-targeted (un-biased) metabolomics, which is used to develop hypotheses and identify relevant biomarkers. The other is targeted metabolomics used to verify any specific hypothesis. The most common technique applied for targeted metabolomics is mass spectrometry, which enables a low level of detection and quantification [52].

#### *1.2.1.1 Approaches of metabolomics studies:*

Metabolomics can be classified into three main approaches; targeted, semi-targeted and untargeted metabolomics which all enable the evaluation of metabolic disruptions accompanying various diseases or treatments.

- **Untargeted approach (hypothesis assessment)**

This approach provides the most suitable technique to detect unbiased changes in metabolites levels between different biological samples. Untargeted metabolomics aim to maximise the number of identified metabolites and provide the opportunity to monitor unexpected alterations. Mass spectrometry can analyse a massive number of metabolites. However, one single analytical method cannot detect all of the metabolites in a biological system. Therefore, a combination of analytical methods can be used to maximise the coverage of the metabolome. One of the most challenging parts in untargeted metabolomics is the identification of metabolites. The generation of the hypothesis depends on the outcomes and observations of the final analysis [55].

- **Targeted approach (hypothesis formation)**

In this approach, an experiment is designed to study a small number of targeted metabolites, typically up to twenty metabolites, or a targeted pathway. It is a quantitative method concerned with ensuring accuracy and specificity for the targeted metabolites based on established biological knowledge of the sample before data analysis. The use of authentic chemical standards of the metabolites is necessary to perform the study. The targeted approaches examine and evaluate a hypothesis that has been generated through untargeted or semi-targeted studies [55].

- **Semi-targeted approach**

The semi-targeted approach falls between targeted and untargeted approaches. This approach aims to quantify hundreds of metabolites. Unlike targeted approaches, one calibration curve can be used for a set of metabolites which have similarity in their structure [55].

### 1.2.2 Metabolomics flux

High glycolysis rates in the presence of oxygen, is known as the Warburg effect and this is a distinctive feature of malignant cells. Glucose metabolism plays an important role in cancer cell survival and growth [16]. Flux analysis is a complementary approach used in metabolomics which uses stable isotope labelled compounds, such as  $^{13}\text{C}$  labelled glucose [56]. Many studies have used flux analysis with different ratios of  $^{13}\text{C}$  glucose and normal glucose ( $^{12}\text{C}$ ), for example, labelled glucose may be used alone at high enrichment (100%), or in a mixture (50%  $^{13}\text{C}$ : 50%  $^{12}\text{C}$ ), or mixtures of  $^{13}\text{C}$ :  $^{12}\text{C}$  (90:10, 80:20, and 60:40) [56] thus producing typical incorporation patterns which are easy to spot following data extraction. The advantage of flux analysis is that it allows

some estimation of the rate at which different pathways operate, whereas a simple metabolomics experiment just gives a static snapshot of the metabolite levels in a biological system with no information about metabolic rates.

## 1.3 Metabolomics in prostate Cancer

### 1.3.1 Prostate cancer

Cancer is a destructive disease that causes changes in metabolic activities of cells and the surrounding environment [57]. In comparison with normal cells, cancer cells are characterised by different metabolic features [14]. At a cellular level, malignant cell growth is associated with various metabolic changes that could be used as a biomarker for diagnosis, prognosis and evaluation of anticancer therapies [24]. For example, cancer cells rely on a high glycolysis rate (Warburg effect) [14], fatty acid synthesis and glutaminolysis for proliferation [57]. Thus, studying the metabolic profile of cancer cells is essential to understand the process of carcinogenesis and the mechanism of chemoresistance leading to the development of better diagnostic tools and drugs [58].

According to “Cancer Research Website” in 2016, prostate cancer is the most common cancer among men and the second most common cancer comparing both genders (Cancer Research UK, 2019). Worldwide, more than 1.3 million men were diagnosed with prostate cancer in 2018. It considered as the fourth most commonly occurring cancer overall (World Cancer Research Fund International, 2019). Research done by “Prostate Cancer UK Charity” in 2018, reported that more than 47,500 men are diagnosed with prostate cancer each year, which means the daily new cases amount to about 130 men. The majority of the newly diagnosed cases were in England, comprising of more than 40,000 men (Prostate Cancer UK Charity, 2019). Prostate cancer has a high survival rate, of 10 years or more (Cancer Research UK, 2019).



Androgen stimulation is responsible for initiating prostate tumorigenesis [59]. Moreover, down-regulation of the androgen receptor (AR) is a key therapeutic strategy for locally advanced and more aggressive tumors. Treatment options include surgical and/or chemical castration (androgen ablation therapy) and/or by inhibiting AR activation using anti-androgen therapy [60]. Indeed, androgen ablation therapy may fail after a period of time and the cells start to grow again independently without the requirement for androgen, which usually happens within 18 months from starting the treatment. This stage is known as hormone-refractory prostate cancer (HRPC) and is expected to be less than 24 months [61]. The mechanism of this phenomenon remains not fully understood.

Prostate cancer is undetectable at an early stage due to the lack of symptoms. The symptoms are quite similar to those of other conditions such as prostatic hyperplasia, thereby making it difficult to diagnose at an early stage. However, it can be screened for using a blood test called the prostate-specific antigen (PSA) test or through a physical examination using a digital rectal examination (DRE) (Cancer Research UK, 2019). Transrectal ultrasound-guided (TRUS) prostate tissue biopsies are also used as a diagnostic tool. While the use of PSA for screening remains controversial [62], it can be used in HRPC stage as the levels of PSA increased hugely at this stage [63].

## **1.4 Prostate cancer treatment**

### **1.4.1 Current chemotherapy**

It has been long thought that hormonal therapy is the best treatment option for androgen-dependent prostate cancer until these cells adapt to the new environment and develop to grow independently without relying on androgen [64]. The first metastatic prostate cancer documented was the 1940s and treated by surgery [65]. Chemotherapy has generally a good success rate with metastatic castration-resistance prostate cancers (mCRPC) [66] and androgen sensitive prostate cancer [67], which improves overall survival [66]. Many studies have demonstrated that the combination of androgen deprivation therapy and chemotherapy showed an advantage of overall survival in comparison with androgen ablation.

### **1.4.2 Sphingosine kinase inhibitors**

Sphingosine kinase (SK) is a therapeutic target for the treatment of cancer. The objective is to control the relative levels of ceramide and S1P thereby directing cancer cells to ceramide-dependent death **Figure 1.1-6**. There are different types of inhibitors, which are non-selective (SK1/ SK2 inhibitors), such as SKi (2-(p-hydroxyanilino)-4- (p-chlorophenyl) thiazole), SK1 selective inhibitors such as SK1-I (BML-258, SK1 (2R,3S,4E)-N-methyl- 5-(4-pentylphenyl)- 2-aminopent-4-ene-1,3-diol). In addition, there are SK2 selective inhibitors such as ABC294640 (3-(4-chlorophenyl)- adamantane-1-carboxylic acid (pyridin-4-ylmethyl)amide) or FTY720-OMe (ROME) [38]. Several inhibitors have been examined on different cell lines and been demonstrated to inhibit cancer cell proliferation and to induce apoptosis [38].

**Table 1-1 Some examples for SK inhibitors and a summary of their activity [27]**

Sphingosine kinase inhibitor name	Vivo or vitro	Comment
<p>SK1 - I (BML - 258, SK1 (2R,3S,4E) - N - methyl - 5 - (4 - pentylphenyl) - 2 - aminopent - 4 - ene - 1,3 - diol)</p> <p><b>(SK1 inhibitor)</b></p>	<i>In vitro</i>	Inhibition of growth and survival, induction of apoptosis in leukaemia[68] and glioblastoma cells[69].
	<i>In vivo</i>	<ul style="list-style-type: none"> <li>-Inhibition of AML xenograft growth[68].</li> <li>- Inhibition of tumor growth and vascularization and induction of apoptosis in a glioblastoma xenograft[69].</li> <li>- Increase survival of mice with orthotopic glioblastoma[69].</li> </ul>
<p>SKi 2-(p - hydroxyanilino) - 4 - (p - chlorophenyl) thiazole)</p> <p><b>(SK1 and SK2 inhibitor-non-selective)</b></p>	<i>In vitro</i>	- Proliferation inhibition and apoptosis enhanced in several tumor cell lines[70].
	<i>In vivo</i>	<p>Inhibition of growth of syngeneic mammary adenocarcinoma cells[70].</p> <ul style="list-style-type: none"> <li>- Inhibition of inflammation in mice with ulcerative colitis[70].</li> </ul>

Sphingosine kinase inhibitor name	Vivo	Sphingosine kinase inhibitor name
ABC294640	<i>In vitro</i>	<ul style="list-style-type: none"> <li>- Inhibition of proliferation and migration of various tumor cell lines[71].</li> <li>- Induction of autophagic cell death in kidney, prostate and breast tumor cell lines[72].</li> </ul>
(3 - (4chlorophenyl) - adamantane - 1 - carboxylic acid (pyridin - 4 - ylmethyl) amide)  <b>(SK2 selective)</b>	<i>In vivo</i>	<ul style="list-style-type: none"> <li>- inhibition of tumor growth and induction of apoptosis in mammary adenocarcinoma xenografts[71].</li> <li>Inhibition of tumor growth and induction of autophagic cell death in kidney tumor xenografts[72].</li> </ul>

### 1.4.3 Study on LNCaP cell lines using SKi

The effect of sphingosine kinase inhibitors on two prostate cancer cell lines, namely androgen sensitive LNCaP and androgen independent LNCaP-AI, was investigated by Pyne et al (2012). A previous study demonstrated that the expression levels of androgen receptor (AR), which is a type of nuclear receptor, in androgen-sensitive prostate cancer cell lines in response to SKi was reduced [73], [74]. The expression of AR was reduced by SKi via a post-translational dependent mechanism. Likewise, treating LNCaP cells with two SK1 inhibitors, (S)- FTY720

vinylphosphonate and FTY720 reduced AR expression. In contrast, treating LNCaP cells with (10 $\mu$ M, 24 h) the SK2 inhibitor, (R)-FTY720 methyl ether (ROME) **Figure 1-7**, failed to reduce AR expression [5]. In addition, a previous study demonstrated that protein (p53) expression increased in LNCaP-AI cells but not in androgen-sensitive LNCaP cells when they were treated with SKi (10  $\mu$ M) [74].

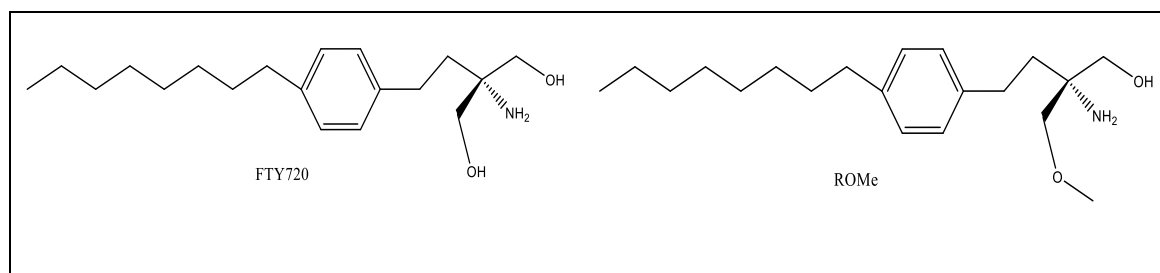


Figure 1.4-1 Chemical structures of FTY720 [64] and ROME [75].

## 1.5 Techniques used in Metabolomics Studies.

A biological sample may contain various groups of metabolites with different physicochemical properties whose analysis can be performed by employing the same techniques as those used in regular chemical analysis. These analytical techniques can be used to monitor alteration occurring in cell extracts, such as cancer cells, followed by a treatment or changing the growing conditions, and comparing them with other conditions or a negative control. The most common techniques used in metabolomics are liquid chromatography (LC), gas chromatography (GC), coupled with a suitable detector such as mass spectrometer (MS) [76]. In addition to those techniques, NMR is also commonly used in such studies [77].

### 1.5.1 Principles of chromatographic separation

The term of chromatography describes a physical separation technique based on an interaction

between a metabolite or a chemical or an element and two phases, one of which is a stationary phase, while the other, a mobile phase, is running in a specific direction [78]. Generally, choosing the most suitable method of separation depends on the nature of the targeted analytes. For instance, GC is used for volatile compounds while LC is used for non-volatile compounds. The most common high-performance liquid chromatography (HPLC) methods used in the pharmaceutical analysis are reversed-phase (RP), normal phase (NP) and hydrophilic interaction liquid chromatography (HILIC). The proper stationary and mobile phases depend on the nature of the analysis, for example, polar compounds required a polar stationary phase (NP) while reversed-phase columns provide better separation for non-polar compounds with the use of proper mobile phases.

### 1.5.2 Mobile phase

In an LC-MS system, the mobile phase is normally a solvent, or mixture of solvents, consisting of polar and organic components which are miscible with each other. Polar solvents may contain buffer salts at low concentrations such as ammonium carbonate, ammonium formate, ammonium acetate, or ammonium chloride with stationary phases, such as HILIC and C-18 reversed-phase, in order to modify the retention on an analyte [79]. For example, ammonium carbonate is used with HILIC columns to increase the retention of the polar analytes by increasing the thickness of the aqueous layer on the HILIC surface [79]. Thus, the choice of a mobile phase depends on the stationary phase. For example, typically a non-polar mobile phase, such as hexane, is used with a polar stationary phase, such as unmodified silica gel or silica gel with diol, in order to retain polar analytes. Opposite of this, a highly polar mobile phase (e.g: water) with a small amount of an organic modifier is used with hydrophobic columns, such as C<sub>4</sub>, C<sub>8</sub> and C<sub>18</sub> columns, in order to

retain non-polar analytes. In GC-MS, the mobile phases used is an inert gas such as nitrogen, helium or hydrogen [78]. This is the main difference between GC and LC in mobile phases.

### 1.5.3 Stationary phases

There is a wide range of stationary phases available, the most common phases are reversed-phase (RP), normal-phase (NP) and hydrophilic interaction liquid chromatography (HILIC). Since, HILIC is employed extensively in the metabolomics field due to the fact that many hydrophilic metabolites such as carbohydrates cannot be sufficiently retained in a RP column and often elute close to the column void volume, this study will focus on the of HILIC columns.

#### *1.5.3.1 hydrophilic interaction liquid chromatography (HILIC)*

HILIC is a technique used to separate polar analytes using a polar stationary phase and a less polar mobile phase, which compatible with a mass spectrometer [80]. It works in an orthogonal manner to reversed phase chromatography, for example, whereas the organic solvent is the strong solvent in reversed phase partition, water is the stronger one in HILIC. It has recently established itself as the method of choice for highly polar and hydrophilic compounds instead of RPLC [81],[82]. The actual retention mechanism of HILIC is complex and depends on solute characteristics, type of the stationary phase, and mobile phase composition. HILIC columns are classified according to their chemical properties which indicate the exact mechanism in separation. There are various types of columns available commercially, such as bare silica, silicon hydride columns, diol silica, amide silica, zwitterionic both silica gel and polymer-based columns. The current study used a polymer based zwitterionic column and a bare silica gel column

Silica gel consist of silanol groups bonded to the silica atoms of the particles. The chemical environment of the silanol groups has an effect on their acidic activity. Some examples of the most

common silanol groups are isolated silanol groups, vicinal silanol group and geminal silanol group

**Figure 1.7.**

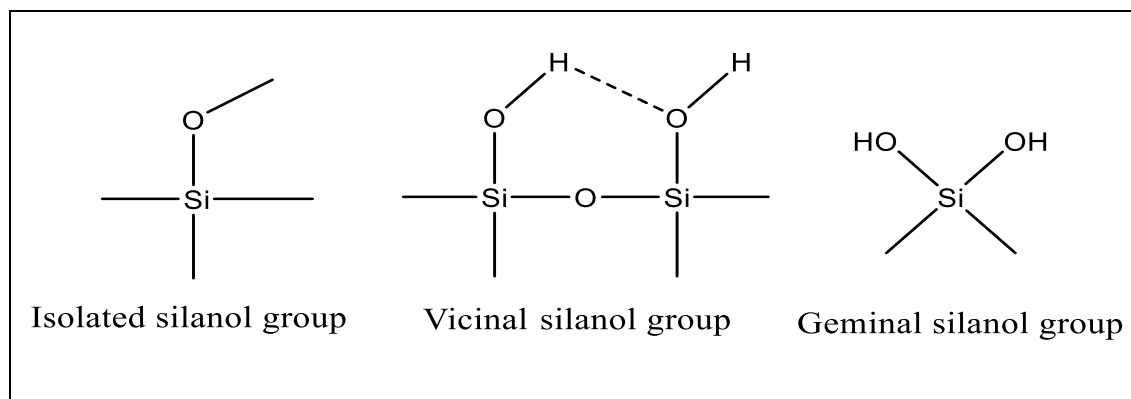


**Figure 1-1.5-1 different types of silanol in a silica gel column.**

Silanol groups on the surface of silica gel make the stationary phase polar. This polar stationary phase can be used in HILIC since water can form a layer on the gel and provides partitioning with analytes for the separation [82]. Besides partitioning, analytes can form hydrogen bonds with silanols and there is a possibility for ion exchange interactions with the more acidic silanols depending on the pH of the mobile phase [83],[84]. The mobile phase used is a mixture of a high percentage of organic solvent (>70%), such as acetonitrile and isopropanol, and aqueous solvent/buffer [85]. Silica can be used for lipid fractionation, as non-polar analytes are first recovered in non-polar solvents. Hence, polar compounds such as phospholipids are more strongly adsorbed by the silica sorbent than by neutral lipids such as triglycerides [86].

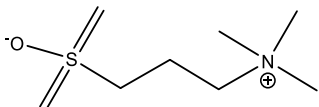
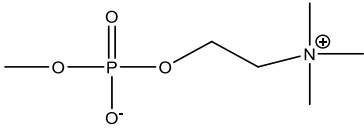
### *1.5.3.2 Zwitterionic phases*

Zwitterionic phases are characterised by the embedding a compound that carries both positive and negative charges to the silanol groups such as the sulfobetaine and phosphocholine ligands shown in **Table 1-2**. This column gains importance in metabolomics when a high pH of 9.2 is used since it can successfully detect most phosphates [81]. The sulfobetaine group can be found in ZIC-HILIC



and ZIC-pHILIC, which are differ in the type particles to which it is bonded. The particles in ZIC-pHILIC are polymeric particles instead of silica which provides the basis of the ZICHILIC column. The ZIC-cHILIC has a phosphorylcholine functional group attached to silica particles. These columns have shown reproducible efficiency at separating metabolites in various biological samples. For this reason, they offer the best results in comparative studies for untargeted metabolomic applications [83]. Various retention mechanisms are involved in HILIC columns which include partitioning between the MP and SP, anion and cation exchange, and weak non-polar interactions with the carbon backbone [87]. For instance: neutral hydrophilic analytes are retained based on their partitioning between the polar MP and water layer form on the stationary phase [82],[88] whereas acids and bases may undergo additional ion-exchange interactions.

**Table 1-2 examples of zwitterionic phases and their functional groups.**

Column	Functional group	Particle	Structure
ZIC-HILIC	Sulfobetaine	Silica	
ZIC-pHILIC	Sulfobetaine	Polymer	
ZIC-cHILIC	Phosphorylcholine	Silica	

#### 1.5.4 Mass spectrometry MS

Generally, mass spectrometry systems used in conjunction with gas chromatography (GC-MS) or

liquid chromatography (LC-MS) provide some of the most powerful techniques used in metabolomics. A mass spectrometer has three main components, which are: an ion generator, a mass analyser and a detector [89] as shown in **Figure 1.5-2**

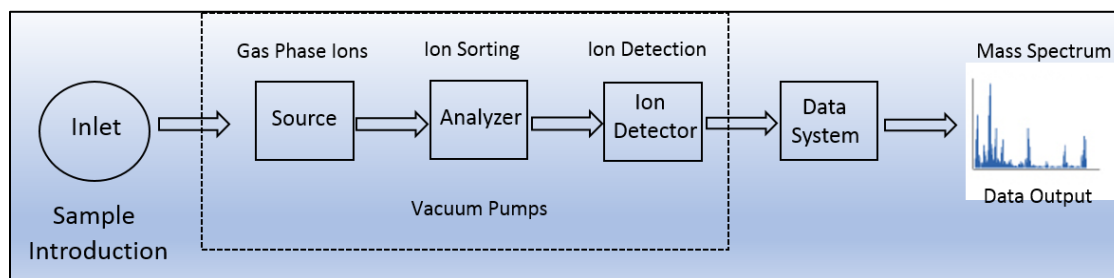


Figure 1.5-2 Schematic diagram of the main components of a mass spectrometer.

#### 1.5.4.1 Ion sources

The first main part of a mass spectrometer is the ion generation source. Negative or positive ions are produced when an analyte passes through the ionization chamber [89]. There are many kinds of ion generators, for example, electrospray ionization (ESI), atmospheric pressure chemical ionisation (APCI) and electron impact (EI), which are currently the most popular techniques used [89]. Matrix assisted laser desorption ionisation (MALDI) is another example of an ion source which is typically used in conjunction with time of flight instrument (TOF) [89]. The ions generated by the ion source are accelerated through a region of electric and magnetic fields so that only those ions with  $m/z$  in a selected range can reach the analyser and be detected [89]. It has been observed that several adducts can be formed when in an ion source such as ammonium sodium and potassium [90]. These adducts could arise from glassware or mobile phases or solvent impurities [90]. ESI is more compatible with LC-MS while EI is more compatible with GC-MS [89].



than ESI since ESI can ionized most drug molecules [78]. However, APCI can be used for low polarity compounds and can be applied at high flow rates [78].

### 3- Electron impact (EI)

EI is used with GC-MS while it not compatible with LC-MS [78]. Therefore, it is suitable to ionize volatile analytes by evaporating a sample at the end of a probe. Evaporation can be carried out by the high vacuum within the system or *via* a capillary column. A vaporised sample is then introduced to the ionisation chamber *via* the sample inlet. In this chamber, a high electric potential is applied (70eV) to electrons produced by heating a rhenium or tungsten filament. The analyte passing between the filament and the target electrode are then ionised. The Positive ions produced in the source are pushed out by a repeller voltage which carries a positive charge thus pushing the analytes from the ion source towards the analyser. Extensive fragmentation of the analyte occurs since the positive ions produced by using energy higher than the strength of the bonds within the analyte **Figure 1-10**. The EI ionisers have the advantage of a provide a unique fingerprint for a molecule [78].

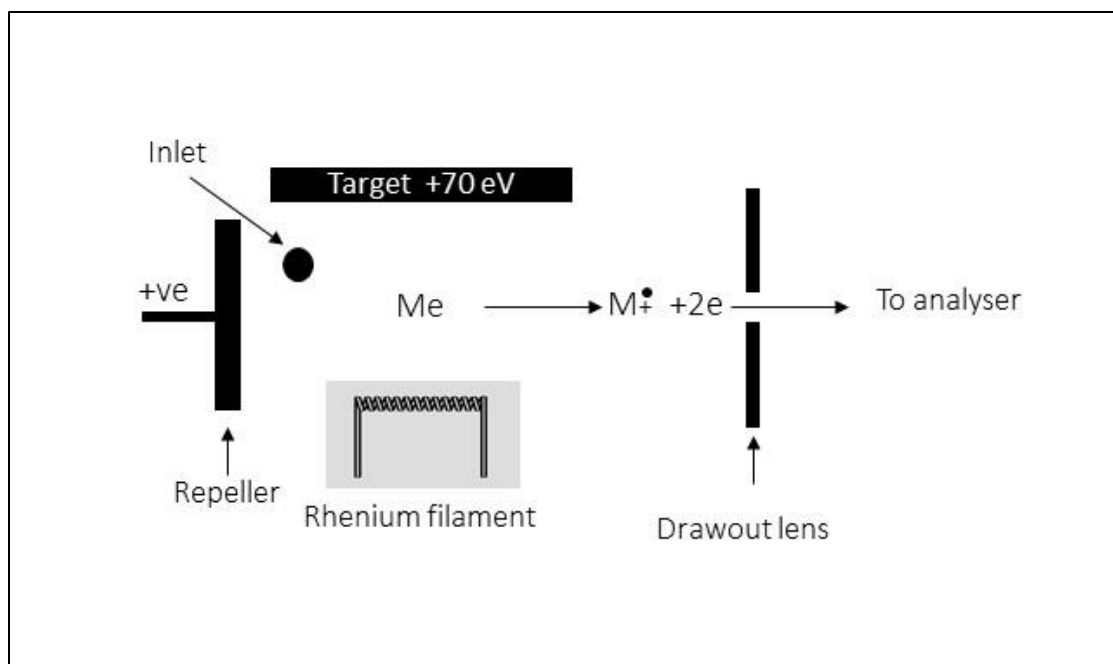


**Figure 1.5-4** Ion generator in an electron impact source. where: M=molecule; e=electron. modified from. [78]

#### 1.5.4.2 Mass analysers

The mass analyser is the second main component of a mass spectrometer instrument. This part responsible for separating ions produced in the ion source according to their ( $m/z$ ) ratio. There are many kinds of mass analysers in use, for example, quadrupole mass analyser (Q), triple quadrupole ion trap (QIT), time of flight (TOF), Fourier transform ion cyclotron resonance (FT-ICR), and Orbitrap analysers are all commonly used to separate ions according to their mass to charge ratio [78]. The main differences between these mass analysers arise from their resolving power, mass accuracy, sensitivity, dynamic range and fragmentation capabilities for MS studies. In the last decades, hybrid mass analyzers were combined in order to improve the capabilities based on the ion separation techniques being incorporated in the system. Examples of this combination are QTOF, TOF-TOF, IT-Orbitrap and Q-exactive [92]. In the experiments carried out in the current work an Orbitrap Exactive instrument was used.

## Quadrupole mass analyser

A quadrupole analyser Error! Reference source not found. has a great sensitivity and a high resolution in comparison with other analysers, especially older analyzers such as a magnetic sector. This analyser consists a set of four solid rods, which are arranged in parallel to the direction of ion beam. An oscillating electrostatic field is generated between the rods by applying a direct-current (DC) voltage and oscillating radiofrequency (RF) voltage. Ions oscillate within this electrostatic field depending on the ratio between the two currents. Depending on the ratio between the two fields, ions acquire an oscillation in the electrostatic field. For out of range ions, the  $m/z$  is too small or too large to undergo a stable oscillation. Ions with the correct  $m/z$  ratio for a particular combination of voltages remain stable and travel down the quadrupole to reach the detector. Some quadrupoles have  $m/z$  ranges up to 2000.

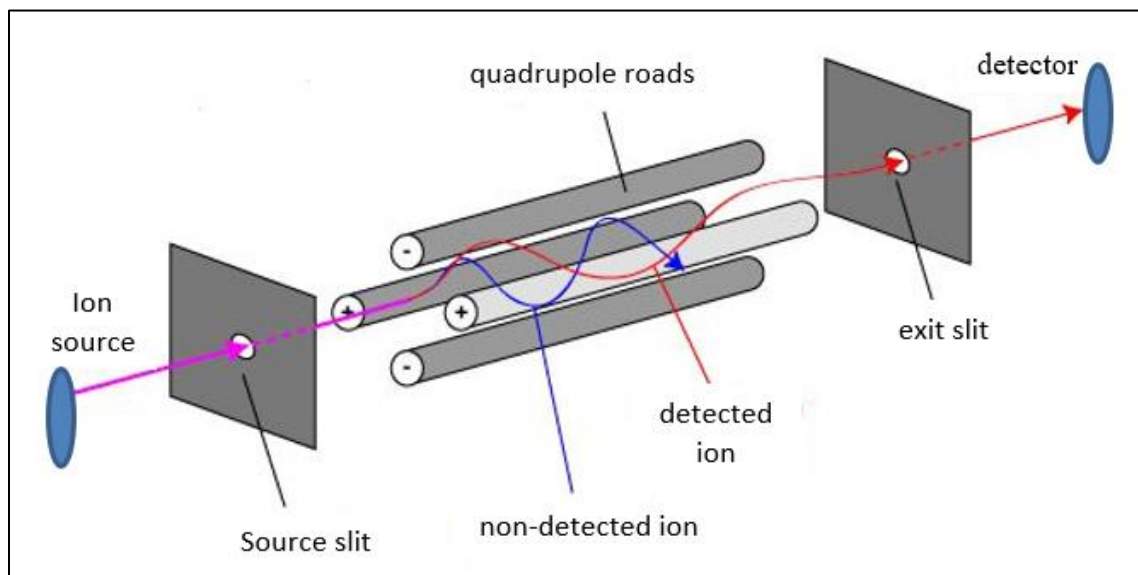


Figure 1.5-5 Separation of ions using a quadrupole mass analyser. Resonant ions with specific  $m/z$  values pass into the detector. Obtained and modified from [93].

### **The orbitrap mass spectrometer**

The heart of Orbitrap mass analyzer is an axially-symmetrical mass analyzer, which consists of a spindle-shape central electrode surrounded by a pair of bell-shaped outer electrodes as shown in Figure 1.5-6 schematic diagram representing the Orbitrap Mass Spectrometer. Obtain and modified from [92]. **Figure 1.5-6.** Firstly, ions generated by an ion source and then transferred into quadrupole. The quadrupole rod selects the ions according to  $m/z$  ratios. Then, the ions transferred into the C-trap and then injected into the Orbitrap mass analyser. In an orbitrap mass analyser, ions are trapped due to their electrostatic attraction to the inner electrode. Then, the ions rotate around the inner electrode on oval path. The field between electrodes is reduced and then ions are injected from an external ion source while the electric field is increased when ion packets are injected tangentially into the field. Ions are squeezed towards the inner electrode until they reach the trap and at this time ramping is stopped and the field becomes static and detection starts. Because each packet contains many ions of different velocities, the rotational frequencies are different. This means that ions of a specific mass-to-charge ratio spread into rings which oscillate along the inner spindle. Axial oscillations of the ion rings are detected by their image current induced on the outer electrode which is divided in two symmetrical pick-up sensors. The ions are detected simultaneously over a given period of time [93].

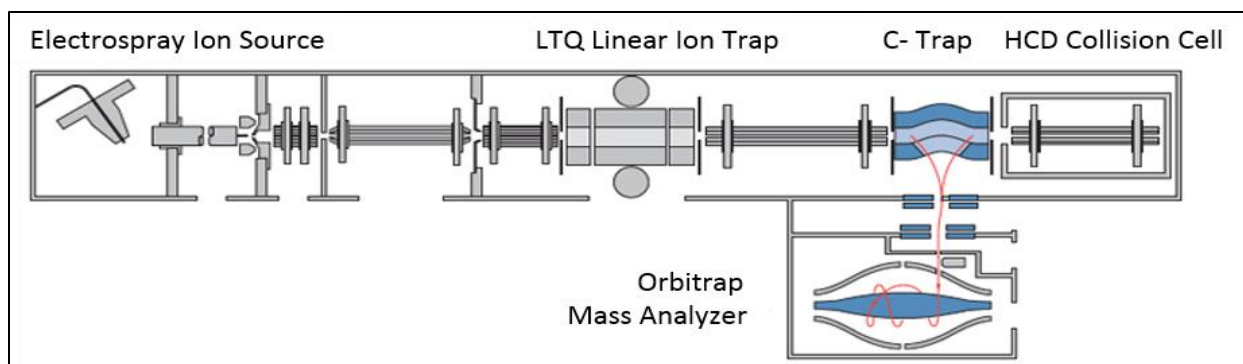


Figure 1.5-6 schematic diagram representing the Orbitrap Mass Spectrometer. Obtain and modified from [92].

### **Time of flight (TOF) mass analyser**

The basis of the separation technique in TOF depends on the relation between the speed of travel and molecular weight, where smaller ions reach the detector quicker than larger ions. In order to avoid spectral overlap, a ‘reflectron’ device is used to focus the kinetic energy of the ions and send the ions back in the opposite direction. This increases the length of the flight tube and increases the instrument resolution. TOF instruments are often combined with matrix-assisted laser desorption ionisation (MALDI) as an ion source [89]. ESI and APCI can be also used as an ion source with TOF [78]. a unique combination between quadrupole and TOF was developed using ESI as an ion source [78], which produces the high compound fragmentation efficiency of quadrupole and high mass resolution capability of TOF [94].

#### *1.5.4.3 Detectors*

The Detector is the last main component in the MS instrument. The detector is responsible for converting the separated ions into signals (as  $m/z$  values) on the computer screen and displaying their abundances [78]. Various mass detectors are used in MS systems, such as electron or photomultiplier [78], conversion dynodes and cryogenic detectors.



## 1.6 Data Extraction and Processing

Analysis of biological samples produces a vast amount of data of a very complex nature which are difficult to be interpreted until statistical software is used to simplify it. Processing the data in this way allows all relevant information about the analytes that were found in the sample to be extracted while, at the same time, making subsequent data analysis and interpretation easier by minimising background noise. Therefore, LC-MS data must be processed and metabolites identified properly for easier interpretation. Data usually passes through two different steps: data processing using a software, followed by data analysis. In data processing, firstly, the raw data is transformed into a format that can be used by a software for further data processing as it will be described in the next section [95]. Software for data processing is available commercially, such as SIEVE and TraceFinder [96] are developed by Thermo Fisher Scientific; and non-commercially, such as MzMine [97] and MzMatch. Then, in the data analysis, the processed data is visualised and analysed using multivariate analysis producing clustering of metabolic profiles and determining the difference between groups [95]. Examples of software for data analysis are SIMCA-P [80], which is available commercially, and Metaboanalyst [98], which is web-based and open source.

### 1.6.1 Mz-Mine.

There are many types of software used for extraction and profiling data collected by mass spectrometry software programs while running biological samples with LCMS. Nevertheless, data processing is quite a challenging technique for molecular profiling[99]. Katajamaa et al, 2006, presented a compatible program for extracting mass spectrometry data and profiling it, which was Mz-Mine version (2.10)[99]. Firstly, the raw data files (Thermo-Xcalibur format) were initially split into a single ESI positive and negative data set, and also converted into mzML format by

using ProteoWizard. The Mz-Mine tool provides numerous functions for data processing **Figure 1.6-1**, including peak picking, chromatogram deconvolution, retention time normalization, peak alignment, and data base search among others[99]. However, in this experiment, version (2.10) was employed as it has more features allowing for filtering of the data during extraction.

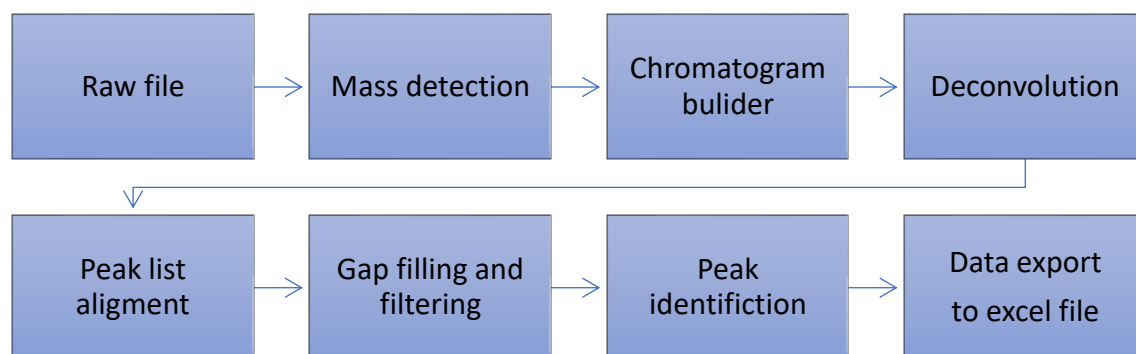


Figure 1.6-1 schematic diagram of data processing using MzMine 2.10.

### 1.6.2 Multivariate analysis

Data of biological samples obtained by LC-MS to study metabolomics or genomics or proteomics are vast and complex. The data yielded is multi-dimensional and contains variables such as the area under the curve (AUC), RT and m/z values. Pooled samples and blanks can be used to minimise variance contributions from random technical processes such as sample analysis and sample preparation. This provides a better understanding between different groups and/or classes [100]. The huge data sets generated by a mass spectrometer require the use of multivariate analysis (MVA). The multivariate analysis packages Metaboanalyst (open-access source) and SIMCA-P (commercial), were used in the current study.

SIMCA-P is a recognized tool for multivariate analysis particularly for high numbers of samples for determining within-class variability[101]. This program has many features that provide a good

representation of differences between classes *via* using unsupervised or supervised techniques. Examples of unsupervised techniques; principle component analysis (PCA) and Hierarchical Cluster Analysis (HCA). The use of PCA is considered as the main tool for data reduction that could extract meaningful information [102]. Whereas, Orthogonal Partial Least Square Discriminant Analysis (OPLS-DA) and partial least square discriminant analysis (PLS-DA) are examples of supervised techniques [101]. OPLS-DA is applied to discriminate between groups of samples [103]. Typically,  $R^2$  and  $Q^2$  are the most often used parameters for validating models. Since OPLS-DA is a supervised technique OPLS-DA it requires an internal validation such as a permutation test or Receiver Operating Characteristic (ROC) [104].

Supervised OPLS-DA model is an expansion of PLS-DA model, which can separate the variation in X that correlates to Y (horizontally) called predictive variation, and also separate variation in X that is uncorrelated to Y (orthogonal) **Figure 1.6-2**. This supervised technique is considered as the most powerful technique used to examine the difference between groups [103]. OPLS-DA can also distinguish reliable biomarkers that have a strong association with separation between groups (Trygg et al., 2007) and it correlates disease to perturbations in metabolic pathways (Goodacre, 2007). Therefore, OPLS-DA helps expand our understanding of pathophysiology and future therapeutic targets.

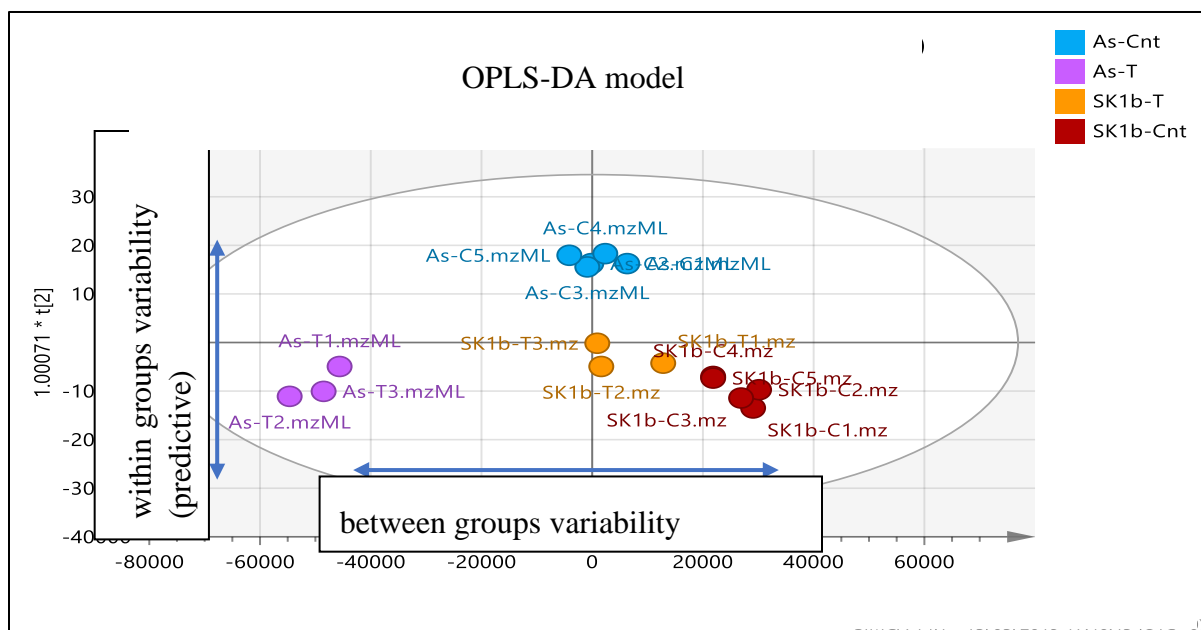


Figure 1.6-2 Orthogonal Partial Least Discrimination Analysis (OPLS-DA) score plot.

### 1.6.2.1 Permutation test

The permutation test compares the  $R^2$  and  $Q^2$  obtained from the original model to randomly permuted  $R^2$  and  $Q^2$  produced when some variables are omitted from the model this process can be repeated several times to generate new quality parameters [105]. This test is applied to examine whether the specific classification of observations into two groups is significantly better than any other random grouping in two arbitrary classes [105]. The validity of this test depends on two factors; (i) the original  $R^2$  and  $Q^2$  should be higher than generated values, (ii) the regression line of the predictive model should cross zero line [106] as shown in **Figure 1.6-3**. In addition, the accuracy of the model in discriminating observations based on their metabolic profile should be evaluated using area under the ROC.

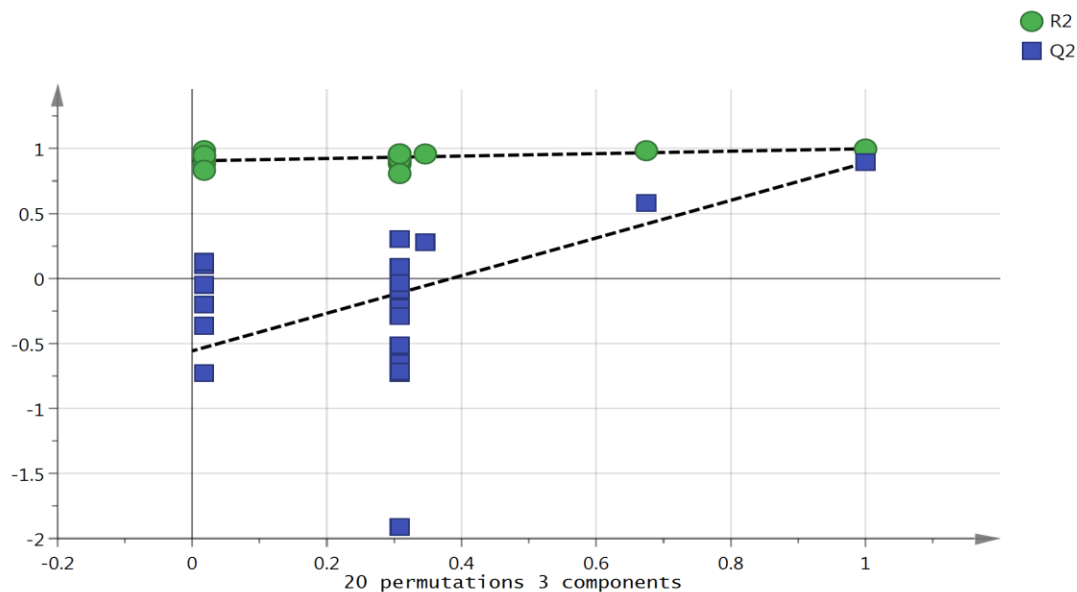


Figure 1.6-3 permutations test. It shows the vertical axis gives the R2Y and Q2Y -values of each model. The horizontal axis represents the correlation coefficient between the original Y, which has correlation 1.0 with itself, and the permuted Y.

### 1.6.2.2 Receiver Operating Characteristic (ROC)

The area under the ROC curve (AUROCC) is an important model to check any classification model's performance, which is a reflection of how accurate a supervised model is at discriminating between variables/observations sharing the same metabolomics profile and those that do not. The greater the AUROCC, the better the model is capable to distinguish between classes. The ROC curve designed by several points of sensitivity and specificity, which are inversely proportional to each other [107]. The goodness of the ROC curve depends on AUROCC values as it is shown in **Table 1-3** [108]. For example, when AUC is between 0.5-0.6, it means that the model has no discrimination capacity to distinguish between classes as shown in **Figure 1.6-4, B**. On the other hand, when AUC is between 0.90-1, it means that the model has a high capability to distinguish between classes [108].

Table 1-3 The predictability of ROC model

AUC	0.9-1.0	0.8-0.9	0.7-0.8	0.6-0.7	0.5-0.6
The predictability	Excellent	Good	Fair	Poor	Fail

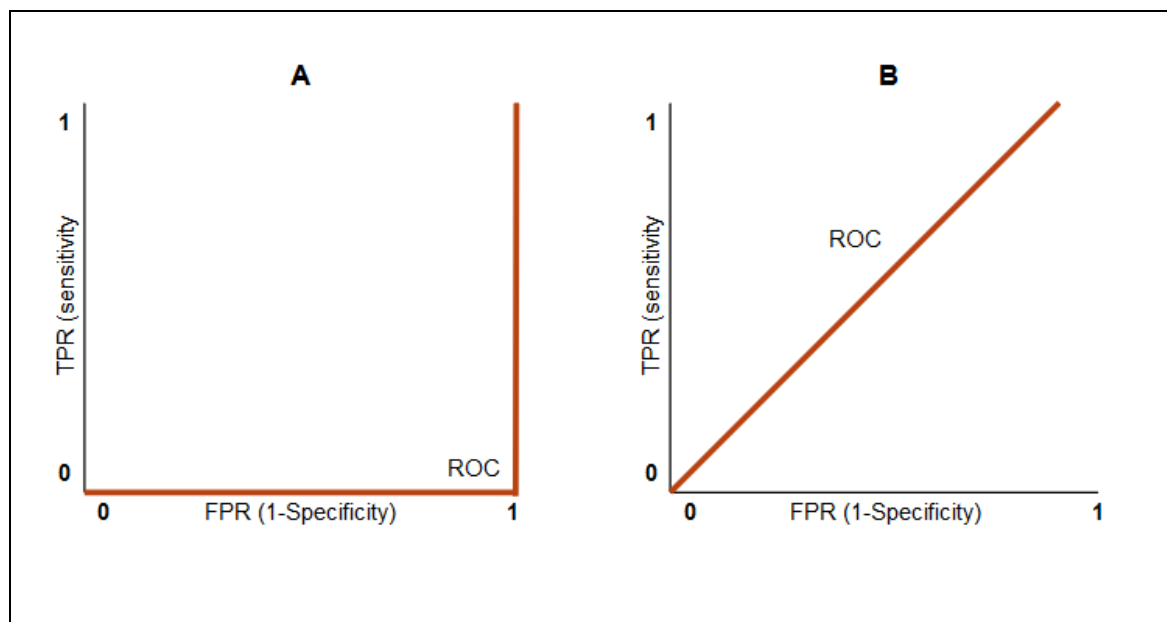


Figure 1.6-4 the ROC curve shows sensitivity (true positive rate (TPR)) on the y-axis versus (false positive rate (FPR = 1 - Specificity)) on the x-axis, the value of both normalised to 1 which represents the value of AUC for a group. (A) excellent AUC accuracy= 1; (B) fail model AUC= 0.5, which is the worst model. Where; TPR= true positive rate. FPR=false a positive rate.

## 1.7 Aims

The overall aim of this study was to investigate the metabolome of three human prostate cancer cell lines: LNCaP (androgen sensitive), LNCaP-AI (androgen-independent) and LNCaP-SK1b cells (SK1b gene over expressed) in response to different sphingosine inhibitors by using high-resolution LC-MS. Changes identified in the metabolome due to a treatment or gene expression

can then be used to generate hypotheses regarding the role of SK1 and SK2 in prostate cancer. In addition, observed changes in pathways and/or metabolites can potentially support an established mechanism, which was proven by other technique such as Western blot, or indicate novel mechanisms. The following objectives were used to achieve the main aims of the study:

- 1- To study the metabolomics effect of SKi on LNCaP-AI cells using  $^{13}\text{C}_6$ -glucose (pulse-chase experiment).
- 2- To measure ROS production in response to SKi in LNCaP-AI cells.
- 3- To study the effect of the expression of SK1b on LNCaP cells.
- 4- To compare metabolomic changes induced by SKi between LNCaP and over expressed LNCaP-SK1b cells.
- 5- To investigate the effect of the SK2 inhibitor ROME on the metabolome of LNCaP and LNCaP-SK1b cells.
- 6- To perform a lipidomic analysis of the effect of new SK inhibitors (PLR24, ST55, ST81) on the metabolome of LNCaP-AI.
- 7- To perform a lipidomic analysis of the effect of new SK inhibitors (PLR24, ST55, ST81) on the metabolome of LNCaP-SK1b cells.

## **Chapter II**

---

### **Materials and Methods**

---



## 2 Materials and methods

### 2.1 Chemicals and solvents

#### 2.1.1 Solvents and chemicals

HPLC grade 99% acetonitrile (ACN), methanol (MeOH), and isopropanol (IPA) were purchased from Sigma-Aldrich (Poole, UK). A Direct Q-3 water purification system (Millipore, Walford, UK) was used to produce the HPLC water that was in all of the analyses. Ammonium carbonate HPLC grade was obtained by VWR chemicals, UK. Ammonium acetate was obtained by Sigma-Aldrich, (Poole UK).  $^{13}\text{C}_6$ -Glucose,  $^{13}\text{C}_2$ -Glycin and all the analytical standards used to evaluate the column were purchased from Sigma-Aldrich, (Poole UK).

#### 2.1.2 Materials used in cell culture:

- RPMI 1640 medium, obtained by Life Technologies, cat. No. 12633012, Paisley UK.
- RPMI 1640 without glucose, obtained by Life Technologies, cat. No. 11879020, Paisley UK.
- Trypsin 0.25% Solution was from Thermo Scientific, cat no. 25050014.
- L-Glutamine, was from Thermo Scientific, cat. No. 25030081.
- Foetal Bovine Serum European Grade, Origin: Brazil EU Grade, Batch No. 26140079.
- Foetal charcoal/dextran stripped (FBS) serum, Catalogue number is DE14-820F, supplier is Cambrex, South America.
- LNCaP cells, LNCaP-SK1b and LNCaP-AI cells.
- Dimethyl Sulfoxide (DMSO), was from Sigma-aldrich, cat no. 276855.
- Geneticin G-418 sulphate, potency 732, Gibco. CAS. no.108321-42-2

- Cryogenic vials, 1ml, screw caps, E3110-6112 obtained by Stra Lab.
- Phosphate buffered saline, Cat no. P4417, obtained by SIGMA, USA.
- Sphingosine kinase inhibitor (SKi), 2-(p-hydroxyanilino)-4-(p-chlorophenyl) thiazole.HCl obtained by Calbiochem, Merck Millipore, Darmstadt, Germany.
- (R)-FTY720 methyl ether (ROME), obtained by Merck Avanti. Cat. No. 857392O.
- PLR24, ST55 and ST81 gifted from Dr.Simon Mackay's lab at Strathclyde.
- 96 well cell culture black with clear bottom plates, Lot. 13608025, costar, USA.
- Dihydroethidium, lot. 1689834, cat no: D1168, Thermo Fisher Scientific, USA.

## 2.2 Method:

### 2.2.1 Preparation of LNCaP, LNCaP-SK1b and LNCaP-AI

LNCaP and LNCaP-AI cells were grown in full RPMI medium, which containing 10% of Foetal Bovine Serum (FBS) for the Androgen sensitive LNCaP cell line or 10% charcoal/dextran stripped FBS serum for the androgen independent LNCaP-AI cell line plus 1% of streptomycin/penicillin and 1% of L-glutamine. Cell passage involved removing the old medium followed by washing the cells using 5-7ml of serum free medium and then adding 1ml trypsin and putting the flask in an incubator under humidified conditions, 37°C with 5% CO<sub>2</sub>. Then 1ml of cell suspension was transferred from confluent flasks into two new flasks and then 9 ml of full medium was added to each flask. One flask was used for experimental work, as described in the next section, when both flasks had reached confluence and one of these was used for splitting into two new flasks with a new passage number. The difference between LNCaP and over

expressed cells, LNCaP-SK1b, was that LNCaP-SK1b maintained in RPMI media with 0.3 % Geneticin.

### 2.2.2 Cell Extraction

Aliquots of medium containing  $75 \times 10^4$  cells were plated into seven T-25 flasks with 3 ml of full media. Three flasks were used for controls and three flasks for treatment and two for counting. The flasks were included the  $10 \mu\text{M}$  SKi inhibitor and three its vehicle (DMSO) and were incubated before extraction after 24 hours. After counting cells by using a haemocytometer slide the volume of extraction solution required could be calculated so that it was set at 1ml/2 million cells. For extraction, the medium was completely aspirated and the cells were gently washed with 3ml of  $37^\circ\text{C}$  PBS twice, this step was very quick, and was followed by adding a calculated volume of pre-cooled extraction solution (methanol:acetonitrile:water 50:30:20), which was kept in a dry ice/methanol mixture. The cells were harvested by using a cell scraper and after that each mixture was transferred into clear marked Eppendorff tubes. Subsequently, all tubes were shaken in Thermo mixer in a cold room at  $4^\circ\text{C}$  for 12 minutes. After shaking had finished then centrifugation was carried out at  $0^\circ\text{C}$  at 15300 rpm for 15 minutes. When this step was finished the supernatant was transferred to new Eppendorff tubes and stored at  $-20^\circ\text{C}$  until injection into the mass spectrometer.

### 2.2.3 Cell extraction for flux-analysis

LNCaP-AI cells were plated in 16 T-25 flasks, 3 flasks for each condition and one for counting. Cells for grown for approximately 24 hours before adding (50:50) labelled: unlabelled glucose with the treatment and extracting the cells at 4 different time points, 3, 6, 12 and 24 h. Cells were extracted as described in the previous section 2.2.2.

#### 2.2.4 Cell extraction for pulse-chase analysis

The same method 2.2.4 used. The difference is that (50:50) labelled U-<sup>13</sup>C<sub>6</sub>: unlabelled glucose was added at the same time as the treatment then removed by replacing RPMI media with a new unlabelled media. Then the cells were extracted at 4 different times (1 hour, 4 hours, 12 hours and 24 hours).

#### 2.2.5 ROS Assay

To measure ROS generation by SKi, dihydroethidium (DHE) fluorescent dyes were used to detect the superoxide (O<sub>2</sub><sup>-</sup>) level. LNCaP-AI cells were plated at 5 x 10<sup>3</sup> / well in 96 well, four wells for each condition, and maintained in full RPMI media for 24 hours in a normal CO<sub>2</sub> incubator. Then, four wells were exposed to SKi for 24 hours. At the end of the 24 h stimulation, 2.0 μL of dihydroethidium (100nM DHE) were added to each well for 30 minutes in the dark before fluorescence microscopy was performed to measure ROS production. Also, angiotensin II (100nM) were added to four well for 1 hour as a positive control. Plate reader wavelengths adjusted to 485 and 520 nm [109].

#### 2.2.6 LC-MS conditions

##### *2.2.6.1 Chromatographic conditions and MS conditions for analyses on a ZIC-pHILIC column*

Polar metabolite separation was achieved by using a ZICpHILIC column (150 x 4.6 mm, 5 μm), HiChrom, Reading UK on an Accela HPLC interfaced to an Orbitrap Exactive system (Thermo Fisher, Hemel Hempstead UK) coupled with an electrospray Ionization Source (ESI) in operated both positive and negative modes. Data collection was carried out via XCalibur Software (Thermo

Fisher, Bremen). The separation was achieved by running samples in a random sequence to minimize bias after running a blank (extraction solution). Using binary mobile phases, mobile phase A (20mM ammonium carbonate) and mobile phase B (100 % Acetonitrile), in a gradient system for 46 minutes as shown in Table 2-1. Mobile phase A (aqueous phase) was prepared by dissolving 1.92g of ammonium carbonate in 1 L of distilled water, pH was approximately 8.8. Mobile phase B was 100 % acetonitrile (organic phase).

Table 2-1: The gradient system used in the LCMS experiment.

Time (min)	Mobile phase A%	Mobile phase B%
0	20	80
30	80	20
31	92	8
36	92	8
37	20	80
46	20	80

Note: This method developed by Watson and their group in 2013.

The samples were kept in a vial tray which was set at constant temperature of 7°C to avoid any possible degradation of samples. All mobile phase solutions were freshly prepared and were stored at room temperature for up to 48 hours.

#### 2.2.6.2 *Chromatographic conditions for analysis of lipids on silica gel*

An ACE silica gel column (150 x 4.6 mm, 3µm), Hichrom Reading UK was used for the analysis of lipids. The mobile phase for the ACE silica gel column consisted of (A) 20% isopropyl alcohol

(IPA) in acetonitrile (ACN) (v/v) and (B) 20% IPA in 0.02M ammonium formate (v/v). The flow rate was 300  $\mu$ L/min and the gradient was as follows:

Time (min)	Mobile phase A%	Mobile phase B%
0	92	8
5	91	9
10	80	20
16	75	25
23	65	35
26	92	8
40	92	8

### 2.2.7 Standards preparation

Approximately 300 metabolites were prepared at 1 mg/ml as stock solutions with (1:1) HPLC grade methanol: water then stored at -20°C. Seven standard mixtures prepared by taking 100  $\mu$ l from each standard stock solutions according **Table 2-2**. The metabolites were distributed into seven mixtures in order to identify the retention times of isomers which have identical molecular weights such as the common hexoses.

Table 2-2 The distribution of metabolite standards into seven mixed standard solutions. Where S.N.= standard number.

S.N	Standard name	S.N	Standard name	S.N	Standard name
1	Inosine	2	Imidazole-4-acetate	4	UTP
1	Xanthosine	2	N-Formyl-L-	4	Lactic acid
1	IMP	2	O-Acetylcarnitine	4	Cysteine
1	Adenosine	2	trans-cinnamic acid	4	Ribose 1,5-diphosphate
1	Maltose	2	2-Indolecarboxylic acid	4	5-phospho-D-ribose-1-diphosphate
1	Uridine 5'-diphosphoglucose	2	Caffeate	4	Indole
1	Riboflavin	2	3-indole acetate	4	L-Cysteic acid
1	Malonate	2	Indole-3-lactic acid	5	Acetylcholine
1	CoA	3	Sarcosine	5	3-Methyl-L-histidine
1	FAD	3	2-phosphoglycerate	5	N-Acetylhistamine
1	Taurine	3	xylose	5	3-hydroxybutyric acid
1	UDP-N-acetyl-D-glucosamine	3	D-Xylulose 5-phosphate	5	3-(2-Hydroxyphenyl) propanoic acid
1	L-Alanine	3	Itaconate	5	Hydroxyectoine
1	L-Serine	3	mannose	5	L-2-Aminoadipic acid
1	Glyceraldehyde 3-phosphate	3	Galactose-1-phosphate	5	DL-2-Methyl-3(3,4-dihydroxy-phenyl)alanine
1	D(+)-2-Phosphoglyceric acid	3	Picolinic acid	5	7-Methyladenine
1	Putrescine	3	D-Glucuronolactone	5	3-O-Methyluridine

1	Fumarate	3	Paraxanthine	5	2-Ketobutyric acid
1	Cytosine	3	L-Kynurenine	5	Lasparagine
1	Acetoacetate	3	Guanosine	5	S-Methyl-L-cysteine
1	Methylmalonate	3	Thymidine	5	5-methyluridine
1	L-Aspartate	3	dAMP	5	Xanthurenic acid
1	L-Threonic acid	3	AMP	5	UDP
1	creatine	3	L-Metanephrine	5	Carnitine
1	L-Homoserine	3	Spermine	5	1-Methylguanine
1	L-Glutamine	3	Kynurenic acid	5	B-Glutamic acid
1	L-Arabinose	3	5-Hydroxyindoleacetate	5	Glycocholic acid
1	Betaine	3	L-Saccharopine	5	3-(2-Hydroxyphenyl) propanoic acid
1	L-Methionine	3	NADPH	5	4-methyl-2-oxovaleric acid
1	D-Ribose 5-phosphate	3	Glycocholic acid	5	N-Acetylneuraminic acid
1	Xylitol	3	Glycine	5	Malonic acid
1	Choline(+)	3	Pyruvate	5	γ-Aminobutyric acid
1	Xanthine	3	5-Oxoproline	5	5-hydroxy-L-tryptophan
1	Citraconate	3	Histamine	5	Tyramine
1	2-Oxoglutarate	3	Acetylcysteine	5	N'-Methylnicotinamide
1	Citramalate	3	Galactarate	5	D-Mannose 1-phosphate



1	L-Proline	3	D-Glucosamine	5	DL-Indole-3-lactic acid
1	Cis-4-Hydroxy-D-Proline	3	6-Phospho-D-gluconate	5	2-Deoxyadenosine 5-monophosphate dAMP
1	L-Glutamate	3	L-Arginine	5	2-Deoxycytidine
1	Ectoine	3	D-Glucosamine 6-Phosphate	5	Cytidine 2':3'-cyclic monophosphate
1	D-Galacturonate	3	L-Histidine	5	L-Norvaline
1	L-Cystine	3	N-Acetyl-L-aspartate	5	L-Fucose
1	rhamnose	3	N <sub>2</sub> -Methyl-L-histidine	5	N $\alpha$ -Acetyl-L-ornithine
1	glucose	3	N-Acetyl-L-glutamate	5	Chenodeoxycholic acid
1	L-isoleucine	3	Dopamine	6	pyridoxine
1	glucose 1 phosphate	3	6-Hydroxydopamine	6	Maleic acid
1	D-Sorbitol	3	Pyridoxamine	6	DL-Leucine
1	Isonicotinic acid	3	Lipoate	6	Xanthine
1	Ascorbate	3	N <sub>6</sub> -Acetyl-L-Lysine	6	Taurocholic acid
1	Isocitrate	3	Pyridoxal	6	D-panthenol
1	N-Acetyl-D-Glucosamine	3	Uridine	6	D(-)-quinic acid
1	2-Phenylglycine	3	UMP	6	N-acetyl-L-glutamine
1	Pantothenate	3	Cytidine	6	5-methyluridine
1	N <sub>6</sub> -Trimethyl-L-lysine	3	CDP	6	DL-valine
1	2-phenyl imidazole	3	CTP	6	D-sorbitol
1	4-Coumarate	3	O-Acetylcarnitine	6	myo-Inositol

1	Hippuric acid	3	Lithocholic acid	6	L-Gulonic gamma-lactone
1	Ribothymidine	3	2-deoxyribose-5-phosphate	6	Oxaloacetic acid
1	Inosine	3	4-Hydroxy-L-glutamate	6	2-Pyrrolidone-5-carboxylic acid
2	Sucrose	3	Homo-arginine	6	Mucic acid
2	B-Alanine	3	2,6-Quinolinediol	6	Picolinic acid
2	DHAP	3	Deoxy uridine	6	indole-3-acetic acid
2	3-Phosphoglycerate	4	Fructose	6	6-phosphogluconic acid
2	Maleic acid	4	Fructose 6 phosphate	6	D-Fructose-1-phosphate
2	Ketobutyric acid	4	Octopamine	6	Guanosine-5-triphosphate
2	Succinate	4	Tryptophanol	6	L-Histidine
2	L-Threonine	4	GMP	6	D-(-)-Erythrose
2	Ribose	4	5-methylcytidine	6	Erythritol
2	L-Valine	4	GDP	6	Succinic acid
2	D-Ribulose 5-phosphate	4	ATP	6	2-Imino-1-imidazolidine acetic
2	Oxypurinol	4	L-Glutathione oxidized	6	inosine-5-monophosphate
2	Mesaconate	4	L-Tryptophan	6	N-acetyl-L-lysine
2	D-2-Hydroxyglutaric acid	4	5'-Methylthioadenosine	6	1-Methyl-L-histidine
2	5-Aminolevulinate	4	7-Methylguanosine(+)	6	Fructose-1-phosphate

2	O-Acetyl-L-serine	4	Thiamine (+)	6	2-O-Methyluridine
2	D-Glucuronate	4	Melatonin	6	Glycodeoxycholate
2	Fucose	4	S-Adenosyl-L-homocysteine	6	serotonin creatinine sulfate
2	Galactose	4	NAD+	6	Deoxycholic acid
2	L-Leucine	4	Cholate	6	5-hydroxy-l-tryptophan
2	Glucose 6 phosphate	4	Taurocholate	6	Taurocholate
2	Mannitol	4	Ethanolamine phosphate	6	Oxalacetic acid
2	Nicotinate	4	Phosphocreatine	6	Spermidine
2	D-Isoascorbic acid	4	(L)-Malate	6	D-(+)-Trehalose
2	Citrate	4	L-Homoserine Lactone	6	D-Mannose 6-phosphate
2	Theobromine	4	2-Hydroxybutanoic acid	6	Ursodeoxycholic acid
2	N-Acetyl-D-mannosamine	4	L-Homocysteine	6	S-(5-Adenosyl)-L-homocysteine
2	Hydroxyphenylacetaldoxime	4	Urate	6	2-Deoxy-D-ribose
2	Biopterin	4	Guanine	6	Hydroxyphenyllactic acid
2	Serotonin	4	D-Galactono-1,4-lactone	6	Folic acid
2	ADP	4	D-Gluconic acid	6	4-methyl-2-oxovaleric acid
2	Biotin	4	L-Citrulline	7	Glycine <sup>13</sup>
2	Glutathione	4	L-Lysine	7	xanthine

2	3-Phenylpropionylglycine	4	beta-D-Fructose-1,6-bisphosphate	7	D-mannose-6-phosphate
2	Lactoylglutathione	4	Triethanolamine	7	Creatine
2	S-Adenosyl-L-methionine	4	Nicotinamide	7	shpingosine
2	Folate	4	Cis-Aconitate	7	Rhanmnisone
2	NADP <sup>+</sup>	4	N-Acetylglutamine	7	GTP
2	Oxalate	4	Cystathionine	7	NADP
2	Bilirubin	4	methyl-L-lysine	7	2-O-methyluridine
2	Phosphoenolpyruvate	4	Spermidine	7	UTP
2	sn-Glycerol 3-phosphate	4	Gallate	7	a-ketoglurate
2	Uracil	4	2-(4-Hydroxyphenyl) ethanol	7	Ursodeoxycholic acid
2	Allantoin	4	L-Noradrenaline	7	N,N-dimethylsphingosine
2	Creatinine	4	N-Acetyl-D-glucosamine 6-	7	3,4-Dihydroxyphenylacetic
2	D-3-hydroxy-butyrate	4	Dimethyl-L-lysine	7	Acetylcholine
2	DL-3-aminobutyrate	4	Hydroxyphenylacetate	7	3-Methyl-L-histidine
2	Deoxyribose	4	Homogentisate	7	N-Acetyl histamine
2	L-Ornithine	4	L-Phenylalanine	7	DL-2-Methyl-3(3,4-dihroxy-phenyl)alanine
2	Hypoxanthine	4	L-Tyrosine	7	L-Cysteic acid
2	Adenine	4	Dihydrobiopterin	7	a-ketoglurate

## 2.2.8 LC-MS conditions

### 2.2.8.1 *Accela HPLC-ESI-Exactive Orbitrap*

Liquid chromatographic separation was carried out on an Accela HPLC system interfaced to an Exactive Orbitrap mass spectrometer (Thermo Fisher Scientific, Bremen, Germany). The nitrogen sheath and auxiliary gas flow rates were maintained at 50 and 17 mL/min. The electrospray ionisation (ESI) interface was operated in a positive/negative dual polarity mode. The spray voltage was 4.5 kV for positive mode and 4.0 kV for negative mode, while the ion transfer capillary temperature was 275°C. Full scan data was obtained in the mass-to-charge ratio ( $m/z$ ) range of 75 to 1200 for both ionisation modes with settings of AGC target and resolution as Balanced (1E6) and High (50,000) respectively. Mass calibration was performed for both positive and negative ESI polarities before the analysis using the standard Thermo Calmix solution (Thermo Fisher Scientific, Bremen, Germany) with additional coverage of the lower mass range with signals at  $m/z$  83.0604 ( $2\times\text{ACN}+\text{H}$ ) for the positive and  $m/z$  91.0037 ( $2\times\text{HCOO}^-$ ) for the negative modes respectively. The resulting data were recorded using the XCalibur 2.1.0 software package (Thermo Fisher Scientific, Bremen, Germany).

### 2.2.8.2 *Finnigan HPLC- LTQ Orbitrap*

$\text{MS}^2$  analysis of lipids was carried out on an LTQ Orbitrap using the ACE silica gel column. Instrument settings were as for the Exactive instrument except that the instrument was operated in negative ion mode alone. The PC lipids of interest were analysed in negative ion mode by setting the source collision energy to 35V to remove formic acid and methyl from the formic acid adducts of the molecular ions (Zheng et al., 2010) and then carrying of  $\text{MS}^2$  with a collision energy of 35V using the LTQ ion trap as the detector.

### 2.2.9 Data extraction, processing and analysis

Data extraction for each of the samples was carried out by MZmine-2.10 software (Pluskal et al., 2010) ([mzmine.github.io/](http://mzmine.github.io/)) using identical parameters for peak detection, deconvolution, deisotoping, alignment, filtering, gap filling and identification in order to make multiple data files comparable (Zhang et al., 2013). The raw data files (Thermo-Xcalibur format) were initially split into a single ESI positive and negative data set, and also converted into mzML format by using ProteoWizard. The procedure and the settings of each step used in MZmine-2.10 are described in **Figure 2.2-1**.

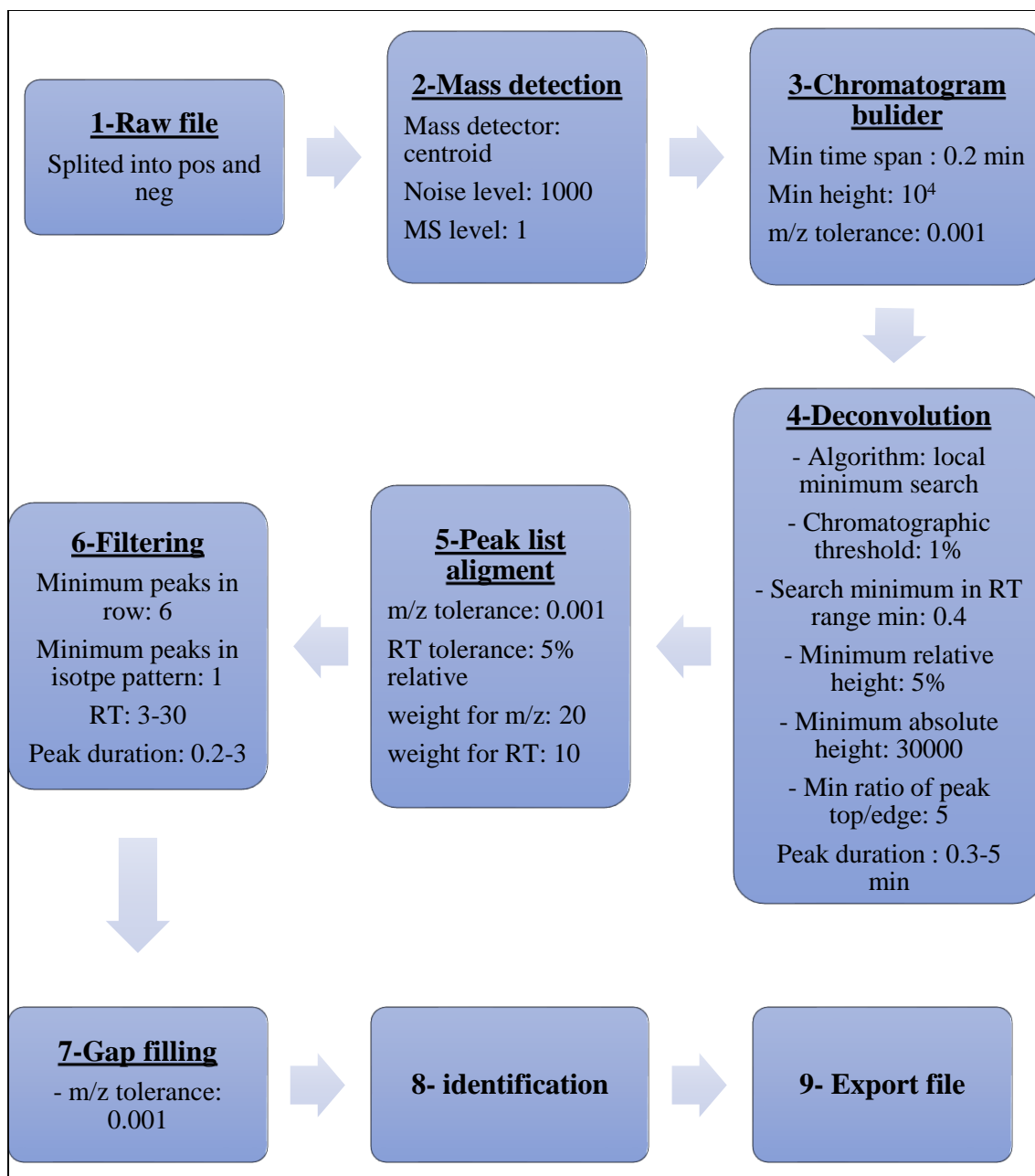


Figure 2.2-1 MZMine 2.10 procedure and settings

### 2.2.10 Databases used for identification of metabolites

The extracted data, which include m/z values, retention time (RT) and peak areas, in Mz-Mine can then be searched against an in-house metabolite database, which uses a range of public online databases such as Kyoto Encyclopedia of Genes and Genomes (KEGG), Human Metabolome

Database (HMDB), METLIN Metabolomics Database, MassBank and LipidMap, sources displayed in **Table 2-3**. Final result then exported into Microsoft Excel for further analysis using chemometric tools.

Table 2-3 Online databases used in the in-house macro

Source	Website
KEGG	<a href="http://www.genome.jp/kegg/">http://www.genome.jp/kegg/</a>
HMDB	<a href="http://www.hmdb.ca/">http://www.hmdb.ca/</a>
METLIN Metabolomics Database	<a href="https://metlin.scripps.edu/">https://metlin.scripps.edu/</a>
MassBank	<a href="https://massbank.eu/MassBank/">https://massbank.eu/MassBank/</a>
LIPID MAPS	<a href="http://www.lipidmaps.org/">http://www.lipidmaps.org/</a>

### 2.2.11 Xcalibur

Xcalibur version (2.1.0) is software produced by Thermo Fisher Scientific to record data from a mass spectrometry run. Data include peaks shape, retention time, peak area, peak height, accurate mass, suggestions of chemical formula and other useful information.



## **Chapter III**

---

**Metabolomics profiling of the effect of the sphingosine  
kinase inhibitor SKi on the metabolome of LNCaP-AI cells  
using pHILIC column and flux analysis using  $^{13}\text{C}_6$  glucose**

### 3 Metabolomics profiling of the effect of sphingosine kinase inhibitor SKi on the metabolome of LNCaP-AI cells using pHILIC column and flux analysis using $^{13}\text{C}_6$ glucose

#### 3.1 Introduction

There have been several studies which have shown that the bioactive lipid, sphingosine-1-phosphate (S1P), which is responsible for regulating cell survival, growth and migration, may play a vital role in many diseases, such as cancers, inflammation and cardiovascular diseases. Therefore, it has been proposed that controlling the sphingolipid rheostat by targeting sphingosine kinase might be a useful therapeutic approach for treating cancer [28]. Loveridge et al, 2010 demonstrated that the SK1/SK2 inhibitor SKi (2-(p-hydroxyanilino-4-(p-chlorophenyl) thiazole) induces proteasomal degradation of SK1 in LNCaP and LNCaP\_AI cells and this leads to the accumulation of glycolytic and pentose phosphate metabolites [5]. SKi also promotes cell stress as indicated by the accumulation of GSSG and the reduction of NADPH levels [5].

Under stress conditions, glucose appears to be diverted into the pentose phosphate pathway through oxidation of G6P into 6-phosphogluconate then into ribulose-5-phosphate in order to generate two molecules of NADPH. NADPH is a reducing agent that maintains the GSSG/GSH balance at a normal ratio [110] and it is also required for fatty acid synthesis [20]. Physiologically, the normal proportion of GSSG:GSH is about 1:100 to 1:10 [12]. When cells is exposed to stress, there are changes in the GSSG:GSH ratio. In this regard, GSH buffers oxidative stress by scavenging ROS (e.g  $\text{H}_2\text{O}_2$ ) to release  $\text{H}_2\text{O}$  and GSSG, catalysed by glutathione peroxidase. GSSG is subsequently converted back to GSH in the presence of NADPH by glutathione reductase. A high ratio of GSSG:GSH correlates with high levels of ROS, while a low ratio is associated with

low oxidative stress [111]. Therefore, GSSG:GSH has been used as a critical biomarker to measure cellular oxidative stress [111].

SKi has also been shown to promote cell cycle arrest leading to inhibition of cell proliferation and promotion of senescence of LNCaP-AI cells. Interestingly, this was associated with a reduction in c-Myc levels [112]. Previous studies have shown that the c-Myc oncogene regulates multiple metabolic pathways, including reprogramming glucose metabolism, glutamine and nucleotide biosynthesis. c-Myc overexpression is responsible for enhancing proliferation through such metabolic reprogramming and through promoting other cellular changes in cancer cells [113]. For instance, overexpression c-Myc enhances aerobic glycolysis *via* the activation of enzymes such as hexokinase II (HK2), pyruvate kinase isozyme (PKM1/2) and lactate dehydrogenase A (LDHA) [112][114]. Similarly, it has been found that c-Myc is also overexpressed in prostate cancer [115], where it has a critical role in tumor initiation and progression [116]. Due to the direct roles of c-Myc in the regulation of multiple glycolytic enzymes, it has been suggested that targeting this transcription factor will inhibit cell growth by reprogramming of glycolytic metabolism.

While the signalling mechanism linking c-Myc and ROS has been shown to involve p53 activation, the metabolic fingerprint occurring during this process is not yet clear. p53 regulates a diverse range of biological functions including apoptosis [117], senescence [118], DNA metabolism [119] and inhibition of angiogenesis [120]. Therefore, the de-regulation of p53 promotes tumorigenesis and it is the most mutated gene in primary human cancers [121]. The activation of p53 by hypoxia or cytotoxic agents has been shown to inhibit cell growth [117].

The aim of this chapter is to examine the effect of SKi (10  $\mu$ M, 24 hours) on LNCaP-AI prostate cancer cells using labelled  $^{13}\text{C}_6$ -glucose (pulse-chase study). To investigate this, the metabolomic profile of LNCaP-AI cells was measured to:

- 1- Identify the effect of SKi on the cellular metabolism.
- 2- Understand how glycolytic metabolites are altered in response to the treatment of these cells with SKI.
- 3- Establish the effect on SKi on ROS production.
- 4- Determine the effects of SKi on carbon flux through different pathways using  $^{13}\text{C}_6$  labelled glucose.

## 3.2 Materials and methods

### 3.2.1 Cell lines chemical and culture

As described in section 2.2.1, Chapter II.

### 3.2.2 Cell Extraction

As described in section 2.2.2, Chapter II.

### 3.2.3 Cell extraction for flux-analysis and pulse-chase experiment

Utilising the extraction method used previously, but in this case, the  $^{13}\text{C}$  glucose was added with the treatments and the cells extracted at 4 different time points, 3, 6, 12 and 24 hours. While in the pulse-chase analysis experiment, cells were extracted after replacing the media with  $^{13}\text{C}$  glucose containing media at the different time points, 1, 4, 12, 24 hours. As detailed in section 2.2.4, Chapter II.

### 3.2.4 ROS measurement

ROS measurement was carried out as described in section 2.2.5, Chapter II.

### 3.3 Results

#### 3.3.1 Metabolomic profile of the effect of SKi on LNCaP-AI

Hydrophilic interaction liquid chromatography (ZIC-pHILIC) with gradient elution in combination with high-resolution mass spectrometry was used to determine changes in metabolite levels in SKi-treated *versus* control LNCaP-AI prostate cancer cells. Metabolites were identified by their accurate masses and retention times, by comparison with standards (all had less than 2 ppm mass deviation). Treatment of the cells with SKi caused alterations in the metabolic profile of LNCaP-AI prostate cancer cells and these included changes in glycolytic metabolites, pentose phosphate metabolites, nucleotides, amino acids, fatty acids and lipids.

**Figure 3.3-1** and **Figure 3.3-2** show the changes induced by SKi in the ratios of glycolytic, TCA, pentose phosphate metabolites and related molecules associated with oxidative stress. Some of these findings confirm those reported by Watson et al. (2013), but also provide a more extensive analysis that adds information on the mechanism of action of this SK inhibitor. The levels of the metabolites (e.g. gluconic acid) in response to SKi were increased with the exception of ribose, NADPH and TCA metabolites, which were decreased. NADPH levels are lowered as this molecule is required to recycle GSSG back to GSH and indeed oxidized GSSG accumulates in cells treated with SKi. Phosphogluconate and ribulose-5-phosphate are metabolites of the pentose phosphate pathway and their levels are elevated. Ribulose-5-phosphate is an important precursor for nucleotide biosynthesis. The accumulation in the levels of PPP metabolites and the decline in the levels of these nucleotides in the SKi-treated cells support the possibility that glycolysis is inhibited.

Metabolites summarised in **Figure 3.3-3** represent changes in nucleotide metabolism, the levels of which were decreased with the exception of GMP, which in contrast, was increased. These metabolites are produced during purine and pyrimidine synthesis, and which are intermediates for RNA and DNA synthesis. These findings indicate that SKi may downregulate the metabolites in these pathways, thereby interfering with DNA and RNA synthesis that might ultimately, impact on cell survival. However, this possibility requires further investigation.

Fumarate, citrate and malate levels were decreased indicating that the TCA cycle is also modulated by SKi. In general, SKi elevates the levels of most of the metabolites in the glycolytic and pentose phosphate pathways. In contrast, the levels of NADPH, sorbitol and three metabolites in TCA cycle, citrate, fumarate and malate, were decreased **Figure 3.3-4**. These findings suggest that SKi might prevent utilization of pyruvate by the TCA cycle.

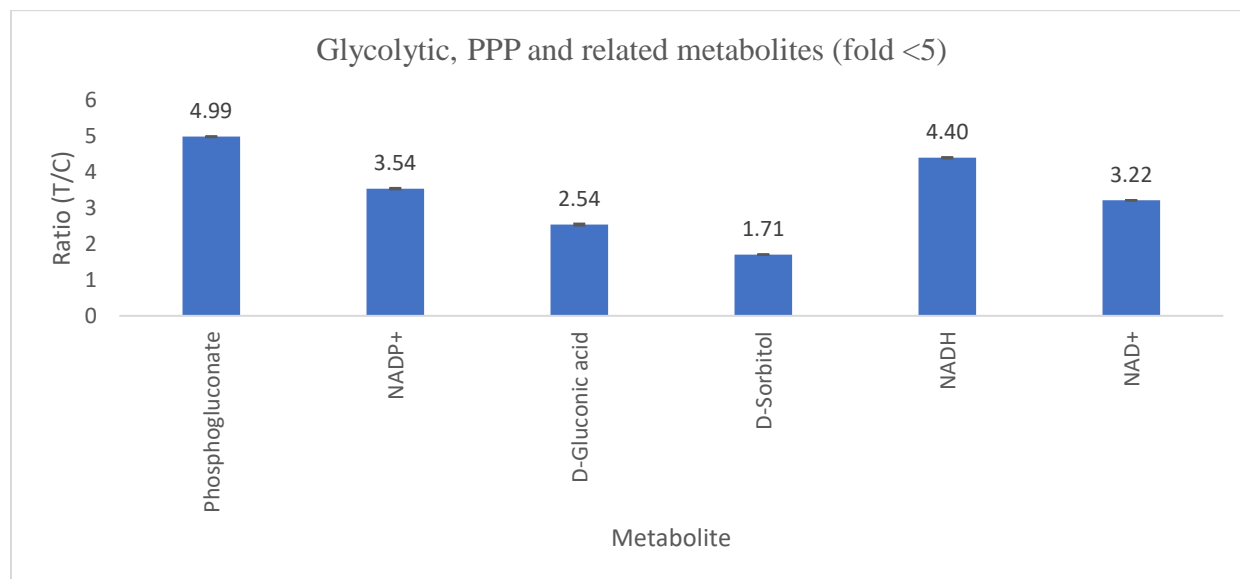


Figure 3.3-1 The bar graph is a comparison of the changes in some metabolites in the pentose phosphate pathway (linked with oxidative stress) in response to the treatment of LNCaP-AI cells with SKi, where T/C = the ratio of the average amount of a given metabolites in samples from treated cells compared with the average amount of a given metabolites in samples from control cells (n=3), numbers above bars represent ratios.

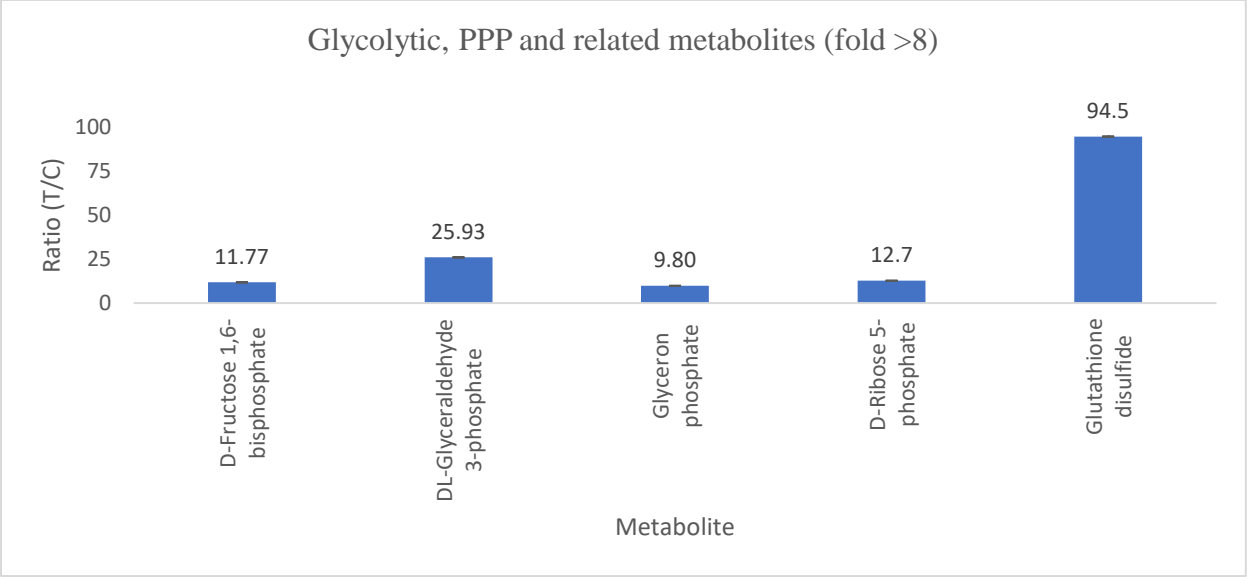


Figure 3.3-2 The bar graph is a comparison of the changes in some metabolites in the pentose phosphate pathway (linked with oxidative stress) in response to the treatment of LNCaP-AI cells with SKi, where T/C = the ratio of the average amount of a given metabolites in samples from treated cells compared with the average amount of a given metabolite in samples from control cells (n=3), numbers represent the ratio for each metabolite.

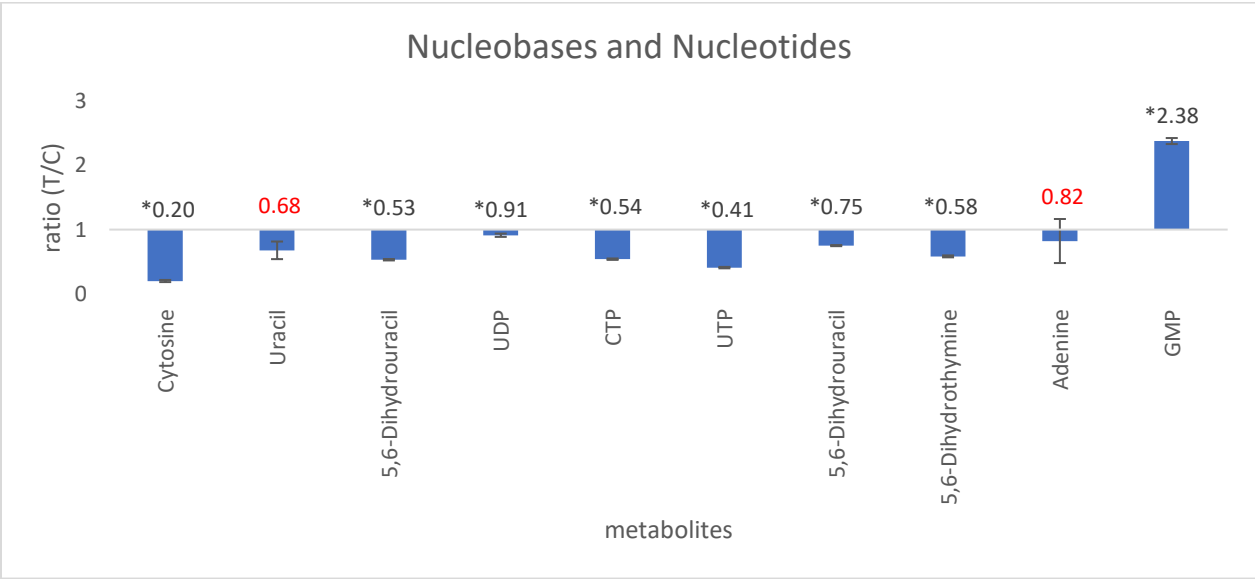


Figure 3.3-3 Bar graph is a comparison of changes in some metabolites in the Nucleotide pathways in response to treatment of LNCAP-AI cells with SKi, where T/C = the ratio of the average amount of a given metabolites in samples from treated cells compared with the average amount of a given metabolites in samples from control cells (n=3), numbers above bars represent the ratio for each metabolite. \* significant.



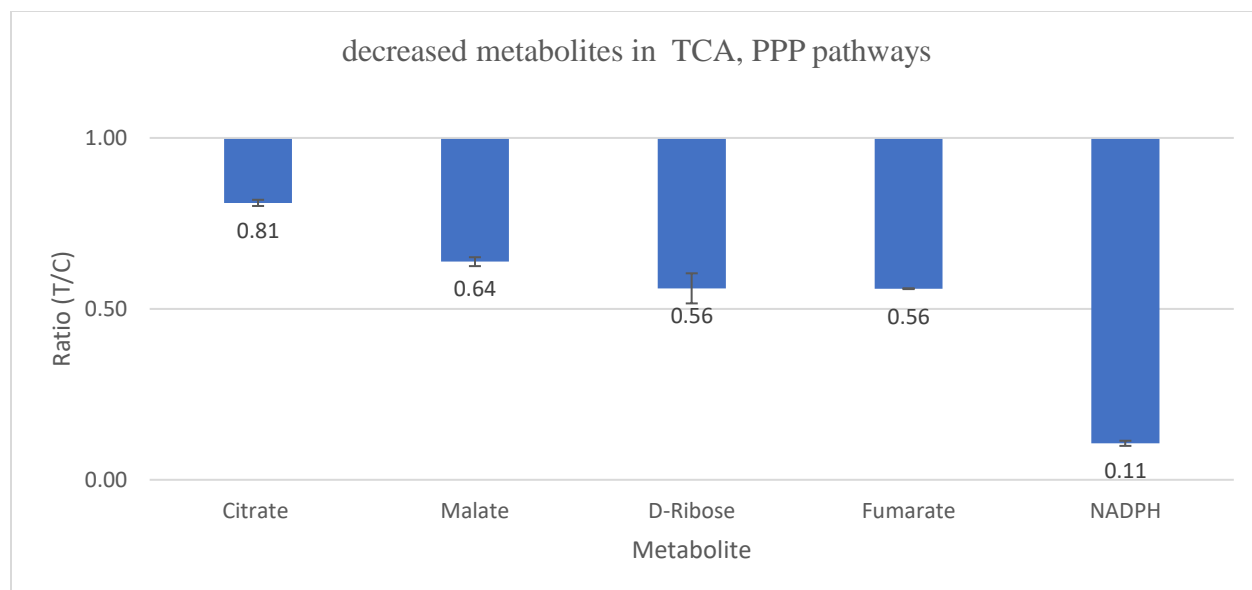


Figure 3.3-4 Bar graph is a comparison of the changes in ribose, NADPH and TCA metabolites, citrate, malate, fumarate in response to the treatment of LNCaP-AI with SKi, where T/C = the ratio of the average amount of a given metabolites in samples from treated cells compared with the average amount of a given metabolites in samples from control cells (n=3), numbers represent the ratio for each metabolite.

There was a significant effect of SKi on cellular amino acids metabolism. **Figure 3.3-5** and **Figure 3.3-6** show that SKi induced a decrease in the levels of serine, glutamate-5-semialdehyde, alanine, creatine, N<sub>6</sub>-trimethyl-lysine, 2-aminomuconate, hypotaurine, cystathionine and aspartate. However, the levels of other metabolites were significantly increased including L-proline, valine, glycerol, cysteinylglycine disulfide, N-acetyl-glutamate, N-formimino-L-glutamate, hydroxyphenyl lactate,  $\gamma$ -glutamyl-cysteine and S-glutathionyl-L-cysteine. The increase in  $\gamma$ -glutamyl-cysteine and S-glutathionyl-L-cysteine were substantial and were 14.7- and 7.3-fold respectively. These metabolites are intermediates in glutathione biosynthesis and the formation of glutathione cysteine, which are oxidative stress metabolites. The elevation of these metabolites suggests that SKi induces a profound oxidative stress response in LNCaP-AI cells.

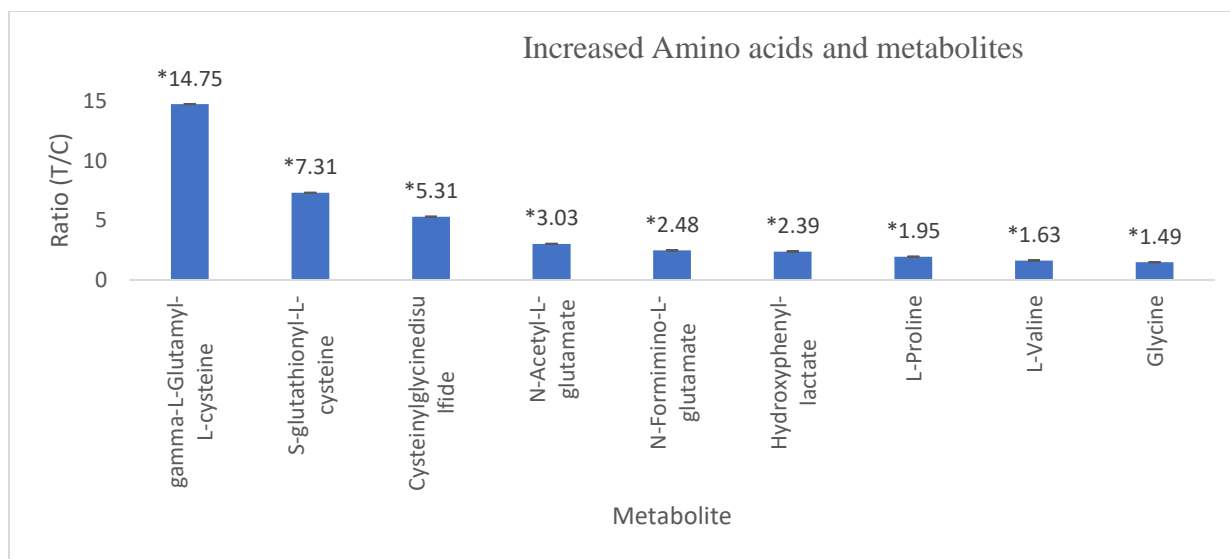


Figure 3.3-5 Bar graph is a comparison of changes occurring in some metabolites in the amino acid pathways in response to treatment of LNCAP-AI cells with SKi, where T/C = the ratio of the average amount of a given metabolites in samples from treated cells compared with the average amount of a given metabolites in samples from control cells (n=3), numbers above bars represent ratios of each metabolite.

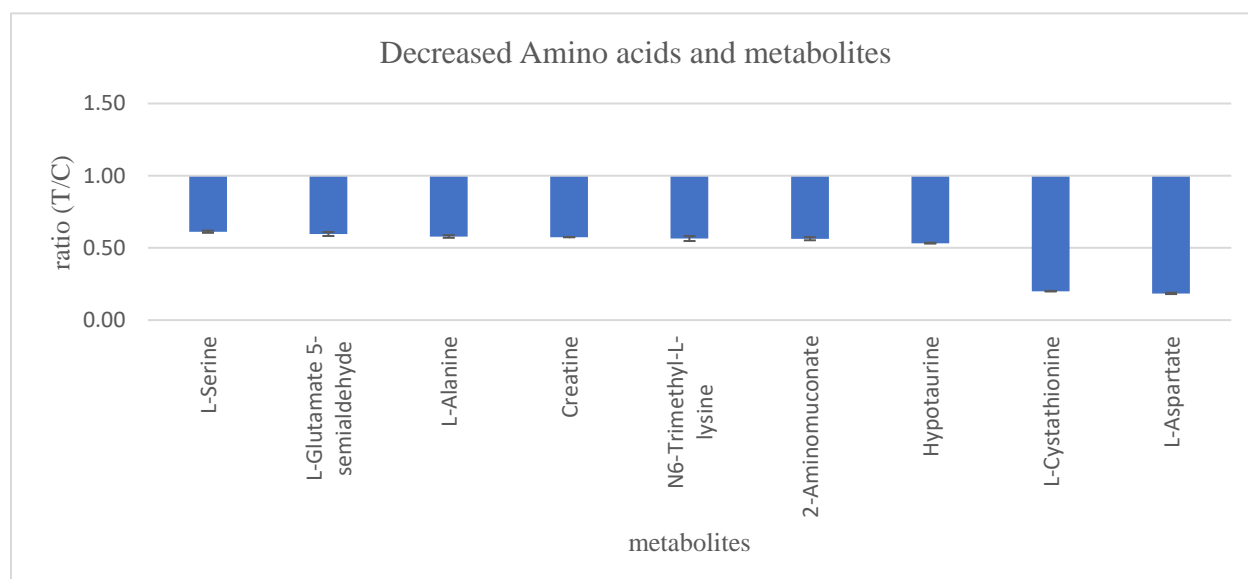


Figure 3.3-6 Bar graph is a comparison of changes occurring in some metabolites in the amino acid pathways in response to treatment of LNCAP-AI cells with SKi, where T/C = the ratio of the average amount of a given metabolites in samples from treated cells compared with the average amount of a given metabolites in samples from control cells (n=3), numbers above bars represent the ratio of each metabolite.

Phosphate donors, phosphocreatine and/or phosphocreatinine are important molecules in regulating the conversion of AMP into ADP and ADP into ATP to maintain the energy [122].

**Figure 3.3-7** shows that SKi induced a decrease in the levels of creatinine/creatinine and creatinine/creatinine phosphate suggesting that these molecules might be consumed in order to maintain the cellular ATP levels in the face of compromised glycolysis. Carnitine and its derivatives are also responsible for transport fatty acid into and out of the mitochondria [123]. Other changes induced by SKi include a minor alteration in carnitines, such as L-carnitine and butanoylcarnitine as shown in **Figure 3.3-8**. The treatment of LNCaP-AI prostate cancer cells with SKi also modestly reduced some carnitines while having no effect or small effect on L-carnitine and acetylcarnitine **Figure 3.3-8**.

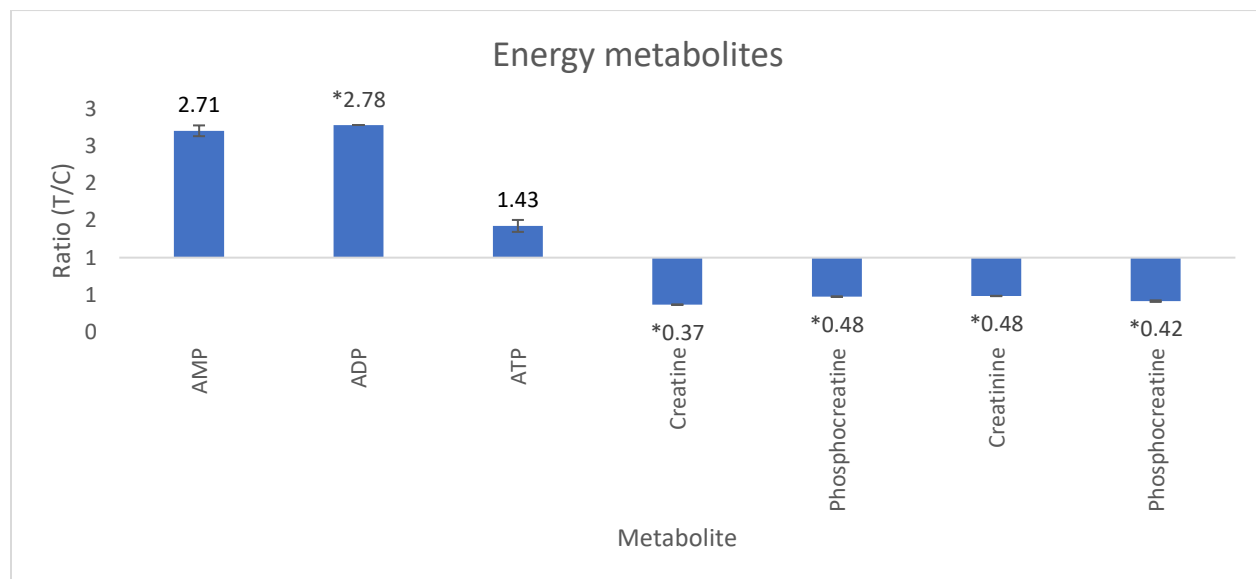


Figure 3.3-7 Bar graph is a comparison of changes occurring in some energy metabolites in response to treat LNCaP-AI cells with SKi, where T/C = the ratio of the average amount of a given metabolites in samples from treated cells compared with the average amount of a given metabolites in samples from control cells (n=3), numbers above bars represent the ratio of each metabolite. \*significant.

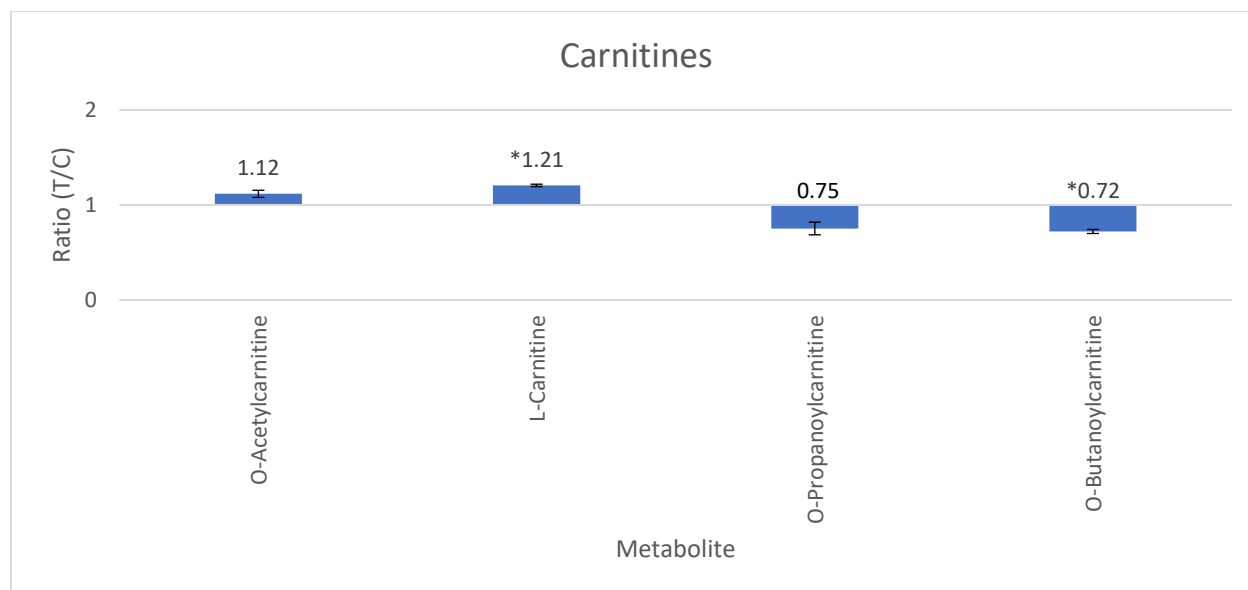


Figure 3.3-8 Bar graph is a comparison of changes occurring in some metabolites in the fatty acid (carnitines) in response to treat LNCAP-AI cells with SKi, where T/C = the ratio of the average amount of a given metabolites in samples from treated cells compared with the average amount of a given metabolites in samples from control cells (n=3), numbers above bars represent the ratio of each metabolite.

**Figure 3.3-9** shows that SKi induces increased formation of choline (1.42-fold and p-value= 0.007), choline phosphate (1.73-fold and p-value= 0.015), *sn*-glycerol 3-phosphate (*sn*-G3P) (9.25-fold and p-value= 0.017), PC (16:2) (3.32-fold and p-value= 0.015) and PC (28:0) (2.21 fold and p-value= 0.011). These findings indicate that there might be an increased turnover of membrane phospholipids, particularly since choline and choline phosphate levels are elevated. *sn*-G3P is important as it is derived from glycolysis to form the backbone of glycerophospholipids. This is of interest as glycerol, in the inner mitochondrial membrane, formed by glycerophosphate dehydrogenase [124] and the oxidation of *sn*-G3P in the mitochondria is considered a major source for ROS production [124]. Lipids will be studied in more depth in chapters four and five. The chromatograms shown in **Figure 3.3-10** indicate higher levels of *sn*-G3 in SKi treated cells compared with control cells, and mass spectroscopy traces determined an accurate mass of 171.0067. All metabolites mentioned in **Figure 3.3-1** to **Figure 3.3-9**, which is from one run with

3 replicates of each condition were also almost consistent in the pattern of change with the presented results. The results are listed in **appendix 1** as a table.

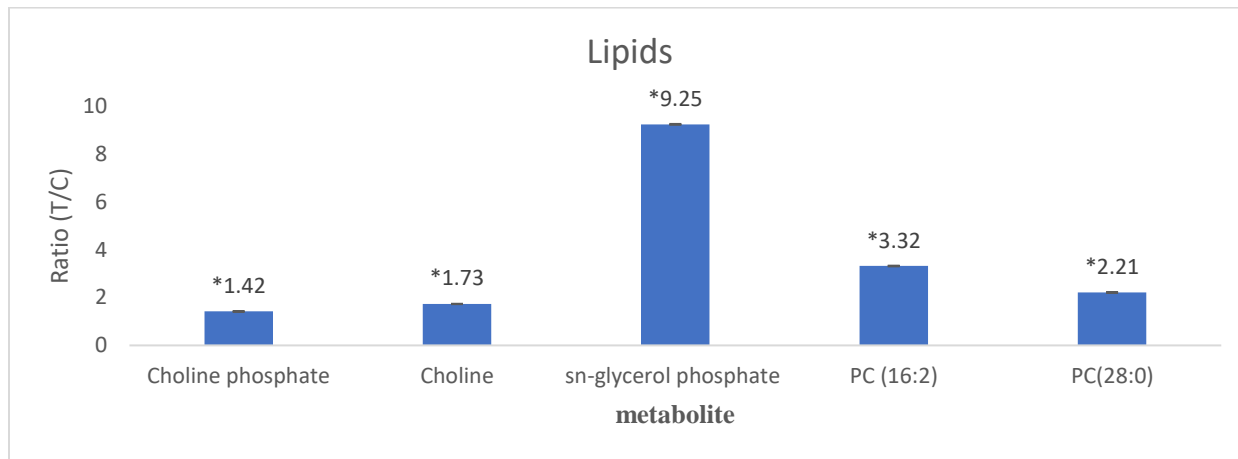


Figure 3.3-9 Bar graph is a comparison of changes in some metabolites in lipid metabolism in response to treat LNCAP-AI cells with SKi, where T/C = the ratio of the average amount of a given metabolites in samples from treated cells compared with the average amount of a given metabolites in samples from control cells (n=3), numbers above bars represent ratio of each metabolite. \* p-value < 0.05

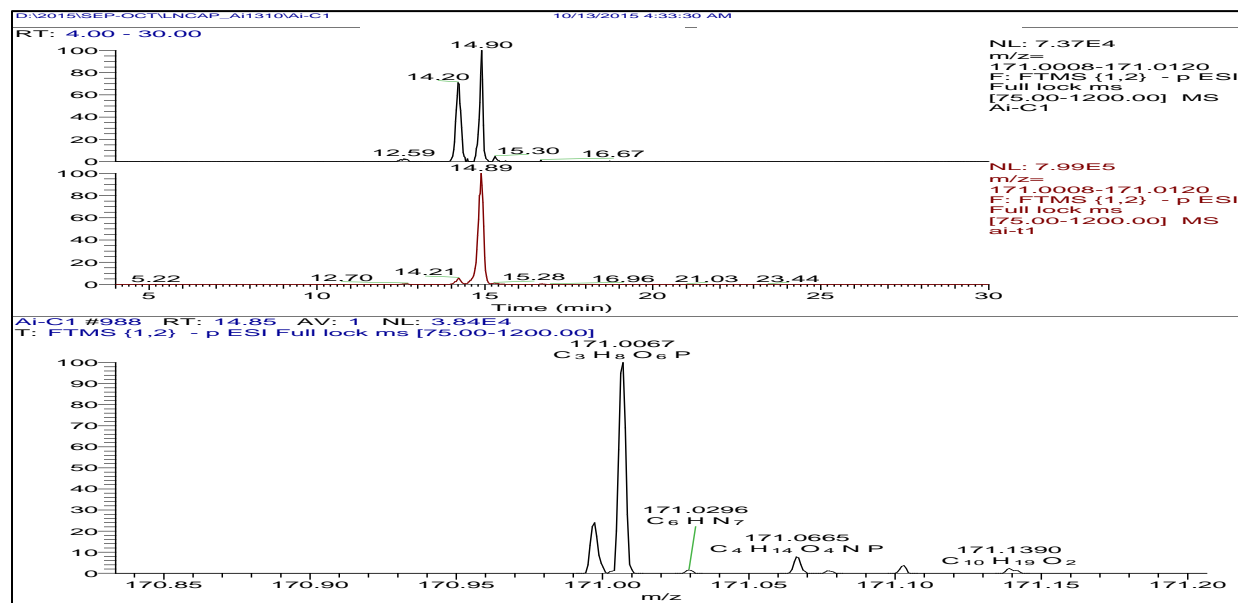


Figure 3.3-10 *sn*-glycerol 3-phosphate chromatograms in untreated and treated samples with the mass spectra.

### 3.3.2 Effect of SKi on LNCaP-AI cells using $^{13}\text{C}_6$ -glucose (pulse-chase analysis)

Over the last decades, flux analysis has been considered to be an important technique to understand the dynamic changes in metabolism in living cells [125]. This methodology enables the fate of particular metabolites to be tracked. This is achieved by following the conversion of an isotope tracer such as  $^{13}\text{C}$  or  $^{14}\text{C}$  in glucose or  $^{13}\text{C}$ -glycine or  $^{13}\text{C}$ -glutamine into isotopically labelled metabolites. In this experiment,  $^{13}\text{C}_6$ -glucose was used to detect changes in glycolytic and pentose phosphate metabolites [125]. This was achieved using the same method as described in section 2.2.3; with a small alteration, which was adding  $^{13}\text{C}_6$ -glucose into the media to obtain a new media with 50:50 glucose/ $^{13}\text{C}_6$ -glucose. Isotopically labelled metabolites of glycolysis and other pathways were identified by their accurate masses and retention times, which all had less than 3 ppm mass deviation from their calculated mass.

Using isotopic labeling procedures, the dynamic nature of glycolysis and conversion of metabolites via anabolic pathways, such as amino acid and glycerol phospholipid synthesis can be analysed. The use of snapshot analysis of metabolites as described previously might allow inference as to whether a pathway is inhibited or activated e.g. diversion of glucose from the glycolytic pathway to the pentose phosphate pathway, but it is not definitive. For this, it is necessary to determine flux. Therefore, a pulse-chase experiment was employed to further probe the metabolomics changes occurring by using medium containing  $^{13}\text{C}_6$ -glucose. This experiment focused on the changes of several endogenous isotopic metabolites, which were identified in the previous experiment. The flux analysis was performed at several time points (25, 28, 36 and 48 hours) in LNCaP-AI cells treated with and without SKi. Generally, this type of experiment consists two stages. First, metabolites were determined in LNCaP-AI cells treated with and without SKi (10  $\mu\text{M}$ ) for 24 hours in RPMI with normal glucose and  $^{13}\text{C}_6$ -glucose. In the second stage (pulse-

chase), the  $^{13}\text{C}_6$ -glucose containing media was replaced with media that did not contain  $^{13}\text{C}_6$ -glucose and washed with a RPMI free media in order to remove any traces of the  $^{13}\text{C}_6$ -glucose. The cells were then incubated for various additional times (1-24 hours) and changes in the levels of the glycolysis metabolites measured. Combined results of these studies provide more metabolic information from monitoring the metabolism of  $^{13}\text{C}_6$ -glucose through the glycolytic and connected pathways.

Several metabolic pathways were considered. These were: (i) metabolites linked with the oxidative stress; (ii) glycolytic and pentose phosphate pathway metabolites; (iii) nucleotides and related metabolites, (iv) metabolites linked with energy metabolism; (v) lipids including, *sn*-G3P, GPE, GPC, PC 34:0 and LPA; (vi) TCA cycle metabolites. A list of the unlabelled and labelled metabolites is shown in **table 3.1** and **Figure 3.3-11** summarises the  $^{13}\text{C}$  incorporation from glucose into several pathways.

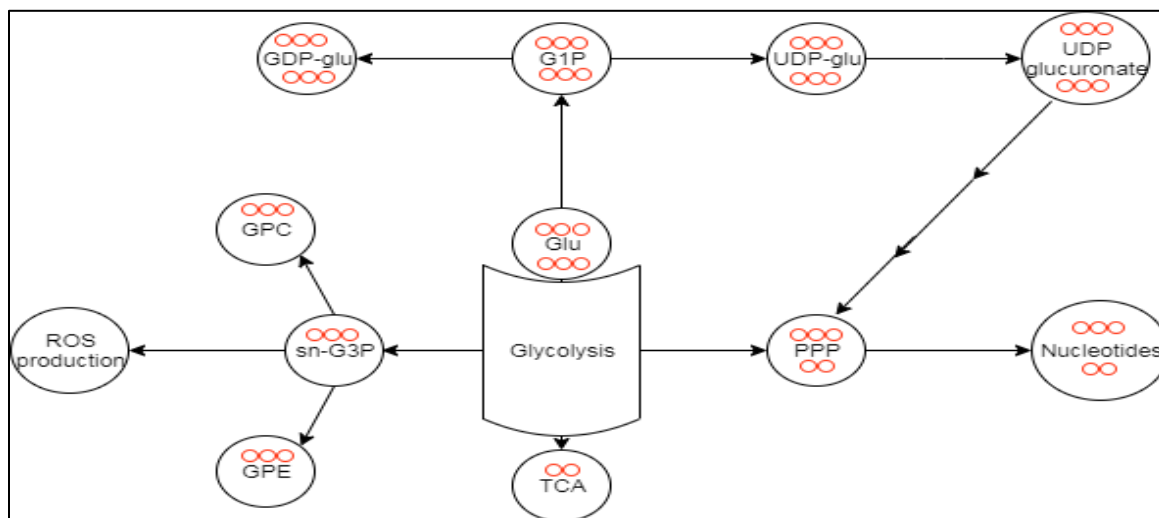


Figure 3.3-11 summary of  $^{13}\text{C}$  incorporation from  $^{13}\text{C}_6$ -glucose into pathways in LNCaP-AI cells

Table 3-1 Summary of the alteration in unlabelled and labelled metabolites in LNCaP-AI cells in the pulse-chase experiments.

m/z	RT (min)	Metabolite	24h (labelled)		1h (chase exp)		4h (chase exp)		12h (chase exp)		24h (chase exp)	
			Ratio	P-value	Ratio	P-value	Ratio	P-value	Ratio	P-value	Ratio	P-value
Glycolysis and PPP												
338.9876	17.82	Fructose 1,6-bisphosphate	5.68	0.0318	1.97	0.2018	2.41	0.0592	0.6	0.2044	0.42	0.0066
<b>341.9977</b>		<b><sup>13</sup>C<sub>3</sub>- F-2,6-P<sub>2</sub></b>	<b>20.71</b>	<b>0.0618</b>	<b>Not detected</b>							
<b>345.0079</b>		<b><sup>13</sup>C<sub>6</sub>- F-2,6-P<sub>2</sub></b>	<b>6.72</b>	<b>0.0181</b>	<b>Not detected</b>							
168.9908	15.80	GAP	20.27	0.0028	3.87	0.0915	2.34	0.0491	1.25	0.5879	1.39	0.3066
		<b><sup>13</sup>C<sub>3</sub>- GAP</b>	<b>11.15</b>	<b>0.0173</b>	<b>Not detected</b>							
184.9850	16.69	Phosphoglycerate	1.80	0.0403	1.22	0.6269	2.77	0.4214	1.30	0.6485	0.86	0.2240
<b>187.9952</b>	<b>16.69</b>	<b><sup>13</sup>C<sub>5</sub>- phosphoglycerate</b>	<b>2.13</b>	<b>0.0421</b>	<b>Not detected</b>							
275.0179	17.53	Phosphogluconate	3.03	0.0120	3.04	0.1590	5.14	0.0069	2.89	0.1315	1.57	0.0097
<b>281.0367</b>		<b><sup>13</sup>C<sub>6</sub>-Phosphogluconate</b>	<b>3.05</b>	<b>0.0266</b>	<b>Not detected</b>							
229.0121	16.33	Ribulose-5-phosphate	6.24	0.0546	1.99	0.2671	3.43	0	1.8	0.2249	1.14	0.3607
<b>234.0281</b>		<b><sup>13</sup>C<sub>5</sub>-ribulose phosphate</b>	<b>3.95</b>	<b>0.0711</b>	<b>Detected in treated cells only</b>						<b>Not detected</b>	



m/z	RT (min)	Metabolite	24h (labelled)		1h (chase exp)		4h (chase exp)		12h (chase exp)		24h (chase exp)	
			Ratio	P-value	Ratio	P-value	Ratio	P-value	Ratio	P-value	Ratio	P-value
<b>TCA</b>												
808.1161	11.99	Acetyl-CoA	1.01	0.8827	0.72	0.4137	0.93	0.6333	0.66	0.1600	0.57	0.1733
<b>110.1226</b>		<b><sup>13</sup>C<sub>2</sub>- acetyl-CoA</b>	<b>0.80</b>	<b>0.1685</b>	0.33	0.0736	0.51	0.0264	0.49	0.0374	0.40	0.1086
204.1282	11.03	Acetyl carnitine	0.85	0.0280	0.55	0.0352	0.71	0.0845	0.32	0.0268	0.52	0.1342
<b>206.1347</b>		<b><sup>13</sup>C<sub>2</sub>. acetyl carnitine</b>	<b>0.96</b>	<b>0.5112</b>	1.14	0.7348	1.33	0.1638	0.64	0.1553	0.52	0.1364
191.0191	17.78	Citrate	0.56	0.0032	0.47	0.0456	0.96	0.7920	0.74	0.3769	0.87	0.7704
<b>193.0256</b>		<b><sup>13</sup>C<sub>2</sub>- citrate</b>	<b>0.38</b>	<b>0.0034</b>	0.53	0.3523	0.91	0.6366	0.76	0.4502	0.85	0.7360
145.0137	15.35	Oxoglutarate	0.98	0.7772	0.43	0.0049	0.83	0.5818	0.32	0.0550	0.53	0.2318
		<b><sup>13</sup>C<sub>2</sub>- Oxoglutarate</b>	<b>0.42</b>	<b>0.0038</b>	<b>N/D</b>		<b>N/D</b>		<b>N/D</b>		<b>N/D</b>	
<b>Lipids</b>												
171.0056	12.62	<i>Sn</i> -Glycerol-3-	2.92	0.0099	0.81	0.3807	1.54	0.0516	1.74	0.0416	1.69	0.0018
174.0157	12.62	<b><sup>13</sup>C<sub>3</sub><i>sn</i>-Glycerol phosphate</b>	4.37	0.0028	1.02	0.9470	2.03	0.0404	1.96	0.1114	2.05	0.0012

m/z	RT (min)	Metabolite	24h (labelled)		1h (chase exp)		4h (chase exp)		12h (chase exp)		24h (chase exp)	
			Ratio	P-value	Ratio	P-value	Ratio	P-value	Ratio	P-value	Ratio	P-value
214.0478	15.51	GPE	0.86	0.0025	0.67	0.4058	0.99	0.9247	1.05	0.8642	1.18	0.7184
217.0577	15.50	<b><sup>13</sup>C<sub>3</sub> GPE</b>	0.63	0.0004	0.64	0.3827	1.00	0.9987	1.09	0.7705	1.30	0.5870
256.0948	14.37	GPC	1.18	0.0308	0.87	0.7573	1.18	0.2564	1.32	0.4179	1.42	0.4869
259.1048	14.36	<b><sup>13</sup>C<sub>3</sub> GPC</b>	1.39	0.0094	1.34	0.5078	1.91	0.0507	1.79	0.1897	2.13	0.0671
820.5679	4.13	PC 34:0	4.66	0.0262	<b>N/D</b>		<b>N/D</b>		<b>N/D</b>		<b>N/D</b>	
<b>822.5745</b>	<b>4.13</b>	<b><sup>13</sup>C<sub>2</sub> PC 34:0</b>	3.92	0.0324	<b>N/D</b>		<b>N/D</b>		<b>N/D</b>		<b>N/D</b>	
409.2352	4.60	LPA 16:0	1.65	0.0026	4.08	0.0995	1.22	0.4540	1.14	0.7673	1.36	0.6094
410.2385	4.60	<b><sup>13</sup>C LPA 16:0</b>	1.61	0.0068	0.92	0.1171	1.28	0.1976	1.21	0.5479	1.61	0.0671
<b>Energy metabolism</b>												
505.9870	16.18	ATP	1.10	0.2386	0.62	0.1010	1.13	0.3624	1.40	0.2384	0.70	0.0184
511.0036	16.18	<b><sup>13</sup>C<sub>5</sub>-ATP</b>	<b>0.60</b>	<b>0.0009</b>	<b>0.14</b>	<b>0.0027</b>	<b>0.59</b>	<b>0.0230</b>	<b>1.23</b>	<b>0.6205</b>	<b>0.60</b>	<b>0.0268</b>
662.1002	14.00	NAD	1.36	0.0269	0.73	0.2161	1.36	0.1462	1.63	0.0378	1.04	0.6934
667.1169	14.01	<b><sup>13</sup>C<sub>5</sub>NAD</b>	<b>1.21</b>	<b>0.0253</b>	<b>0.60</b>	<b>0.0035</b>	<b>0.94</b>	<b>0.6663</b>	<b>1.46</b>	<b>0.1679</b>	<b>0.92</b>	<b>0.3724</b>

m/z	RT (min)	Metabolite	24h (labelled)		1h (chase exp)		4h (chase exp)		12h (chase exp)		24h (chase exp)	
			Ratio	P-value	Ratio	P-value	Ratio	P-value	Ratio	P-value	Ratio	P-value
664.1160	13.15	NADH	5.91	0.0062	1.98	0.0189	3.17	0.0176	1.46	0.4134	2.07	0.0059
669.1326	13.15	<b><sup>13</sup>C<sub>5</sub> NADH</b>	4.89	0.0063	1.41	0.0111	2.11	0.0479	1.26	0.5568	1.46	0.0085
Nucleotides, nucleotide-sugar and related metabolites												
259.0214	15.72	α-D-Glucose-1-phosphate	0.98	0.7782	0.63	0.3825	2.21	0.0125	1.82	0.2288	0.89	0.7865
265.0415	15.72	<b><sup>13</sup>C<sub>6</sub> glucose-1 phosphate</b>	0.96	0.8020	<b>0.22</b>	<b>0.0007</b>	<b>0.28</b>	<b>0.0013</b>	<b>0.29</b>	<b>0.0303</b>	<b>0.27</b>	<b>0.0187</b>
259.0216	16.58	α-D-Glucose-6-phosphate	0.58	0.0840	0.87	0.6940	2.21	0.0125	2.18	0.1040	0.99	0.8280
265.0417	16.59	<b><sup>13</sup>C<sub>6</sub> glucose-6 phosphate</b>	0.73	0.0612	<b>N/D</b>		<b>N/D</b>		<b>N/D</b>		<b>N/D</b>	
604.0694	17.92	<b>GDP-glucose</b>	2.74	0.0023	1.39	0.0619	2.07	0.0492	2.06	0.0777	1.42	0.0898
610.0890	17.92	<b><sup>13</sup>C<sub>6</sub> GDP-glucose</b>	2.16	0.0040	1.47	0.1043	4.83	0.0164	9.17	0.0369	<b>N/D</b>	
565.0460	16.09	UDP-glucose	1.28	0.0137	0.70	0.1837	1.16	0.3362	0.74	0.2345	0.62	0.0022
571.0661	16.09	<b><sup>13</sup>C<sub>6</sub> UDP glucose</b>	1.12	0.0300	<b>Below LOD</b>		<b>Below LOD</b>		<b>Below LOD</b>		<b>Below LOD</b>	

m/z	RT (min)	Metabolite	24h (labelled)		1h (chase exp)		4h (chase exp)		12h (chase exp)		24h (chase exp)	
			Ratio	P-value	Ratio	P-value	Ratio	P-value	Ratio	P-value	Ratio	P-value
579.0256	18.67	UDP-D-galacturonate	1.58	0.0525	0.65	0.1410	1.53	0.0812	1.47	0.1932	0.64	0.0030
585.0457	18.67	<b><sup>13</sup>C<sub>6</sub> UDP galacturonate</b>	0.97	0.4487	0.49	0.0353	1.29	0.1927	1.78	0.0193	1.08	0.5792
606.0730	14.90	UDP-N-acetyl-glucosamine (E6)	1.37	0.0002	1.45	0.3458	1.91	0.0201	1.45	0.2895	1.37	0.5045
611.0890	14.90	<b><sup>13</sup>C<sub>5</sub> UDP N-acetyl-glucosamine</b>	0.48	0.0001	0.99	0.9717	1.40	0.1152	1.39	0.3131	1.45	0.4603
426.0212	14.87	ADP	3.33	0.0147	0.64	0.2094	1.26	0.4088	1.62	0.0516	0.98	0.8952
431.0379	14.87	<b><sup>13</sup>C<sub>5</sub> ADP</b>	1.78	0.0382	0.35	0.0063	0.71	0.0332	1.01	0.9817	2.31	0.0049
442.0159	18.91	GDP	0.83	0.3747	0.51	0.0325	1.01	0.8934	0.71	0.3101	0.52	0.0271
447.0334	18.91	<b><sup>13</sup>C<sub>5</sub> GDP</b>	0.67	0.0219	<b>N/D</b>		<b>N/D</b>		<b>N/D</b>		<b>N/D</b>	
521.9822	18.92	GTP	1.20	0.2749	0.55	0.0692	1.01	0.9363	0.71	0.2746	0.57	0.0126
528.0025	18.91	<b><sup>13</sup>C<sub>5</sub> GTP</b>	0.45	0.0057	0.18	0.0001	0.56	0.1174	0.95	0.9003	ND/t	0.0028

### 3.3.2.1 Oxidative stress metabolites:

**Figure 3.3-12** shows the effect of treating LNCaP-AI cells with SKi (0-24 hours) on a metabolite linked with oxidative stress. It can be seen that the GSSG level was increased over time until this reached a maximum at 4 hours (22.4-fold) in the chase experiment. The drop in the ratio between the experiments, could be explained by the media exchange. It is also notable that NADPH levels were decreased or depleted significantly during the incubation. In addition, peak areas of NADPH were hardly detectable (in some cases, lower than the detection limit,  $10^3$ , as shown in **Figure 3.3-13** or absent in some treated cells, which could explain the accumulation in GSSG.

In the pulse-chase experiments,  $\text{NADP}^+$  was barely detectable and NADPH is depleted. This was coincident with the accumulation of oxidised glutathione, suggesting that the low levels of  $\text{NADP}^+$  might be due to rapid turnover.

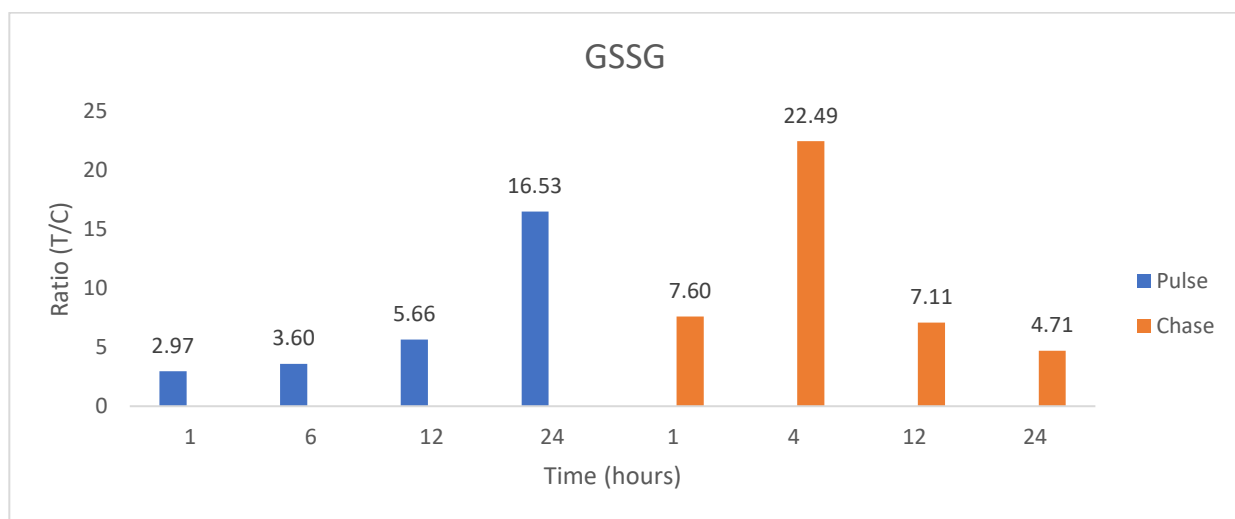


Figure 3.3-12 Bar graph is a comparison of the changes in GSSG in the pulse-chase experiments, where T/C = the ratio of the average amount of a given metabolites in samples from treated cells compared with the amount of a given metabolites in samples from control cells (n=3), numbers above bars represent ratio of each metabolite.

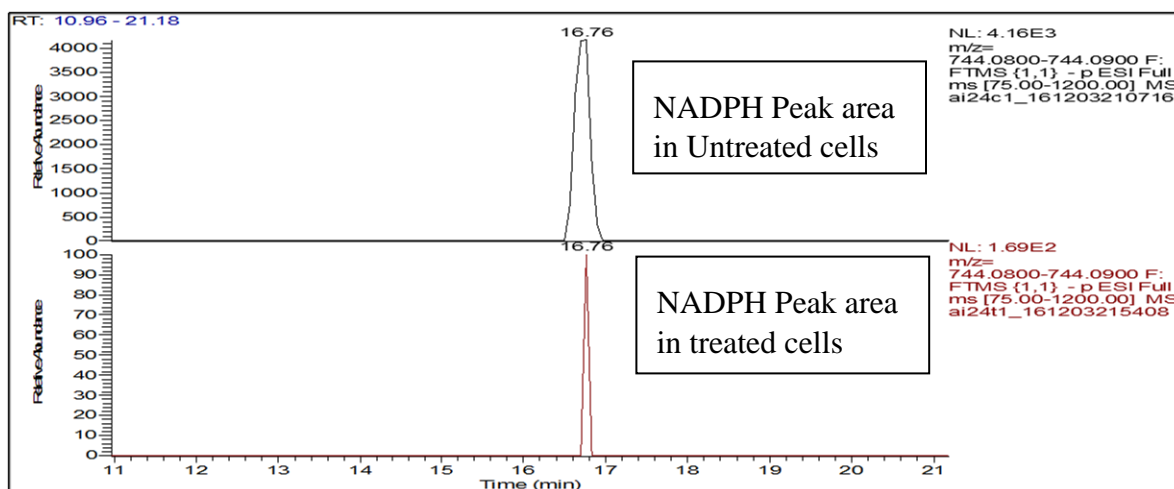


Figure 3.3-13 Chromatograms of NADPH of untreated and treated LNCaP-AI cells with SKi (24 hours).

### 3.3.2.2 The glycolysis and pentose phosphate pathways

**Figure 3.3-14 A and B** show the changing ratios in some metabolites in the glycolytic and pentose phosphate pathways; both labelled and unlabelled. D-glyceraldehyde-3-phosphate is converted reversibly to its isomer, dihydroxyacetone phosphate (DHAP), catalysed by triose phosphate isomerase. This is a precursor for the synthesis of glycerol lipids. (Hans-Walter Heldt, 2011, Plant biochemistry). *Sn*-glycerol 3-phosphate is a product of the reduction of DHAP and which converts back into DHAP between the outer layer and inner mitochondrial membrane *via* glycerophosphate dehydrogenase enzyme and  $\text{NAD}^+/\text{NADH}$ . Therefore, it is important to monitor this route besides TCA metabolites.

**Figure 3.3-15** and **Figure 3.3-16, A-D** monitoring the actual peak intensities of the glycolytic and the pentose phosphate pathway metabolites, F-1,6-P<sub>2</sub>, GAP, phosphoglycerate, phosphogluconate and R5P and their isotopes during the pulse experiment, while **Figure 3.3-16, E and F** show intensities of R5P in the chase experiment at several time points. Generally, intensities of R5P were low in both experiments as demonstrated in extracted chromatogram in **Figure 3.3-17**. However, it is ultimately an important metabolite as a precursor for nucleotides, amino acids, vitamins, RNA and DNA synthesis.[13] Results in **Figure 3.3-16,D** and **Figure 3.3-16, F** show the dynamic changes of <sup>13</sup>C<sub>5</sub>-R5P in SKi-treated cells in the pulse-chase experiments, indicating that labelled R5P accumulated in the SKi-treated cells only at the first time point (3 h) and remained higher at all time points. In the chase experiment **Figure 3.3-16,F**, <sup>13</sup>C<sub>5</sub>-R5P was detected in the first hour in the control cells before it disappeared in the next time points (4 h), while it was detected in the treated cells until 12 h after removing the labelled media.

It has been confirmed that the glycolysis rates and glucose consumption in tumor cells are much higher; at least 30 times more when compared with normal cells (Michael, 2011). Thus, perhaps not surprisingly, all labelled glycolytic metabolites turned over (disappeared) in the chase experiment at all-time points with the exception of R5P which might indicate that the rate of glycolysis is very high in both the treated and untreated cells. However, other labelled metabolites were detected in the chase study, consisting of acetyl-CoA, acetylcarnitine and citrate by chasing (tracking) <sup>13</sup>C<sub>6</sub>-glucose through the TCA cycle.

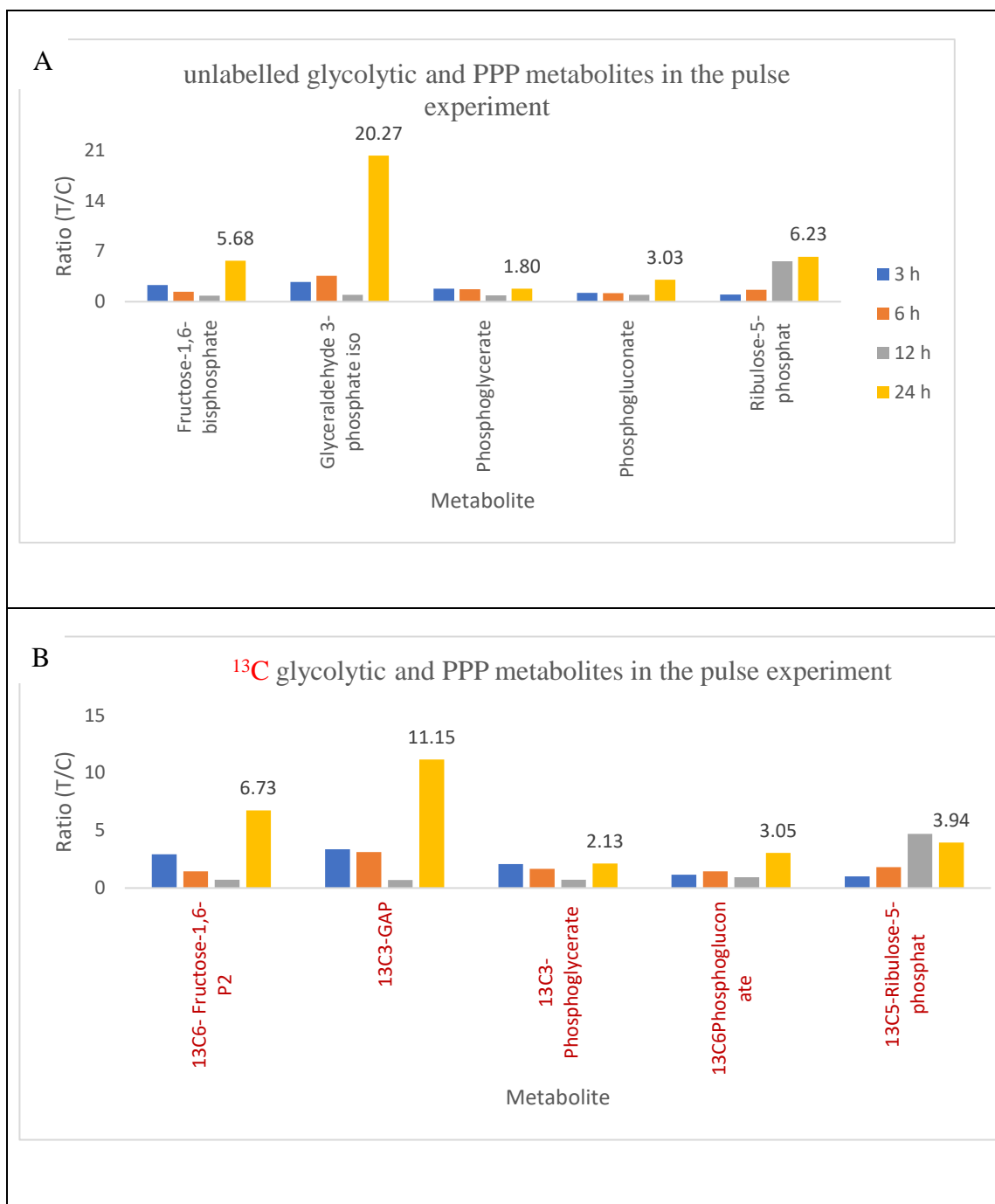


Figure 3.3-14 (A) Bar chart is a comparison of the changes occurring in certain metabolites in the glycolysis and PPP and (B) their isotopes. Where T/C = the ratio of the average amount of a given metabolites in samples from treated cells compared with the amount of a given metabolites in samples from control cells (n=3), the numbers above bars represent the ratio of each metabolite at time point 24 hours.



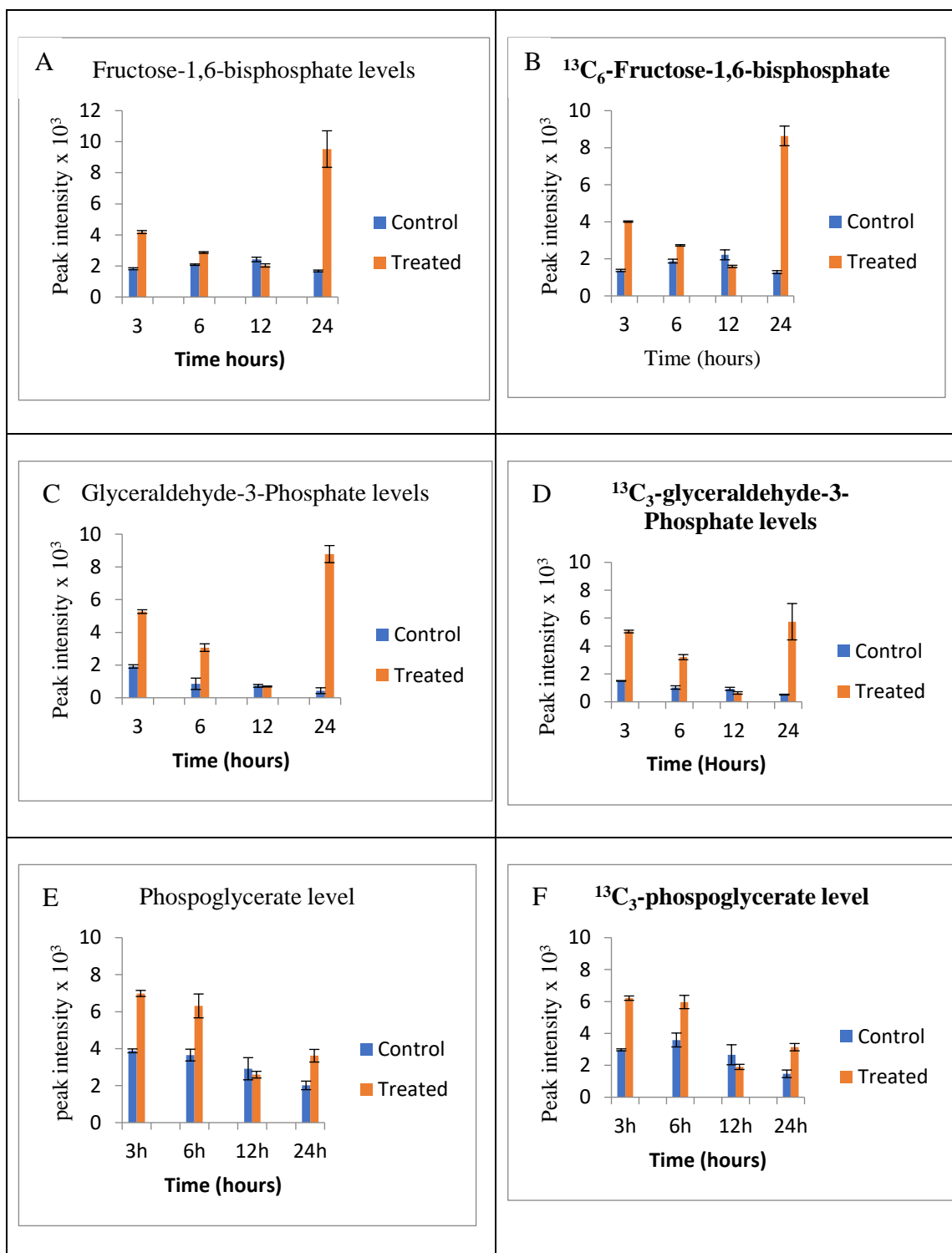


Figure 3.3-15 Bar graphs represent absolute levels of (A) F-1,6,P2, (B) <sup>13</sup>C<sub>6</sub>-F-1,6 P2, (C) GAP, (D) <sup>13</sup>C<sub>3</sub>-GAP, (E) phosphoglycerate and (F) <sup>13</sup>C<sub>3</sub>-phosphoglycerate in the pulse experiment.

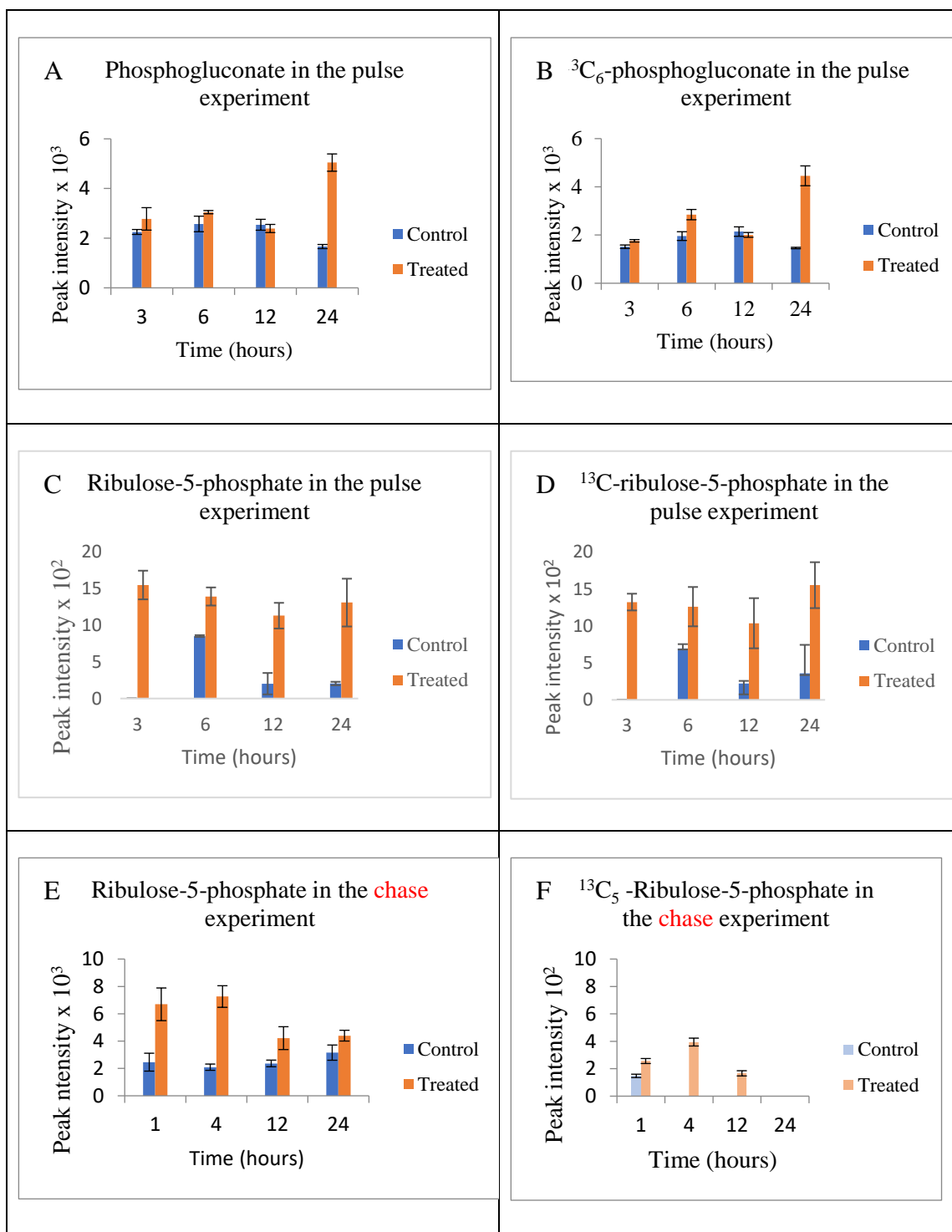


Figure 3.3-16 Bar graphs represent absolute levels of (A) phosphogluconate, (B) <sup>13</sup>C<sub>6</sub>-phosphogluconate, (C) R5P and (D) <sup>13</sup>C<sub>5</sub>-R5P in the pulse experiment. (E) R5P and (F) <sup>13</sup>C<sub>5</sub>-R5P in the chase experiment.

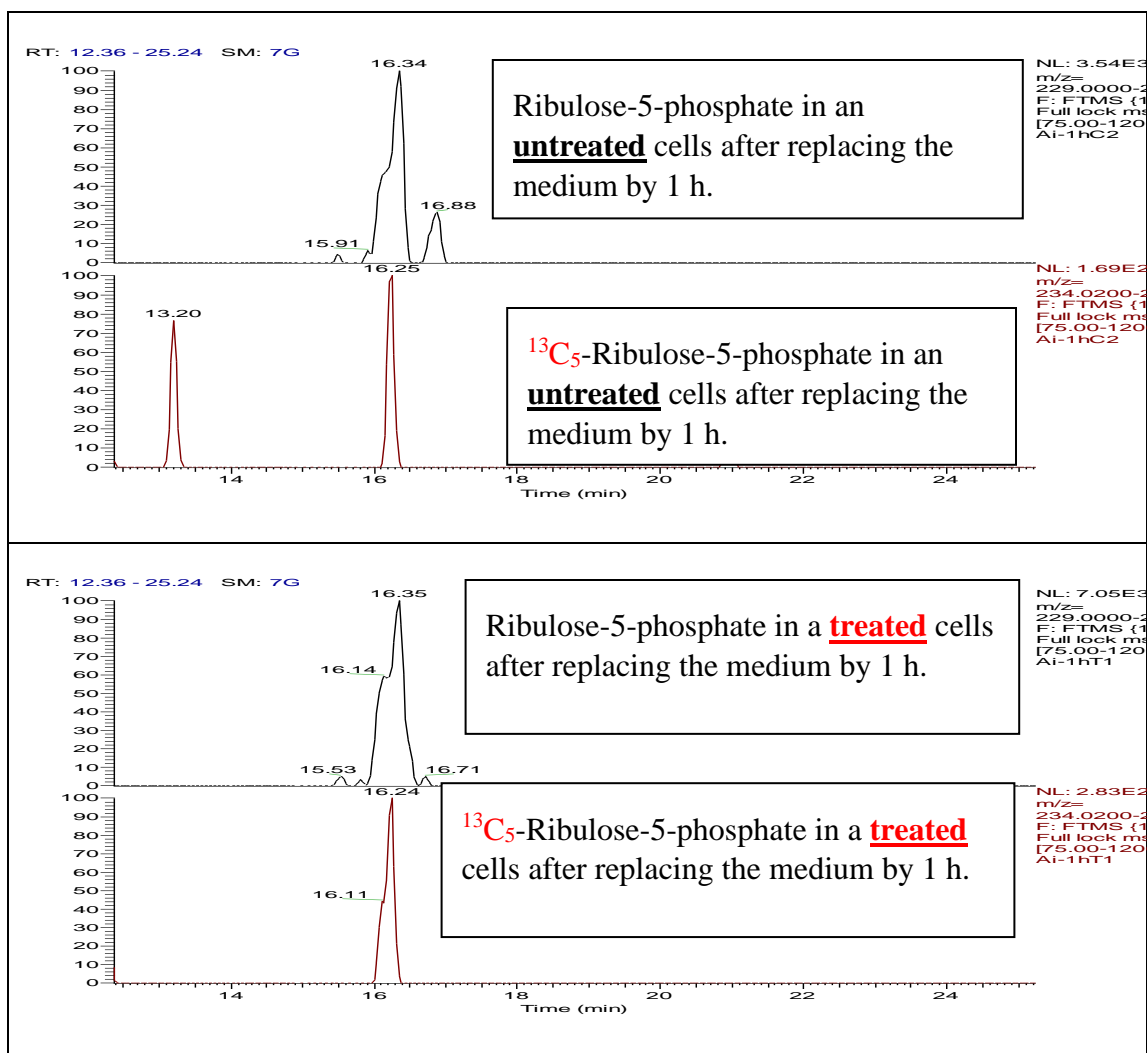


Figure 3.3-17 Extracted chromatograms of peak intensities of R5P and its isotopically labelled equivalent in the control and SKi-treated cells in the pulse-chase experiments.

### 3.3.2.3 Alteration in nucleotide sugar metabolites

Interestingly, this study found that <sup>13</sup>C<sub>6</sub>-glucose was incorporated into pentose glucuronate through glucose-1-phosphate (G1P), which is then converted into GDP-glucose or UDP-glucose at different rates. **Figure 3.3-18** may signpost the conversion rate of <sup>13</sup>C<sub>6</sub>-glucose into <sup>13</sup>C<sub>6</sub>-G1P, since the intensity of labelled G1P at the chase experiment (1 h – 24 h) was

much higher in untreated cells as well at the first time point in the pulse experiment (3 h) and this could be either due to increase uptake of glucose or decrease the removal into other pathways. The results shown in **Figure 3.3-18, B** suggest that the elimination rate of  $^{13}\text{C}_6$ -G1P during the chase experiment is almost the same in both SKi-treated and untreated cells, since the ratios were the same over time (approximately 0.27-fold), even though the intensity of  $^{13}\text{C}_6$ - G1P is higher in the control cells. On the other hand, more unlabelled G1P accumulated in SKi-treated cells compared with untreated cells.

This study provides a new insight into the relationship between G1P and nucleotide sugars metabolites. **Figure 3.3-19** shows nucleotide sugar metabolites; GDP-glucose, UDP- glucuronic acid and UDP-N-acetyl-glucosamine and their isotopes. In the chase experiment,  $^{13}\text{C}_6$ -GDP-glucose levels started to decline faster in the untreated cells from the first time point after exchanging the media. This tends to suggest that the removal of GDP-glucose was slower in the SKi-treated cells (**Figure 3.3-19, B**) as the ratio increased from 1.47 to 4.84 and 9.17 at 1, 4 and 12 hours, respectively, and the metabolites disappeared completely in the last time point. This might suggest inhibition of nucleotide synthesis in SKi-treated cells.

Levels of UDP-galacturonic acid and UDP-N-acetyl-glucosamine (**Figure 3.3-19 D and F**) were increased up to 4 h in the SKi-treated cells, while their levels were decreased in the untreated cells over time.

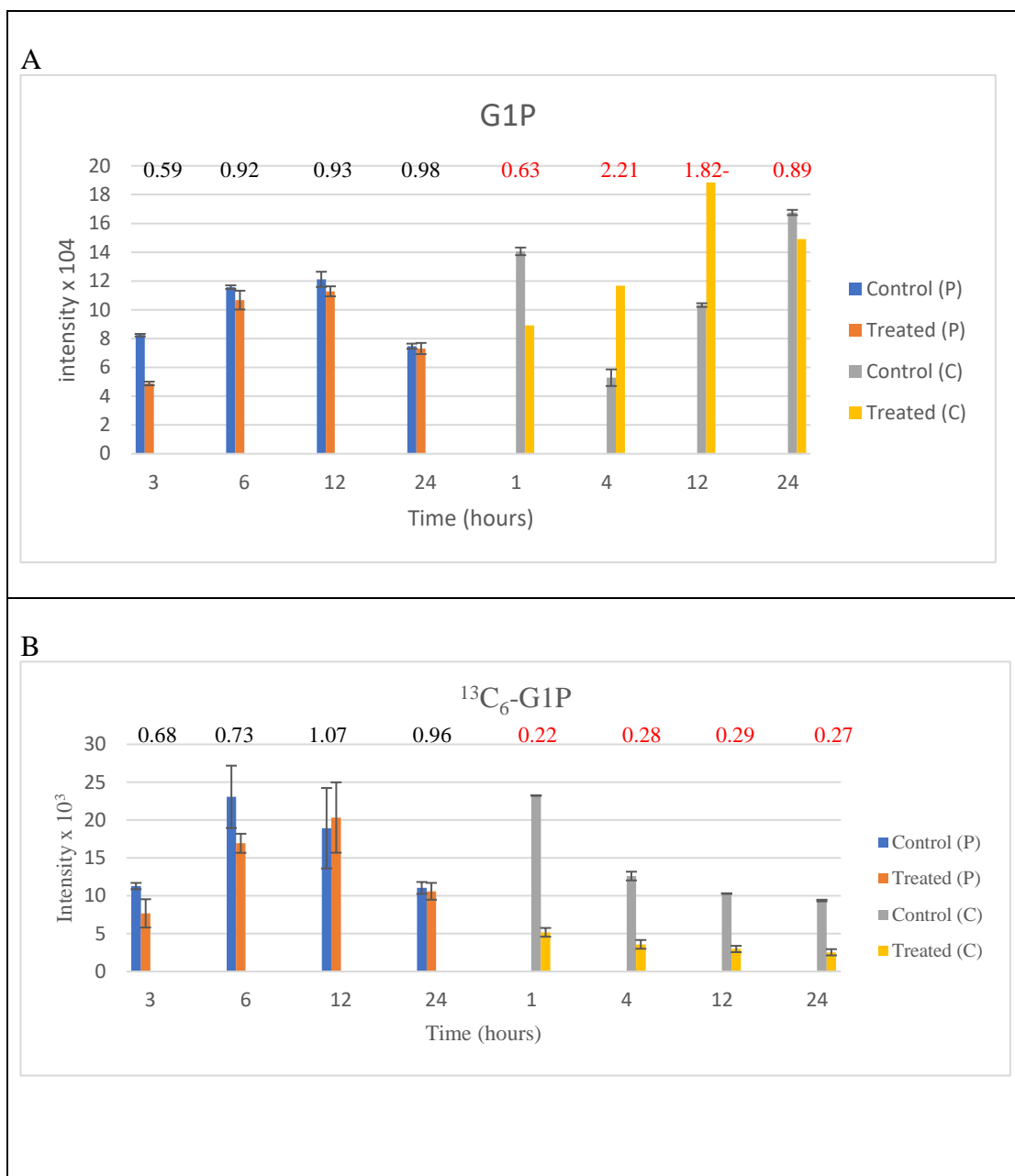


Figure 3.3-18 intensity levels of G1P (left) and its isotope (right) over time in the pulse-chase experiment. Number above bars represent ratios (Treated/Control) of each time point.

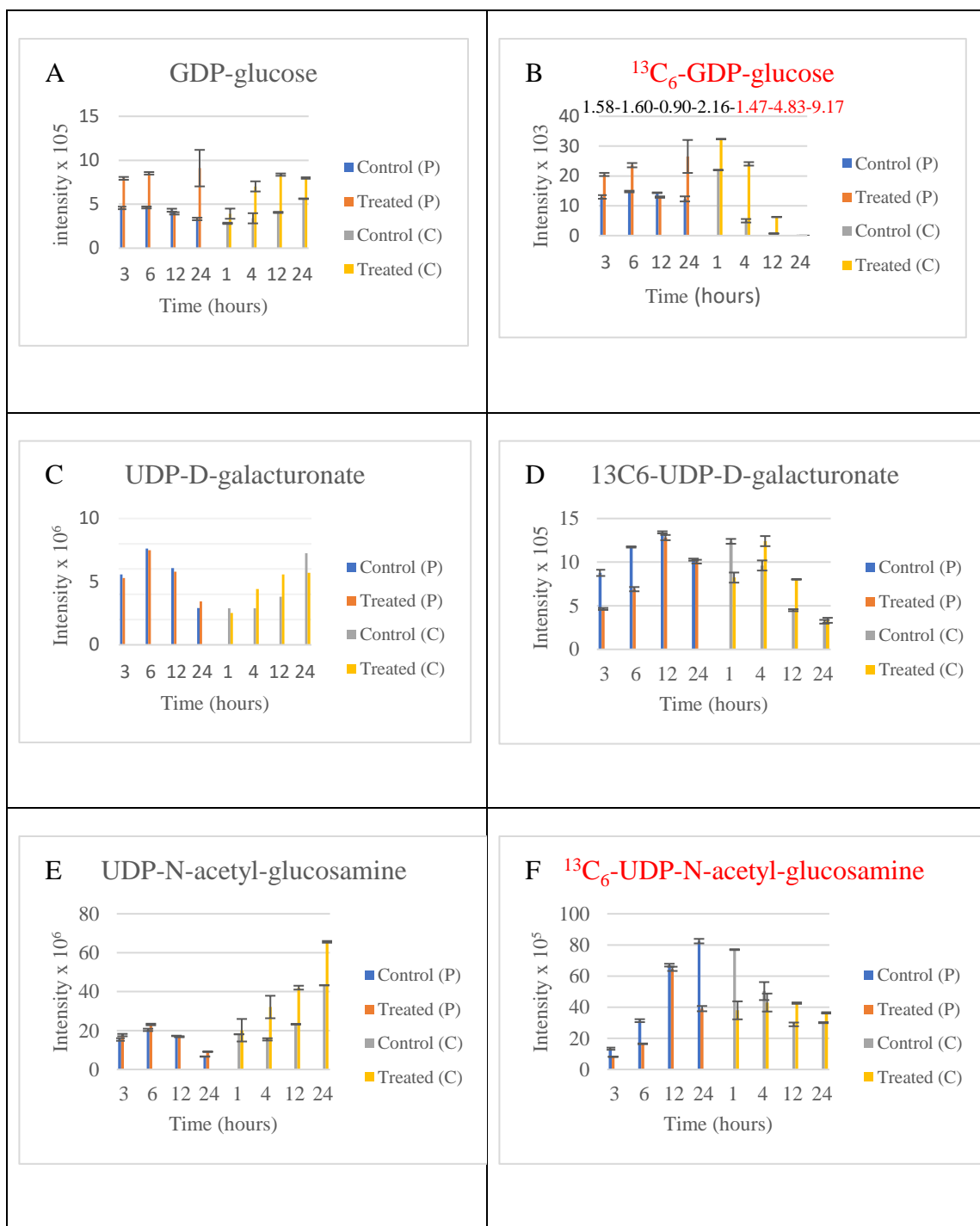


Figure 3.3-19 Bar graphs show absolute levels of (A) GDP-glucose, (B) <sup>13</sup>C<sub>6</sub>- GDP-glucose, (C) UDP-galacturonate and (D) <sup>13</sup>C<sub>6</sub>- UDP-galacturonate; (E) UDP-N-acetyl-glucosamine and (F) <sup>13</sup>C<sub>6</sub>- UDP-N-acetyl-glucosamine.

#### 3.3.2.4 *Alteration in nucleotides*

Since ribose is incorporated in nucleotide structures, all detected nucleotides contain five  $^{13}\text{C}$ -atoms in their chemical structure. ATP, ADP, NAD, NADH, GTP and GDP were detected in this pathway. During the chase, a reduction in labelled and unlabelled ATP production in treated-SKi cells after 48 hours was observed. Conversely, labelled and unlabelled ADP production increased as shown in **Figure 3.3-20, C and D**. The loss of labelled ATP was faster in the untreated cells in comparison with SKi-treated cells. Likewise, GTP levels were higher and GDP levels were lower (**Figure 3.3-21 A and C**). In **Figure 3.3-21 C**, the level of labelled GTP was higher in untreated LNCaP-AI cells and eliminated faster compared with SKi-treated cells. In **Figure 3.3-21 D**, the levels of  $^{13}\text{C}_5$ -GDP were higher in the untreated cells at the first time point but eliminated completely after 12 hours of exchanging the media. The levels of  $^{13}\text{C}_5$ -GDP in the SKi-treated cells increased by 1.56-fold after 4 hours in the chase experiment before starting to decline after which it disappeared and was replaced by unlabelled GDP at the last time point.

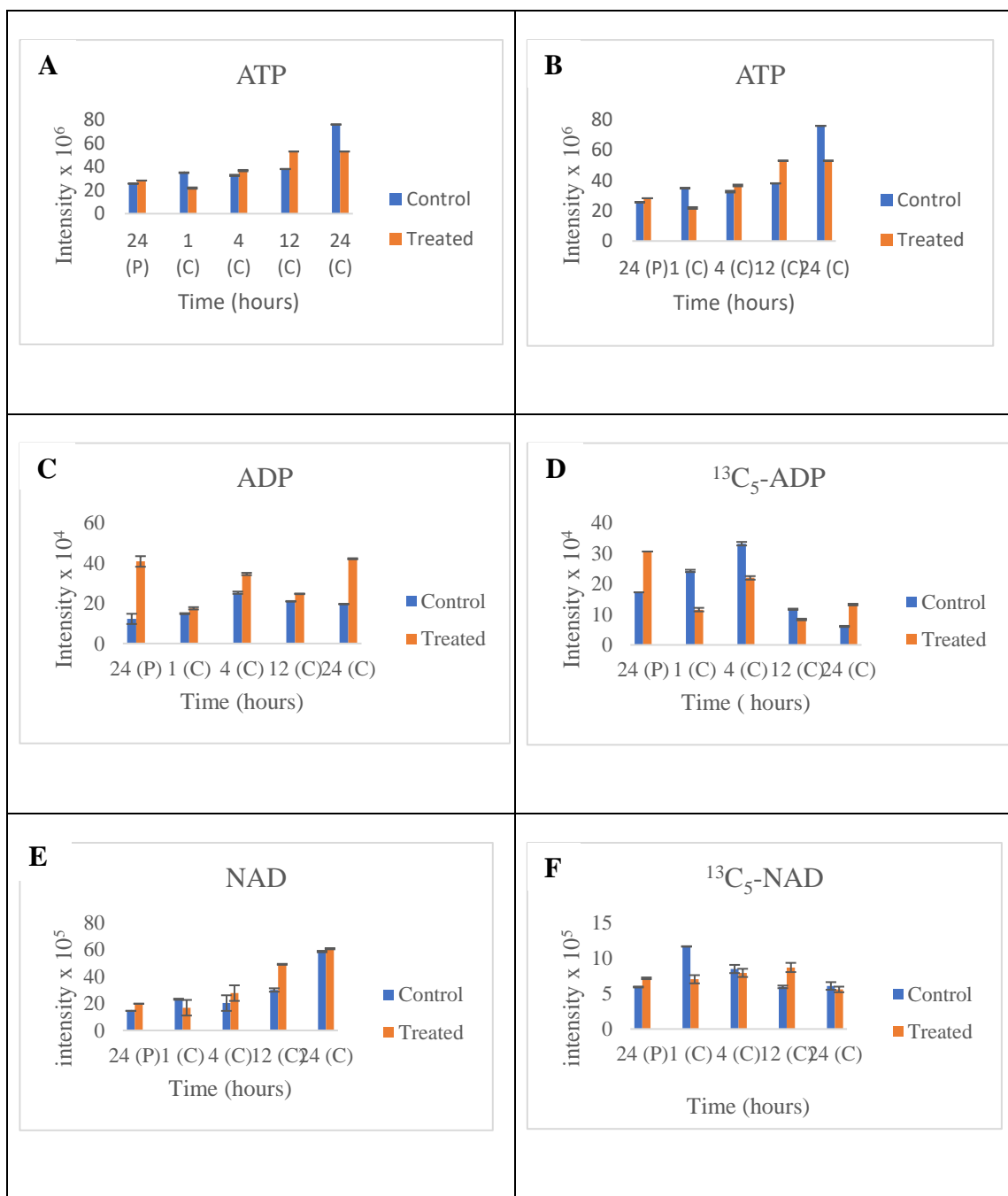


Figure 3.3-20 Bar graphs show absolute levels of (A) ATP; (B) <sup>13</sup>C<sub>5</sub>- ATP; (C) ADP; (D) <sup>13</sup>C<sub>5</sub>-ADP; (E) NAD; (F) <sup>13</sup>C<sub>5</sub>- NAD



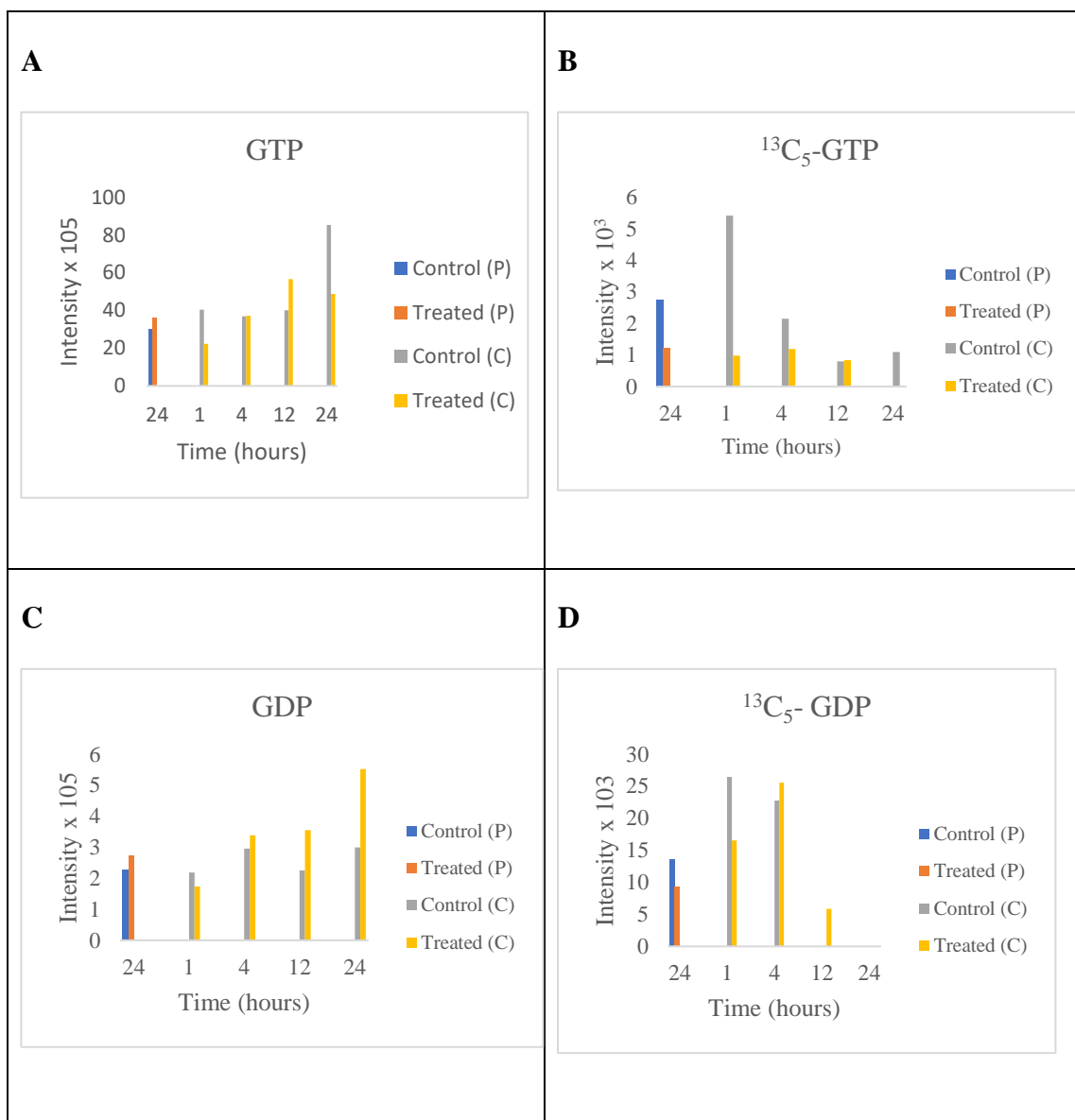


Figure 3.3-21 GTP and GDP and their isotopes levels in the pulse-chase experiment.

### 3.3.2.5 Alteration in TCA metabolites

**Figure 3.3-22** and **Figure 3.3-23** show the changes in the levels of four metabolites in TCA cycle in LNCaP-AI cells treated with SKi for 0-24 hours. All the levels of the

metabolites of interest as well as the levels of their  $^{13}\text{C}$  equivalents were found to be decreased in response to SKi, with the exception of  $^{13}\text{C}_2$ -acetyl-carnitine which slightly increased at the first two time points (3 and 6 hours) and oxoglutarate; the ratio of which increased at 3 hours before declining thereafter.

$^{13}\text{C}_2$ -oxoglutarate was not detected suggesting that this metabolite might be rapidly converted to amino acids; such as lysine and arginine[126] or other metabolites. Therefore, the fate of oxoglutarate is not clear from this study. The ratios of the other TCA metabolites, which are acetyl-CoA, acetyl-carnitine and citrate, were decreased with time, with the exception of acetyl-carnitine which increased transiently at 25 and 28 hours, before declining at 48 hours. This suggests that SKi has some effect on acetyl-CoA, acetylcarnitine and citrate and on the mitochondrial TCA cycle. The removal of  $^{13}\text{C}_2$ -acetyl-CoA levels in cells treated with and without SKi were almost the same in the chase experiment as shown in **Figure 3.3-22, D**.

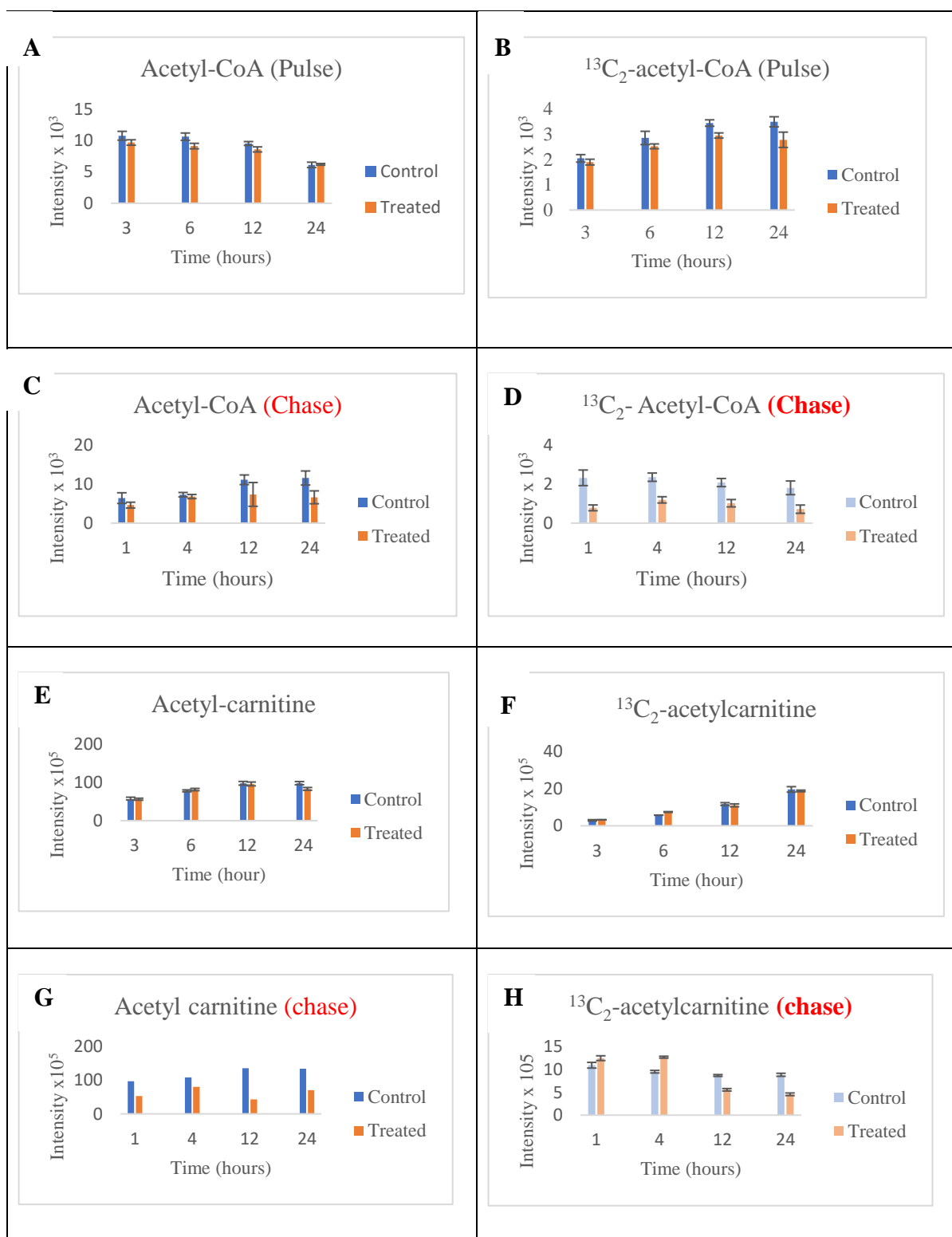


Figure 3.3-22 Bar graphs show a comparison of the changes in levels of acetyl-CoA and acetyl-carnitine and the intensities of <sup>13</sup>C-labelled isotopologues in untreated and SKi-treated cells over time in the pulse-chase experiment, where bars represent the average amount of a given metabolites in samples from untreated (blue) or treated (red) LNCaP-AI cells with SKi, (n=3)

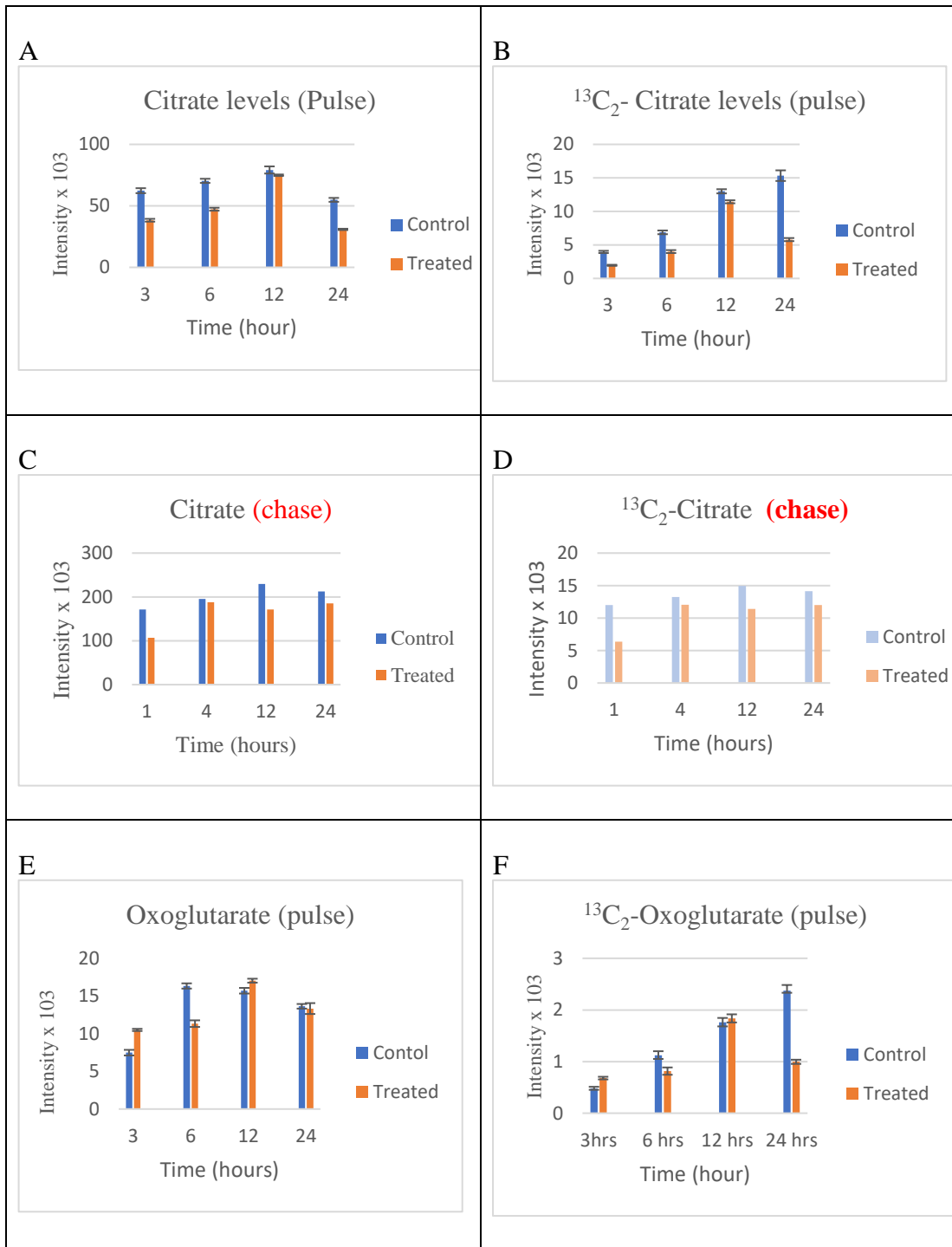


Figure 3.3-23 bar graphs is a comparison of the changes in levels of citrate, oxoglutarate and the intensities of <sup>13</sup>C-labelled isotopologues untreated and SKi-treated cells over time in the pulse-chase experiment, where bars represent the average amount of a given metabolites in samples from untreated (blue) or treated (red) LNCaP-AI cells with SKi, (n=3).

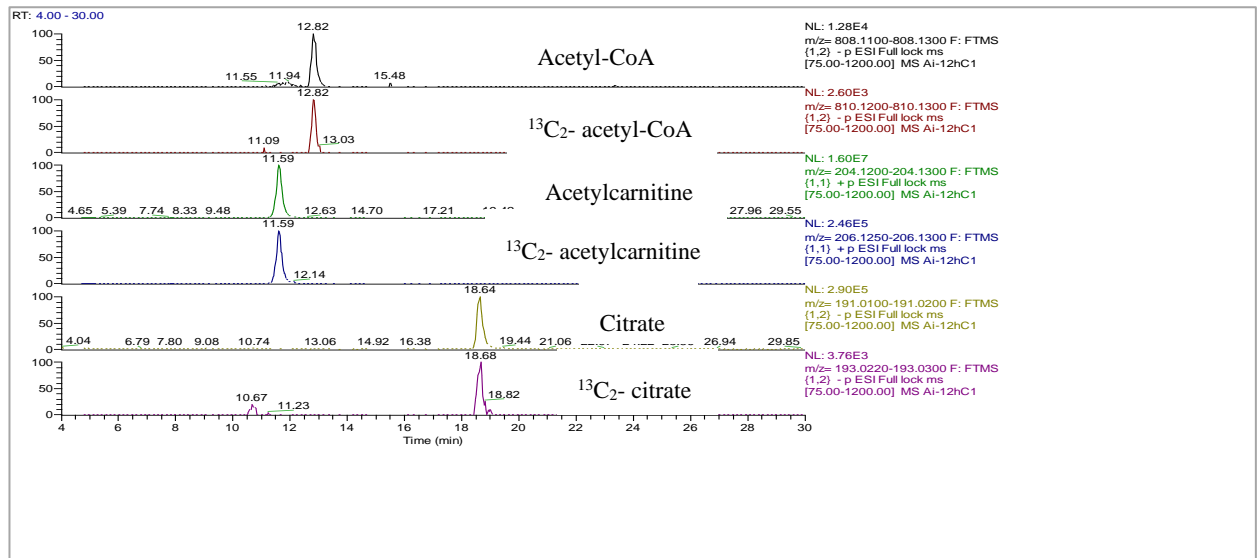


Figure 3.3-24 Extracted chromatograms of acetyl-CoA, acetylcarnitine, citrate and their isotopologues from 12 hours untreated cells in the chase experiment.

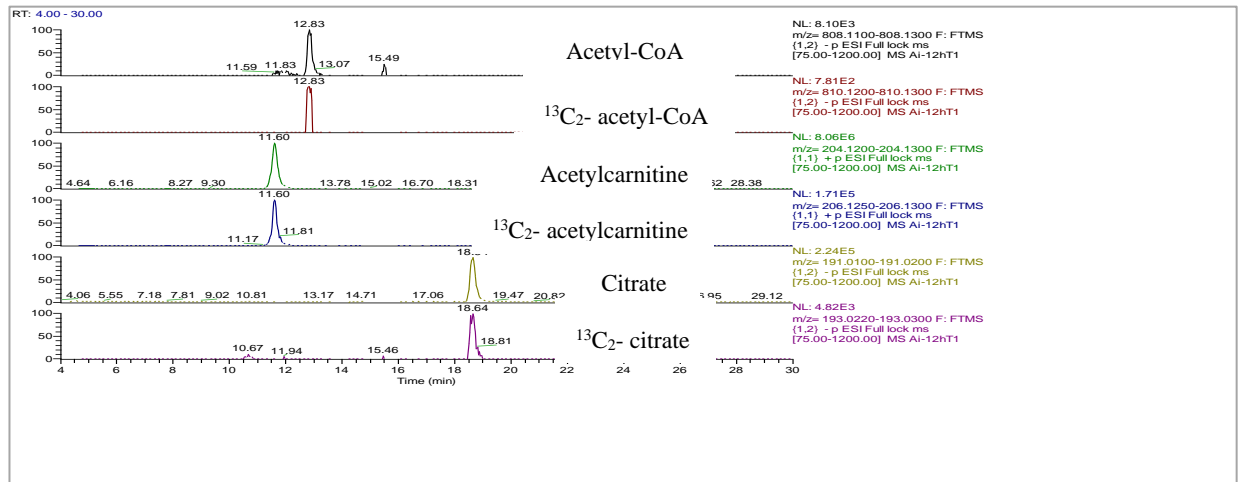


Figure 3.3-25 Extracted chromatograms of acetyl-CoA, acetylcarnitine, citrate and their isotopologues from 12 hours treated cells in the chase experiment.

### 3.3.2.6 Alteration in lipids

The inner mitochondrial membrane is impermeable to NADH. Hence, *Sn*-glycerol 3-phosphate (*Sn*-G3P) functions as a carrier for the NADH protons from the cytosol and which is produced from glycolysis. In this manner, *sn*-G3P can regulate the electron transport chain in the mitochondria [127]. *sn*-G3P is a reduced form of the DHAP and represents the first metabolite branch of the glycolytic pathway, and which can lead to the *de novo* synthesis of glycerol phospholipids [124]. Orr et al. (2012) demonstrated that *sn*-G3P is oxidized at the intermembrane face of mitochondrial inner membrane and cytosol by *sn*-glycerol-3-phosphate dehydrogenase (mGPDH) to produce DHAP. H<sub>2</sub>O<sub>2</sub> produced as a result of the mitochondrial oxidation of *sn*-G3P in presence of FADH<sub>2</sub> as proton donor [124] is shown in **Figure 3.3-26**. Enhancing *sn*-G3P production from the glycolysis leads to increased ROS production by increasing electron flow through the coenzyme Q pool, and which can results in leaking electrons from electron transport chain (ETC) complex [128].

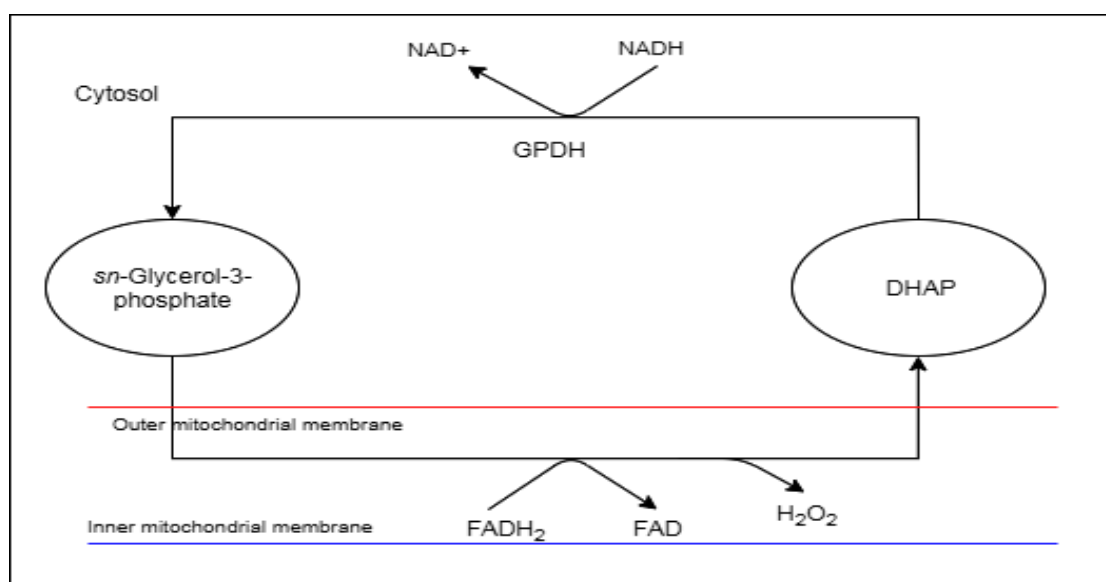


Figure 3.3-26 reaction between <sup>13</sup>C<sub>2</sub>-*sn*-G3P and DHAP in the cytosol and mitochondrial membrane.

**Figure 3.3-27** shows the changes in intensity levels of *sn*-G3P (A) and its isotope (B) in cells treated with and without SKi in the pulse-chase experiment.  $^{13}\text{C}_2$ -*sn*-G3P ratios increased from 0-24 h indicating that SKi can either promote synthesis or reduce further metabolism of *sn*-G3P. Thus,  $^{13}\text{C}_3$ -DHAP is converted to  $^{13}\text{C}_3$ -*sn*-G3P, and which can produce  $\text{H}_2\text{O}_2$  or is involved in glycerophospholipid synthesis, such as GPC and GPE. **Figure 3.3-28** shows the changes in some labelled lipids intensities, such as GPC, GPE and LPA, during the pulse-chase experiments. It can be seen in **Figure 3.3-28,B** that during the chase experiment, the incorporation of labelled carbons continue to accumulate in both untreated and SKi-treated cells with higher accumulation in the latter, while labelled GPE incorporations were reduced during the chase.

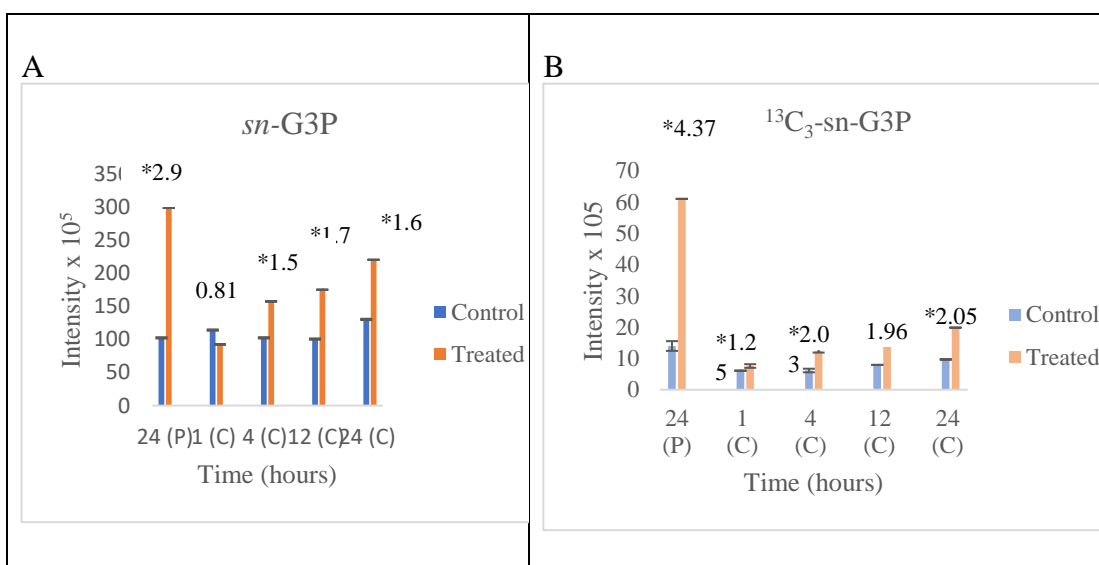


Figure 3.3-27 bar graphs show the changes of *sn*-G3P and acetyl-carnitine and the intensities of  $^{13}\text{C}$ -labelled isotopologues in untreated and SKi-treated cells over time at 24 hours in the pulse experiment and 1, 4, 12 and 24 hours in the chase experiment. \* significant.

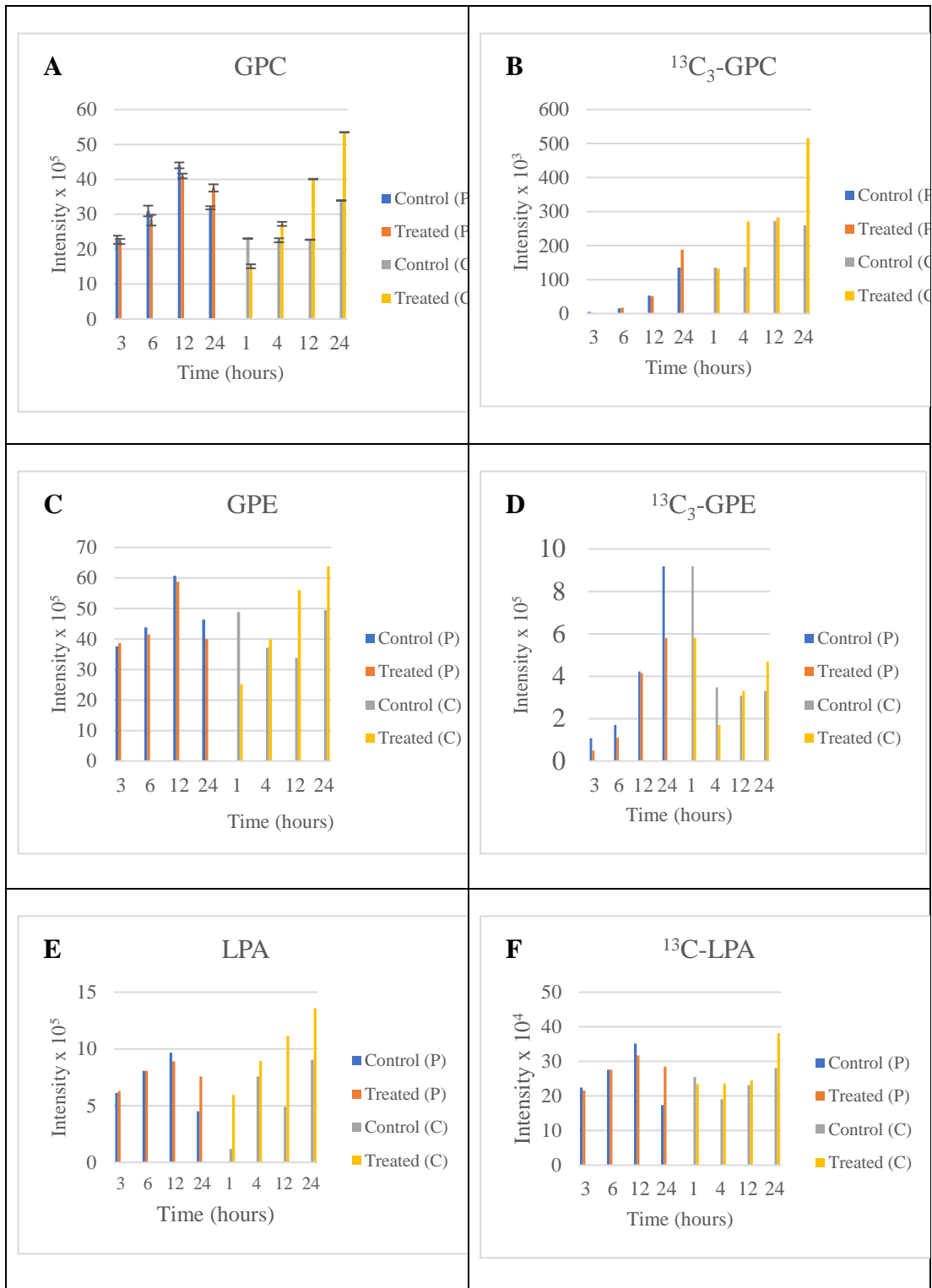


Figure 3.3-28 bar graphs show the changes of GPCm GPE, LPA and the intensities of <sup>13</sup>C-labelled isotopologues in untreated and SKi-treated cells over time 0-24 hours in the pulse experiment and 1, 4, 12 and 24 hours in the chase experiment.



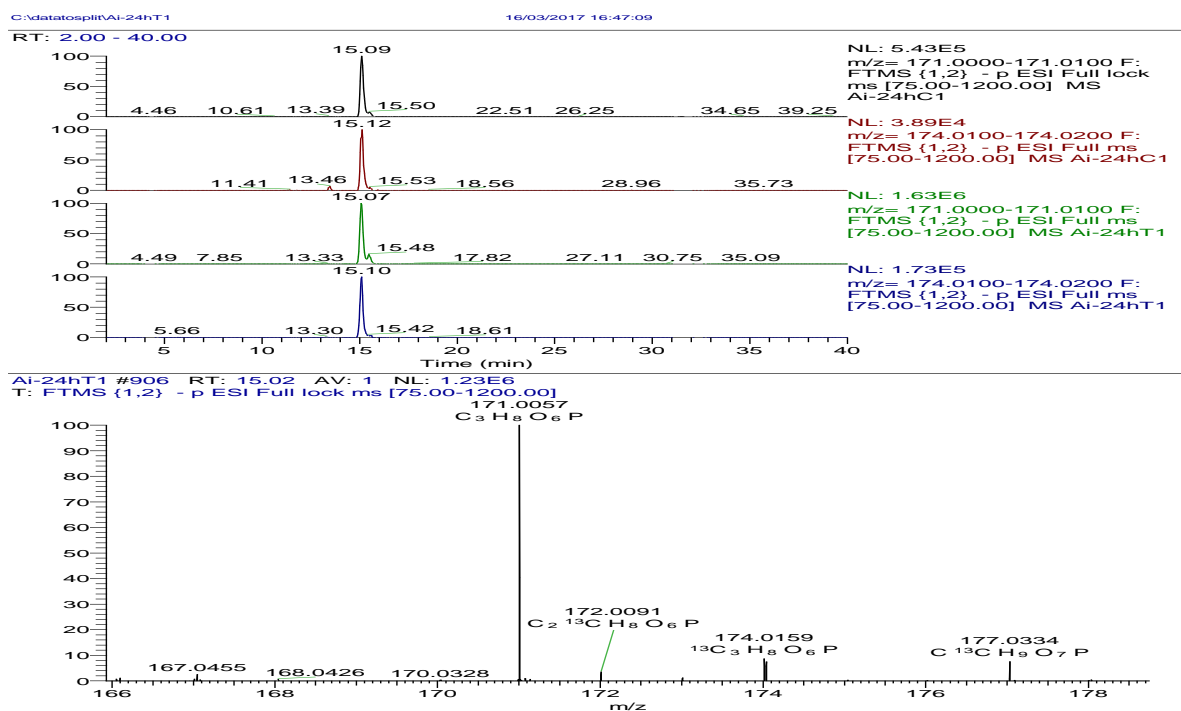


Figure 3.3-29 Extracted ion chromatograms showing *sn*-glycerol 3-phosphate and its isotope detected in negative ion mode and eluted at the same retention time (15.10). The accurate mass spectra of *sn*-glycerol 3-phosphate and its isotope, 171.0057 and 174.0159, in untreated and treated LNCaP-AI cells.

### 3.3.3 ROS measurement

Reactive oxygen species (ROS) are characterised by the presence of a single unpaired electron in the oxygen electron field example of which are superoxide ( $O_2^{\cdot-}$ ), hydroxyl radical ( $\cdot OH$ ), nitric oxide ( $NO^{\cdot}$ ), peroxy radicals ( $ROO^{\cdot}$ ), termed oxygen-free radicals. Non-radical ROS includes singlet oxygen ( $O_2^*$ ), ozone ( $O_3$ ), hydrogen peroxide ( $H_2O_2$ ), prexynitrite ( $ONO^-$ ), dinitrogen dioxide ( $N_2O_2$ ) and other compounds. The production of ROS is a normal process in living organisms that enables regulation of the redox balance within living cells [129]. Moreover, several studies have confirmed that elevated ROS levels are a feature of cancer cells and induces some of the hallmarks of these cells, in terms of their interaction with the microenvironment, metabolic changes and genetic instability [129].

**Figure 3.3-30** shows ROS measurements performed by using of dihydroethidium (DHE) to monitor intracellular superoxide ( $O_2^{\cdot-}$ ) levels produced in LNCaP-AI cells in response to SKi. **Figure 3.3-30** shows that superoxide ( $O_2^{\cdot-}$ ) levels were enhanced significantly by approximately 32.5% and 39.85% in SKi- or angiotensin II-treated cells. Angiotensin II is used as a positive control because of its ability to produce ROS species, such as  $O^{\cdot-}$  and  $H_2O_2$  via stimulation of NADH and NADPH oxidase [130].

The increase in ROS production in SKi-treated cells may cause damage and degrade the lipid membrane integrity to induce senescence and/or cell death.

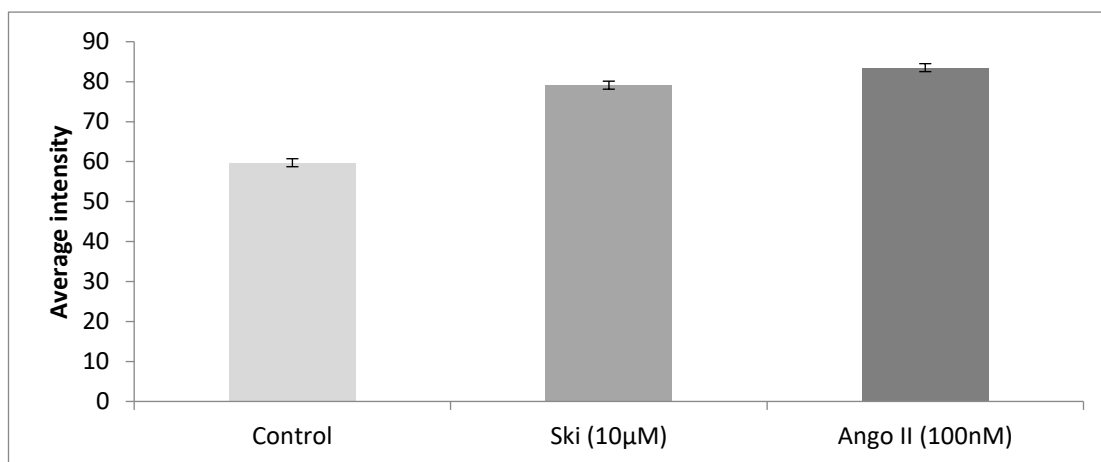


Figure 3.3-30 The effect of 10  $\mu$ M SKi (24 hours) on ROS production in LNCaP-Ai cells using dihydroethidium (DHE) as a detector and angiotensin II (100nM) as a positive control for 1 hour. (n=4 and P.value <0.05). error bars represent the standard error of the mean (SEM).

## 3.4 Discussion

### 3.4.1 Metabolomic profile of the effect of SKi on LNCaP-AI cells.

In a previous study, it was found that treating androgen sensitive and independent prostate cancer cells (LNCaP-AS and LNCaP-AI cells respectively) with the SK inhibitor, SKi induces metabolic alterations in glycolytic intermediates, pentose phosphate metabolites, fatty acids and diadenosine triphosphate formation [5]. It has been previously shown that the treatment of LNCaP-AI with SKi does not cause cell apoptosis [131], but instead senescence[131]. In the current study, the effects of SKi on the metabolomic profile and flux (using pulse-chase experiment) in the LNCaP-AI cells were investigated by employing pHILIC-MS analysis. The treatment of LNCaP-AI cells with SKi induced changes in glycolytic, pentose phosphate metabolites, nucleotide sugars, TCA and energy metabolites and lipid precursors; such as *sn*-G3P.

The current study confirms changes observed previously in proline and glycine levels in response to SKi [5]. Moreover, high elevation of glutathione disulfide (GSSG) levels was observed. GSSG is formed by the reaction of glutathione and peroxide catalyzed by glutathione peroxidase and which indicates that SKi induces an oxidative stress response. Moreover, NADPH levels were almost completely depleted in SKi treated cells, probably a consequence of its use in recycling GSH. Nevertheless, the recycling of GSSG appears to be overwhelmed, although there is a modest increase in GSH. This interpretation is supported by results showing that the levels of cystathione, which is an important intermediate in cysteine biosynthesis and is required for GSH formation, is decreased in SKi-treated cells. Moreover, the levels of N-acetyl-L-glutamate, S-glutathionyl-L-cysteine and gamma-L-glutamyl-cysteine were

significantly increased in response to SKi. This is significant because these metabolites are involved in glutathione and glutathione cysteine biosynthesis and oxidative stress responses.

The current findings also suggest an important role for *sn*-G3P as this metabolite induces oxidative stress. The levels of *sn*-G3P are higher in SKi-treated cells. This is possibly due to the inhibitory effect of SKi on glycolysis and nucleotide synthesis, as will be discussed later. This would enhance the production of *sn*-glycerol-3-phosphate through the G3P shuttle in order to generate ATP via the action of complex I and III. The mitochondrial inner membrane is impermeable to NADH. Therefore, a free H<sup>+</sup> from NADH is used to reduce DHAP to form *sn*-G3P. In turn, *sn*-G3P can cross the outer mitochondrial membrane, where it is then oxidised to DHAP in the ETC. This oxidative processes generates ROS as a by-product (H<sub>2</sub>O<sub>2</sub>) within the mitochondria [124]. Therefore, these results suggest that SKi induces oxidative stress in LNCaP-AI cells.

The results in part 3.3.1 also demonstrate that SKi reduces the levels of TCA metabolites; notably citrate, fumarate and malate. The accumulation of glycolytic metabolites was also observed. Therefore, higher levels of glycolytic metabolites and lower levels of TCA metabolites suggest that the glycolysis flux towards the TCA cycle is reduced by SKi. Indeed, these changes are consistent with previous studies, which have shown that SKi inhibits DNA synthesis at G1, resulting in senescence of LNCaP-AI cells [131]. It has also been previously demonstrated that SKi activates the proteasome to remove c-Myc [132]. This is significant because c-Myc regulates enzymes involved in glycolysis and other pathways [113]. Therefore, it will be

interesting to determine whether there is a functional link between the metabolic changes induced by SKi and the proteasomal degradation of c-Myc.

#### 3.4.2 Effect of SKi on LNCaP-AI cells using $^{13}\text{C}_6$ -glucose

A major objective was to establish the effect of SKi on the metabolism of  $^{13}\text{C}_6$ -glucose in LNCaP-AI cells. It is necessary to use pulse-chase in order to define flux through these pathways and to determine whether or not SKi can alter this flux. In this manner, one can attribute an inhibitory or stimulatory effect of any given pharmacological intervention. **Figure 3.4-1** summarises the number of carbons that incorporate into several pathways from  $^{13}\text{C}_6$ -glucose. The pathways which will be discussed include: (i) glycolysis; (ii) PPP; (iii) nucleotide sugars; (iv) TCA; (v) energy metabolites and nucleotides and (vi) lipids.

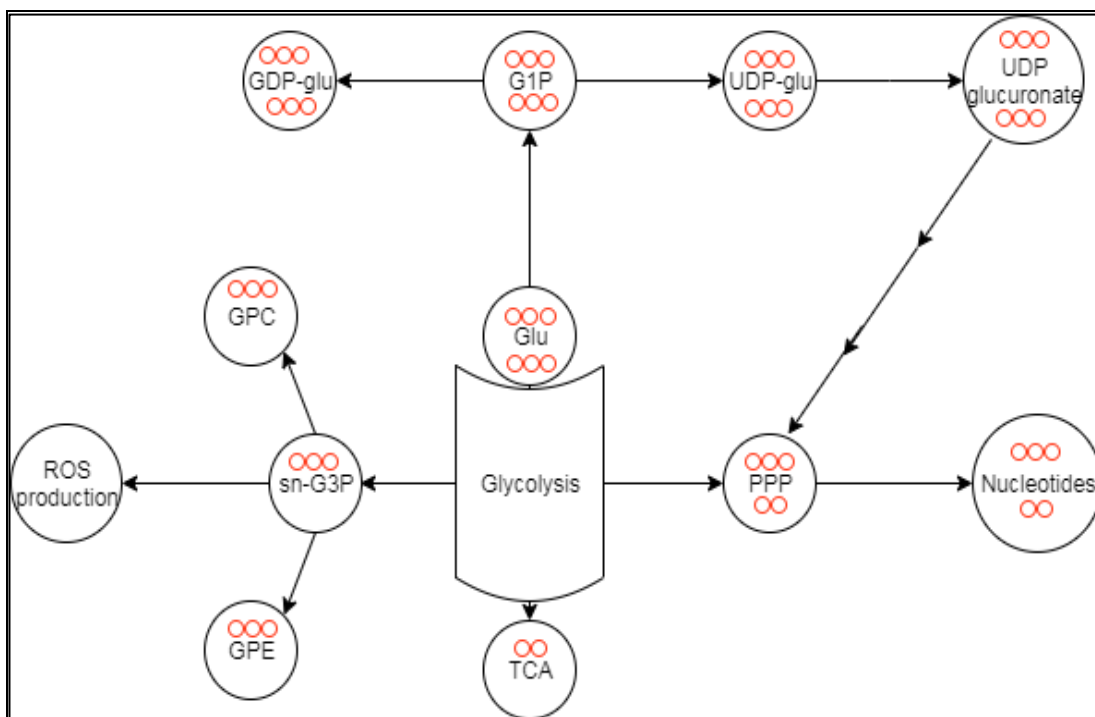


Figure 3.4-1 Flux map of  $^{13}\text{C}_6$ -glucose in LNCaP-AI cells that have been treated with SKi. Several pathways include glycolysis, pentose phosphate pathway (PPP), nucleotides, nucleotide-sugar and glycerolipids biosynthesis.

It was observed during the pulse that SKi induced an elevation of  $^{13}\text{C}$ -labelled glycolytic and pentose phosphate metabolites. When comparing with results obtained using unlabelled glucose, the fold increase in these metabolites in response to SKi were similar. The highest levels of  $^{13}\text{C}$ -glycolytic metabolites were  $^{13}\text{C}_6$ -fructose1,6-bisphosphate (F1,6-P<sub>2</sub>) and  $^{13}\text{C}_3$ -glyceraldehyde-3-phosphate (GAP). GAP is a product of the breakdown of F1,6-P<sub>2</sub>. Elevation in PPP metabolite levels, such as 6-phosphogluconate and R5P were also noted.

Shortly after chase (1 hour), the labelled glycolytic and PPP metabolites disappeared from untreated and SKi-treated cells with the exception of R5P. R5P was detected at low concentration at the 1 hour time point in the untreated cells and up to 12 h in the SKi-treated cells as shown in **Figure 3.3-16, F**. Disappearance of 6-phosphogluconate

at 1 hour in both cell treatments and the detection of R5P at 1 h until 12 h in the untreated cells and SKi-treated cells suggests that the removal of  $^{13}\text{C}_5\text{-R5P}$  is slower in SKi-treated cells. Therefore, SKi may reduce the flux through PPP thereby affecting nucleotide and DNA synthesis. A slower elimination rate of R5P in the SKi-treated cells is, in line, with a previous study by McNaughton et al. (2016), which showed that SKi induces growth arrest at G1, thereby inhibiting DNA synthesis. These changes were also associated with a reduction in the percentage of cells in the S phase [131]. This could explain why the R5P metabolite were still observed for a longer period in the pulse-chase in SKi-treated cells. R5P is a key metabolite for phosphoribosyl pyrophosphate (PRPP) synthesis, which is essential in nucleotide synthesis *via* the salvage pathway and/or *de novo* synthesis [57]. Nucleotides require larger amounts of R5P produced from both branches of the PPP [133].

A second observation related to the interconversion of pentose glucuronate in labelled glucose-treated LNCaP-AI cells. Metabolites such as G1P, GDP-glucose, UDP-glucose and UDP galacturonate were investigated. At the first time point of the pulse (3 h) the levels of unlabelled G1P and  $^{13}\text{C}_6\text{-G1P}$  were lower in the SKi-treated cells, after which they returned to baseline. Interestingly, the results of  $^{13}\text{C}\text{-G1P}$  in the chase experiment showed different patterns in comparison with unlabelled G1P. The ratio (T/C=0.27) of  $^{13}\text{C}\text{-G1P}$  might indicate that the elimination rate of the isotope was the same in both SKi-treated and untreated cells during the chase experiment.

Interestingly, in contrast with labelled G1P which is reduced in SKi-treated cells, the levels of unlabelled G1P increased. This might be as a result of increased glycogen

degradation to generate G1P *via* glycogen phosphorylase. G1P can be converted into other metabolites, such as GDP-glucose and UDP-glucose.

It was observed during the pulse-chase experiment that SKi induced an elevation of  $^{13}\text{C}_6$ -GDP levels until 12 h of the chase. Interestingly, it was observed during the chase that the removal rate of  $^{13}\text{C}$  GDP-glucose from the SKi-treated cells was slower suggesting that SKi induces a reduction in further metabolism of GDP-glucose. For instance,  $^{13}\text{C}$  GDP-glucose can be hydrolysed in the presence of  $\text{H}_2\text{O}$  into GDP and glucose or into GMP and G1P. Both nucleotides, GMP and GDP are involved in RNA and DNA synthesis [134]. Therefore, the reduction in the rate of flux through this pathway to enable nucleotide biosynthesis, support the previous finding that SKi induces inhibition of DNA synthesis in LNCaP-AI cells [131].

$^{13}\text{C}_6$ -UDP-galacturonate and UDP-N-acetyl-glucosamine levels increased until 4 hours in the chase experiment before their levels start to decline. The levels in the untreated cells were higher at the first time point (1 h) but declined thereafter. This supports the possibility that SKi reduces the flux through the pentose phosphate pathway. It seems that much of the glucose flux in these cells goes through this pathway and although this is difficult to explain it appears to be a novel observation.

Another effect of SKi is that it might modulate GTP-GDP exchange reactions by for instance, G protein, *via* increasing the hydrolysis of GTP or reducing the phosphorylation of GDP to form GTP. GTP is a high energy molecule that can activate Ras. When GTP is hydrolysed to GDP by the GTPase- activating protein, Ras is converted into an inactive form [135]. Ras is involved in cell signaling and the regulation of cell proliferation. Therefore, Ras plays critical role in the development



of human diseases, such as cancer [136]. A previous study suggested that inhibiting GDP-GTP exchange might play an important role in reducing DNA synthesis in LNCaP cells [136]. The reduction in GTP levels and accumulation in GDP observed in response to SKi might support the possibility that Ras function is impaired and this might result in the inhibition of DNA synthesis by SKi.

An important effect of SKi on the metabolome of LNCaP-AI cells is in the downregulation of TCA metabolites. This might be attributed to a reduction of acetyl-CoA, acetyl-carnitine or citrate. The chase experiment showed a stable rate of elimination of  $^{13}\text{C}_2$ -acetyl-CoA and  $^{13}\text{C}_2$ -citrate with lower levels in SKi-treated cells.  $^{13}\text{C}_2$ -Oxoglutarate disappeared in the chase experiment, which might be explained by its possible conversion into other metabolites. These results suggest that SKi reduces the glycolytic flux and subsequently the restriction of pyruvate for use by the TCA cycle.

Due to of the destructive effect of the treatment on the glycolysis, cells seem to reprogram their metabolism by shifting toward ETC to help increase ATP synthesis. This is achieved using a proton from cytosolic NADH *via* the *sn*-G3P shuttle. In addition, the current results suggest that SKi accelerates the conversion of glycero phosphate to *sn*-glycerol 3-phosphate in the mitochondrial membranes and thereby resulting in the production of ROS. This could provide an explanation for oxidative stress induced by SKi and is supported by the much higher incorporation of label into  $^{13}\text{C}_3$ -G3P in SKi-treated cells compared with untreated cells **Figure 3.3-27**.

### 3.4.3 Reactive oxygen species (ROS)

ROS is usually generated in normal cells to induce cellular function but dysregulation could lead to a variety of diseases [129][137]. Studies have shown multiple explanations for the function of ROS in cancer [138]. For example, ROS has been shown to promote cancer development [139]. This correlates with the observation that cancer cells have a higher ROS level in comparison with normal cells [140]. Therefore it has been suggested that reducing ROS levels might suppress cancer by abrogating the requirement for ROS to promote the metabolism and survival of cancer cells [129]. On the other hand, others have suggested that higher levels of ROS can be detrimental to cancer cells. For example, increasing the levels of ROS have been shown to promote apoptosis or senescence of cancer cells; as observed here and which suggests a possible therapeutic approach.

In the current study, ROS production and mitochondrial depolarization might also cause senescence [141]. Studies have shown that SKi promotes apoptosis of androgen-sensitive LNCaP cells due to the proteasomal degradation of SK1a/b. In contrast, SKi does not stimulate the proteasomal degradation of SK1b in LNCaP-AI cells thereby limiting apoptosis of these cells. However, combined treatment with SK1 siRNA and SKi removed SK1b and subsequently promoted apoptosis of LNACaP-AI cells. [131].

ROS overproduction alongside the inhibition of the PPP (a major source for NADPH production [20] by SKi might explain the depletion of NADPH and the accumulation of GSSG. The ratio of GSH/GSSG in cells has been found to be 100:1, whereas this ratio was reduced to 10:1 when cells are exposed to oxidative stress [142]. This imbalance or quantitative change in the GSH/GSSG ratio is considered to be an

indicative biomarker of oxidative damage [143]. The observed 1:94 ratio of GSH:GSSG **Figure 3.3-2**, therefore supports the conclusion that SKi induces oxidative stress in LNCaP-AI cells and this is linked to senescence of these cells. Indeed, SKi promotes p53 and p21-dependent senescence of LNCaP-AI cells [131] and this occurs multiple via the up-regulation of p21 and p53 expression and which is dependent on the loss of both Des1 and SK1a (McNaughton et al. 2016). The role of oxidative stress is evident by the finding that the anti-oxidant, N-acetylcystin (NAC) blocks the increase in p53 expression in these cells (McNaughton et al. 2016)

Overall, the observation that SKi enhanced *sn*-G3P synthesis, which promotes ROS when metabolized within mitochondria, suggests that SK is a key regulator of oxidative stress-induced senescence in LNCaP-AI cells.

### **3.5 Summary**

In current study, the *in vitro* effect of SKi on the metabolomic alteration of LNCaP-AI was examined using  $^{13}\text{C}_6$ -glucose in a pulse-chase experiment. The metabolomic profile demonstrated that SKi increases the levels of glycolytic, some PPP metabolites and *sn*-G3P. In addition, significant decreases in NADPH, acetyl-CoA, acetyl-carnitine, citrate and oxoglutarate levels were observed. On the other hand, the pulse-chase experiment revealed that glycolytic and PPP metabolites and oxoglutarate were undetectable, while levels of *sn*-G3P, GPC and GPE were found to be increased. Levels of acetyl-CoA, acetyl-carnitine and citrate levels were found to be lower in SKi-treated cells. These results suggest that SKi modulates the Warburg effect and shifts glycolytic flux toward *sn*-G3P. This might be necessary in order to transfer an

electron from NADH from the cytoplasm into mitochondria, thereby producing excessive ROS as a byproduct. This correlates with a model in which increased ROS production increase p53 expression to induce senescence in LNCaP-AI cells [131]. In conclusion, SK regulates metabolic reprogramming from glycolysis to other pathways and which results in the accumulation of ROS in LNCaP-AI cells.

## **Chapter IV**

---

**Lipidomics analysis of the effects of the  
sphingosine kinase inhibitors SKi and  
ROME on LNCaP and LNCaP-SK1b  
prostate cancer cells using Mass  
spectrometry**

## 4 Lipidomics analysis of the effects of the sphingosine kinase inhibitors SKi and ROME on LNCaP and LNCaP-SK1b prostate cancer cells using Mass spectrometry

### 4.1 Introduction

Cancer cells have alterations in cellular metabolism for promoting proliferation and producing energy. These changes can be used as tools for diagnosis, prognosis or evaluation of anti-tumor agents [144]. For example, in contrast to normal cells, cancer cells activate glycolysis to provide energy for the cells, by consuming glucose at a high rate. The cells also use intermediate glycolytic metabolites as precursors for biosynthesis, such as glycerol phosphate and citrate for lipids biosynthesis and ribose sugars for nucleotide biosynthesis [145]. Moreover, numerous studies have shown that the sphingolipid rheostat plays a vital role in regulating cell fate and cancer [146]. Hence, assessment of alterations of a particular metabolite can suggest a dysfunctional role for such a pathway in cancer cells. The metabolic profile of cancer cells might also provide meaningful information that enhances understanding of the mechanism of action and resistance of the cells to drugs, thus contributing to the development of better therapeutic tools [58].

Lipidomics is an emerging field of science which focuses on profiling lipid species present in an organism. Lipidomics provides a comprehensive analysis using combined technological tools, especially mass spectrometry, with the principles of analytical chemistry to map the massive diversity of the lipid composition of metabolome. However, it is still quite a challenging field because of the complexity and specificity of lipids species. For example, some lipids have an identical molecular formula but different spatial configuration, termed isobaric molecular species. Also,

some lipids share identical elemental composition but are different chemical species, termed iso-elemental. These similarities make the identification of lipids complicated and which, therefore, requires extended investigation for each molecule using additional techniques such as MS/MS or NMR. This science has grown rapidly in recent years, for different aspects such as the identification of lipid biomarkers for diagnosis and disease management [147], drugs targeting and improved understanding pharmacological mechanisms [148].

A number of lipid metabolic pathways have been linked to prostate cancer, particularly sphingolipids which play a vital role in cell signaling [149]. For instance, SK1 is expressed in many tumor cells including LNCaP cells. Higher expression levels of SK1 in these tumors correlate with shorter disease specific survival in patients [150]. It has been previously shown that both the expression levels of SK1a and SK1b are increased in aggressive androgen-independent LNCaP-AI prostate cancer cells compared with androgen-sensitive LNCaP prostate cancers cells [28]. SK1b evades the proteasome in response to the SK inhibitor, SKi ((2-(p-hydroxyanilino)-4-(pchlorophenyl) thiazole) in androgen-independent LNCaP-AI cells and these cells undergo senescence [131]. In contrast, SK1b is degraded by the proteasome in androgen-sensitive cells in response to SKi, and these cells undergo apoptosis. We, therefore, over-expressed SK1b in androgen-sensitive LNCaP cells in order to recapitulate a more aggressive phenotype, akin the LNCaP-AI cells. The effect of over-expressing SK1b on the lipidome of LNCaP cells was then investigated and compared with LNCaP cells.

Mammalian cells produce unusual sphingoid bases, such as 1- deoxysphingoid [151], and dimethylsphingosine (DMS) [152]. 1-deoxysphingoid bases are atypical and neurotoxic sphingo-bases [153]. These bases are formed by serine palmitoyltransferase (SPT) but with the use of other amino acids instead of serine [153]. For instance, SPT can use alanine to form deoxy-sphinganine (doxSA) or can use glycine to form deoxymethyl-sphinganine [154]. A previous study showed that 1-deoxysphingoid bases are substrates for ceramide synthase (CerS) [154], [155], which is responsible for the conversion of sphinganine into dihydroceramide (DHcer). In addition, 1-deoxysphinganine has been found to reduce SK1 activity and inhibit DNA synthesis [156]. DMS acts as an inhibitor for sphingosine kinase (SK), which is synthesised endogenously from the catabolism of ceramide [157]. It can also inhibit protein kinase C which is responsible for PC lipids hydrolysis [152].

The synthesis of ether lipids involves multi-step processes involving the peroxisome and the ER [158]. Firstly, glycerol-3-phosphate (G3P) is shuttled into peroxisomes where it is converted to DHAP, acyl-DHAP and alkyl-DHAP. Alkyl-DHAP is converted to 1-O-Alkyl-G3P which enters the ER and subsequently converted to alkyl-acylglycerol (AAG). In the ER, AAG is further converted to ether-lipids by the addition of conjugates such as CDP- choline or CDP-ethanolamine at the Sn-3 position. Similarly, G3P or acyl-DHAP is also interconverted to lysophosphatidic acid to synthesize ester phospholipids [159].

The sphingosine kinase inhibitor SKi (10  $\mu$ M, 24h) reduces the activity of SK1a and SK1b in LNCaP prostate cancer cells [28] and has a similar effect to FTY720, which is also an SK1 inhibitor [160]. In this regard, SKi induces a reduction in the



intracellular S1P levels and an accumulation in sphingosine and C22:0 ceramide has been noted to be associated with apoptosis as a result of SK1a and SK1b degradation [73].

ROME is a low potency SK2 selective inhibitor, which has a similar structure compared with the SK1 inhibitor, FTY720 but with methoxy group instead of hydroxyl group [75]. ROME reduces S1P levels in MCF7 breast cancer cells [75] as well as LNCaP-AI cells [5]. Unlike SKi, ROME fails to reduce c-Myc expression or to induce apoptosis, but instead promotes growth arrest in MCF-7 cancer cells. However, ROME also induces autophagy in LNCaP prostate cancer cells, but fails to reduce the expression of SK1 [5]. It also has been found that ROME has no effect on most of ceramide species with the exception of Cer (22:0)[28],[161].

The current study aimed to examine the effect of SKi and ROME on LNCaP and LNCaP-SK1b metabolome to determine how overexpression of SK1b might affect the response of the cancer cell metabolism to SK inhibitors. Analysis employed mass spectrometry-based lipidomic profiling. Each of the cell lines was separately treated with 10  $\mu$ M SK inhibitor for 24 hours before extraction and global metabolite analysis of cell lysates by LC-MS using a high-performance liquid chromatography (HPLC) system coupled to an Orbitrap Exactive mass spectrometer using a silica gel column. The resulting data were extracted by MZMine and subsequently analysed by univariate and multivariate approaches with SIMCA-P.

## **4.2 Materials and Methods**

### **4.2.1 Cell lines and cultures**

As detailed in section 2.2.1, Chapter 2.

### **4.2.2 Chromatographic conditions for columns**

As detailed in section 2.2.6, Chapter 2.

### **4.2.3 Data extraction and analysis**

As detailed in section 2.2.9, Chapter 2.

## 4.3 Results

### 4.3.1 Effect of SKi on the lipidome of LNCaP and LNCaP-SK1b cell lines

The effects of SKi on the lipid composition of prostate cancer cells (LNCaP and LNCaP-SK1b cells) were measured using LC-MS based on lipidomics. In order to gain a better understanding of the role of the SK1b in regulating the lipidome, differences in the levels of lipids induced by treating cells with SKi (10 $\mu$ M) were assessed. In this study, combination of MzMine and Microsoft-excel were used for processing the raw data obtained by mass spectrometry, producing thousands of metabolites. The metabolites shown in Error! Reference source not found. **and appendix 2** were identified according to their accurate masses *via* in-house database that used public databases such as KEGG, MassBank, Human Metabolome Database and Lipidmap. Univariate analysis was carried out to describe the data obtained by MzMine after minimising data by excluding unidentified metabolites, metabolites with RSD more than (30%) in pooled samples and unwanted pathways.

Cell populations were counted using a haemocytometer before extraction in order to evaluate the effect of SKi on both cell lines. It was found that the survival rate of LNCaP was somewhat improved compared with LNCaP-SK1b cells. **Table 4-1** and **Figure 4.3-1** show that SKi is more effective in reducing the cell number of LNCaP-SK1b cells compared with LNCaP cells. Thus, SKi reduced the LNCaP-SK1b cell populations by 40-53%, while it reduced the LNCaP cell populations by 19-42%.

Treatment of cells with SKi produced different effects on metabolic pathways in LNCaP-SK1b cells compared with LNCaP cells. The changes were classified according to the class of lipid as shown in Table 4 2. The classes are: (i) sphingolipids; (ii) phosphatidylglycerol (PG) and phosphatidylserine (PS); (iii) phosphatidylcholine (PC); (iv) lysophosphatidylcholine (lysoPC); (v) phosphatidylethanolamine (PE) and phosphatidylinositols (PI); and (vi) fatty acids.

Firstly, Error! Reference source not found. shows that the treatment of LNCaP and LNCaP-SK1b cells with SKi altered sphingolipids, SM and ceramide levels. Importantly, there were differences in sphingolipid composition between the untreated LNCaP-SK1b (C-1b) cells and LNCaP cells (C) and these were also altered by SKi (T-1b/T). For example, the levels of sphingomyelins (SMs) and sphinganine in LNCaP-SK1b cells were lower than in LNCaP cells. This effect was reversed significantly after the treatment with SKi, leading to an accumulation of SMs and other sphingolipids in LNCaP-SK1b cells. This indicates that SKi has a larger effect in LNCaP-SK1b cells. It was also observed that levels of dimethylsphingosine, deoxy sphinganine and long-chain ceramides were higher in LNCaP-SK1b cells compared with LNCaP cells. The levels of these lipids were further increased by SKi in both cell lines.

The abundance of PG and PS species was lower in LNCAP-SK1b cells compared with LNCaP cells. While the treatment of LNCaP cells with SKi reduced the levels of these phospholipids, the opposite effect was seen in LNCaP-SK1b cells, with substantial fold increases being observed. Interestingly, the effects of overexpressing SK1b on PS levels appears to be dependent on the number of carbon atoms present in the PS

species. For example, the overexpression of SK1b reduced PS species with carbon chain length and degree on unsaturation of 32:1, 34:1 and 36:2 chain lengths. In contrast, SK1b overexpression increased the levels of longer-chain unsaturated PS containing 36:3, 38:4 and 40:6 chains. Further increases were observed after the treatment of LNCaP-SK1b with SKi. Another class of lipids that were affected were the PC lipids. In LNCaP cells, the levels of some phosphocholine metabolites increased upon treatment of cells with SKi. These changes were markedly enhanced in LNCaP-SK1b cells.

The treatment of LNCaP cells with SKi altered (both increase and decrease) some lysoPC species. SKi markedly increased the levels of all lysoPC metabolites in LNCaP-SK1b cells compared with LNCaP cells. These included lysoPC (17:0), which was increased by 2-fold in LNCaP-SK1b compared with LNCaP cells. In addition, LysoPC (18:0) was significantly lower by approximately 50% in LNCaP-SK1b cells compared with LNCaP cells. The treatment of LNCaP and LNCaP-SK1b with SKi increased levels of PE, especially ether-PE, and downregulated some PE lipids and had no effect on others. These effects were enhanced by over-expression of SK1b. Ether PE levels were increased more robustly compared with ester PE lipids.

The treatment of LNCaP cells with SKi differentially altered fatty acids and acyl-carnitines metabolites as shown in the **appendix 2**. Five of the 10 detected fatty acids metabolites (e.g. oxooctadecanoic acid, oxo-docosanoic acid, oxo-heneicosanoic acid, hydroxy-tetracosenoic acid and octadecenamide) were significantly increased by SKi. In contrast, SKi treatment of LNCaP cells resulted in a significant reduction of hexadecenoic acid and eicosapentaenoic acid levels. However, in SK1b overexpressed

cells, SKi treatment significantly increased the levels of all the 10 fatty acid species. Interestingly, the overexpression of SK1b alone increased the levels of hexadecenoic acid, oxooctadecanoic acid, oxo-docosanoic acid, oxo-heneicosanoic acid, hydroxy-tetracosenoic acid and eicosapentaenoic acid but reduced markedly octadecenamide. The levels of all fatty acid species, with the exception of eicosapentaenoic acid, were significantly higher in SKi-treated LNCaP-SK1b cells when compared to SKi-treated LNCaP cells. These findings suggest that the overexpression of SK1b further promotes the effects of SKi on fatty acid metabolism.

The treatment of LNCaP cells with SKi altered (both increase and decrease) some acyl-carnitine metabolites. Six of nine metabolites decreased and two increased significantly. In contrast, relative to untreated, SKi markedly increased the levels of all acyl-carnitine metabolites in LNCaP-SK1b cells. Importantly, the levels of three metabolites of acyl-carnitine were also increased significantly in LNCaP-SK1b cells compared with LNCaP cells as shown in the **appendix 2**. For example, both O-hexanoyl-carnitine and O-Butanoylcarnitine levels increased by 2-fold in LNCaP-SK1b compared with LNCaP cells. However, all acyl-carnitine metabolites significantly increased in SKi treated LNCaP-SK1 cells compared with SKi-treated LNCaP cells.

SIMCA-P was used as a tool of data visualisation and statistical analysis, to examine the correlation between samples using the peak intensities of metabolites and classified samples into groups. Principle component analysis (PCA), is an example of unsupervised model, and was able to classify samples into groups. This plot can convert the vast amount and complex data into a simple graph (Prelorendjos, 2014)

and it can be used as the first step in the visualisation of metabolomics data (Kirwan *et al.*, 2012, Trygg *et al.*, 2007). In this study, PCA and OPLS-DA models were used to assess the differences of the lipids in the two cell lines and between treated and untreated cells. Both models gave a clear separation between the treated and untreated cell samples, as shown in **Figure 4.3-2 A and B**. The OPLS-DA model was built on actual values of peak areas of identified metabolites with RSD less than 20% in the pooled sample. The samples were classified into four groups, untreated LNCaP (As-C), treated LNCaP cells (As-T), untreated LNCaP-SK1b (SK1b-C) and treated LNCaP-SK1b (SK1b-T). This model shows a significant separation between the four groups with CV-ANOVA= 2.0263e-006. OPLS-DA model was validated using a permutation test and ROC as shown in **Figure 4.3-2 (C and D)**.

Table 4-1 table shows cell population of untreated and treated LNCaP and LNCaP-SK1b with SKi in two different experiments

Experiment number	LNCaP cells count		Survival rate	LNCaP-SK1b cells count		Survival rate
	Untreated	Treated		Untreated	Treated	
<b>1</b>	$2.25 \times 10^6$	$1.84 \times 10^6$	81%	$0.80 \times 10^6$	$0.48 \times 10^6$	60%
<b>2</b>	$1.82 \times 10^6$	$1.04 \times 10^6$	58%	$2.20 \times 10^6$	$1.03 \times 10^6$	47%

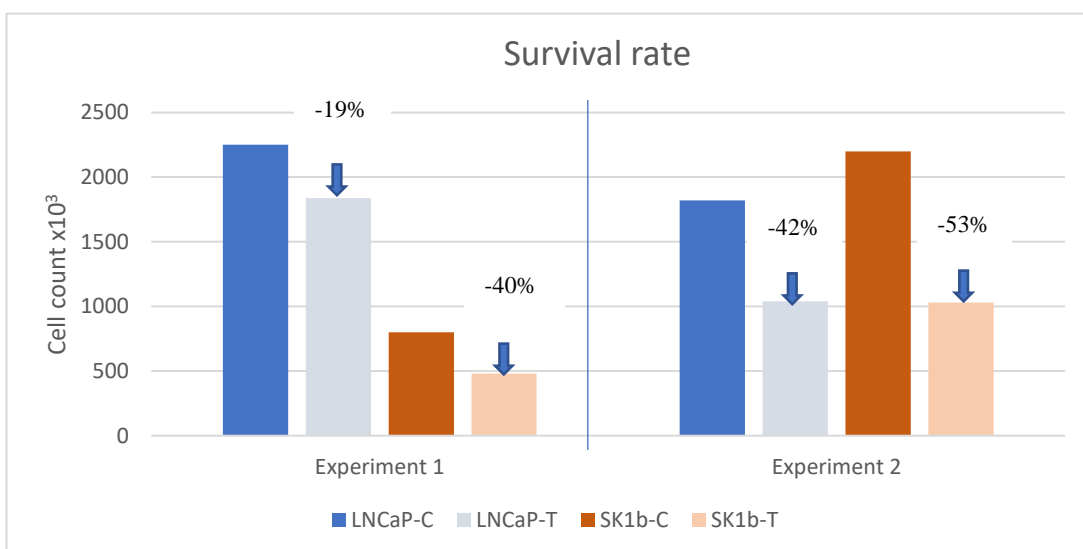


Figure 4.3-1 Bar chart illustrates cell numbers in untreated and treated LNCaP and LNCaP-SK1b cells with 10 $\mu$ M SKi for 24 hours in two different experiments.



Table 4-2 summary of Alterations in lipids metabolites of LNCaP and LNCaP-SK1b cells treated with SKi. Where: (T/C)= treated cells /untreated cells, (C-1b/C)= peak intensity of untreated of (LNCaP-SK1b / LNCaP. (T-1b/T) = peak intensity of treated of (LNCaP-SK1b

Metabolite name	Ratio (treated/untreated)				Ratio (SK1b / LNCaP)			
	(As) (T/C)	P- Value	SK1b (T/C)	P-Value	Ratio C/C	P-Value	Ratio T/T	P-Value
<b>Sphingolipids</b>								
Sphingosine	1.23	ns	4.43	<0.001	1.08	ns	3.90	<0.001
Sphinganine	1.54	<0.001	9.27	<0.001	0.77	ns	4.63	<0.001
N,N-Dimethylsphingosine	1.28	<0.001	1.32	<0.050	3.23	<0.050	3.31	<0.001
1-deoxy-sphinganine	1.19	<0.001	1.63	<0.001	2.96	<0.001	4.05	<0.001
Hexadecasphinganine	1.21	<0.001	1.40	<0.001	2.62	<0.001	3.04	<0.001
SM(d18:0/22:0)	15.2	<0.001	773	<0.001	0.47	ns	24.0	<0.001
SM(d18:1/18:1)	1.03	ns	4.43	<0.001	0.64	<0.050	2.75	<0.050
SM(d18:1/22:0)	1.07	ns	5.49	<0.001	0.71	<0.050	3.68	<0.001
SM(d18:1/23:0)	2.73	<0.050	7.16	ns	1.47	ns	3.86	ns
SM(d18:0/24:1)	0.98	ns	5.95	<0.001	0.81	<0.050	4.93	<0.001
SM(d18:1/24:1)	0.94	ns	4.91	<0.001	0.60	<0.050	3.16	<0.001
Cer (d18:1/20:2)	1.70	<0.050	14.7	<0.05	1.41	0.0242	12.0	<0.050
Cer (d18:1/24:1)	1.91	<0.050	14.3	<0.05	1.78	0.0453	11.6	<0.001
Cer (d18:1/23:1)	1.97	<0.050	15.1	<0.05	1.78	0.0126	12.4	<0.050
<b>PG</b>								
Sn-glycerol-3-phosphate	0.86	ns	4.43	<0.050	0.24	<0.050	1.24	<0.050
PG (30:0)	0.43	<0.001	3.36	ns	0.18	<0.001	2.75	ns
PG (38:4)	0.58	<0.001	1.43	<0.050	0.49	<0.001	1.17	<0.050
PG (36:1)	0.86	<0.050	5.24	<0.050	0.53	<0.005	4.28	<0.010
<b>PC</b>								
PC (36:1)	1.39	<0.001	3.67	<0.001	1.59	<0.005	3.00	<0.001
PC (36:2)	0.88	<0.050	2.29	<0.001	1.14	ns	1.87	<0.001
PC (38:4)	1.39	<0.001	7.20	<0.001	1.13	ns	5.88	<0.001
PC (38:5)	1.68	<0.001	7.89	<0.001	0.74	<0.050	6.44	<0.001
PC (40:2)	0.58	<0.001	1.99	<0.001	1.07	<0.050	1.62	<0.001
PC (40:3)	0.81	<0.001	3.53	<0.001	0.73	<0.005	2.88	<0.001
PC (42:1)	0.37	<0.005	2.05	<0.001	1.64	<0.001	1.67	<0.001
PC (42:2)	0.45	<0.050	1.63	<0.001	1.20	<0.050	1.33	<0.001
PC (42:3)	0.47	<0.050	2.49	<0.001	0.74	ns	2.03	<0.001
<b>Ether-PC</b>								
PC (P-36:0)	0.85	<0.050	3.01	<0.001	0.35	<0.005	2.46	<0.005
PC (P-36:2)	0.97	<0.005	3.18	<0.005	0.85	<0.050	2.60	<0.001
PC (P-36:3)	1.61	<0.001	7.63	<0.001	0.77	<0.005	6.23	<0.001

PC (P-36:4)	4.47	<0.005	13.20	<0.050	1.73	<0.005	10.8	<0.050
PC (P-38:2)	1.20	<0.001	3.95	<0.001	0.55	<0.005	3.22	<0.001
	Ratio (treated/untreated)				Ratio (SK1b / LNCaP)			
Metabolite name	(As) (T/C)	P- Value	SK1b (T/C)	P-Value	Ratio C/C	P-Value	Ratio T/T	P-Value
PC (P-40:5)	1.86	<0.001	10.70	<0.001	0.62	<0.050	8.78	<0.001
<b>Lyso-PC</b>								
LysoPC (17:0)	1.47	<0.050	19.2	<0.050	2.73	<0.050	15.7	<0.050
LysoPC (18:0)	0.71	<0.001	4.01	0.0200	0.46	<0.001	2.67	<0.050
LysoPC (22:1)	0.74	<0.050	6.76	<0.001	1.36	ns	5.52	<0.001
LysoPC (24:0)	0.39	<0.050	6.10	<0.001	0.82	ns	4.98	<0.001
<b>PS</b>								
PS (32:1)	0.39	<0.005	2.09	<0.05	0.73	<0.05	1.71	<0.05
PS (34:1)	0.73	<0.050	3.49	<0.001	0.76	<0.05	2.85	<0.001
PS (36:2)	0.77	<0.05	3.07	<0.001	0.69	<0.05	2.50	<0.001
PS (36:3)	0.87	ns	2.41	<0.005	1.26	<0.05	1.97	<0.005
<b>PE</b>								
PE (36:2)	1.29	<0.001	2.38	<0.001	1.56	<0.001	1.95	<0.001
PE (36:3)	0.69	<0.050	2.34	<0.001	0.96	ns	1.91	<0.005
PE (36:4)	1.24	<0.050	2.97	<0.001	2.12	<0.001	2.43	<0.005
PE (38:4)	1.19	<0.001	2.81	<0.001	1.89	<0.001	2.30	<0.001
PE (40:3)	0.94	<0.050	2.03	<0.001	1.43	<0.005	1.66	<0.001
PE (40:7)	1.68	<0.001	3.75	<0.001	1.75	<0.005	3.06	<0.001
PE (P-34:1)	1.10	<0.050	2.24	<0.001	1.79	<0.001	1.83	<0.001
PE (P-36:4)	1.28	<0.050	2.83	<0.001	1.81	<0.050	2.31	<0.001
PE (P-38:1)	1.37	<0.001	2.49	<0.001	1.44	<0.050	2.03	<0.001
PE (P-38:2)	1.10	<0.050	2.31	<0.001	1.16	ns	1.89	<0.001
PE (P-38:3)	1.40	<0.001	3.43	<0.001	1.17	<0.050	2.80	<0.001
PE (P-38:5)	1.57	<0.001	3.94	<0.001	1.82	<0.050	3.22	<0.001
PE (P-40:3)	1.55	<0.001	4.51	<0.001	0.87	ns	3.68	<0.050
PE (P-40:4)	1.99	<0.001	6.75	<0.001	1.14	ns	5.51	<0.001
PE (P-40:5)	1.88	<0.001	4.66	<0.001	1.68	<0.050	3.81	<0.001

- Appendix 2 shows all results obtained by MzMine with the retention time (RT) and m/z values .

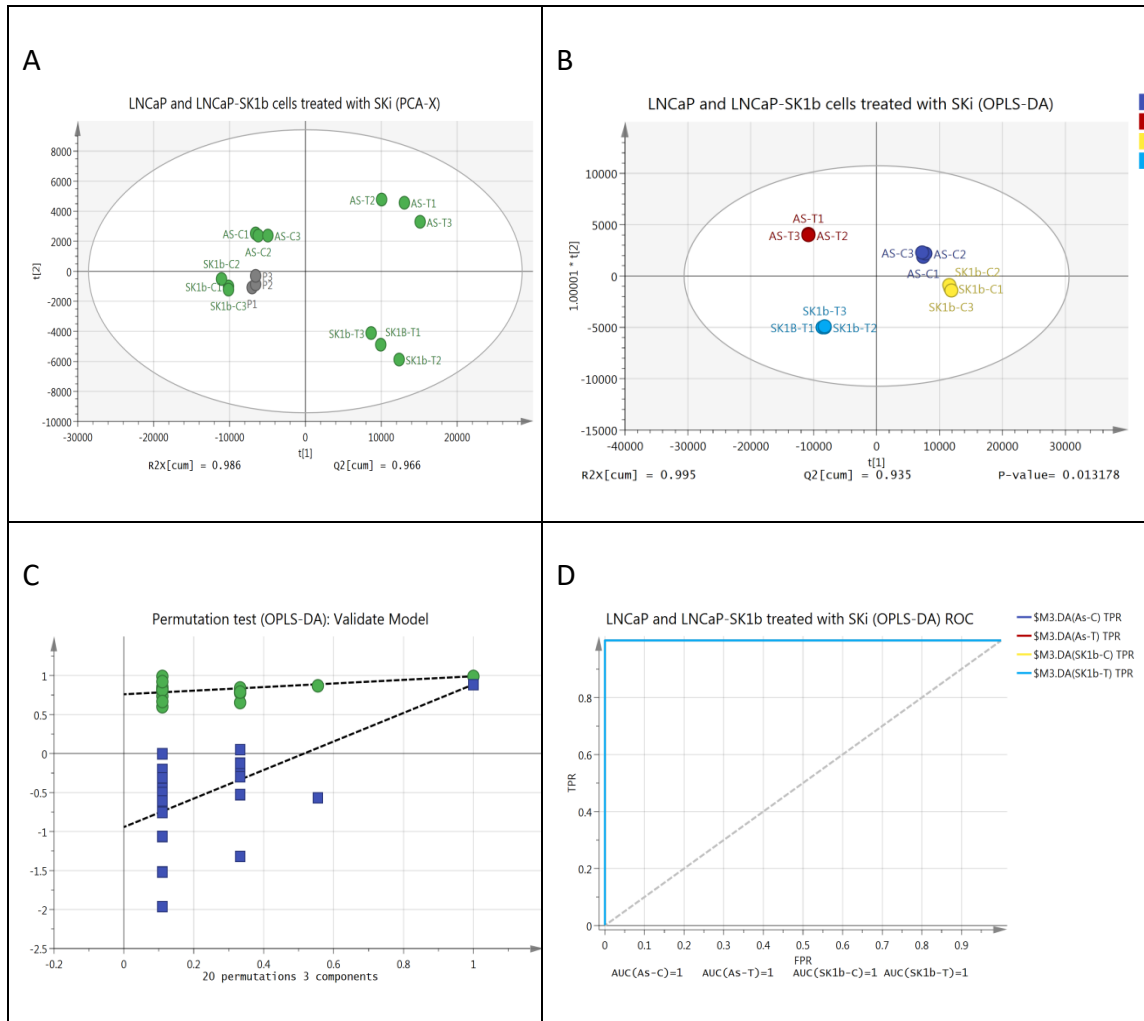


Figure 4.3-2 (A) PCA score plot of LNCaP and LNCaP-SK1b cell lines before and after treatment with SKi with pooled samples (P). (B) OPLS-DA score plot of LNCaP and LNCaP-SK1b before and after treatment with SKi. The groups: As-C= untreated LNCaP cells; As-T= LNCaP treated cells; SK1b-C= untreated LNCaP-SK1b cells; SK1b-T= LNCaP-SK1b treated cells. (C)= Permutation analysis of OPLS-DA model derived from model-B; (D) Receiver Operating Characteristics (ROC) curve shows the sensitivity (true positive rate (TPR)) on the y-axis versus (false positive rate (FPR)) on the X-axis. The area under ROC curve (AUROCC)=1 for MS and C groups.

#### 4.3.2 Effect of ROME on LNCaP and LNCaP-SK1b cell lines

The effects of the SK2 selective inhibitor, ROME on the lipid composition of prostate cancer cells was measured using LC-MS based on lipidomics. In order to gain a better understanding of the role of SK2 in LNCaP and LNCaP-SKb cells, differences in the levels of lipids induced by treatment of cells with ROME (10 $\mu$ M, 24 h) were assessed. This analysis enables the role of SK2 and its functional interaction with SK1b in terms of regulation of the lipidome in LNCaP cells to be investigated.

Initially, cell populations were counted using a haemocytometer before extraction in order to evaluate the effect of ROME on both cell lines. The data in **Table 4-3** demonstrates the effect of ROME is viability more substantial in LNCaP cells compared with LNCaP-SK1b cells (22.5 *versus* 11% loss of cells respectively). The treatment of LNCaP and LNCaP-SK1b cells with ROME produced different effects compared with SKi. Whereas, SKi has more pronounced effects on the lipidome of LNCaP-SK1b cells, ROME was more effective on LNCaP cells.

Table 4-4 shows the metabolic alteration of sphingolipids in both cell lines in response to ROME. Generally, the treatment of LNCaP cells with ROME has a greater impact on the sphingolipid rheostat compared with LNCaP-SK1b cells. For example, ROME induced a larger fold increase in sphinganine, sphingadiene, SM (d18:1/22:0), SM (d18:1/26:1) and some glycosphingolipids levels in LNCaP cells compared with LNCaP-SK1b cells as shown in the **table 4-4**.

Other alterations in some lipid metabolism in both cell lines were observed after the treatment with ROME. The levels of some PC lipids and ether-PC lipids were slightly

increased in both cell lines after the treatment with ROME. Moreover, ROME markedly increase the levels of PS and long-chain PG lipids in both cell lines with a greater effect on the LNCaP cells. Moreover, ROME slightly increase the levels of PE in LNCaP cells and had no effect on these lipids in LNCaP-SK1b cells. A list of the lipid metabolites is shown in Error! Reference source not found.. In this study, PCA and OPLS-DA models were used to assess the difference of the lipids in the two cell lines. Both models gave a clear separation between the treated and untreated samples, as shown in **Figure 4.3-3 (A and B)**. OPLS-DA model was built on actual values of peak areas of identified metabolites with RSD less than 20% in the pooled sample. Observation classified into four groups, untreated LNCaP (As-C), treated LNCaP cells (As-T), untreated LNCaP-SK1b (SK1b-C) and treated LNCaP-SK1b (SK1b-T). This model shows a significant separation between the four groups with CV-ANOVA= 0.00179. OPLS-DA model was validated using a permutation test and ROC as shown in **Figure 4.3-4 (A and B)**.

Table 4-3 cells count in LNCaP and LNCaP-SK1b cells with and without ROME.

LNCaP cells count		Survival rate	LNCaP-SK1b cells count		Survival rate
Control	Treated		Control	Treated	
1.60 x 10 <sup>6</sup>	1.24 x 10 <sup>6</sup>	77.5%	2.92 x 10 <sup>6</sup>	2.60 x 10 <sup>6</sup>	89%

Table 4-4 summary of changes in sphingolipids, other lipids occurred in response to the treatment of LNCaP and LNCaP-SK1b with ROME, where T/C= the ratio of the average amount of a given metabolites in samples from treated cells compared with the average amount of a given metabolite in samples from control cells (n=3),

Metabolite name	M/z	RT (min)	Ratio (T/C)	P-Value	Ratio (T/C)	P-Value
<b>Lipids: Sphingolipids</b>			<b>LNCaP</b>		<b>LNCaP-SK1b</b>	
Sphingosine	300.2895	11.48	1.64	0.0053	1.62	<0.001
Sphinganine	302.3051	12.33	3.20	0.0164	1.66	<0.001
SM(d18:1/18:0)	731.6052	21.41	1.65	0.0284	1.17	0.0291
SM(d18:1/18:1)	729.5893	21.36	1.44	0.0705	1.19	0.0135
SM(d18:1/20:0)	759.6362	21.29	1.90	0.0167	1.36	0.0036
SM(d18:1/22:1)	785.6518	21.15	1.95	0.0148	1.33	0.0029
SM(d18:1/22:0)	787.6674	21.20	2.02	0.0097	1.50	<0.001
SM(d18:1/26:1)	841.7141	21.08	2.78	0.0208	1.15	0.1491
<b>Phosphatidylcholine (PC)</b>						
LysoPC (16:0)	496.3386	22.65	2.46	<0.01	1.26	<0.001
LysoPC (16:0)	496.3386	22.65	2.46	<0.01	1.26	<0.001
PC (30:2)	692.5583	20.58	1.54	<0.05	1.48	<0.001
PC (34:3)	756.5534	19.76	1.64	<0.05	1.14	<0.05
PC (36:1)	788.6163	19.91	1.13	<0.05	1.05	ns
PC (P30:0)	690.5428	20.2	1.33	<0.05	1.31	<0.05
PC (P-32:0)	718.5741	20.16	1.56	<0.05	1.23	<0.01
PC (P-34:0)	746.6051	20.26	1.45	<0.01	1.32	<0.01
PC (P-36:0)	774.6364	20.18	1.45	<0.01	1.27	<0.01
<b>Phosphatidylethanolamine (PE)</b>						
PE (32:2)	688.491	12.45	2.25	<0.01	1.44	<0.001
PE (34:3)	714.5069	12.63	1.67	<0.001	1.13	<0.05
PE (36:4)	740.5213	12.48	1.28	<0.05	1.08	<0.001
PE (36:5)	738.5057	12.47	1.68	<0.001	1.17	<0.001
PE (42:6)	820.5843	12.28	1.15	<0.05	1.08	<0.001
PE (P-36:2)	728.5584	12.58	1.2	<0.05	1.05	ns
PE (P-36:3)	726.5429	12.55	1.24	<0.05	1.01	ns
PE (P-40:2)	784.6199	12.49	1.48	<0.05	1.04	ns

Metabolite name	M/z	RT (min)	Ratio (T/C)	P-Value	Ratio (T/C)	P-Value
<b>Phosphatidylglycerol (PG )</b>						
PG (40:6)	823.5462	3.75	3.37	<0.01	2.82	<0.001
PG (40:7)	821.5308	3.62	3.28	<0.01	2.33	<0.001
<b>Phosphatidylserine (PS)</b>						
PS (34:0)	764.5433	3.85	5.31	<0.01	4.12	<0.001
PS (36:0)	792.5744	3.83	5.58	<0.01	3.35	<0.01
PS (38:0)	820.6060	3.81	3.73	<0.01	2.88	<0.01
<b>Phosphatidylinositol (PI)</b>						
PI (34:0)	837.5521	6.15	2.12	<0.05	1.75	<0.05
PI (36:0)	865.5832	6.11	2.03	<0.01	1.59	<0.05
PI (36:3)	861.5476	5.80	1.79	<0.05	2.05	<0.05
PI (38:2)	891.5932	5.94	1.64	<0.01	1.28	<0.05
PI (38:3)	889.5789	5.71	1.50	<0.01	1.21	<0.05
PI (38:4)	887.5625	5.70	1.32	<0.01	1.24	<0.001

- All results obtained by MzMine are listed in appendix 3 and appendix 4.

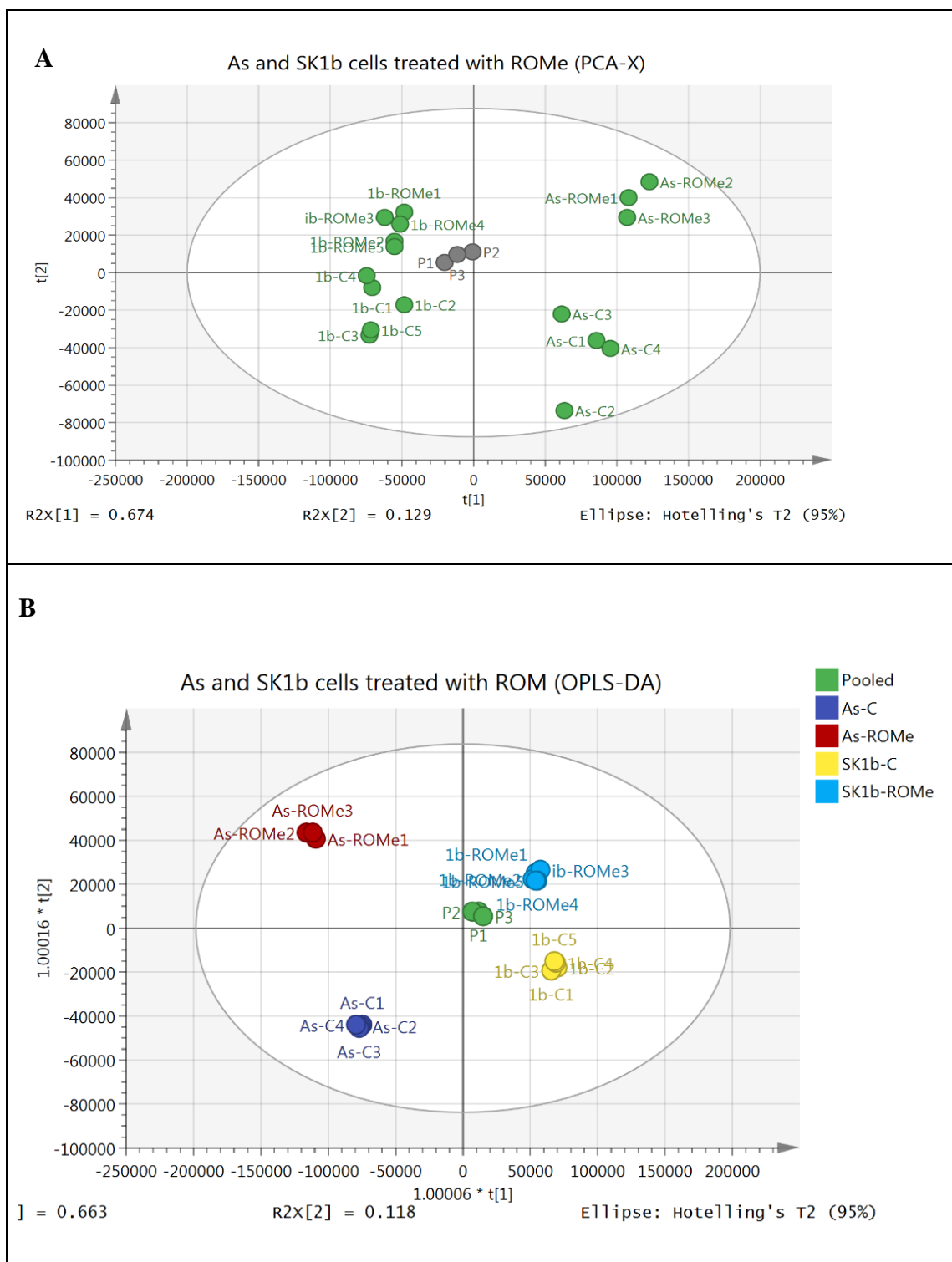


Figure 4.3-3 (A) PCA and (B) OPLS-DA show the separation between LNCaP and LNCaP-SK1b treated with ROME inhibitor. The groups: Pooled (green); As-control (dark blue); As-ROME (red); LNCaP-SK1b control (yellow); LNCaP-SK1b-ROME (bright blue).



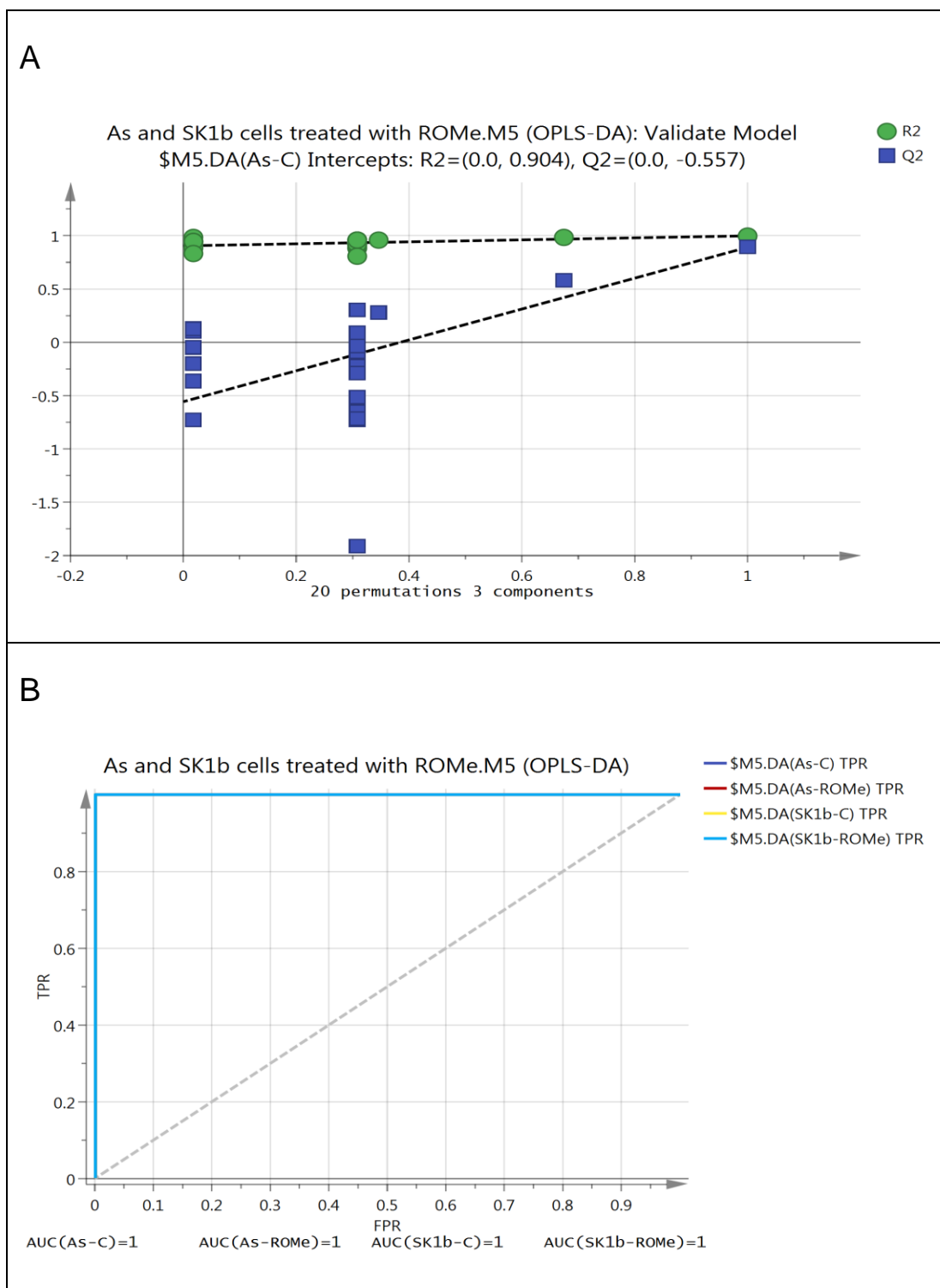


Figure 4.3-4 (A)= Permutation analysis of OPLS-DA model derived from model-B; (B) Receiver Operating Characteristics (ROC) curve shows the sensitivity (true positive rate (TPR)) on the y-axis versus (false positive rate (FPR)) on the X-axis. The area under ROC curve shows the sensitivity (true positive rate (TPR)) on the y-axis versus (false positive rate (FPR)) on the X-axis. The area under ROC curve (AUROCC)=1 for MS and C groups.

## 4.4 Discussion

### 4.4.1 Effect of SKi on the lipidome of LNCaP and LNCaP-SK1b cells

To gain a better understanding of the role of SK1b in prostate LNCaP cells, mass spectrometry in conjunction with LC was used to characterise the lipid profiles of cells over-expressing SK1b. A method to analyse lipids had been developed previously in the Watson group which provides high throughput of information about lipids composition [162]. In addition, ESI-MS has offered a great technique to identify and quantify lipids [163],[164].

Cell counts indicated that the survival rate of LNCaP cells was better compared with LNCaP-SK1b cells in response to SKi as shown in **Table 4-1** and **Figure 4.3-1**. This suggests that SKi induces a stronger apoptotic/senescent effect in LNCaP-SK1b cells compared with LNCaP cells. This observation can be correlated with an alteration in the sphingolipid rheostat as shown in the data in **Error! Reference source not found.** and suggests that SK1b alters flux through this pathway such that its subsequent inhibition by SKi has a greater impact on apoptotic/senescent sphingolipids.

It can be seen from **Error! Reference source not found.** that lower levels of SMs and non-significant changes in sphinganine were observed in LNCaP-SK1b cells compared with LNCaP cells. Therefore, the over-expression of SK1b appears to increase sphingomyelin hydrolysis or inhibit synthesis by sphingomyelin synthase (SMS). In a previous study, it was found that the over-expression of SK1 promotes the conversion of sphingomyelin to SIP through sphingolipid rheostat, thereby impacting proliferation [165]. However, slightly higher levels of apoptotic sphingosine and other ceramides such

as Cer (d18:1/24:1) were also observed. These elevations in ceramide species correlate with the reduction of sphingomyelin and might be expected to increase flux through to the synthesis of S1P, which might then be hydrolysed by S1P lyase at a faster rate due to substrate induction [161]. These observations along with lower levels of SMs in the SK1b overexpressed cells agree with previous studies reporting that SK1 enhances the production of S1P resulting in proliferation and increased tumor grade [27].

Importantly, higher levels of DMS and 1-deoxysphinganine, which have an inhibitory effect on SK enzyme, were detected in the LNCaP-SK1b compared with LNCaP cells. 1-deoxysphinganine can also act as a substrate for ceramide synthase (CerS) [154],[155], which might explain the increase in ceramide levels in SK1b overexpressed cells. The treatment with SKi does not alter DMS levels but led to a modest increase in 1-deoxysphinganine levels. It has previously been shown that SKi inhibits dihydroceramide desaturase (Des1) by promoting its proteasomal degradation in LNCaP-AI cells [131]. This increases the levels of several DHCer species [28]. It should be noted that the treatment of LNCaP-SK1b cells with SKi also results in a substantial increase in the levels of ceramide, which are more robust than in LNCaP cells.

SKi reduces the activity of Des1, resulting in the accumulation of sphinganine (4.6-fold) and SM (d18:0/22:0) (24-fold) and this is more robust in LNCaP-SK1b prostate cancer cells compared with LNCaP cells. Ceramides are converted to sphingomyelins by sphingomyelin synthase (SMS) as summarised in **Figure 4.4-1**. Therefore, the effects of SKi on ceramide levels and the inhibition of Des1 suggest that the major source of ceramide, in this case, is likely from sphingomyelin hydrolysis rather than from *de novo* synthesis.

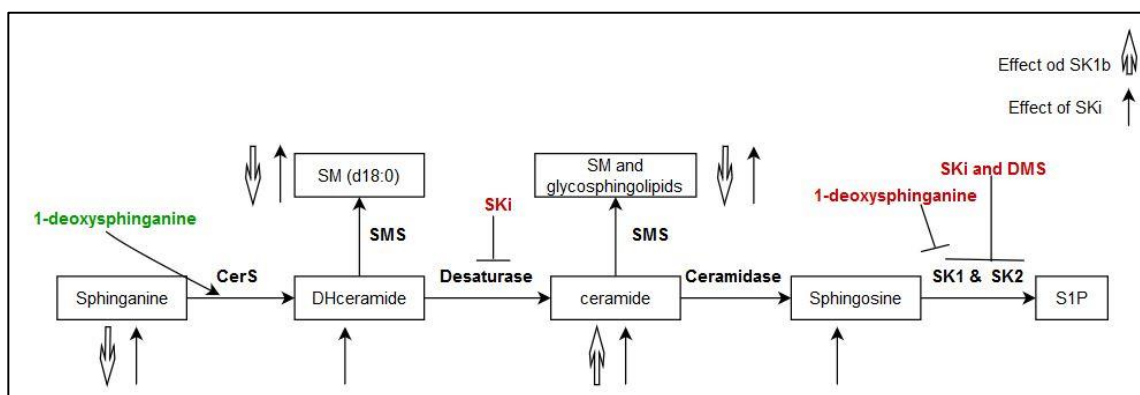


Figure 4.4-1 summaries of the changes occurred on sphingo-bases in the LNCaP cells due to the over expression of SK1b gene then the treatment of LNCaP-SK1b cells with SKi. Where: CerS: ceramide synthase; SMS: sphingomyelin synthase; DMS: dimethylsphingosine.

In this regard, a previous study showed that C22:0 and C24:0 ceramide levels increased in LNCaP cells after the treatment with SKi [28]. Ceramidase 2 (ACER2), which is responsible for the conversion of ceramide to sphingosine, has been found to be upregulated in response to cellular stimuli, such as DNA damage and serum starvation [166]. This enzyme was found to be regulated by p53 and to promote apoptosis by enhancing ROS production [167]. Another study showed that fenretinide, which induces apoptosis in many cancer cells does so by increasing ceramide levels. The current findings are consistent with these studies showing that the levels of sphinganine, which is the precursor for DHCer, are elevated in response to SKi; with a larger effect in LNCaP-SK1b cells compared with LNCaP cells. These findings demonstrate that overexpression of SK1b in LNCaP cells might promote survival by shifting sphingolipid rheostat towards S1P, and that treatment with SKi induces a stronger apoptotic/senescent effect in these cells compared with LNCaP cells. This is possibly due to a more dynamic effect on ceramide biosynthesis. In this regard, S1P has been shown to inhibit CerS2 [168] and

predicted relief of this inhibition by SKi might promote back conversion of sphingosine into ceramide.

A previous study has shown that SK1 and some other lipids kinases, such as phosphatidylglycerol kinase (YegS) and (DGK), exhibit similarity in their amino acid sequences [169], although it is not known whether SKi inhibits these enzymes as an ‘off-target’ effect. In this respect, PG levels were significantly lower in LNCAP-SK1b cells compared with LNCaP cells. A reduction in *sn*-G3P levels in LNCaP cells was also noted, and this was even more robustly reduced in LNCaP-SK1b cells, consistent with SK1b promoting the Warburg effect. In chapter III, we found *sn*-G3P levels are upregulated through glycolysis after the treatment of LNCaP-AI cells with SKi. It has also been reported that SKi fails to increase p53 expression in LNCaP cells but does increase p53 in LNCaP-AI cells, suggesting that oxidative stress is likely reduced in LNCaP cells compared with LNCaP-AI cells [74]. Here, we found a stronger accumulation of *sn*-G3P levels in LNCAP-SK1b cells in response to SKi compared with LNCaP cells. Therefore, these findings suggest that inhibition of SK in LNCAP-SK1b cells might result in a stronger *sn*-G3P-induced oxidative stress response, possibly mediated by a more profound impact of SKi on the Warburg effect in LNCaP-SK1b cells.

The levels of PC, PI, lysoPC, PE and PS were increased in SKi-treated LNCAP-SK1b cells. The changes in phospholipid levels might be through alterations in S1P levels. In this case, S1P is known to activate phospholipase C (PLC) in hepatocytes [170] and many solid tumors [171] via S1P receptor-dependent mechanisms. PLC catalyzes the hydrolysis of PC and PI to form diacylglycerol (DAG) [172],[173]. PC lipids also donate the

phosphorylcholine headgroup to ceramide to form sphingomyelins and to additionally produce DAG, catalyzed by sphingomyelin synthase [174]. Previous studies have also shown that the activity of PLA<sub>2</sub> to form lysolipids is regulated by complex sphingolipids such as sphingosine and ceramide, which activate the release of fatty acids from these phospholipids [175]. The overexpression of SK1b in LNCaP-SK1b cells might increase S1P levels more robustly compared with LNCaP cells and thereby increase the hydrolysis of PC and PI lipids via an autocrine loop involving the release of S1P from cells and activation of S1P receptors. However, the levels of PC lipids were not decreased in the LNCaP-SK1b cells. This might indicate that the re-synthesis rate in LNCaP-SK1b cells is faster than in LNCaP cells and when SK1 and S1P are inhibited by SKi, the lipids accumulate because the breakdown is reduced while re-synthesis is maintained. Since the treatment with SKi is predicted to reduce the S1P levels more robustly in LNCaP-SK1b cells due to abrogating increased flux through the sphingolipid rheostat, this might explain why PC and PI levels are increased more robustly in these cells compared with LNCaP cells. A similar effect might impact S1P receptor-dependent regulation of PLA<sub>2</sub>, thereby affecting lysolipids in a similar manner. LysoPC and fatty acids are synthesized from PC hydrolysis by phospholipase-A<sub>2</sub> (PLA<sub>2</sub>) and the accumulation of lysoPC promotes apoptosis by stimulating caspase-3 activation [167].

LysoPC species are known as metabolic biomarkers for apoptosis [176]. This agrees with a model in which SKi promotes apoptosis through multiple signaling pathways that might involve these lysolipids. LysoPC has also been shown to promote ROS accumulation, which induces apoptosis via cytochrome c release [177]. Here, we found that LysoPC (18:0) levels are 2-fold higher in LNCaP-SK1b cells compared with LNCaP cells. In

addition, lysoPC also promotes phagocytosis by binding and recruiting phagocytes to apoptotic cells [178]. Therefore, SKi appears to reprogram cellular metabolism to alter apoptosis.

Alterations in PI lipids were also observed with higher levels in LNCaP-SK1 cells compared with LNCaP cells and this was enhanced by SKi. Again, this might be consistent with changes in PLC regulation by S1P. It was also observed that the effects of overexpressing SK1b on PS levels were dependent on the number of carbon atoms present in the PS. For example, the overexpression of SK1b reduced PS metabolites that have between 32:1 and 36:2. In contrast, SK1b increased the levels of PS lipids containing 36:3 to 40:6. The exact mechanism promoting changes in these lipids in response to the SKi or the overexpression of SK1b requires further investigation.

Exogenous ether phospholipids have been shown to have anti-tumor activities [179]. It has been suggested previously by Watson et al (2013) and in chapter III that SKi inhibits glycolysis and the PPP which leads to the accumulation of GSSG and an increase in ROS levels. Because of the inhibitory effect of SKi on PPP, the major source for NADPH, the result presented herein suggests that inhibition of SK1b with SKi reprograms metabolism to generate another endogenous ROS scavengers, which are the ether phospholipids. This route could disturb the phospholipid composition [180] and activate ER stress leading to apoptosis [172, 173]. This possibility requires more investigation because ER stress is involved in several pathways, such as the generation of ATP through mitochondria metabolism and as a precursor for glycerophospholipids. The exact mechanism of ether lipids accumulation remains unclear. It is possible that the treatment of LNCaP-SK1b cells

with SKi increases cellular ether lipids from cytosolic DHAP. This may promote apoptosis as a result of enhanced mitochondrial-dependent lipid metabolism.

Generally, ether lipids play an important role in cell membrane integrity [182], which can affect membrane fluidity and fusion [183]. They are also involved in various cellular functions such as differentiation and cellular signaling. Cytosolic DHAP is a precursor for ether lipids biosynthesis, which occurs in the peroxisomes [184]. The current finding might suggest that the accumulations of ether lipids could be as a result of the enhancement of DHAP – *sn*-G3P conversion, consequently, increasing the synthesis of ether-lipids.

The roles of fatty acids have not been fully elucidated. However, some of fatty acid metabolites are critical regulators of cell functions, such as proliferation and the regulation of oxidative stress. For example, arachidonic acid is involved in cellular inflammation. SK1b overexpression led to the reduction of some fatty acid metabolites. Therefore, LNCaP-SK1b cells are more sensitive to the effects of SKi on fatty acid metabolites. It will be interesting to further study how changes in fatty acid metabolites affect cellular functions.

#### 4.4.2 Effect of ROME on LNCaP and LNCaP-SK1b cell lines

The multivariate analysis techniques used in this study included PCA and OPLS-DA. A good clustering in the pooled sample showed on a PCA score plot indicate the high precision of the LC-MS. It is also revealed a good separation between the two cell lines and between controls and treated cells. A clear separation of ROME-treated LNCaP and LNCaP-SK1b cells, and their respective untreated controls, was achieved indicating



different profiles for the treated and untreated cells on an OPLS-DA scores plot. Clustering of each group in both score plots indicates a good sample preparation and extraction.

There was a larger decrease in the viability of LNCaP cells in response to ROME (10 $\mu$ M, 24 h) compared with LNCaP-SK1b cells. Therefore, the survival of LNCaP cells was enhanced by overexpression of SK1b.

Sphingosine is phosphorylated by SK1/SK2 in the sphingolipid rheostat and sphinganine is converted to sphinganine 1-phosphate in the *de novo* ceramide synthesis pathway. The effects of ROME on sphingolipids were more robust in LNCaP cells compared with LNCaP-SK1b cells, suggesting that SK1b provides some protection to the sphingolipid changes induced by inhibiting SK2. This suggests that there might be some overlap in the pools of sphingolipid that can be regulated by SK2 and SK1. However, access of the subsequently formed SIP/ceramide in terms of regulating other lipidomic changes, such as phospholipids and lysophospholipids appears restricted and determined by SK isoform selectivity. ROME has previously been shown to stimulate autophagy, while SKi inhibits autophagy [5], suggesting opposing role for SK1 and SK2. These findings indicate that the distinct lipid profiles induced by SKi and ROME might be linked with different biological outcomes.

#### **4.5 Summary**

In conclusion, this study shows that SK1b and SK2 appear to regulate flux through the sphingolipid pathway. Treatment with SKi modulated the levels of SM, ceramides, lysoPC and PC more robustly in LNCaP-SK1b cells compared with LNCaP cells and this was

linked with a stronger apoptotic effect. On the other hand, ROME, elevated sphingosine significantly but had a weaker effect on other lipids such as SM, PCs and lysoPC. This was more robust in LNCaP cells compared with LNCaP-SK1b cells, suggesting that SK1b and SK2 are functionally linked.

## **Chapter V**

---

**Metabolomic Profiling of the Effects of Different SK  
Inhibitors on LNCaP-AI and LNCaP-SK1b Prostate  
Cancer Cells Using Mass Spectrometry**

## 5 Metabolomic Profiling of the Effects of Different SK Inhibitors on LNCaP-AI and LNCaP-SK1b Prostate Cancer Cells Using Mass Spectrometry.

### 5.1 Introduction

Prostate cancer is one of the most diagnosed cancers in men and responsible for over 10000 deaths per year in the UK [185]. Early diagnosed prostate cancer can be treated using androgen ablation therapy and/or radiotherapy and/or chemotherapy. However, the majority of patients with prostate cancer become resistant to these approaches of treatment after a period of time, by developing a new type of cells that grow independently of androgen, termed LNCaP-AI [186]. The treatment of these cells is challenging as they failed to respond to anti-androgen therapy because they grow independently of androgen [160]. Growing evidence has demonstrated several mechanisms that could be involved in resistance, for example; drug-detoxifying mechanisms, gene expression which could lead to acquiring the ability to evade drug-induced apoptosis [187],[188]. A good example related to our study is that androgen-independent prostate cancer evades the proteasomal degradation of SK1b when SKi, a dual inhibitor, is used as a treatment, causing cell senescence [131]. Therefore, a new therapy innovation required to overcome the drug resistance, poor prognosis and spread of these cells. Therefore, it is necessary to develop innovative therapeutic strategies to overcome the limitations of current therapy.

Sphingosine Kinase (SK) functions were initially thought to be limited to sphingolipid metabolism after sphingosine was discovered and isolated in the 18<sup>th</sup> century [189]. SK was later suggested to regulate other cellular functions after it was reported that sphingolipids are critical metabolic-regulators involved in the immune response, cell

differentiation and platelet functions [190],[191]. SK has two isoforms which are responsible for phosphorylating sphingosine but they differ in their enzyme kinetic properties and spatial distribution, therefore, each isoform has a distinct physiological function [192]. These initial studies opened research into the molecular characterization and sequencing of the two isoforms SK1/2 which led to interests in the development of SK inhibitors [193], [194], [195].

SK inhibitors were initially developed as sphingosine analogues and were demonstrated to actively compete with sphingosine substrates hence targeting and blocking both SK1 and SK2. Sphingosine-based inhibitors have been grouped based on the composing backbone such as sphingoguanidine, amidine, bicyclic aryl and amino-alcohol [196]. However, ‘off-target’ effects and low specificity of these inhibitors have been widely reported [196], [131]. These limitations led to the development of small-molecule inhibitors with better specificity for SK. For example, lipidic small molecule inhibitors such as MP-A08 specifically bind to the ATP-binding pocket of SK1/2 [197] and non-lipidic small molecule inhibitors such as SKI-I, SKI-II, SKI-III and SKI-IV had similar mechanisms [198], [70], [199], [200], [201].

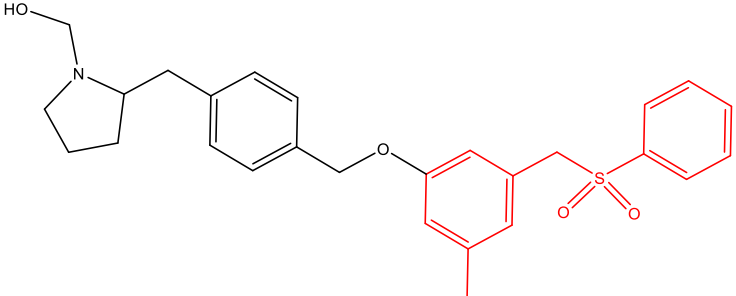
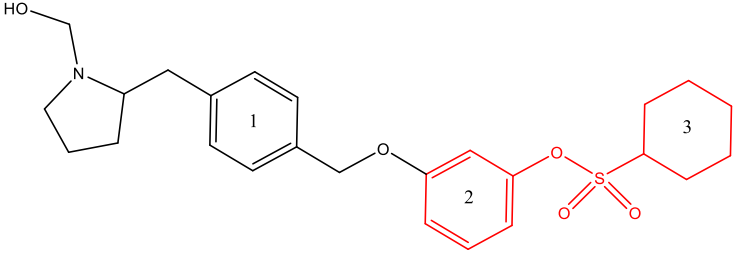
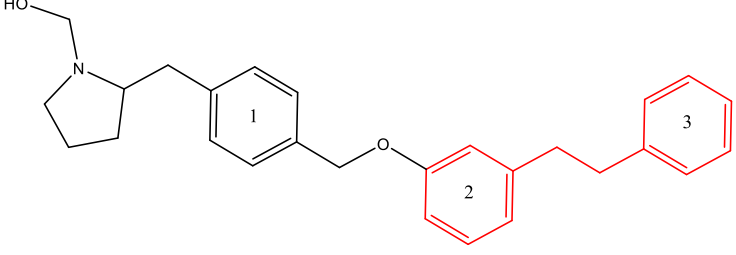
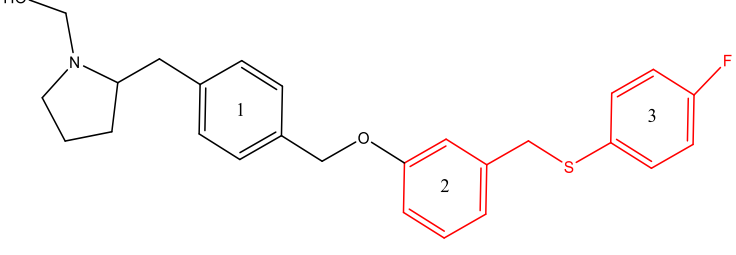
Moreover, some of these small molecule inhibitors such as SKI-II inhibit cellular processes such as the lysosomal degradation pathways [199] hence promoting the exploration of novel inhibitors as used in this thesis. Utilising a rational structure-based approach, in-depth analysis of the residues in the J-channel region of SK1 and SK2 coupled with the co-crystal structure of PF-543/SK1 highlighted subtle differences in the J channel regions between SK1 and SK2. These include that the toe region of the J-channel

extends further in SK2 relative to SK1. Also, SK2 has a slightly wider J-channel throat region relative to SK1. These were used to create new analogues PLR24, ST55 and ST81 as a result of modifications in the hydrophobic tail regions of PF-543, as shown in **Table 5-1**, *via* a synthetic process producing the new inhibitors with different potency and/or selectivity relative to PF-543. ST55 varied from PF-543 in the loss of the methyl group on the ring 2 and convert the ring 3 from benzene to cyclohexane ring, which increases the selectivity for SK1.

In PLR24, the entire methyl ((phenylsulfonyl)methyl)benzene tail group from PF-543 was replaced with a 1,2-diphenylethyl group resulting in a non-selective inhibitor probably as a result of the reduction in the overall length of the molecule. In ST81, the entire methyl((phenylsulfonyl)methyl) benzene tail group from PF-543 was replaced with a (4-fluorobenzyl)(phenyl) sulfane group resulting in a SK2 selective inhibitor probably as a result of the presence of the fluorine in the para position in ring 3, which increase the overall length and its ability to form halogen bond interactions.

Because of the accumulated evidence of the involvement of SK in cancer, many of SK inhibitors have been prepared to reduce cell survival, which has a great success rate with prostate cancer [202]. Therefore, the current study explored the metabolome, particularly sphingolipids, of androgen-independent LNCaP-AI and LNCaP-SK1b prostate cancer cells using different types of SK inhibitors which target SK1, SK2 and dual SK1/2 inhibitor (Table 5-1).

Table 5-1 information of inhibitors used in this experiment

Inhibitor name	Pharmacological action	Structure formula
PF-543	SK1 –selective  M.Wt: 465	
ST55	SK1 –selective  M.Wt: 459.60	
PLR24	Non-selective  M.Wt: 401	
ST 81	SK2- selective  M.Wt: 437	

## 5.2 Materials and Methods

### 5.2.1 Cell lines and cultures

Cell lines used in this experiment were LNCaP-AI and LNCaP-SK1b cell lines

As detailed in section 2.2.1, Chapter 2.

### 5.2.2 SK inhibitors

Inhibitor name	PLR24	ST55	ST81
Concentration	1 $\mu$ M	100 nM	1 $\mu$ M

### 5.2.3 Chromatographic conditions for columns

Bare silica gel column method was used in the current study as detailed in section 2.4.1

### 5.2.4 Data extraction and analysis

As detailed in section 2.2.9, chapter 2.

## 5.3 Results

### 5.3.1 Effect of new sphingosine kinase inhibitors (SKIs) on LNCaP-SK1b cells.

The multivariate analysis techniques used in this study included PCA and OPLS-DA score plots. Supervised OPLS-DA model **Figure 5.3-1, A** showed a clear separation between the control and treated LNCaP-SK1b samples with the SK1/SK2 inhibitor, PLR24



Separation between the control and treated samples with selective inhibitors, ST55 and ST81 were noted but the metabolomics changes with these inhibitors were similar or there were small variations between them. The validity of this model was tested using a permutation test (**Figure 5.3-1, B**). An unsupervised HCA model **Figure 5.3-2** was used as a clustering analysis tool in order to find a natural grouping of the data. It can be seen that there is a clear separation and between treated LNCaP-SK1b cells with PLR24 and other groups, while the treated cells with ST55 and ST81 had the lowest variations between groups. However, a separation was noted between cells treated with selective inhibitors and untreated samples. The OPLS-DA model parameters and validation of the plot suggested a strong model (R2X (cum) 0.950, Q2 (cum) 0.904) and the CV-AVOVA for this model was ( $< 0.001$ ).

**Table 5-2** shows the metabolic alterations in LNCaP-SK1b cell lines in response to PLR24, ST55 and ST81. It can be seen that levels of six sphingolipid metabolites were increased in response to all the inhibitors. The increase in the levels of sphingoid bases indicate that there is a perturbation of the sphingolipid rheostat. It was noted that ST55 had the weakest effect in LNCaP-SK1b cells and is consistent with the possibility that over-expression of SK1b can dampen the effect of the selective SK1 inhibitor. Significant increases in phosphoethanolamine levels were also observed with the use of the inhibitors, suggesting that the inhibition of SK1 might increase phosphatidylethanolamine hydrolysis.

The SK inhibitors increased the levels of all of the fatty acids in LNCaP-SK1b cells. For example, linolenic acid levels increased significantly by at least 5.8-fold in response to

PLR 24, 6.78-fold in response to ST55 and 7.2-fold in response to ST81. Fatty acids are important molecules in the cell signaling that can induce apoptosis. The levels of acyl-carnitine metabolites were lowered in the SKIs-treated cells.

LysoPC levels increased in response to SK inhibitors, and in particular to ST55. PLR24 has the weakest effect on LNCaP-SK1b cells. For example, lysoPC (20:0) levels were increased by approximately 5.6-fold in response to ST55 and 2.2-fold in response to PLR24. For some classes such as PC, ether-PC, ether-PE and PE only weak effects were observed or there was no effect on lipid compositions in these classes in response to the different SK inhibitors. The SK inhibitors produced clear increases in the levels of PG and PS lipids.

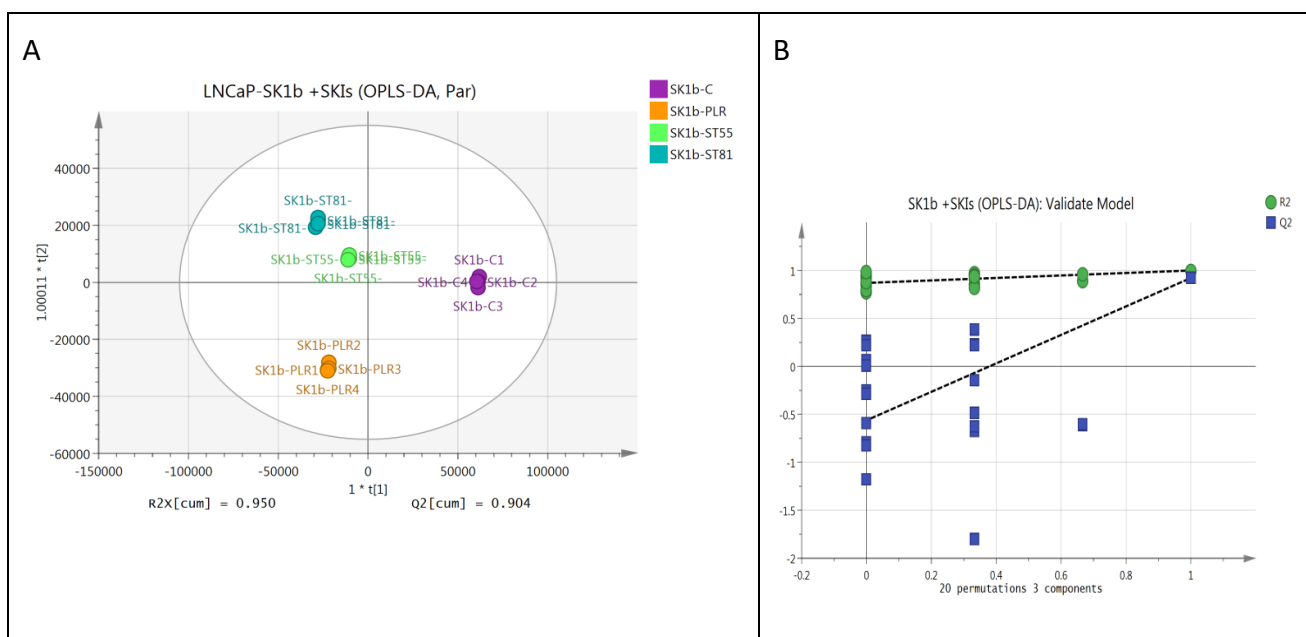


Figure 5.3-1 (A) OPLS-DA model for SK1b cells and (B) permutation test

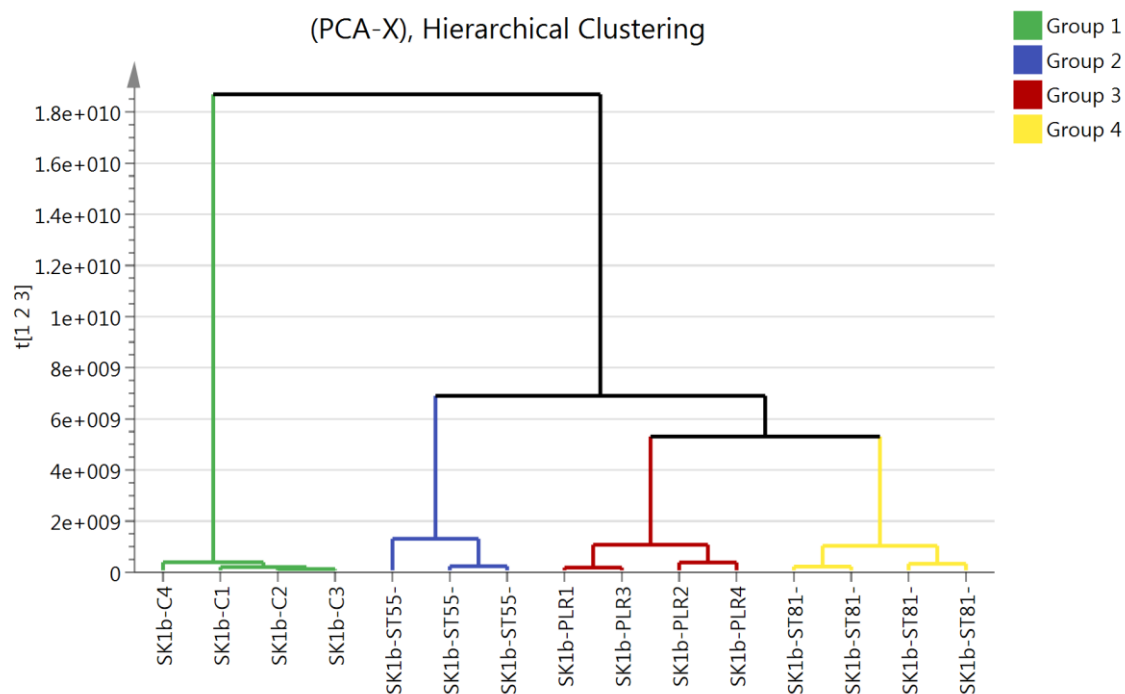


Figure 5.3-2 HCA analysis of 16 prostate cancer LNCaP-SK1b samples. It shows two main groups and four sub-groups. The groups: Group 1 (green), control of LNCaP-SK1b cells; Group 2 (blue): ST-55-treated LNCaP-SK1b cells; Group3 (red): PLR24-treated LNCaP-SK1b cells; Group 4 (yellow): ST-81-treated LNCaP-SK1b cells.

Table 5-2 summary of the effect of different inhibitors, non-selective (PLR24), and SK II selective (ST55 and ST81) on LNCaP-SK1b cells using Silica gel conjugated with high resolution mass spectroscopy. Where ratio represent the mean of the intensity of treated cells / the mean of the peak intensity of untreated cells.

Met name	RT	M/Z	Ratio PLR	Ratio-ST55	Ratio ST81	PLR	ST55	ST81
Shphingolipids								
Sphingobase			Treated/ untreated LNCaP-SK1b cells			P-Value		
Sphingosine	12.28	300.2891	4.96	3.88	5.82	<0.001	<0.01	<0.001
Sphinganine	12.89	302.3045	4.4	3.42	5.24	<0.001	<0.01	<0.001
N,N-Dimethylsphingosin	12.23	328.3203	19.27	13.33	18.85	<0.001	<0.01	<0.001
sphingadienine	12.02	298.2734	6.23	4.61	7.14	<0.001	<0.01	<0.001
Ceramides								
Cer(d18:0/22:0)	7.41	624.6294	1.92	1.76	2.81	ns	<0.05	<0.05

Met name	RT	M/Z	Ratio PLR	Ratio- ST55	Ratio ST81	PLR	ST55	ST81
<b>Cer(d18:1/18:1)</b>	<b>3.84</b>	<b>564.5346</b>	<b>1.63</b>	<b>1.07</b>	<b>1.31</b>	<b>&lt;0.05</b>	<b>ns</b>	<b>&lt;0.05</b>
SM(d18:1/18:1)	22.3	729.5895	1.37	1.16	1.25	<0.001	ns	<0.05
<b>Cer(d18:1/18:0)</b>	<b>4.41</b>	<b>566.5508</b>	<b>1.91</b>	<b>1.63</b>	<b>1.99</b>	<b>&lt;0.05</b>	<b>&lt;0.05</b>	<b>&lt;0.05</b>
SM(d18:1/18:0)	22.33	731.6049	1.51	1.26	1.39	<0.05	ns	<0.05
Glucosylcer (d18:1/18:0)	4.4	728.604	1.33	1.01	1.27	<0.05	ns	ns
LacCer(d18:1/18:0)	4.89	890.6564	1.85	1.78	2.33	<0.05	<0.05	<0.05
<b>Cer(d18:1/20:0)</b>	<b>5.31</b>	<b>594.5822</b>	<b>2.68</b>	<b>2.17</b>	<b>2.54</b>	<b>&lt;0.05</b>	<b>&lt;0.01</b>	<b>&lt;0.001</b>
<b>Fatty acids</b>								
Linolenic acid	4.1	277.217	5.79	6.78	7.2	<0.050	<0.001	<0.001
Linoleate	4.21	279.233	3.07	3.26	3.47	<0.001	<0.01	<0.001
Dihomo- linolenate	4.14	305.249	2.01	1.92	2.15	<0.050	<0.01	<0.001
<b>Fatty acyls -Carnitines</b>								
O-Butanoylcarnitine	27.3	232.155	0.75	0.6	0.65	<0.001	<0.001	<0.001
O-decanoyl-carnitine	24.57	316.248	0.56	0.47	0.5	<0.001	<0.001	<0.001
O-Palmitoyl-carnitine	23.61	400.341	0.76	0.65	0.65	<0.05	<0.001	<0.001
<b>LysoPC</b>								
LysoPC (18:0)	23.31	524.371	1.76	3.96	2.36	<0.001	<0.01	<0.001
lysoPC (20:0)	23.08	552.402	2.28	5.64	3.98	<0.001	<0.001	<0.001
LysoPC (20:1)	23.14	550.386	1.73	3.72	2.74	<0.001	<0.01	<0.001
LysoPC (22:1)	22.89	578.417	2.76	8.15	6.25	<0.001	<0.01	<0.001
<b>Phosphatidylcholine (PC)</b>								
PC (38:1)	20.79	816.648	1.21	1.2	1.27	<0.001	<0.01	<0.001
PC (30:2)	21.65	692.558	1.58	1.92	1.91	<0.05	<0.01	<0.001
PC (32:2)	21.60	720.589	1.89	2.11	2.35	<0.05	<0.05	<0.05
<b>Ether-PE</b>								
PE (P-38:1)	13.64	758.605	1.39	1.26	1.65	<0.05	ns	<0.05
PE (P-40:1)	13.80	786.636	1.64	1.56	1.75	<0.05	ns	<0.05
PE (P-40:2)	13.46	784.62	1.2	1.13	1.42	<0.05	ns	<0.05
PE (P-40:3)	13.33	782.605	1.19	1.14	1.29	<0.05	ns	<0.001

### 5.3.2 Effect of SKIs; namely, PLR24, ST55 and ST81 inhibitors on LNCaP-AI cell lines

**Figure 5.3-3** showed a clear separation between the LNCaP-AI treated with and without the nM potent SK1/SK2inhibitor, PLR24. The effect of the SK1 inhibitor, ST55 and the selective SK2 inhibitor, ST-81 on metabolic changes were similar with relatively small differences. Therefore, an unsupervised HCA model **Figure 5.3-4** was used as a clustering analysis tool in order to find a natural grouping of the data. It can be seen that there is a clear separation and between PLR24-treated LNCaP-AI cells with other groups. While the treated cells with ST55 and ST81 had the lowest variations between groups there are some differences. The OPLS-DA model parameters and validation of the plot suggested a strong model (R2X (cum) 0.965, Q2 (cum) 0.963) and the CV-AVOVA for this model was (< 0.0000). The validity of this model was tested using ROC and permutation tests **Figure 5.3-5, A** and **Figure 5.3-5, B**.

Lipids were extracted from 16 samples, four replicates of each condition, using the optimised extraction procedure that cover a wide range of lipids in the non-polar extraction and using a silica gel column for separation coupled with high-resolution mass spectroscopy (HRMS),.

The alteration of lipids between treated and untreated cells would be expected since cell death might be observed as a result of an accumulation of ceramides, SMs, and lipids formed in other metabolic pathways. The main interest of this study was to measure changes in lipids in response to the inhibitors, especially in the sphingolipid pathway. Error! Reference source not found. shows the metabolic alterations in LNCaP-AI cell lines i n response to PLR-24, ST-55 or ST-81. It can be seen that levels of six out of eight

sphingolipid metabolites were increased in response to all the inhibitors. The elevations of sphingoid bases after treating cells indicate that these inhibitors successfully blocked flux through the sphingolipid rheostat. For example, the treatment of LNCaP-AI cells with the inhibitors induced an increase in sphingosine, sphinganine, sphingodienes and dimethylsphingosine levels,

Generally, the treatment of LNCaP-AI cells with 10  $\mu$ M (24 h) PLR24 or ST55 increased the levels of ceramides, SMs and sugar-ceramides (e.g: glucosylceramide or lactosylceramide) with a stronger effect of PLR24. The treatment with SK2 inhibitor (ST81) had no effect on ceramide, such as DHcer 22:0; Cer (d18:1/22:0) and Cer (d18:1/26:1), or weak effects such as on Cer (d18:1/18:1) and Cer (d18:1/18:0). Therefore, the effect on SMs and glucosylceramides had the same trend as ceramides with the exception of long-chain SM and glucosyl-ceramide (C=20:0 and C26:1).

The treatment of LNCaP-AI cells with these inhibitors increased the majority of the fatty acids with the exception of tridecadienoic acid, oxo-hexadecanoic acid and FA (12:3). It is also noted that PLR24 had the strongest effect on fatty acids. The treatment of LNCaP-AI cells with PLR24 increased the levels of some acyl-carnitine metabolites, while O-Propanoylcarnitine and O-Butanoylcarnitine levels decreased when the cells were treated with ST55 and ST81.

The levels of lysoPCs were increased in response to inhibitors with the strongest effect exhibited by ST-55, suggesting a prominent role for SK1. For example, lysoPC (20:0) and lysoPC (22:0) levels were increased by approximately 8-fold and 29-fold in response to ST-55. Modest changes in PC, PG and PS levels with ST-55 and PLR-24 were observed,

while ST-81 induced considerably weaker responses, suggesting a predominant role for SK1. The levels of PE lipids were modestly increased in response to PLR24, while ST55 and ST81 were without effect suggesting that PE is controlled by SK1 and SK2. An increase in ether lipids was observed in LNCaP-AI cells treated with PLR24, while the levels of these lipids were not altered in response to ST-55. A significant decrease in the levels of long-chain ether-PC such as PC (P-38:2) and PC (P-38:3) was observed with the selective inhibitors.

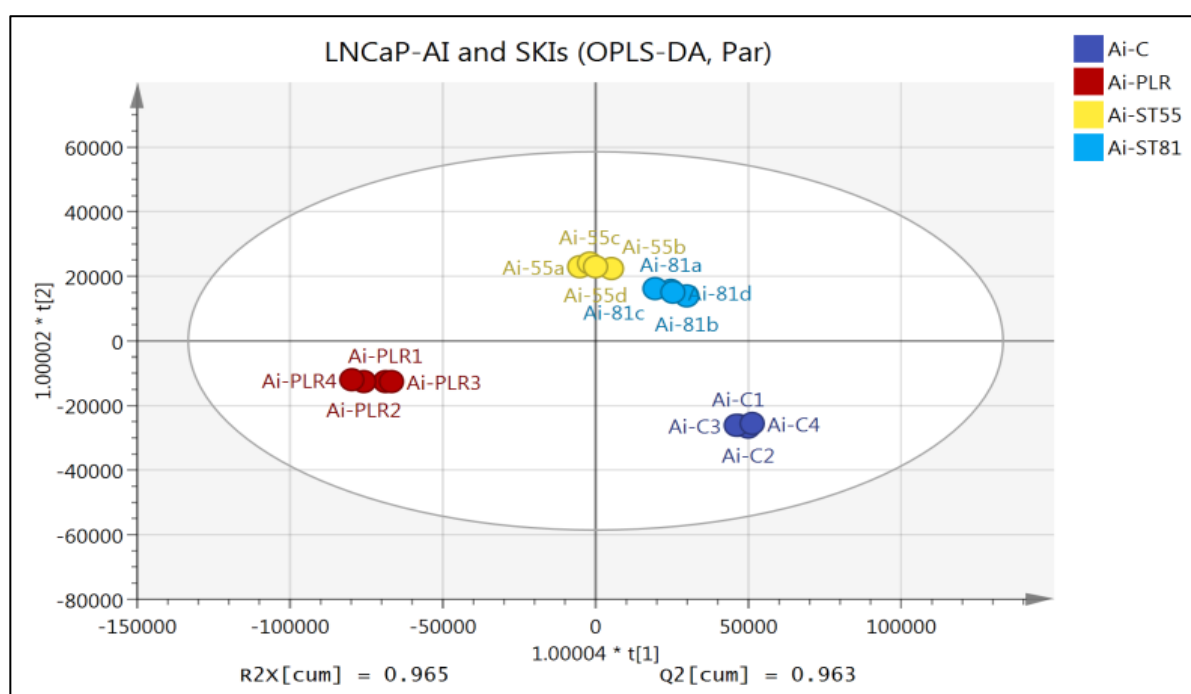


Figure 5.3-3 OPLS-DA model of androgen independent (LNCaP-AI) prostate cancer cells treated with SKIs, PLR24 (red); ST55 (yellow) and ST81 (bright blue).

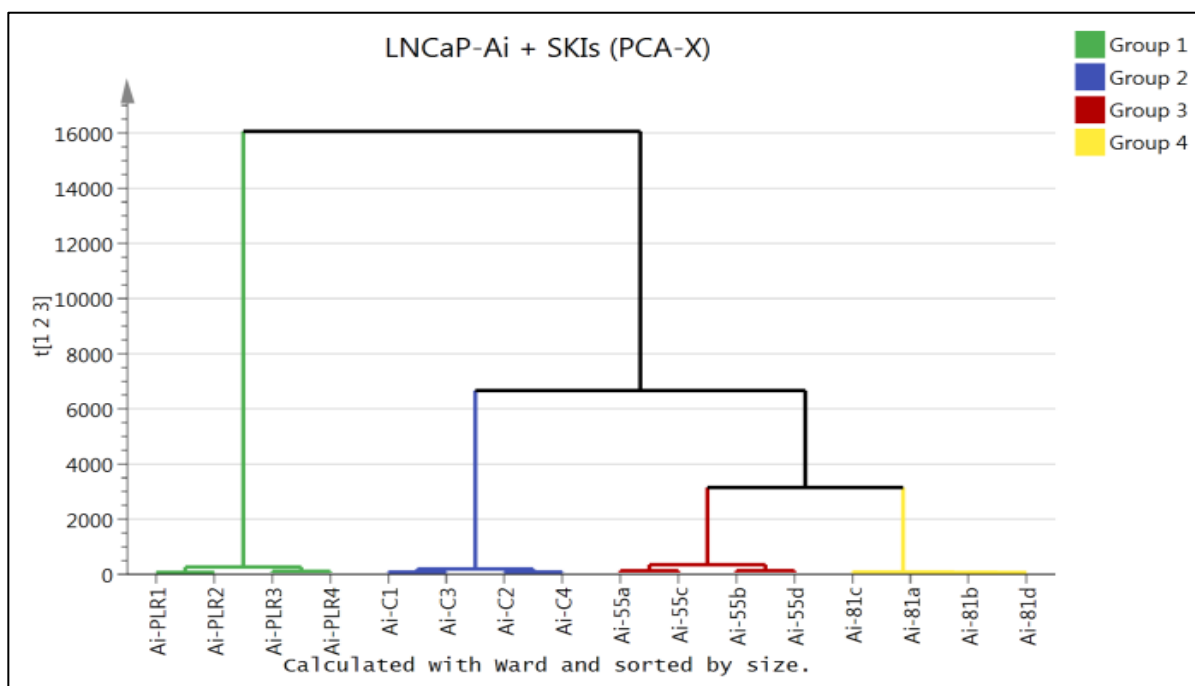


Figure 5.3-4 Hierarchical clustering analysis (HCA) of 16 prostate cancer LNCaP-AI cell samples, four replicates of each condition. It shows two main groups and four subgroups. The groups; group 1 (green): LNCaP-AI treated cells with PLR; group 2 (blue): LNCaP-AI untreated cells; group 3 (red); LNCaP-AI treated cells with ST55 and group 4 (yellow): LNCaP-AI treated cells with ST81.

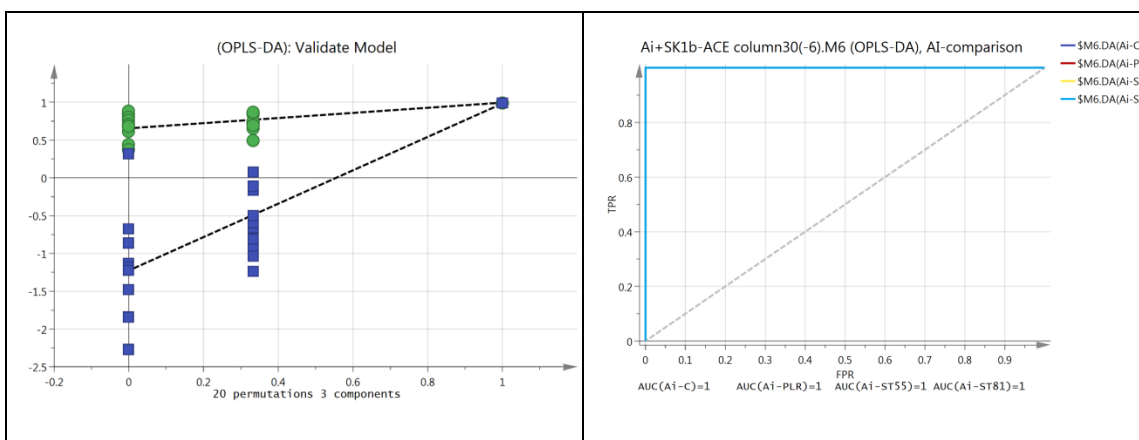


Figure 5.3-5 (A) Permutation analysis of OPLS-DA model derived from LNCaP-AI cells treated with SKi inhibitors and untreated cells. Statistical validation of the OPLS-DA model by permutation analysis using 20 different model permutations. The goodness of fit ( $R^2$ ) and predictive capability ( $Q^2$ ) of the original model are indicated on the far right and remain higher than those of the 100 permuted models to the left. OPLS-DA, orthogonal partial least squares discriminant analysis. (B) Receiver Operating Characteristics (ROC) curve shows sensitivity (true positive rate (TPR)) on the y-axis versus (false positive rate (FPR = 1 - Specificity)) on the x-axis. The area under ROC curve (AUROC) = 1 for SOR and CR groups.



Table 5-3 shows a summary of the effect of different inhibitors, non-selective (PLR24) and SK2 selective inhibitors (ST55 and ST81) on LNCaP-AI cells using silica gel conjugated with high resolution mass spectroscopy. Where: T/C= treated cells/ untreated cells.

Fatty acids			Ratio (T/C)			P-value		
Metabolite name	RT	M/z	PLR24	ST55	ST81	PLR24	ST55	ST81
Linolenic acid	4.10	277.2173	3.38	3.20	2.84	<0.001	<0.001	<0.001
Linoleate	4.21	279.2330	3.41	2.94	2.69	<0.001	<0.001	<0.001
Dihomo-linolenate	4.14	305.2488	3.04	2.65	2.43	<0.001	<0.001	<0.001
Arachidonic acid	4.04	303.2331	3.01	2.92	2.75	<0.001	<0.001	<0.001
Eicosenoic acid	4.52	309.2800	2.76	1.68	1.79	<0.001	<0.001	<0.001
FA methoxy (16:0)	4.14	285.2424	2.41	1.69	1.58	<0.001	<0.001	<0.001
FA methyl (18:0)	4.24	293.2490	3.26	2.53	2.46	<0.001	<0.001	<0.001
FA methyl (18:1)	4.39	295.2644	2.79	1.73	1.82	<0.001	<0.001	<0.001
<b>Fatty acyls -Canitine</b>								
O-Propanoylcarnitine	28.71	218.1384	1.35	0.64	0.75	<0.01	<0.010	<0.010
O-Butanoylcarnitine	27.30	232.1546	1.60	0.72	0.87	<0.001	<0.010	<0.050
O-decanoyl-R-carnitine	24.57	316.2476	3.16	3.24	2.09	<0.001	<0.010	ns
Hexadec-enoylcarnitine	23.55	398.3258	1.58	2.12	1.56	<0.01	<0.010	<0.010
<b>LysoPC</b>								
<b>LysoPC (20:0)</b>	23.08	552.4021	4.57	8.38	4.32	<0.001	<0.001	<0.001
<b>LysoPC (22:0)</b>	22.87	580.4337	6.71	29.69	18.40	<0.05	<0.05	<0.05
LysoPC (24:0)	22.71	608.4654	5.03	4.97	4.91	<0.05	<0.001	<0.001
<b>Phosphatidylethanolamine (PE)</b>								
PC (36:0)	20.94	790.6300	1.52	1.23	1.14	<0.001	<0.001	0.0013
PC (38:1)	20.79	816.6475	1.40	1.15	1.11	<0.001	<0.05	<0.05
PC (40:7)	20.28	832.5871	1.45	1.34	1.00	<0.05	<0.05	ns
PC (P-38:2)	20.88	798.6382	1.27	0.88	0.86	<0.001	<0.05	<0.05
PC (P-38:3)	20.64	796.6228	1.28	0.84	0.79	<0.001	<0.05	<0.05
<b>Phosphatidylethanolamine (PE)</b>								
PE (36:2)	13.37	744.5526	1.39	1.11	1.01	<0.001	<0.05	ns

PE			Ratio (T/C)			P-value		
Metabolite name	RT	M/z	PLR24	ST55	ST81	PLR24	ST55	ST81
PE (38:2)	13.46	772.5841	1.44	1.05	0.93	<0.001	ns	ns
PE (38:4)	13.10	768.5524	1.2	0.81	0.74	<0.001	<0.001	<0.001
PE (40:1)	13.71	802.6306	2.49	1.33	1.12	<0.05	ns	ns
PE (42:2)	13.74	828.6469	2.59	1.26	1.13	<0.001	ns	ns
PE (P-38:1)	13.64	758.6053	2.54	1.24	1.01	<0.05	ns	ns
PE (P-40:1)	13.80	786.6362	3.88	1.63	1.07	<0.05	<0.05	ns
PE (P-40:2)	13.46	784.6202	1.57	1.23	1.13	<0.001	<0.001	<0.05
<b>Phosphatidylglycerol (PG)</b>								
PG (32:0)	4.60	723.5149	6.63	3.81	2.92	0.0035	<0.05	<0.05
PG (36:3)	4.24	771.5191	3.73	3.00	2.75	<0.001	<0.001	<0.001
PG (36:5)	4.28	769.4996	3.5	2.58	2.39	<0.001	<0.001	<0.001
PG (36:6)	4.13	767.4837	3.43	2.82	2.5	0.0035	<0.05	<0.001
PG (38:3)	4.35	799.5505	3.22	2.25	2.21	<0.001	<0.001	<0.001
PG (40:4)	4.30	827.5789	2.51	1.81	1.73	<0.001	<0.001	<0.001
PG (40:6)	4.34	823.5464	2.52	1.82	1.74	<0.001	<0.001	<0.001
PG (40:7)	4.12	821.531	2.57	2.2	1.94	<0.001	<0.001	<0.001
PG (42:5)	4.35	825.5626	2.36	1.61	1.54	<0.001	<0.05	<0.001
<b>Phosphatidylserine (PS)</b>								
PS (32:1)	14.08	734.4953	2.08	1.14	0.74	<0.050	ns	ns
PS (34:1)	14.13	762.5267	2.47	1.28	0.74	<0.050	ns	ns
PS (34:2)	13.99	760.5109	1.92	1.11	0.84	<0.050	ns	ns
PS (36:1)	14.12	790.5577	3.21	1.68	0.84	<0.050	ns	ns
PS (36:2)	14.04	788.542	2.18	1.21	0.85	<0.050	ns	ns
PS (40:5)	13.91	838.5573	2.41	1.34	0.83	<0.050	ns	ns
PS (40:6)	13.87	836.5426	2.09	1.09	0.67	<0.050	ns	ns

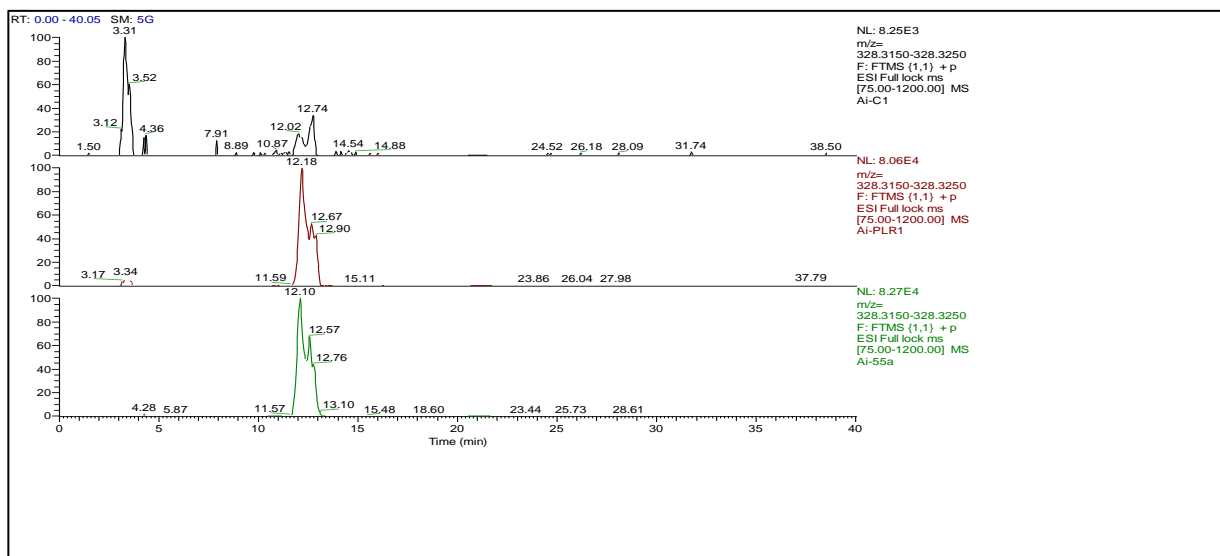


Figure 5.3-6 Extracted chromatogram of (dimethylsphingosine) DMS from control and PLR and ST55-treated LNCaP-AI cells.

## 5.4 Discussion

SK inhibitors might be utilized in a therapeutic manner to perturb the sphingolipid rheostat and to thereby kill cancer cells [201]. In the current study, the *in vitro* effects of new SK inhibitors, PLR24 (non-selective), ST55 (SK1-selective) and ST81 (SK2-selective), were treated on LNCaP-SK1b cells and androgen-independent LNCaP-AI cells using LC-MS lipidomics-based approach. ESI-MS has been shown to have an important role in identification, characterisation and quantification of lipids. Untargeted lipidomics was performed in order to compare the metabolic profile of the lipid composition of LNCaP-SK1b prostate cancer treated with PLR24, ST55 and ST81 (new inhibitors or SK inhibitors) and compared with SKi and ROME inhibitors. Also, untargeted lipidomics was performed to explore the effect of SK inhibitors on LNCaP-AI cells. A shotgun lipidomics

platform was established to measure alterations in a variety of lipid classes, including sphingolipids, lysoPC, PC, PE, PS and PG, in response to the compounds. In addition, some changes in metabolites belonging to fatty acid and acyl-carnitine classes were observed.

#### 5.4.1 The effect of SK inhibitors (SKIs) on lipids metabolism on a LNCaP-SK1b cell line.

The SKIs increased the levels of sphingoid bases, such as sphingosine, sphinganine and sphingadienine in LNCaP-SK1b prostate cells. The levels of DMS were also markedly increased with PLR24 (19.2-fold), ST55 (13.3-fold) and ST81 (18.85-fold). Interestingly, the treatment of cells with ST81 produced the strongest effect on sphinganine and Cer (d18:0/22:0) in comparison with PLR24 and ST55, suggesting that SK2 might regulate the conversion of sphinganine to sphinganine 1-phosphate. Interestingly, the ceramide levels were increased with ST81 but not with ROME, which fails to alter ceramides as can be seen in Chapter 4, suggesting that ST81 might be a more efficient and potent a SK2 inhibitor. Generally, the evidence is strong that all three inhibitors modulate the sphingolipid rheostat. However, ST81 has more profound effects on phospholipid metabolism than ROME, and these changes are similar compared with ST-55 and PLR24. This might suggest that ST-81 has ‘off-target’ effects or efficiency of inhibition is improved for ST-81 compared with ROME. Therefore, ST81 could provide a promising molecule to treat androgen-independent prostate cancer cells. However, more investigation is required to the effect of these compounds on prostate cancer cell fate (apoptosis, autophagy and senescence).

lysoPC is synthesized via PC hydrolysis by phospholipase-A2 and the accumulation of lysoPC promotes apoptosis by stimulating caspase-3 activation [176]. Indeed, previous studies have shown that lysoPCs are known as metabolic biomarkers for apoptosis [176]. LysoPCs have also been shown to promote ROS generation, which induces apoptosis via cytochrome C release [177]. The levels of fatty acids, lysoPC and PC were higher in SKIs-treated LNCaP-SK1b cells. The effects on these pathways are similar to the effect of SKi on LNCaP-SK1b cells, suggesting the same mechanism of action of these new inhibitors compared with SKi. The expected reduction in S1P bioavailability is likely to reduce S1P/S1P receptor-dependent activation of PLA2 or PLA1.

The levels of acyl-carnitine metabolites were lower in the SKIs-treated cells. This was similar to the effect of ROME in LNCaP-SK1b cells and opposite to the changes induced by SKi, suggesting that the SK2 might have a predominant role in regulating acyl-carnitine metabolism. Carnitine serves a critical role in the regulation of energy production from fatty at the cellular level. Acyl-carnitines facilitate the transport of long-chain fatty acid across the inner mitochondrial membrane to serve energy [203]. For example, carnitine palmitoyltransferase I (CPT1) is located at the outer mitochondrial membrane and facilitates the translocation of long fatty acids from the cytosol into mitochondria for  $\beta$ -oxidation [204]. A previous study showed that CPT1 is a key enzyme in regulating sphingolipids and inhibition of CPT induces programmed cell death [205]. The mechanism underlying the reduction in acyl-carnitine metabolism requires more investigation. However, acyl-carnitine may conjugate with long-chain fatty acids to cross the inner mitochondrial membrane.

As previously mentioned, diacylglycerol kinase (DGKs) shows some similarity to SK1 in amino acid sequence and domain organisation [169]. DGKs are important enzymes, which catalyze the formation of bioactive phosphatidic acids (PA) from diacylglycerols (DAG) and play an important role in cell signaling and DNA synthesis [206],[207]. The treatment of LNCaP-SK1b cells with PLR24 or ST55 induced a similar effect to SKi on increasing PG and PS levels and ST81 induced a similar effect to ROME. Thus, our observation suggests that SK might be involved in PS and PG synthesis/hydrolysis.

Generally, ether lipids play an important role in cell membrane integrity [182], which can affect membrane fluidity and fusion [183]. Ether lipids can also function as an endogenous antioxidant to reduce oxidative stress [183]. SKIs fail to alter ether-PC and have a slight effect on ether-PE lipids. This was similar to the effect of ROME in LNCaP-SK1b cells, suggesting that unlike SKi, the new SKIs might have a weak effect on cell fluidity and migration. However, more investigations in this manner are required.

#### 5.4.2 The effect of SK inhibitors (SKIs) on lipids metabolism on LNCaP-AI cell line.

The multivariate analysis techniques used in this study included OPLS-DA and HCA. It is revealed a good separation between controls and treated cells. A clear separation of SKIs-treated LNCaP-AI cells from controls was achieved indicating different effects of the compounds.

Treatment of LNCaP-AI prostate cells with the SKIs increased the levels of sphingoid bases such as sphingosine, sphinganine and sphingadienine. Interestingly, the levels of dimethylsphingosine (DMS) were markedly increased with PLR24 (29.5-fold), ST55

(33.2-fold) and ST81 (21.1-fold). DMS is an endogenous metabolite that can act as an inhibitor for both SK isoforms by competing with sphingosine [194]. DMS also inhibits other kinases such as ceramide kinase [208] and protein kinase C [152]. Consequently, DMS is likely to inhibit other processes, such as Ceramide 1-P biosynthesis and PC hydrolysis, and abrogate the sphingolipids rheostat to form ceramide and SM. The increase in the levels of sphingoid bases, ceramides, SM and PC lipids appear linked with the inhibitory effect of DMS on SK, Cer kinase and protein kinase C. However, the SK2 inhibitor, ST81 has a weak or negligible effect on ceramide and PC lipids, indicating the SK2 has little role in the back conversion of sphingosine to form ceramides. In addition, the levels of phosphoethanolamine were higher in PLR24-treated LNCaP-AI cells compared with control.

The majority of fatty acids, including arachidonic acid, and lysoPC levels were increased in SKI-treated LNCaP-AI cells. The mechanism of fatty acids production is likely through multiple pathways to regulate cellular function. Cancer cells promote *de novo* synthesis of fatty acids and store it as lipid droplets, containing triglycerides [209]. Fatty acids can be generated *via* triglyceride hydrolysis by triglyceride lipase (ATGL) [210] or synthesis *via* fatty acid synthase (FAS) [211] or breakdown of phospholipids. Interestingly, the levels of PS were lower in ST81-treated LNCaP-AI cells and higher in PLR24- and ST55-treated cells, suggesting a different role of SK1 and SK2 in regulating PS and fatty acid metabolism. The exact mechanisms of the accumulation of fatty acids remain unclear and require further investigation. The treatment of cells with PLR24, ST55 and ST81 might inhibit *de novo* synthesis and activate ATGL as alternative pathway to support cell

survival. Also, ST81 might inhibit PS synthesis or enhance PS hydrolysis, causing an increase in fatty acids levels.

PC lipids were increased after the treatment of LNCaP-AI cells with PLR24 and ST55 but not ST81, suggesting a key role for SK1 in regulating PC metabolism. It is unclear why ST81 fails to alter PC lipids. However, these findings suggest that SK1 and SK2 might have different roles in regulating fatty acids, lysoPC, PC and PS lipids in LNCaP-AI cells.

The levels of acyl-carnitine metabolites were found to be higher in the SKIs-treated LNCaP-AI cells compared with control. A previous study showed that CPT1 is a key enzyme in enhancing sphingolipid synthesis an inhibition of CPT1 induces programmed cell death [205]. Therefore, it is important to examine the effect of SKIs on CPT1 in LNCaP-AI cells to explain some of the effects of SK inhibitors on cell survival. The levels of PG lipids were higher in PLR24-treated LNCaP-AI cells compared with ST55 and ST81-treated AI cells. This suggests that targeting both SK1 and SK2 has a more substantial effect on PG lipids than targeting SK1 or SK2 alone.

## **5.5 Conclusion**

Based on the different effects of the SK inhibitors one can attribute effects to SK1 or SK2 or both; and this is facilitated by lipidomic analysis using MS analysis. PLR24 and ST55 have some similar metabolic effects on some pathways and differ in their effects on other pathways in LNCaP-SK1b prostate cancer cell lines in comparison with SKi. In common with PLR24, the treatment of LNCaP-SK1b cell line with ST81 (SK2-selective) show a significant increase in the levels of the pro-apoptotic metabolites (ceramides) and DMS. The effects of the SKI inhibitors on the lipid metabolome of both the LNCAP AI cells and



the LNCAP SK1b cells are quite marked. Moreover, it is clear that lipid metabolism is a target for these drugs. Since the effects of the SKI inhibitors might be mediated via sphingosine bases it would be interesting to see what the effect of treating directly with these bases might have on the metabolome. In addition, an important experiment would be to carry out more detailed structure elucidation experiments for key lipid markers using MS<sup>n</sup> experiments. In the current work, this approach was only partially successful due to the low intensity of many of the marker compounds in combination with an old LTQ Orbitrap.

## **Chapter VI**

---

### **Summary and future work**

## 6 Summary

Metabolomics represents a critical tool for studying phenotypic diversity at the molecular level. Metabolomics can provide an important role in understanding a mechanism of drug action, the molecular biology state of disease and biomarker discovery [212]. This thesis describes comprehensive investigations of the metabolic responses to different sphingosine kinase inhibitors on three prostate cell lines. Metabolomic profiling could help in understanding and elucidating the mechanisms of action of different SK inhibitors and the role of SK1 and SK2 play in cancer cell biology. This profiling was achieved through the use of LC-MS as an analytical technique. The use of this technique to study the effect of SK inhibitors on prostate cancer cells, illustrate alteration in several pathways. In the current study,  $^{13}\text{C}_6$ -glucose was used to explore the effect of SKi on several pathways including the Warburg effect in LNCaP-AI cells using a ZIC-pHILIC chromatographic separation method in conjugation with HRMS. Also, the effect of SKi and ROME on the lipid composition of LNCaP and LNCaP-SK1b were assessed using LC-MS. Finally, the current study explored the effect of new inhibitors, PLR24, ST55 and ST81 on LNCP-Sk1b and LNCaP-AI cells.

The results in chapter 3 reported the effect of SKi on the metabolome of LNCaP-AI prostate cancer cells as demonstrated using  $^{13}\text{C}$  glucose. The use of pulse-chase experiment illustrates a better interrogation for the effects of SKi on the glycolysis and other pathways by tracking labelled carbon. These effects include the inhibition of glycolysis, PPP, TCA, nucleotide metabolism and the increase in the production of *sn*-G3P. Moreover, the flux of  $^{13}\text{C}$  experiment suggested that much of glucose flux in LNCaP-AI cells go through the pentose glucuronate interconversion pathway. Interestingly, this

observation is a novel and would be relevant in the understanding of metabolic reprogramming in prostate cancer. Also, the results suggested that SKi promotes glycogen breakdown to produce G1P. The current study also observed that the levels of GSSG were elevated, indicative of oxidative stress and indeed, SKi promoted ROS production. The findings also potentially link *sn*-G3P with ROS production, suggesting that SK promotes cell survival by limiting oxidative stress. Indeed, previous studies have shown that SKi promotes p53-dependent senescence via oxidative stress in LNCaP-AI cells [131]. Therefore, these findings suggest that the inhibition of SK with SKi modulates the Warburg effect and shifts glycolytic flux toward *sn*-G3P. This might be necessary to transfer an electron from the cytoplasm into mitochondria, producing excessive ROS as a byproduct.

The current study in Chapter 4 sought to determine how overexpression of SK1b might affect the response of the cancer cells to SKi using LC-MS based lipidomic analysis. The findings reveal that the inhibition of SK1b with SKi alters lipid compositions and this is likely to have an effect on cell survival. For example, the levels of SM were lower in the LNCaP-SK1b compared with LNCaP cells. This agrees with previous studies reporting that SK1 enhances the production of S1P, leading to an increase in proliferation [27]. Also, it was observed that the levels of DMS and 1-deoxysphinganine, which have an inhibitory effect on SK enzyme, were higher in SKi-treated LNCaP-SK1b compared with LNCaP cells. Since, 1-deoxysphinganine can also enhance the ceramide synthesis [154],[155], this might explain the reason for the accumulation of ceramides. Previous studies have shown that over-expression of SK1 leads to an increase in S1P levels [161], which has been shown to regulate other enzymes, such as PLC [172] and CerS2 [168]. Based on this,

the suggested higher levels of S1P in LNCaP-SK1b cells should activate the PLC, leading to an increase in PC hydrolysis thereby reducing the PC levels. However, the levels of PC lipids were not decreased in the LNCaP-SK1b cells as expected. The larger increase in PC lipids in LNCaP-SK1b cells compared with LNCaP cells after the treatment with SKi suggests that the re-synthesis rate of PC lipids in LNCaP-SK1b cells is faster than in LNCaP cells. A previous study showed that the treatment of LNCaP cells with SKi induces a reduction in the S1P levels and an accumulation in sphingosine and C22:0 ceramide [28]. SKi also reduced the activity of Des1 in LNCaP-AI cells [131]. The current study showed that SKi results in a substantial increase in the levels of sphingosine, SM and ceramides in LNCaP-SK1b cells compared with LNCaP cells. The reduction in S1P with SKi might also relieve S1P-dependent inhibition of CerS2 thereby enhancing the back conversion of sphingosine into ceramide. It is notable that the SK2 inhibitor, ROME fails to alter ceramide levels, suggesting that the pool of S1P that is regulated by SK2 does not affect CerS2

Other lipids were also altered by SKi in LNCaP-SK1b cells include PG, PI, lysoPC, PE and PS. Therefore, these changes might be associated with the changes in S1P levels, which in turn may affect other enzymes such as PLC and PLA<sub>2</sub>. All these lipid classes were increased in LNCaP-SK1b treated with SKi compared with LNCaP with the exception of PG, which is found to be lower in SK1b over-expressing cells. Generally, we found that the levels of these lipids increased more robustly in treated SKi-LCaP-SK1b cells compared with treated SKi-LNCaP cells. A previous study showed that the treatment of LNCaP cells with SKi reduced the levels of S1P [28]. Interestingly, the changes in the PG lipids between the two cell lines before and after expression suggest that inhibition of

SK in LNCaP-SK1b cells likely results in a stronger *sn*-G3P-induced oxidative stress response. This effect was similar to the effect of SKi on LNCaP-AI in Chapter three.

In contrast, the effects of ROME on LNCaP cells were more robust compared with LNCaP-SK1b cells. It has been shown that ROME stimulates autophagy [132] and SKi inhibits autophagy [5], suggesting the opposite role for SK1 and SK2. These findings demonstrate that overexpression of SK1b in LNCaP cells might promote survival by shifting sphingolipid rheostat towards S1P, and the treatment of cells with SKi has more pronounced effects on LNCaP-SK1b cells. However, ROME has more pronounced effects on LNCaP cells compared with the effect on LNCaP-SK1b cells. This indicates that the over-expression of SK1b provides some protection against ROME.

The work carried out in Chapter 5 examined the effect of three different SK inhibitors (SKIs), namely; PLR24, ST55 and ST81 on LNCaP-SK1b and LNCaP-AI cells using LC-MS based lipidomics to gain a better understanding of the role of SK1 and SK2 in prostate cancer cells. The new inhibitors were chemically derived from the SK1 inhibitor, PF-543. In general, the alterations in lipid metabolism in LNCaP-SK1b in response to the new inhibitors were similar. All inhibitors increased the levels of sphingoid bases, DMS, sphinganine and ceramides, and this effect was similar to SKi. The results also showed that the treatment of LNCaP-SK1b cells with ST81 produces a stronger effect on ceramide and sphinganine in comparison with ROME, suggesting that ST81 might be a more efficient SK2 inhibitor; it is certainly ~500 x more potent than ROME in purified SK2 assays. The treatment of LNCaP-SK1b cells with the new SK inhibitors induced the same effect of SKi on several pathways including lysoPC, PC, PG, PS and fatty acids,

suggesting a role for SK1/SK2 on several pathways. The effects of these inhibitors were different on acyl-carnitine and ether lipids compared with SKi and similar to ROME. This includes acyl-carnitines, suggesting that SK might have an important role in regulating acyl-carnitine metabolism, but not ether lipids metabolism.

In LNCaP-AI cells treated with SKIs, the levels of DMS increased. SM levels were increased by PLR24 and ST55 but not ST81, suggesting that SK2 has little effect on the SM synthesis from ceramide; probably a consequence of ceramide synthesis being unaltered by inhibition of SK2. The levels of PS lipids were higher in PLR24- and ST55-treated LNCaP-AI cells and lower in the ST81-treated LNCaP-AI cells, suggesting that SK1 and SK2 might have opposing roles in regulating PS metabolism. The SKIs increased the levels of LysoPC and fatty acids and this might be linked with apoptosis/senescence [176], [177]. Lastly, the levels of PG lipids in PLR24-treated cells were higher compared with ST55 and ST81, suggesting that targeting both SK1 and SK2 has a more substantial effect on PG lipids than targeting SK1 or SK2 alone.

The results presented in the current study showed that the use of different SK inhibitors helps to understand the role of SK1 and SK2 in prostate cancer cell biology. In addition, this study highlights several pathways that can be studied at a genomic level to determine the gene-metabolism relationship and to provide information concerning the best therapeutic approach for the treatment of the advanced stage of prostate cancer.

## **6.1 Proposed future work**

The results from the metabolomics profiling in this study could potentially offer more evidence about this promising potential therapy for prostate cancer which utilises sphingosine kinase inhibitors. This includes their use in profiling the effects of SKi in LNCaP-AI cells using pHILIC column; investigation of the lipid profiles on the effect of overexpression of the SK1b gene of androgen-sensitive LNCaP cells and the evaluation of the effect of SKi and ROME on both cell lines; as well as profiling the responses of LNCaP-AI and LNCaP-SK1b cell lines to different SKIs (namely; PLR24, ST55 and ST81). However, besides the evidence and information generated by this study, there remains a need for additional analytical research and biological work in the future inclusive of the following areas:

- The use of other labelled substrates such as  $^{13}\text{C}$  glutamine to probe metabolism.
- Better characterisation of the lipids using MSn methods.
- Measurement of mitochondrial dysfunction in LNCaP-AI after the exposure of SKi treatment using mitochondrial membrane potential assay
- Investigation of the effect of SKi on Ras protein in LNCaP-AI cells.
- Measurements of cell fate (apoptosis/ senescence/ autophagy) in LNCaP and LNCaP-SK1b cells in response to the new developed SKIs.



## 7 Appendix

**Appendix 1:** Summary of the alteration in untreated and SKi-treated LNCaP-AI cells. (second run). Where ratio= average of the mean of treated cells/ untreated cells (n=3).

Metabolite name	RT (min)	m/z	Ratio (T/C)	P-Value
Phosphogluconate	17.7	275.0179	2.31	<0.010
NADP+	16.87	742.0683	1.80	<0.050
NADPH	17.33	744.0843	0.14	<0.001
D-sorbitol	13.85	181.0721	1.07	NS
NADH	13.27	664.1181	8.41	<0.010
NAD+	13.38	664.1165	1.77	<0.001
Fructose 1,6 bisphosphate	14.83	338.9876	7.23	<0.050
Glyceraldehyde-3-phospahte	16.17	168.9908	12.03	<0.001
Ribulose 5-phosphate	15.65	229.0121	6.54	<0.001
GSSG	17.55	613.1593	38.57	<0.001
Uracil	11.89	111.0199	0.70	NS
5,6-Dihydrouracil	14.64	113.0356	1.10	NS
UDP	16.58	402.9953	1.12	NS
CTP	18.5	481.9777	1.01	NS
UTP	17.94	482.9617	0.70	<0.010
5,6-Dihydrothymine	12.25	127.0513	1.06	NS
Adenine	16.97	136.0617	0.96	NS
Citrate	17.84	191.0200	0.80	<0.010
Malate	16.17	133.0143	0.63	<0.010
gamma-L-Glutamyl-L-cysteine	13.98	251.0693	13.02	<0.001
S-glutathionyl-L-cysteine	17.02	427.0947	6.34	<0.001
Cysteinylglycinedisulfide	15.15	296.0382	4.36	<0.001
N-Acetyl-L-glutamate	14.08	188.0565	3.36	<0.001
N-Formimino-L-glutamate	10.95	173.0567	2.70	<0.010
Hydroxyphenyl-lactate	8.62	181.0508	2.67	<0.001
L-Proline	12.77	114.0560	2.16	<0.001
L-Valine	10.2	116.0862	2.82	<0.001
Glycine	15.65	76.0393	2.54	<0.050
L-Histidine	17.29	156.0766	1.66	<0.050
L-Serine	15.62	106.0498	0.59	<0.001
L-Glutamate 5-semialdehyde	14.25	132.0654	0.28	NS
L-Alanine	14.65	90.05499	0.40	<0.001

Metabolite name	RT (min)	m/z	Ratio (T/C)	P-Value
2-Aminomuconate	14.64	156.0303	0.57	<0.010
Hypotaurine	14.91	110.0270	0.45	<0.010
L-Cystathionine	17.05	223.0744	0.29	<0.010
L-Aspartate	14.87	134.0445	0.12	<0.001
AMP	13.61	348.0698	2.70	<0.050
ADP	14.90	428.0363	2.78	<0.001
ATP	16.22	505.9888	1.42	NS
Creatine	14.62	132.0766	0.33	<0.001
Phosphocreatine	14.99	210.0286	0.45	<0.001
Creatinine	22.36	112.0516	0.54	<0.010
Phosphocreatinine	14.96	192.0182	0.40	<0.001
O-Acetylcarnitine	11.01	204.1282	0.89	<0.010
L-Carnitine	13.06	162.1123	1.39	<0.010
O-Propanoylcarnitine	9.53	218.1382	0.55	<0.010
O-Butanoylcarnitine	8.89	232.1539	0.51	<0.001
Choline phosphate	14.83	184.0732	0.72	<0.05
Choline	14.23	104.1069	1.37	<0.001
sn-glycerol phosphate	12.60	171.0056	7.10	<0.001
PC (16:2)	4.67	482.3602	2.77	<0.050

**Appendix 2:** Table 7-1 Alterations in lipids metabolites of LNCaP and LNCaP-SK1b cells treated with SKi. Where: (T/C)= treated cells /untreated cells, (C-1b/C)= peak intensity of untreated of (LNCaP-SK1b / LNCaP). (T-1b/T) = peak intensity of treated of (LNCaP-SK1b / LNCaP).

Metabolite name	RT (min)	m/z					SK1b / LNCaP			
			Ratio (As) (T/C)	P-Value	Ratio SK1b T/C	P-Value	C/C	P-Value	T/T	P-Value
<b>Sphingolipids</b>										
Sphingosine	11.83	300.2899	1.23	ns	4.43	<0.001	1.08	ns	3.90	<0.001
Sphinganine	12.74	302.3056	1.54	<0.001	9.27	<0.001	0.77	ns	4.63	<0.001
N,N-Dimethylsphingosine	13.14	330.3369	1.28	<0.001	1.32	<0.050	3.23	<0.050	3.31	<0.001
[SP] 1-deoxy-sphinganine	21.52	286.3106	1.19	<0.001	1.63	<0.001	2.96	<0.001	4.05	<0.001
Hexadecasphinganine	13.56	274.274	1.21	<0.001	1.40	<0.001	2.62	<0.001	3.04	<0.001
[SP (14:0)] 1-deoxy-tetradecasphinganine	13.15	230.248	1.19	<0.050	1.46	<0.001	2.67	<0.001	3.27	<0.050
SM(d18:0/22:0)	20.91	789.6850	15.2	<0.001	773	<0.001	0.47	ns	24.0	<0.001
SM(d18:1/22:0)	21.01	787.6690	1.07	ns	5.49	<0.001	0.71	<0.050	3.68	<0.001
SM(d18:1/23:0)	20.96	801.6848	2.73	<0.050	7.16	ns	1.47	ns	3.86	ns
SM(d17:1/24:1)	20.98	799.6686	1.07	ns	5.00	<0.001	0.55	<0.001	2.57	<0.001
SM(d18:1/18:1)	21.22	729.5907	1.03	ns	4.43	<0.001	0.64	<0.050	2.75	<0.050
SM(d19:1/24:1)	20.99	827.6999	1.03	ns	5.14	<0.001	0.51	<0.001	2.55	<0.050
SM(d18:0/24:1)	20.87	815.7003	0.98	ns	5.95	<0.001	0.81	<0.050	4.93	<0.001
SM(d18:1/24:1)	20.96	813.6845	0.94	ns	4.91	<0.001	0.60	<0.050	3.16	<0.001
SM(d18:1/26:0)	21.11	843.7314	0.93	ns	6.65	<0.001	0.48	<0.050	3.46	<0.050
N-(hexacosenoyl)-sphing-4-enine-1-phosphocholine	20.94	841.7158	0.86	ns	4.87	<0.001	0.47	<0.050	2.68	<0.001
Sulfo-Galbeta-Cer(d18:0/2-OH-20:0)	19.72	852.5883	0.83	ns	6.39	<0.001	0.76	ns	5.87	<0.001
Sulfo)Galbeta-Cer(d18:0/2-OH-18:0)	19.79	824.5567	0.78	<0.050	5.59	<0.001	0.89	ns	6.31	<0.001
Sulfo)Galbeta-Cer(d18:1/2-OH-16:0)	19.79	796.5241	0.70	ns	5.13	<0.001	0.97	ns	7.07	<0.001
N-(pentacosanoyl)-sphing-4-enine-1-phosphocholine	21.07	829.715	1.13	ns	6.14	<0.001	0.69	<0.010	3.78	<0.050

							SK1b / LNCaP			
Metabolite name	RT (min)	m/z	Ratio (As) (T/C)	P-Value	Ratio SK1b T/C	P-Value	C/C	P-Value	T/T	P-Value
Heptadecaspheganine	13.24	288.289	1.24	<0.050	1.51	<0.001	2.91	0.0004	3.55	<0.050
Cer (d18:1/20:2)	4.19	590.424	1.70	<0.050	14.7	<0.05	1.41	0.0242	12.0	<0.050
Cer (d18:1/24:1)	4.50	648.468	1.91	<0.050	14.3	<0.05	1.78	0.0453	11.6	<0.001
Cer (d18:1/23:1)	4.52	634.453	1.97	<0.050	15.1	<0.05	1.78	0.0126	12.4	<0.050
<b>Fatty acids</b>										
Hexadecenoic acid	12.65	253.217	0.60	<0.050	1.63	<0.050	1.27	0.0288	1.33	<0.050
Octadecenoic acid	12.56	281.248	0.85	ns	2.73	<0.001	0.99	0.9194	2.23	<0.005
Docosahexaenoic acid	12.19	327.233	1.35	ns	4.47	<0.050	1.30	0.0525	3.65	<0.005
Oxooctadecanoic acid	12.37	297.243	1.11	<0.050	2.55	<0.050	1.53	0.0014	2.08	<0.005
Oxo-docosanoic acid	11.78	353.306	1.15	<0.050	1.89	<0.001	2.28	0.0000	1.54	<0.005
Oxo-heneicosanoic acid	12.27	339.290	1.14	<0.050	2.64	<0.050	1.58	0.0046	2.15	<0.005
Hydroxy-tetracosenoic acid	12.32	381.337	1.08	<0.050	2.72	<0.001	1.51	0.0191	2.22	<0.005
Octadecenamide	12.00	282.279	1.24	<0.050	5.75	<0.001	0.49	0.0009	4.70	<0.005
Eicosapentaenoic acid	12.22	301.217	0.44	<0.050	1.09	<0.001	1.09	0.0162	0.89	<0.005
Arachidonic acid	12.31	303.233	1.15	0.1461	3.87	<0.001	1.10	0.2868	3.16	<0.005
<b>Fatty Acyls- carnitine</b>										
O-Palmitoyl-R-carnitine	22.45	400.342	0.32	<0.050	4.72	<0.001	0.49	ns	3.85	<0.001
Stearoylcarnitine	22.22	428.373	0.25	<0.050	5.28	<0.001	0.35	ns	4.31	<0.001
O-Acetylcarnitine	14.07	204.122	1.64	<0.001	5.56	<0.001	1.07	ns	5.54	<0.001
O-Propanoylcarnitine	26.99	218.138	0.81	ns	1.60	<0.001	1.08	ns	1.31	<0.001
Hydroxybutyrylcarnitine	27.86	248.149	3.04	<0.050	13.9	<0.001	1.18	<0.050	11.3	<0.001
Elaidiccarnitine	22.16	426.357	0.55	<0.050	3.38	<0.001	1.15	ns	2.76	<0.001
Hexadec-2-enoylcarnitine	22.40	398.326	0.50	<0.050	2.43	<0.001	1.54	<0.050	1.98	<0.001
O-hexanoyl-carnitine	24.65	260.185	0.81	<0.050	1.24	ns	2.04	<0.050	1.01	<0.010
O-Butanoylcarnitine	25.94	232.154	0.72	<0.001	2.29	<0.001	2.05	<0.050	1.87	<0.001

							SK1b / LNCaP			
Metabolite name	RT (min)	m/z	Ratio (As) (T/C)	P-Value	Ratio SK1b T/C	P-Value	C/C	P-Value	T/T	P-Value
<b>phosphatidylglycerol (PG)</b>										
Sn-glycerol-3-phosphate	12.43	171.0056	0.86	ns	4.43	<0.050	0.24	<0.050	1.24	<0.050
PG (30:0)	5.28	693.471	0.43	<0.001	3.36	ns	0.18	<0.001	2.75	ns
PG (32:0)	5.16	721.503	0.52	ns	3.02	<0.050	0.28	ns	2.46	ns
PG (38:4)	4.91	797.531	0.58	<0.001	1.43	<0.050	0.49	<0.001	1.17	<0.050
PG (36:2)	5.06	775.550	0.83	ns	5.16	ns	0.42	ns	4.21	ns
PG (36:1)	5.04	777.564	0.86	<0.050	5.24	<0.050	0.53	<0.005	4.28	<0.010
PG (38:4)	4.96	799.546	0.99	<0.050	4.46	ns	0.72	<0.001	3.64	ns
PG (36:2)	5.00	773.534	0.53	ns	2.11	<0.050	0.30	<0.050	1.73	<0.010
PG (46:3)	5.10	771.515	0.64	ns	2.87	ns	0.69	ns	2.35	ns
<b>Glycerophosphocholine (PC)</b>										
PC (36:1)	19.83	788.615	1.39	<0.001	3.67	<0.001	1.59	<0.005	3.00	<0.001
PC (36:1)	20.05	772.621	0.82	<0.005	2.05	<0.001	0.75	<0.005	1.67	<0.001
PC (36:2)	19.71	786.6	0.88	<0.050	2.29	<0.001	1.14	ns	1.87	<0.001
PC (36:3)	19.73	784.585	1.11	ns	4.80	<0.001	1.04	ns	3.92	<0.001
PC (38:2)	19.69	814.631	0.95	ns	2.42	<0.001	1.00	ns	1.97	<0.001
PC (38:4)	19.4	810.599	1.39	<0.001	7.20	<0.001	1.13	ns	5.88	<0.001
PC (38:5)	19.62	794.606	1.68	<0.001	7.89	<0.001	0.74	<0.050	6.44	<0.001
PC (40:1)	19.73	844.678	0.69	ns	1.68	<0.050	1.86	<0.050	1.38	<0.050
PC (40:2)	19.68	842.662	0.58	<0.001	1.99	<0.001	1.07	<0.050	1.62	<0.001
PC (40:3)	19.61	840.647	0.81	<0.001	3.53	<0.001	0.73	<0.005	2.88	<0.001
PC (40:4)	19.49	838.631	1.02	ns	5.38	<0.001	0.80	<0.050	4.39	<0.001
PC (40:5)	19.46	836.615	1.26	<0.001	6.11	<0.001	0.99	ns	4.99	<0.001
PC (40:6)	19.34	834.615	1.29	<0.050	6.77	<0.001	1.18	<0.005	5.53	<0.001
PC (40:7)	19.27	832.584	0.94	<0.001	3.64	<0.001	1.38	<0.050	2.97	<0.001

Metabolite name	RT (min)	m/z					SK1b / LNCaP			
			Ratio (As) (T/C)	P-Value	Ratio SK1b T/C	P-Value	C/C	P-Value	T/T	P-Value
PC (40:8)	19.58	830.568	1.26	<0.001	4.14	<0.050	1.85	<0.050	3.38	<0.005
PC (42:1)	19.72	872.71	0.37	<0.005	2.05	<0.001	1.64	<0.001	1.67	<0.001
PC (42:2)	19.69	870.694	0.45	<0.050	1.63	<0.001	1.20	<0.050	1.33	<0.001
PC (42:3)	19.58	868.679	0.47	<0.050	2.49	<0.001	0.74	ns	2.03	<0.001
PC (42:4)	19.49	866.6633	0.77	<0.005	4.98	<0.001	0.78	<0.050	4.07	<0.001
PC (42:5)	19.39	864.647	1.02	<0.005	5.42	<0.050	0.95	<0.005	4.43	<0.050
PC (42:6)	19.37	862.631	1.21	ns	5.22	<0.050	1.13	<0.050	4.27	<0.050
PC (42:7)	19.21	860.616	1.17	<0.001	4.26	<0.001	1.21	<0.005	3.48	<0.005
PC (42:8)	19.47	858.599	1.17	<0.001	3.71	<0.001	1.34	<0.005	3.03	<0.005
PC (42:9)	19.33	856.584	1.30	<0.001	4.41	<0.001	1.68	ns	3.60	<0.001
PC (P-36:0)	20.22	774.637	0.85	<0.050	3.01	<0.001	0.35	<0.005	2.46	<0.005
PC (P-36:2)	19.71	770.606	0.97	<0.005	3.18	<0.005	0.85	<0.050	2.60	<0.001
PC (P-36:3)	19.72	768.59	1.61	<0.001	7.63	<0.001	0.77	<0.005	6.23	<0.001
PC (P-36:4)	12.36	766.572	4.47	<0.005	13.20	<0.050	1.73	<0.005	10.8	<0.050
PC (P-38:2)	19.84	798.636	1.20	<0.001	3.95	<0.001	0.55	<0.005	3.22	<0.001
PC (P-38:3)	19.65	796.62	1.60	ns	8.50	<0.005	0.52	<0.050	6.94	<0.001
PC (P-38:5)	19.55	792.59	1.69	ns	10.00	<0.001	0.77	ns	8.22	<0.001
PC (P-38:6)	19.32	790.574	1.62	<0.001	10.00	<0.001	0.89	ns	8.22	<0.001
PC (P-40:5)	19.55	820.62	1.86	<0.001	10.70	<0.001	0.62	<0.050	8.78	<0.001
PC (P-40:7)	19.22	816.59	1.54	ns	7.95	<0.005	0.93	<0.005	6.49	<0.050
<b>Lyso-PC</b>										
LysoPC (17:0)	22.21	508.340	1.47	<0.050	19.2	<0.050	2.73	<0.050	15.7	<0.050
LysoPC (O-18:0)	22.86	510.392	1.85	<0.001	20.9	<0.001	0.90	ns	17.1	<0.050
LysoPC (18:0)	22.06	523.3597	0.71	<0.001	4.01	0.0200	0.46	<0.001	2.67	<0.050
LysoPC (20:1)	22.07	550.387	0.88	ns	9.53	<0.001	1.01	ns	7.79	<0.001

							SK1b / LNCaP			
Metabolite name	RT (min)	m/z	Ratio (As) (T/C)	P-Value	Ratio SK1b T/C	P-Value	C/C	P-Value	T/T	P-Value
LysoPC (20:2)	22.11	548.371	1.13	ns	11.6	0.0198	1.41	ns	9.53	<0.050
LysoPC (22:0)	21.81	580.434	0.48	ns	9.50	<0.001	1.04	ns	7.76	<0.001
LysoPC (22:1)	21.87	578.418	0.74	<0.050	6.76	<0.001	1.36	ns	5.52	<0.001
LysoPC (24:0)	21.62	608.465	0.39	<0.050	6.10	<0.001	0.82	ns	4.98	<0.001
<b>Glycerophosphoserines (PS)</b>										
PS (32:1)	12.98	734.497	0.39	<0.005	2.09	<0.05	0.73	<0.05	1.71	<0.05
PS (34:1)	13.02	762.528	0.73	<0.050	3.49	<0.001	0.76	<0.05	2.85	<0.001
PS (36:1)	13.02	790.559	1.10	ns	4.73	<0.001	0.93	0.3746	3.86	<0.001
PS (36:2)	12.35	834.528	0.77	<0.05	3.07	<0.001	0.69	<0.05	2.50	<0.001
PS (36:3)	12.67	784.512	0.87	ns	2.41	<0.005	1.26	<0.05	1.97	<0.005
PS (38:4)	13.05	812.542	1.08	<0.05	3.79	<0.001	1.19	<0.05	3.10	<0.001
PS (40:6)	12.69	836.544	1.14	<0.05	3.63	<0.05	1.34	<0.005	2.96	0.0160
PS (40:6)	12.27	836.541	0.92	<0.05	2.52	<0.001	1.55	<0.05	2.06	<0.005
<b>Glycerophosphoinositols (PI)</b>										
PI (36:3)	5.20	861.549	0.99	ns	4.06	<0.001	1.48	<0.050	3.32	<0.001
PI (36:4)	5.50	859.532	1.41	ns	3.49	<0.050	2.08	<0.050	2.85	<0.050
PI (38:2)	5.29	889.581	1.00	ns	3.56	<0.050	0.75	<0.050	2.90	<0.050
PI (38:5)	5.34	885.548	1.07	ns	2.87	<0.050	1.50	ns	2.34	<0.050
PI (36:0)	5.35	880.592	1.02	ns	3.00	<0.050	1.18	ns	2.45	<0.050
PI (38:4)	5.09	887.564	1.38	<0.050	3.88	<0.050	1.62	<0.050	3.17	<0.050
PI (40:4)	5.19	915.595	1.42	<0.050	4.38	<0.050	1.80	ns	3.57	<0.050
PI (40:5)	5.32	913.578	1.13	ns	3.22	<0.050	1.36	<0.050	2.63	<0.050
PI (40:6)	5.07	911.563	1.12	ns	3.01	<0.050	1.40	<0.050	2.46	<0.050
<b>Glycerophosphoethanolamines (PE)</b>										
PE (32:1)	12.64	686.4769	0.19	<0.005	0.55	ns	1.36	<0.050	0.45	<0.001

Metabolite name	RT (min)	m/z					SK1b / LNCaP			
			Ratio (As) (T/C)	P-Value	Ratio SK1b T/C	P-Value	C/C	P-Value	T/T	P-Value
PE (34:3)	12.53	714.5080	0.57	<0.001	1.08	ns	1.79	<0.001	0.88	<0.001
PE (36:2)	12.52	730.5753	1.29	<0.001	2.38	<0.001	1.56	<0.001	1.95	<0.001
PE (36:3)	12.53	740.5246	0.69	<0.050	2.34	<0.001	0.96	ns	1.91	<0.005
PE (36:4)	12.37	740.5226	1.24	<0.050	2.97	<0.001	2.12	<0.001	2.43	<0.005
PE (38:1)	12.57	772.5860	0.91	ns	2.39	ns	1.13	ns	1.95	<0.001
PE (38:2)	12.48	772.5858	0.95	ns	1.77	<0.001	1.55	<0.001	1.45	ns
PE (38:4)	12.25	768.5539	1.19	<0.001	2.81	<0.001	1.89	<0.001	2.30	<0.001
PE (38:5)	12.30	766.5377	0.95	<0.050	2.16	<0.001	1.85	<0.001	1.76	<0.001
PE (38:6)	12.25	764.5218	1.16	<0.001	2.98	<0.001	2.33	<0.001	2.43	<0.001
PE (38:7)	12.36	762.5070	1.01	ns	2.17	<0.001	2.47	<0.001	1.77	<0.001
PE (40:1)	12.46	802.6324	0.91	ns	1.89	<0.001	2.08	<0.001	1.55	<0.001
PE (40:2)	12.41	800.6165	0.88	<0.001	1.72	<0.001	1.63	<0.001	1.40	<0.001
PE (40:3)	12.37	798.6005	0.94	<0.050	2.03	<0.001	1.43	<0.005	1.66	<0.001
PE (40:6)	12.21	792.5538	1.09	<0.050	2.46	<0.001	2.09	<0.001	2.01	<0.001
PE (40:7)	12.06	776.5589	1.68	<0.001	3.75	<0.001	1.75	<0.005	3.06	<0.001
PE (42:1)	12.44	830.6641	0.14	<0.001	0.75	ns	1.75	ns	0.62	ns
PE (42:2)	12.39	828.6480	0.34	<0.050	0.46	ns	1.51	ns	0.37	<0.050
PE (42:3)	12.34	824.6163	0.18	<0.050	1.80	ns	0.66	ns	1.47	<0.005
PE (42:4)	12.15	824.6165	0.93	<0.050	2.33	<0.001	1.62	<0.001	1.91	<0.001
PE (42:5)	12.15	822.6009	0.95	<0.050	2.30	<0.001	1.55	<0.005	1.88	<0.001
PE (42:6)	12.14	820.5851	0.93	<0.050	2.00	<0.001	1.89	<0.005	1.63	<0.001
PE (42:7)	12.10	818.5695	0.90	<0.005	1.88	<0.001	1.52	<0.005	1.53	<0.001
PE (42:8)	12.35	816.5536	0.99	ns	1.71	<0.001	2.13	<0.001	1.40	<0.001
PE (44:4)	12.07	852.6486	0.89	<0.050	2.49	<0.001	1.73	<0.001	2.03	<0.001



Metabolite name	RT (min)	m/z					SK1b / LNCaP			
			Ratio (As) (T/C)	P-Value	Ratio SK1b T/C	P-Value	C/C	P-Value	T/T	P-Value
PE (44:7)	12.06	846.6013	0.94	<0.050	2.49	<0.001	1.52	<0.005	2.04	<0.005
PE (P-34:1)	12.56	702.5427	1.10	<0.050	2.24	<0.001	1.79	<0.001	1.83	<0.001
PE (P-34:2)	12.54	700.5282	0.82	<0.001	1.49	<0.001	1.60	<0.001	1.22	<0.001
PE (P-34:3)	12.42	698.5123	0.76	ns	0.84	ns	1.58	<0.001	0.69	<0.001
PE (P-36:2)	12.47	728.5595	1.14	<0.050	2.10	<0.001	1.71	<0.001	1.72	<0.001
PE (P-36:3)	12.47	726.5439	0.99	ns	1.98	<0.001	1.58	<0.001	1.62	<0.001
PE (P-36:4)	12.27	724.5280	1.28	<0.050	2.83	<0.001	1.81	<0.050	2.31	<0.001
PE (P-36:5)	12.26	722.5113	1.11	<0.050	2.38	<0.001	1.96	<0.050	1.94	<0.001
PE (P-38:1)	12.48	758.6065	1.37	<0.001	2.49	<0.001	1.44	<0.050	2.03	<0.001
PE (P-38:2)	12.44	756.5906	1.10	<0.050	2.31	<0.001	1.16	ns	1.89	<0.001
PE (P-38:3)	12.42	754.5749	1.40	<0.001	3.43	<0.001	1.17	<0.050	2.80	<0.001
PE (P-38:5)	12.29	750.5436	1.57	<0.001	3.94	<0.001	1.82	<0.050	3.22	<0.001
PE (P-40:3)	12.38	782.6057	1.55	<0.001	4.51	<0.001	0.87	ns	3.68	<0.050
PE (P-40:4)	12.37	780.5911	1.99	<0.001	6.75	<0.001	1.14	ns	5.51	<0.001
PE (P-40:5)	12.25	778.5749	1.88	<0.001	4.66	<0.001	1.68	<0.050	3.81	<0.001

**Appendix 3:** show the changes in sphingolipids occurred in response to the treatment of LNCaP and LNCaP-SK1b with ROME, where T/C= the ratio of the average amount of a given metabolites in samples from treated cells compared with the average amount of a given metabolite in samples from control cells (n=3),

<b>Lipids: Sphingolipids</b>			<b>LNCaP</b>		<b>LNCaP-SK1b</b>	
Metabolite name	M/z	RT (min)	Ratio (T/C)	P-Value	Ratio (T/C)	P-Value
Sphingosine	300.2895	11.48	1.64	0.0053	1.62	<0.001
Sphinganine	302.3051	12.33	3.20	0.0164	1.66	<0.001
Sphingadiene	298.2739	6.50	2.20	0.0358	1.22	0.0803
Sphinganine-1-phosphate	382.2710	24.50	3.40	<0.001	N/D	---
Cer(d18:1/18:1)	564.5347	5.74	1.12	0.4088	1.01	0.7348
Glucosylcer (d18:1/16:0)	700.5721	3.30	0.27	0.0088	0.60	<0.001
Glucosylcer (d18:1/22:0)	784.6654	3.09	1.79	0.0162	1.09	0.1539
Glucosylcer (d18:1/24:1)	810.6820	3.14	1.66	0.0015	0.95	0.7646
Lactosylceramide (d18)	862.6244	3.71	0.42	0.0014	0.51	0.0011
Lactosylcer(d18)	974.7492	3.60	0.54	0.0349	0.95	0.3050
3-O-Sulfogalactosylcer (d18)	862.6108	19.24	1.52	<0.05	1.22	<0.001
<b>Sphingomyelin (SM)</b>						
SM(d18:1/18:1)	729.5893	21.36	1.44	0.0705	1.19	0.0135
SM(d18:1/18:0)	731.6052	21.41	1.65	0.0284	1.17	0.0291
SM(d18:1/20:0)	759.6362	21.29	1.90	0.0167	1.36	0.0036
SM(d18:1/22:1)	785.6518	21.15	1.95	0.0148	1.33	0.0029
SM(d18:1/22:0)	787.6674	21.20	2.02	0.0097	1.50	<0.001
SM(d17:1/24:1)	799.6674	21.14	1.89	0.0135	1.19	0.0263
SM(d18:1/23:0)	801.6833	21.16	1.61	0.0176	1.22	0.0143
SM(d18:1/24:1)	813.6832	21.11	1.96	0.0111	1.43	<0.001
SM(d18:0/24:1)	815.6987	21.12	1.70	0.0202	1.52	<0.001
SM(d19:1/24:1)	827.6985	21.10	1.62	0.0469	1.14	0.3480
SM(d18:0/24:1(OH))	829.6788	20.91	2.15	0.0039	1.81	<0.001
SM(d18:1/25:0)	829.7130	21.16	1.24	0.5060	1.29	<0.001
SM(d18:1/26:1)	841.7141	21.08	2.78	0.0208	1.15	0.1491

**Appendix 4:** shows the changes in PC, PE, PG, PS and PI occurred in LNCaP and LNCaP-SK1b in response to ROME

Phosphatidylcholine (PC)			LNCaP		LNCaP-SK1b	
Name	M/z	RT (min)	Ratio (T/C)	P-Value	Ratio (T/C)	P-Value
LysoPC (16:0)	496.3386	22.65	2.46	<0.01	1.26	<0.001
PC (30:2)	692.5583	20.58	1.54	<0.05	1.48	<0.001
PC (31:0)	720.5545	20.26	1.34	<0.01	1.07	ns
PC (32:0)	734.5685	20.22	1.29	<0.05	1.56	ns
PC (34:0)	762.5999	19.98	1.16	<0.05	1.04	ns
PC (34:2)	748.621	20.34	1.25	ns	1.59	<0.01
PC (34:3)	756.5534	19.76	1.64	<0.05	1.14	<0.05
PC (36:1)	788.6163	19.91	1.13	<0.05	1.05	ns
PC (36:2)	776.651	20.32	1.41	<0.001	2.43	<0.01
PC (36:2)	786.6	19.85	1.56	ns	2.65	<0.05
PC (36:3)	784.5856	19.76	1.29	<0.05	1.29	ns
PC (36:6)	778.537	19.5	1.32	ns	1.21	<0.05
PC (38:7)	804.5522	19.49	1.09	ns	1.09	<0.05
PC (40:4)	838.631	19.51	1.26	<0.05	1.13	<0.01
PC (40:5)	836.6154	19.46	1.11	ns	1.13	<0.01
PC (40:6)	834.6002	19.33	1.15	ns	1.13	<0.01
PC (42:1)	872.7093	20.21	0	ns	1.21	ns
PC (42:3)	868.679	19.56	1.21	ns	1.14	<0.05
PC (42:4)	866.6625	19.47	1.12	ns	1.08	ns
PC (42:5)	864.6464	19.36	1.18	ns	1.09	ns
PC (42:6)	862.6309	19.33	1.15	ns	1.16	<0.001
PC (42:7)	860.6151	19.18	1.18	<0.05	1.10	ns
PC (42:8)	858.5984	19.31	1.13	ns	1.14	<0.01
PC (44:3)	896.7099	19.56	4.5	<0.01	1.06	ns
PC (44:4)	894.6944	19.45	1	ns	0.87	ns
PC (44:5)	892.6776	19.39	1.03	ns	0.98	ns
PC (44:6)	890.6622	19.36	1.18	ns	1.08	ns
PC (44:7)	888.6461	19.18	1.09	ns	1.11	ns

Phosphatidylcholine (PC)			LNCaP		LNCaP-SK1b	
Name	M/z	RT (min)	Ratio (T/C)	P-Value	Ratio (T/C)	P-Value
PC (44:8)	886.6302	19.1	1.33	ns	1.26	<0.05
PC (P30:0)	690.5428	20.2	1.33	<0.05	1.31	<0.05
PC (P-32:0)	718.5741	20.16	1.56	<0.05	1.23	<0.01
PC (P-34:0)	746.6051	20.26	1.45	<0.01	1.32	<0.01
PC (P-36:0)	774.6364	20.18	1.45	<0.01	1.27	<0.01
PC (P-36:4)	764.5585	20.39	1.38	ns	1.06	ns
PC (P-36:5)	762.5422	20.02	1.5	ns	1.18	<0.001
PC (P-38:0)	802.6672	20.16	1.33	ns	1.41	<0.001
PC (P-38:5)	792.5899	19.52	0.95	ns	1.23	<0.001
PC (P-38:6)	788.5586	19.81	1.63	ns	1.18	0.104
PC (P-40:5)	820.6204	19.49	1.1	ns	1.21	<0.01
PC (P-40:7)	816.5891	19.18	1.14	ns	1.18	ns
Phosphatidylethanolamine (PE)						
PE (32:2)	688.491	12.45	2.25	<0.01	1.44	<0.001
PE (34:1)	718.5372	12.77	1.25	<0.05	1.12	<0.05
PE (34:2)	716.5219	12.72	1.77	<0.001	1.17	<0.05
PE (34:3)	714.5069	12.63	1.67	<0.001	1.13	<0.05
PE (36:2)	744.5533	12.66	1.49	<0.001	1.08	ns
PE (36:3)	742.538	12.63	1.5	<0.001	1.08	ns
PE (36:4)	740.5213	12.48	1.28	<0.05	1.08	<0.001
PE (36:5)	738.5057	12.47	1.68	<0.001	1.17	<0.001
PE (38:7)	762.5054	12.48	1.35	<0.05	1.07	ns
PE (40:2)	800.6163	12.55	1.21	<0.05	1.03	ns
PE (40:6)	792.5529	12.33	1.13	ns	1.05	ns
PE (40:7)	790.5363	12.28	1.18	<0.05	1.02	ns
PE (42:5)	822.5998	12.27	1.16	<0.05	1.04	ns
PE (42:6)	820.5843	12.28	1.15	<0.05	1.08	<0.001
PE (42:7)	818.5682	12.24	1.25	<0.001	1.02	ns
PE (42:8)	816.552	12.35	1.04	ns	1.03	ns
PE (P-32:0)	676.5271	12.82	1.2	<0.05	1.09	ns

Phosphatidylcholine (PC)			LNCaP		LNCaP-SK1b	
Name	M/z	RT (min)	Ratio (T/C)	P-Value	Ratio (T/C)	P-Value
PE (P-36:2)	728.5584	12.58	1.2	<0.05	1.05	ns
PE (P-36:3)	726.5429	12.55	1.24	<0.05	1.01	ns
PE (P-36:4)	724.5267	12.38	1.02	ns	1	ns
PE (P-38:5)	750.5423	12.41	1.01	ns	1	ns
PE (P-40:2)	784.6199	12.49	1.48	<0.05	1.04	ns
PE (P-40:3)	782.6049	12.36	1.33	<0.05	0.96	ns
PE (P-40:5)	778.5737	12.36	1.02	ns	1.01	ns
PE (P-40:7)	774.5421	12.2	0.95	ns	0.95	ns
<b>Acyl-carnitines</b>						
Butanoylcarnitine	232.1538	26.27	0.90	<0.05	0.83	<0.001
Tetradecenoylcarnitine	370.2945	22.52	0.72	ns	0.72	<0.001
Hexadec-enoylcarnitine	398.3257	22.31	0.62	<0.05	0.76	<0.001
<b>Phosphatidylglycerol (PG )</b>						
PG (34:1)	749.5317	5.43	1.26	ns	1.13	ns
PG (36:0)	779.5774	5.31	1.28	ns	1.64	ns
PG (36:2)	775.5478	5.29	1.14	ns	1.23	ns
PG (40:6)	823.5462	3.75	3.37	<0.01	2.82	<0.001
PG (40:7)	821.5308	3.62	3.28	<0.01	2.33	<0.001
<b>Phosphatidylserine (PS)</b>						
PS (34:0)	764.5433	3.85	5.31	<0.01	4.12	<0.001
PS (36:0)	792.5744	3.83	5.58	<0.01	3.35	<0.01
PS (38:0)	820.6060	3.81	3.73	<0.01	2.88	<0.01
<b>Phosphatidylinositol (PI)</b>						
PI (34:0)	837.5521	6.15	2.12	<0.05	1.75	<0.05
PI (36:0)	863.5635	5.98	1.54	<0.05	1.41	<0.01
PI (36:0)	865.5832	6.11	2.03	<0.01	1.59	<0.05
PI (36:3)	861.5476	5.80	1.79	<0.05	2.05	<0.05
PI (38:2)	891.5932	5.94	1.64	<0.01	1.28	<0.05
PI (38:3)	889.5789	5.71	1.50	<0.01	1.21	<0.05
PI (38:4)	887.5625	5.70	1.32	<0.01	1.24	<0.001

**Appendix 5:** show the effect of different inhibitors, non-selective (PLR24), and SK II selective (ST55 and ST81) on LNCaP-SK1b cells using Silica gel conjugated with high resolution mass spectroscopy

Met name	RT	M/Z	Ratio PLR	Ratio-ST55	Ratio ST81	PLR	ST55	ST81
<b>Shphingolipids</b>								
<b>Sphingobase</b>			Treated/ untreated LNCaP-SK1b cells			P-Value		
Sphingosine	12.28	300.2891	4.96	3.88	5.82	<0.001	<0.01	<0.001
Sphinganine	12.89	302.3045	4.4	3.42	5.24	<0.001	<0.01	<0.001
N,N-Dimethylsphingosine	12.23	328.3203	19.27	13.33	18.85	<0.001	<0.01	<0.001
C17 sphingosine	12.33	286.2735	1.89	1.55	2.39	<0.001	<0.05	<0.001
sphinga-4E,14Z-dienine	12.02	298.2734	6.23	4.61	7.14	<0.001	<0.01	<0.001
Phosphoethanolamine	13.41	140.0107	2.08	1.67	2.73	ns	<0.01	ns
Cer(d18:0/22:0)	7.41	624.6294	1.92	1.76	2.81	ns	<0.05	<0.05
Met name	RT	M/Z	Ratio PLR	Ratio-ST55	Ratio ST81	PLR	ST55	ST81
<b>Cer(d18:1/18:1)</b>	<b>3.84</b>	<b>564.5346</b>	<b>1.63</b>	<b>1.07</b>	<b>1.31</b>	<b>&lt;0.05</b>	<b>ns</b>	<b>&lt;0.05</b>
SM(d18:1/18:1)	22.3	729.5895	1.37	1.16	1.25	<0.001	ns	<0.05
<b>Cer(d18:1/18:0)</b>	<b>4.41</b>	<b>566.5508</b>	<b>1.91</b>	<b>1.63</b>	<b>1.99</b>	<b>&lt;0.05</b>	<b>&lt;0.05</b>	<b>&lt;0.05</b>
SM(d18:1/18:0)	22.33	731.6049	1.51	1.26	1.39	<0.05	ns	<0.05
Glucosylcer (d18:1/18:0)	4.4	728.604	1.33	1.01	1.27	<0.05	ns	ns
LacCer(d18:1/18:0)	4.89	890.6564	1.85	1.78	2.33	<0.05	<0.05	<0.05
<b>Cer(d18:1/20:0)</b>	<b>5.31</b>	<b>594.5822</b>	<b>2.68</b>	<b>2.17</b>	<b>2.54</b>	<b>&lt;0.05</b>	<b>&lt;0.01</b>	<b>&lt;0.001</b>
SM(d18:1/20:0)	22.32	759.636	2.08	1.81	2.05	<0.05	<0.01	<0.05
Glucosylcer (d18:1/20:0)	5.07	756.635	1.85	1.31	1.63	<0.05	ns	ns
LacCer(d18:1/20:0)	5.43	918.6874	2.03	1.38	1.93	<0.05	ns	<0.05
<b>Cer(d18:1/26:1)</b>	<b>7.88</b>	<b>676.6602</b>	<b>2.34</b>	<b>2.31</b>	<b>1.98</b>	<b>&lt;0.001</b>	<b>&lt;0.05</b>	<b>&lt;0.05</b>
SM(d18:1/26:1)	22.22	841.7147	1.95	1.84	1.94	<0.001	<0.05	<0.05
Glucosylcer (d18:1/26:1)	7.34	838.7148	2.66	2.46	3.14	<0.05	<0.05	<0.05

**Appendix 6:** show the effect of different inhibitors, non-selective (PLR24), SK I selective (ST55) and SK II selective (ST81) on LNCaP-SK1b cells using Silica gel conjugated with high resolution mass spectroscopy

Fatty acids			Treated/ Untreated			P-value		
Metabolite name	RT (min)	M/z	Ratio PLR	Ratio ST55	Ratio ST81	PLR24	ST55	ST81
Linolenic acid	4.1	277.217	5.79	6.78	7.2	<0.050	<0.001	<0.001
Linoleate	4.21	279.233	3.07	3.26	3.47	<0.001	<0.01	<0.001
Dihomo- linolenate	4.14	305.249	2.01	1.92	2.15	<0.050	<0.01	<0.001
Eicosenoic acid	4.52	309.28	2.41	2.22	2.37	<0.050	<0.01	<0.001
Docosahexaenoicacid	3.95	327.233	2.34	1.94	2.19	<0.050	<0.001	<0.001
Hydroxy-eicosadienoic acid	4.27	325.274	2.68	2.58	2.69	<0.050	<0.001	<0.001
Octadecenoic acid	4.34	281.249	2.64	2.57	2.77	<0.001	<0.01	<0.001
Hexadecadienoic acid	4.14	251.202	3.07	2.94	3.47	<0.001	<0.01	<0.001
Cyclohexylundecanoic acid	4.31	267.233	2.9	2.74	2.98	<0.001	<0.01	<0.001
Fatty acids			Treated/ Untreated			P-value		
Metabolite name	RT (min)	M/z	Ratio PLR	Ratio ST55	Ratio ST81	PLR24	ST55	ST81
FA methoxy (16:0)	4.14	285.242	2.93	3.31	3.34	<0.001	<0.001	<0.001
FA methyl (18:0)	4.24	293.249	2.6	2.54	2.78	<0.001	<0.01	<0.001
FA methyl (18:0)	4.39	295.264	2.39	2.24	2.36	<0.001	<0.01	<0.001
FA oxo (19:0)	4.45	313.274	3.01	2.92	3.11	<0.001	<0.01	<0.001
Adrenic Acid	4.13	331.265	2.59	2.6	2.83	<0.001	<0.001	<0.001
Docosatrienoic acid	4.25	333.28	2.77	2.46	2.81	<0.001	<0.01	<0.001
FA oxo(21:0)	4.61	341.305	2.75	2.52	2.65	<0.001	<0.01	<0.001
FA (18:2)	4.35	265.253	2.28	1.91	2.12	<0.001	<0.01	<0.001
Fatty acyls -Carnitines								
O-Propanoylcarnitine	28.71	218.138	1.18	1.23	1.3	<0.05	<0.01	<0.001
O-Butanoylcarnitine	27.3	232.155	0.75	0.6	0.65	<0.001	<0.001	<0.001
O-decanoyl-carnitine	24.57	316.248	0.56	0.47	0.5	<0.001	<0.001	<0.001
O-Palmitoyl-carnitine	23.61	400.341	0.76	0.65	0.65	<0.05	<0.001	<0.001

			Treated/ Untreated			P-value		
Metabolite name	RT (min)	M/z	Ratio PLR	Ratio ST55	Ratio ST81	PLR24	ST55	ST81
Arachidylcarnitine	23.08	456.404	0.9	0.44	0.49	ns	<0.001	<0.001
Stearoylcarnitine	23.36	428.373	0.83	0.44	0.47	ns	<0.001	<0.001
Elaidiccarnitine	23.34	426.357	0.71	0.67	0.73	<0.05	<0.01	<0.05
LysoPC								
LysoPC (18:0)	23.31	524.371	1.76	3.96	2.36	<0.001	<0.01	<0.001
LysoPC(O-18:0)	24.02	510.391	1.62	2.3	1.75	<0.05	<0.01	<0.05
lysoPC (20:0)	23.08	552.402	2.28	5.64	3.98	<0.001	<0.001	<0.001
LysoPC (20:1)	23.14	550.386	1.73	3.72	2.74	<0.001	<0.01	<0.001
LysoPC (22:1)	22.89	578.417	2.76	8.15	6.25	<0.001	<0.01	<0.001
LysoPC (22:0)	22.87	580.434	2.62	6.24	4.96	<0.001	<0.01	<0.001
LysoPC (24:1)	22.82	606.448	2.6	6.75	5.57	<0.001	<0.01	<0.001
LysoPC (24:0)	22.71	608.465	2.11	3.98	3.61	<0.001	<0.01	<0.05
Phosphatidylcholine (PC)								
PC (38:1)	20.79	816.648	1.21	1.2	1.27	<0.001	<0.01	<0.001
PC (30:2)	21.65	692.558	1.58	1.92	1.91	<0.05	<0.01	<0.001
PC (32:2)	21.6	720.589	1.89	2.11	2.35	<0.05	<0.05	<0.05
PC (40:7)	20.28	832.587	1.25	1.22	1.31	<0.001	<0.01	<0.001
PC (P-36:3)	20.74	768.592	1.15	1.04	0.93	<0.001	ns	ns
PC (P-34:3)	21.41	740.559	1.25	1.46	1.39	<0.05	<0.001	<0.001
PC (P-38:2)	20.88	798.638	1.14	1.03	1.08	<0.05	ns	<0.05
PC (P-38:3)	20.64	796.623	1.14	1.02	1.13	<0.05	ns	<0.05
Phosphatidylethanolamine (PE)								
PE (36:1)	13.57	730.573	1.26	1.24	1.46	<0.05	ns	<0.05
PE (36:2)	13.37	744.553	1.08	1.05	1.16	<0.05	ns	<0.05
PE (38:4)	13.1	768.552	0.96	0.76	0.87	ns	<0.01	<0.05
PE (38:4)	13.09	752.558	1.12	1.04	1.15	<0.05	ns	<0.001
PE (40:1)	13.7	802.631	1.73	1.41	1.97	<0.001	ns	<0.05
PE (40:2)	13.58	800.616	1.21	1.15	1.34	<0.001	<0.001	<0.05
PE (40:3)	13.35	798.6	1.11	1.05	1.21	<0.05	ns	<0.001



			Treated/ Untreated			P-value		
Metabolite name	RT (min)	M/z	Ratio PLR	Ratio ST55	Ratio ST81	PLR24	ST55	ST81
PE (40:4)	13.21	796.584	1.08	0.98	1.15	<0.05	ns	<0.05
PE (40:6)	13.01	792.552	1.21	1.09	1.27	<0.05	ns	<0.05
PE (40:7)	12.98	776.559	1.1	1.05	1.15	<0.05	ns	<0.001
PE (42:2)	13.74	828.647	1.7	1.48	1.94	<0.001	<0.05	<0.001
PE (42:3)	13.5	826.632	1.25	1.18	1.28	<0.001	<0.05	<0.05
PE (42:6)	13.01	820.584	1.16	1.17	1.33	<0.001	<0.05	<0.001
PE (42:7)	13	818.568	1.11	1.1	1.25	<0.001	<0.05	<0.001
PE (44:6)	13.06	848.615	1.18	1.16	1.22	<0.001	<0.01	ns
PE (44:7)	12.97	846.6	1.15	1.21	1.3	<0.001	<0.05	<0.001
PE (P-34:3)	13.17	698.512	0.85	0.77	0.84	<0.001	<0.05	<0.001
PE (P-36:3)	13.13	726.543	0.85	0.69	0.76	<0.001	<0.001	<0.001
PE (P-36:5)	13.02	722.511	0.94	0.7	0.81	<0.05	<0.001	<0.001
PE (P-38:1)	13.64	758.605	1.39	1.26	1.65	<0.05	ns	<0.05
PE (P-40:1)	13.8	786.636	1.64	1.56	1.75	<0.05	ns	<0.05
PE (P-40:2)	13.46	784.62	1.2	1.13	1.42	<0.05	ns	<0.05
PE (P-40:3)	13.33	782.605	1.19	1.14	1.29	<0.05	ns	<0.001
PE (P-40:4)	13.18	780.59	1.27	1.36	1.5	<0.05	<0.01	<0.001
PE (P-42:5)	13.08	778.574	1.21	1.24	1.32	<0.001	<0.01	<0.001
PG								
PG (32:0)	4.6	723.515	5.68	6.19	7.34	<0.05	<0.05	<0.05
PG (34:0)	6.32	766.559	1.27	1.03	1.24	<0.05	ns	<0.05
PG (36:3)	4.24	771.519	3.26	3.45	3.94	<0.001	<0.01	<0.001
PG (36:4)	6.3	771.515	1.16	0.97	1.05	<0.05	ns	ns
PG (38:6)	4.23	795.515	2.81	3.08	3.19	<0.001	<0.01	<0.001
PG (36:5)	4.28	769.5	2.95	3.13	3.3	<0.001	<0.01	<0.001
PG (18:0)	4.31	509.289	2.76	2.55	2.83	<0.001	<0.05	<0.001
PG (38:3)	4.35	799.551	2.58	2.49	2.9	<0.001	<0.01	<0.001
PG (38:4)	6.62	799.546	1.23	1.19	1.21	<0.05	<0.01	<0.05
PG (40:4)	4.3	827.579	2.17	1.95	2.28	<0.001	<0.01	<0.001

			Treated/ Untreated			P-value		
Metabolite name	RT (min)	M/z	Ratio PLR	Ratio ST55	Ratio ST81	PLR24	ST55	ST81
PG (40:5)	4.35	825.563	2.08	2.07	2.14	<0.001	<0.01	<0.001
PG (40:6)	4.34	823.546	2.17	2.14	2.28	<0.001	<0.05	<0.001
PG (40:7)	4.12	821.531	2.12	2.06	2.09	<0.001	<0.01	<0.001
PG (36:6)	4.13	767.484	3.18	3.55	3.77	<0.001	<0.01	<0.001
PS								
PS (32:1)	14.08	734.495	1.64	2.16	2.5	<0.05	<0.05	<0.05
PS (34:1)	14.13	762.527	1.7	1.96	2.18	<0.05	<0.05	<0.05
PS (34:2)	13.99	760.511	1.38	1.69	1.93	<0.05	<0.05	<0.05
PS (36:1)	14.12	790.558	2.01	1.8	2.04	<0.05	<0.05	<0.05
PS (40:5)	13.91	838.557	1.6	1.55	1.87	<0.05	<0.05	<0.05
PS (40:6)	13.87	836.543	1.56	1.51	1.56	ns	<0.05	<0.05
PS (36:2)	14.04	788.542	1.46	1.63	1.87	<0.05	<0.05	<0.05

**Appendix 7:** Shows the effect of different inhibitors, non-selective (PLR24), SK I selective (ST55) and SK II selective (ST81) on LNCaP-AI cells using Silica gel conjugated with high resolution mass spectroscopy.

Met name	RT	M/Z	Ratio (Treated / untreated)			P-Value		
Sphingoid base			Ratio	Ratio-	Ratio	PLR	ST55	ST81
Sphingosine	12.28	300.2891	5.94	10.51	3.78	<0.001	<0.001	<0.001
Sphinganine	12.89	302.3045	3.46	3.75	1.73	<0.001	<0.001	<0.001
Dimethylsphingosine	12.23	328.3203	29.46	33.27	21.05	<0.001	<0.001	<0.001
Dihydroceramide	4.16	330.3002	1.22	0.94	0.94	<0.01	ns	ns
sphinga-dienine	12.02	298.2734	9.21	21.55	6.68	<0.001	<0.001	<0.001
Ceramides								
Cer(d18:0/14:0)	3.71	512.5044	1.40	0.83	0.83	<0.001	<0.01	<0.01
Cer(d18:0/16:0)	4.21	540.5360	1.67	0.80	0.91	<0.001	<0.01	ns
Cer(d18:0/22:0)	7.41	624.6294	4.69	2.47	1.07	<0.05	<0.05	ns
Cer (d18:1/16:0)	3.90	538.5198	1.31	0.87	0.88	<0.001	<0.01	<0.05
Glucosylcer (d18:1/16:0)	3.97	700.5726	1.45	0.81	0.91	<0.001	<0.001	<0.05
LacCer(d18:1/16:0)	4.49	862.6252	1.82	0.89	0.82	<0.001	ns	<0.01
Cer(d18:1/18:1)	3.84	564.5346	1.24	1.38	0.71	<0.01	<0.001	<0.01
SM(d18:1/18:1)	22.30	729.5895	1.70	1.30	0.84	<0.001	<0.01	<0.01
Cer(d18:1/18:0)	4.41	566.5508	1.79	1.79	0.83	<0.01	<0.001	<0.001
SM(d18:1/18:0)	22.33	731.6049	2.06	1.67	0.91	<0.001	<0.001	ns
Glucosylcer (d18:1/18:0)	4.40	728.6040	2.04	1.60	0.90	<0.001	<0.001	<0.05
LacCer(d18:1/18:0)	4.89	890.6564	2.43	1.52	0.85	<0.01	<0.05	<0.05
Cer(d18:1/20:0)	5.31	594.5822	2.62	2.59	1.16	<0.001	<0.01	<0.05
SM(d18:1/20:0)	22.32	759.6360	3.12	2.52	1.32	<0.001	<0.001	<0.001
Glucosylcer (d18:1/20:0)	5.07	756.6350	3.28	2.68	1.39	<0.001	<0.001	<0.001
LacCer(d18:1/20:0)	5.43	918.6874	2.81	1.92	1.01	<0.001	<0.05	ns
Cer(d18:1/26:1)	7.88	676.6602	2.50	1.37	0.95	<0.001	<0.05	ns
SM(d18:1/26:1)	22.22	841.7147	3.42	2.19	1.51	<0.001	<0.001	<0.001
Glucosylcer (d18:1/26:1)	7.34	838.7148	4.60	2.03	1.29	<0.01	<0.01	ns

**Appendix 8:** Shows the effect of different inhibitors, non-selective (PLR24) and SK2 selective inhibitors (ST55 and ST81) on LNCaP-AI cells using silica gel conjugated with high resolution mass spectroscopy. Where: T/C= treated cells/ untreated cells.

Fatty acids			Ratio (T/C)			P-value		
Metabolite name	RT	M/z	PLR24	ST55	ST81	PLR24	ST55	ST81
Linolenic acid	4.10	277.2173	3.38	3.20	2.84	<0.001	<0.001	<0.001
Linoleate	4.21	279.2330	3.41	2.94	2.69	<0.001	<0.001	<0.001
Dihomo- linolenate	4.14	305.2488	3.04	2.65	2.43	<0.001	<0.001	<0.001
Arachidonic acid	4.04	303.2331	3.01	2.92	2.75	<0.001	<0.001	<0.001
Eicosenoic acid	4.52	309.2800	2.76	1.68	1.79	<0.001	<0.001	<0.001
Docosahexaenoicacid	3.95	327.2331	2.45	1.52	1.57	<0.001	<0.001	<0.001
Hydroxy-eicosadienoic acid	4.27	325.2736	2.59	1.79	1.79	<0.001	<0.001	<0.001
Octadecenoic acid	4.34	281.2485	3.15	2.21	2.13	<0.001	<0.001	<0.001
Hexadecadienoic acid	4.14	251.2017	3.61	2.69	2.55	<0.001	<0.001	<0.001
Cyclohexylundecanoic acid	4.31	267.2332	3.50	2.47	2.38	<0.001	<0.001	<0.001
Tridecadienoic acid	3.39	211.1693	0.48	0.66	0.83	<0.05	ns	ns
Oxo-hexadecanoic acid	3.41	271.2267	0.56	0.56	0.67	<0.05	<0.05	<0.05
FA (12:3)	3.41	181.1587	0.52	0.54	1.06	<0.001	<0.05	ns
FA methoxy (16:0)	4.14	285.2424	2.41	1.69	1.58	<0.001	<0.001	<0.001
FA methyl (18:0)	4.24	293.2490	3.26	2.53	2.46	<0.001	<0.001	<0.001
FA methyl (18:1)	4.39	295.2644	2.79	1.73	1.82	<0.001	<0.001	<0.001
FA (18:2)	4.35	265.2525	2.15	1.32	1.32	<0.001	0.0017	<0.001
FA oxo (19:0)	4.45	313.2736	2.85	1.80	1.64	<0.001	<0.001	<0.001
FA oxo (21:0)	4.61	341.3047	2.96	1.78	1.61	<0.001	0.0030	<0.001
Adrenic Acid	4.13	331.2645	2.66	1.69	1.78	<0.001	<0.001	<0.001
Docosatrienoic acid	4.25	333.2802	3.20	2.32	2.33	<0.001	<0.001	<0.001
<b>Fatty acyls -Carnitine</b>								
O-Propanoylcarnitine	28.71	218.1384	1.35	0.64	0.75	<0.01	<0.010	<0.010
O-Butanoylcarnitine	27.30	232.1546	1.60	0.72	0.87	<0.001	<0.010	<0.050
O-decanoyl-R-carnitine	24.57	316.2476	3.16	3.24	2.09	<0.001	<0.010	ns

O-Palmitoyl-R-carnitine	23.61	400.3413	1.76	1.58	1.29	<0.001	<0.010	<0.010
Hexadec-enoylcarnitine	23.55	398.3258	1.58	2.12	1.56	<0.01	<0.010	<0.010
Elaidiccarnitine	23.34	426.3569	1.49	1.53	1.26	<0.001	<0.050	<0.010
<b>LysoPC</b>								
LysoPC (16:0)	23.50	496.3389	1.98	2.84	1.56	<0.001	<0.001	<0.001
LysoPC (16:1)	23.11	480.3440	1.93	2.11	1.45	<0.001	<0.001	<0.05
LysoPC (16:2)	24.24	482.3597	1.86	1.90	1.37	<0.001	<0.001	<0.001
LysoPC(18:0)	24.02	510.3912	1.97	1.86	1.33	<0.001	<0.001	<0.05
LysoPC (18:1)	22.87	508.3753	2.33	2.23	1.56	<0.001	<0.001	<0.001
<b>LysoPC (20:0)</b>	23.08	552.4021	4.57	8.38	4.32	<0.001	<0.001	<0.001
LysoPC (20:1)	23.14	550.3858	2.06	3.81	1.88	<0.001	<0.001	<0.001
LysoPC (22:1)	22.89	578.4170	2.86	6.34	3.15	<0.001	<0.001	<0.001
<b>LysoPC (22:0)</b>	22.87	580.4337	6.71	29.69	18.40	<0.05	<0.05	<0.05
LysoPC (24:1)	22.82	606.4482	3.54	6.15	4.56	<0.001	<0.001	<0.001
LysoPC (24:0)	22.71	608.4654	5.03	4.97	4.91	<0.05	<0.001	<0.001
<b>Phosphatidylcholine (PC)</b>								
PC (36:0)	20.94	790.6300	1.52	1.23	1.14	<0.001	<0.001	0.0013
PC (38:1)	20.79	816.6475	1.40	1.15	1.11	<0.001	<0.05	<0.05
PC (30:2)	21.65	692.5580	2.25	1.53	1.39	<0.001	<0.001	<0.001
PC (32:2)	21.60	720.5894	2.81	1.50	1.30	<0.05	<0.05	<0.05
PC (40:7)	20.28	832.5871	1.45	1.34	1.00	<0.05	<0.05	ns
PC (P-36:3)	20.74	768.5917	1.50	1.20	1.06	<0.001	<0.05	ns
PC (P-34:3)	21.41	740.5589	1.45	1.23	1.25	<0.001	<0.05	<0.05
PC (P-38:2)	20.88	798.6382	1.27	0.88	0.86	<0.001	<0.05	<0.05
PC (P-38:3)	20.64	796.6228	1.28	0.84	0.79	<0.001	<0.05	<0.05
<b>Phosphatidylethanolamine (PE)</b>								
PE (36:2)	13.37	744.5526	1.39	1.11	1.01	<0.001	<0.05	ns
PE (36:2)	13.57	730.5733	1.95	1.29	1.05	<0.001	<0.05	ns
PE (36:3)	13.24	742.5382	1.2	0.91	0.85	<0.001	<0.05	<0.05

PE (38:2)	13.46	772.5841	1.44	1.05	0.93	<0.001	ns	ns
PE (38:4)	13.10	768.5524	1.2	0.81	0.74	<0.001	<0.001	<0.001
PE (38:5)	13.09	752.5579	1.24	0.9	0.87	<0.001	<0.05	<0.05
PE (38:5)	13.02	766.5362	1.28	0.98	0.9	<0.001	ns	<0.05
PE (40:1)	13.71	802.6306	2.49	1.33	1.12	<0.05	ns	ns
PE (40:2)	13.58	800.6155	1.65	1.23	1.06	<0.001	<0.05	ns
PE (40:3)	13.35	798.5999	1.46	1.13	1.03	<0.001	<0.05	ns
PE (40:4)	13.21	796.584	1.32	1.04	0.96	<0.001	ns	ns
PE (40:6)	13.01	792.5522	1.44	1.12	0.97	<0.001	<0.05	ns
PE (40:7)	12.98	776.5585	1.27	0.97	0.92	<0.001	ns	<0.05
PE (42:2)	13.74	828.6469	2.59	1.26	1.13	<0.001	ns	ns
PE (42:3)	13.50	826.6319	1.54	1.05	0.98	<0.001	ns	ns
PE (42:4)	13.25	824.6144	1.27	0.98	0.93	<0.001	ns	<0.05
PE (42:6)	13.01	820.5837	1.32	1.05	0.96	<0.001	ns	ns
PE (42:7)	13.00	818.568	1.33	1.12	1.06	<0.001	<0.05	ns
PE (44:4)	13.43	852.6479	1.27	0.86	0.82	<0.05	<0.05	<0.05
PE (44:5)	13.20	850.6307	1.21	0.83	0.81	<0.05	<0.05	<0.05
PE (44:6)	13.06	848.6152	1.53	0.99	0.94	<0.001	ns	ns
PE (44:7)	12.97	846.5999	1.61	1.17	1.11	<0.001	<0.05	ns
PE (P-34:0)	13.17	698.5116	1.28	0.88	0.77	<0.001	ns	<0.05
PE (P-36:2)	13.34	728.5583	1.23	1.05	0.91	<0.05	ns	ns
PE (P-36:3)	13.13	726.5429	1.12	0.75	0.72	<0.05	<0.001	0.0001
PE (P-36:4)	13.04	724.5267	1.48	1.15	1.09	<0.001	<0.05	ns
PE (P-36:5)	13.00	722.5107	1.28	0.9	0.86	<0.001	<0.05	<0.05
PE (P-38:1)	13.64	758.6053	2.54	1.24	1.01	<0.05	ns	ns
PE (P-38:2)	13.37	756.5892	1.34	0.99	0.9	<0.001	ns	<0.05
PE (P-38:3)	13.22	754.5739	1.22	0.91	0.86	<0.001	<0.05	<0.05
PE (P-38:5)	13.04	750.5419	1.39	1.06	0.98	<0.001	ns	ns
PE (P-40:1)	13.80	786.6362	3.88	1.63	1.07	<0.05	<0.05	ns

PE (P-40:2)	13.46	784.6202	1.57	1.23	1.13	<0.001	<0.001	<0.05
PE (P-40:3)	13.33	782.6051	1.36	1.21	1.13	<0.001	<0.001	<0.05
PE (P-40:4)	13.18	780.59	1.26	1.21	1.11	<0.001	<0.001	<0.05
PE (P-42:5)	13.08	778.574	1.33	1.1	1.02	<0.001	<0.05	ns
<b>Phosphatidylglycerol (PG)</b>								
PG (32:0)	4.60	723.5149	6.63	3.81	2.92	0.0035	<0.05	<0.05
PG (34:0)	6.32	766.5593	1.79	1.02	0.93	<0.001	ns	<0.05
PG (36:3)	4.24	771.5191	3.73	3.00	2.75	<0.001	<0.001	<0.001
PG (36:4)	6.30	771.5148	1.67	0.96	0.92	<0.001	ns	<0.05
PG (36:5)	4.28	769.4996	3.5	2.58	2.39	<0.001	<0.001	<0.001
PG (36:6)	4.13	767.4837	3.43	2.82	2.5	0.0035	<0.05	<0.001
PG (38:3)	4.35	799.5505	3.22	2.25	2.21	<0.001	<0.001	<0.001
PG (38:4)	6.62	799.5461	1.78	1.25	0.99	0.0011	<0.05	ns
PG (38:5)	6.18	797.5305	1.49	1.24	0.99	<0.001	<0.05	ns
PG (38:6)	4.23	795.5152	2.99	2.47	2.19	<0.001	<0.001	<0.001
PG (40:4)	4.30	827.5789	2.51	1.81	1.73	<0.001	<0.001	<0.001
PG (40:6)	4.34	823.5464	2.52	1.82	1.74	<0.001	<0.001	<0.001
PG (40:7)	4.12	821.531	2.57	2.2	1.94	<0.001	<0.001	<0.001
PG (42:5)	4.35	825.5626	2.36	1.61	1.54	<0.001	<0.05	<0.001
<b>Phosphatidylserine (PS)</b>								
PS (32:1)	14.08	734.4953	2.08	1.14	0.74	<0.050	ns	ns
PS (34:1)	14.13	762.5267	2.47	1.28	0.74	<0.050	ns	ns
PS (34:2)	13.99	760.5109	1.92	1.11	0.84	<0.050	ns	ns
PS (36:1)	14.12	790.5577	3.21	1.68	0.84	<0.050	ns	ns
PS (36:2)	14.04	788.542	2.18	1.21	0.85	<0.050	ns	ns
PS (40:5)	13.91	838.5573	2.41	1.34	0.83	<0.050	ns	ns
PS (40:6)	13.87	836.5426	2.09	1.09	0.67	<0.050	ns	ns

## References

1. Le Gac, S., Van Den Berg, A.: Single cell electroporation using microfluidic devices. Humana Press, Stockholm (2012)
2. Wang, J., Jin, L., Li, X., Deng, H., Chen, Y., Lian, Q., Ge, R., Deng, H.: Gossypol induces apoptosis in ovarian cancer cells through oxidative stress. *Mol. Biosyst.* (2013). <https://doi.org/10.1039/c3mb25461e>
3. Čuperlović-Culf, M., Barnett, D.A., Culf, A.S., Chute, I.: Cell culture metabolomics: Applications and future directions, (2010)
4. Trock, B.J.: Application of metabolomics to prostate cancer, (2011)
5. Watson, D.G., Tonelli, F., Alossaimi, M., Williamson, L., Chan, E., Gorshkova, I., Berdyshev, E., Bittman, R., Pyne, N.J., Pyne, S.: The roles of sphingosine kinases 1 and 2 in regulating the Warburg effect in prostate cancer cells. *Cell. Signal.* 25, 1011–1017 (2013). <https://doi.org/10.1016/j.cellsig.2013.01.002>
6. Putluri, N., Shojaie, A., Vasu, V.T., Nalluri, S., Vareed, S.K., Putluri, V., Vivekanandan-Giri, A., Byun, J., Pennathur, S., Sana, T.R., Fischer, S.M., Palapattu, G.S., Creighton, C.J., Michailidis, G., Sreekumar, A.: Metabolomic profiling reveals a role for androgen in activating amino acid metabolism and methylation in prostate cancer cells. *PLoS One.* (2011). <https://doi.org/10.1371/journal.pone.0021417>
7. Kupfer, M.E., Ogle, B.M.: Advanced imaging approaches for regenerative medicine: Emerging technologies for monitoring stem cell fate in vitro and in vivo, (2015)



8. Galler, K., Bräutigam, K., Bräutigam, K., Große, C., Popp, J., Neugebauer, U.: Making a big thing of a small cell - recent advances in single cell analysis. *Analyst*. (2014). <https://doi.org/10.1039/c3an01939j>
9. Lee, DA, Brand, J, Salter, D, Akanji, O-O, and C.: Quantification of mRNA Using Real-Time PCR and Western Blot Analysis of MAPK Events in Chondrocyte/Agarose Constructs in 3D Cell Culture. In: Haycock, J.W. (ed.) *3D Cell Culture*. pp. 77–97. Springer Science, Haycock (2010)
10. Stratton, M.R., Campbell, P.J., Futreal, P.A.: *The cancer genome*, (2009)
11. Hanahan, D., Weinberg, R.A.: Hallmarks of cancer: the next generation. *Cell*. 144, 646–74 (2011). <https://doi.org/10.1016/j.cell.2011.02.013>
12. Komoda, T., Matsunaga, T., Komoda, T., Matsunaga, T.: *Metabolic Pathways in the Human Body*. (2015)
13. Icard, P., Lincet, H.: A global view of the biochemical pathways involved in the regulation of the metabolism of cancer cells. *Biochim. Biophys. Acta - Rev. Cancer*. 1826, 423–433 (2012). <https://doi.org/10.1016/j.bbcan.2012.07.001>
14. Warburg, O.: On the origin of cancer cells. *Science* (80-. ). (1956). <https://doi.org/10.1126/science.123.3191.309>
15. Koppenol, W.H., Bounds, P.L., Dang, C. V.: Otto Warburg's contributions to current concepts of cancer metabolism, (2011)
16. Harris, T., Degani, H., Frydman, L.: Hyperpolarized <sup>13</sup>C NMR studies of glucose metabolism in living breast cancer cell cultures. *NMR Biomed*. 26, 1831–1843 (2013). <https://doi.org/10.1002/nbm.3024>
17. Tennant, D.A., Durán, R. V., Gottlieb, E.: *Targeting metabolic transformation for cancer therapy*, (2010)

18. Horecker, B.L.: The Pentose phosphate pathway. In: *The Roots of Modern Biochemistry: Fritz Lippmann's Squiggle and its Consequences* (2011)
19. Kruger, N.J., Von Schaewen, A.: *The oxidative pentose phosphate pathway: Structure and organisation*, (2003)
20. Patra, K.C., Hay, N.: *The pentose phosphate pathway and cancer*, (2014)
21. Raïs, B., Comin, B., Puigjaner, J., Brandes, J.L., Creppy, E., Saboureau, D., Ennamany, R., Paul Lee, W.N., Boros, L.G., Cascante, M.: Oxythiamine and dehydroepiandrosterone induce a G 1 phase cycle arrest in Ehrlich's tumor cells through inhibition of the pentose cycle. *FEBS Lett.* 456, 113–118 (1999). [https://doi.org/10.1016/S0014-5793\(99\)00924-2](https://doi.org/10.1016/S0014-5793(99)00924-2)
22. Boros, L.G., Brandes, J.L., Yusuf, F.I., Cascante, M., Williams, R.D., Schirmer, W.J.: Inhibition of the oxidative and nonoxidative pentose phosphate pathways by somatostatin: A possible mechanism of antitumor action. *Med. Hypotheses.* (1998). [https://doi.org/10.1016/S0306-9877\(98\)90271-7](https://doi.org/10.1016/S0306-9877(98)90271-7)
23. Murray, R.K., Davis, J.C.: *Harper's Illustrated Biochemistry*. Lange Medical Books/McGraw-Hill, London (2003)
24. Maréchal, E., Riou, M., Kerboeuf, D., Beugnet, F., Chaminade, P., Loiseau, P.M.: Membrane lipidomics for the discovery of new antiparasitic drug targets. *Trends Parasitol.* 27, 496–504 (2011). <https://doi.org/10.1016/j.pt.2011.07.002>
25. Abramson, H.N.: *The lipogenesis pathway as a cancer target*, (2011)
26. Brand, K.A., Hermfisse, U.: Aerobic glycolysis by proliferating cells: A protective strategy against reactive oxygen species. *FASEB J.* (1997). <https://doi.org/10.1096/fasebj.11.5.9141507>
27. Pyne, N.J., Pyne, S.: Sphingosine 1-phosphate and cancer. *Nat. Rev. Cancer.* 10, 489–503 (2010). <https://doi.org/10.1038/nrc2875>

28. Loveridge, C., Tonelli, F., Leclercq, T., Lim, K.G., Long, J.S., Berdyshev, E., Tate, R.J., Natarajan, V., Pitson, S.M., Pyne, N.J., Pyne, S.: The sphingosine kinase 1 inhibitor 2-(p-hydroxyanilino)-4-(p-chlorophenyl) thiazole induces proteasomal degradation of sphingosine kinase 1 in mammalian cells. *J. Biol. Chem.* 285, 38841–38852 (2010). <https://doi.org/10.1074/jbc.M110.127993>
29. Okada, T., Ding, G., Sonoda, H., Kajimoto, T., Haga, Y., Khosrowbeygi, A., Gao, S., Miwa, N., Jahangeer, S., Nakamura, S.I.: Involvement of N-terminal-extended form of sphingosine kinase 2 in serum-dependent regulation of cell proliferation and apoptosis. *J. Biol. Chem.* (2005). <https://doi.org/10.1074/jbc.M504507200>
30. Pyne, S., Pyne, N.J.: Sphingosine 1-phosphate signalling in mammalian cells. *Biochem. J.* 349, 385–402 (2000). <https://doi.org/10.1042/0264-6021:3490385>
31. Hofmann, K., Dixit, V.M.: Ceramide in apoptosis--does it really matter? *Trends Biochem. Sci.* 23, 374–7 (1998). <https://doi.org/9810222>
32. Kitatani, K., Idkowiak-Baldys, J., Hannun, Y. a.: The sphingolipid salvage pathway in ceramide metabolism and signaling. *Cell. Signal.* 20, 1010–1018 (2008). <https://doi.org/10.1016/j.cellsig.2007.12.006>
33. Doan, Thao., Melvold, Roger., Viselli, Susan., Waltenbaugh, C.: Lippincott's Illustrated Reviews, Immunology. (2008)
34. Montfort, A., Martin, P.G.P., Levade, T., Benoist, H., Ségui, B.: FAN (factor associated with neutral sphingomyelinase activation), a moonlighting protein in TNF-R1 signaling. *J. Leukoc. Biol.* (2010). <https://doi.org/10.1189/jlb.0410188>
35. Son, J.H., Yoo, H.H., Kim, D.-H.: Activation of de novo synthetic pathway of ceramides is responsible for the initiation of hydrogen peroxide-induced apoptosis in HL-60 cells. *J. Toxicol. Environ. Health. A.* 70, 1310–8 (2007). <https://doi.org/10.1080/15287390701434364>

36. Gómez del Pulgar, T., Velasco, G., Sánchez, C., Haro, A., Guzmán, M.: De novo-synthesized ceramide is involved in cannabinoid-induced apoptosis. *Biochem. J.* 363, 183–8 (2002). <https://doi.org/10.1042/0264-6021:3630183>
37. Wang, F., Nohara, K., Olivera, a, Thompson, E.W., Spiegel, S.: Involvement of focal adhesion kinase in inhibition of motility of human breast cancer cells by sphingosine 1-phosphate. *Exp. Cell Res.* 247, 17–28 (1999). <https://doi.org/10.1006/excr.1998.4327>
38. Pyne, S., Pyne, N.J.: Translational aspects of sphingosine 1-phosphate biology. *Trends Mol. Med.* 17, 463–472 (2011). <https://doi.org/10.1016/j.molmed.2011.03.002>
39. Hait, N.C., Allegood, J., Maceyka, M., Strub, G.M., Harikumar, K.B., Singh, S.K., Luo, C., Marmorstein, R., Kordula, T., Milstien, S., Spiegel, S.: Regulation of histone acetylation in the nucleus by sphingosine-1-phosphate. *Science* (80-. ). (2009). <https://doi.org/10.1126/science.1176709>
40. Alvarez, S.E., Harikumar, K.B., Hait, N.C., Allegood, J., Strub, G.M., Kim, E.Y., MacEyka, M., Jiang, H., Luo, C., Kordula, T., Milstien, S., Spiegel, S.: Sphingosine-1-phosphate is a missing cofactor for the E3 ubiquitin ligase TRAF2. *Nature*. (2010). <https://doi.org/10.1038/nature09128>
41. Parham, K.A., Zebol, J.R., Tooley, K.L., Sun, W.Y., Moldenhauer, L.M., Cockshell, M.P., Gliddon, B.L., Moretti, P.A., Tigyi, G., Pitson, S.M., Bonder, C.S.: Sphingosine 1-phosphate is a ligand for peroxisome proliferator-activated receptor- $\gamma$  that regulates neoangiogenesis. *FASEB J.* (2015). <https://doi.org/10.1096/fj.14-261289>
42. Ross, J.S., Hu, W., Rosen, B., Snider, A.J., Obeid, L.M., Cowart, L.A.: Sphingosine kinase 1 is regulated by peroxisome proliferator-activated receptor  $\alpha$  in response to free fatty acids and is essential for skeletal muscle interleukin-6 production and signaling in diet-induced obesity. *J. Biol. Chem.* (2013).

<https://doi.org/10.1074/jbc.M113.477786>

43. Panneer Selvam, S., De Palma, R.M., Oaks, J.J., Oleinik, N., Peterson, Y.K., Stahelin, R. V., Skordalakes, E., Ponnusamy, S., Garrett-Mayer, E., Smith, C.D., Ogretmen, B.: Binding of the sphingolipid S1P to hTERT stabilizes telomerase at the nuclear periphery by allosterically mimicking protein phosphorylation. *Sci. Signal.* (2015). <https://doi.org/10.1126/scisignal.aaa4998>
44. Strub, G.M., Paillard, M., Liang, J., Gomez, L., Allegood, J.C., Hait, N.C., Maceyka, M., Price, M.M., Chen, Q., Simpson, D.C., Kordula, T., Milstien, S., Lesnefsky, E.J., Spiegel, S.: Sphingosine-1-phosphate produced by sphingosine kinase 2 in mitochondria interacts with prohibitin 2 to regulate complex IV assembly and respiration. *FASEB J.* (2011). <https://doi.org/10.1096/fj.10-167502>
45. Xia, P., Wang, L., Moretti, P.A.B., Albanese, N., Chai, F., Pitson, S.M., D'Andrea, R.J., Gamble, J.R., Vadas, M.A.: Sphingosine kinase interacts with TRAF2 and dissects tumor necrosis factor- $\alpha$  signaling. *J. Biol. Chem.* (2002). <https://doi.org/10.1074/jbc.M111423200>
46. Sablina, A.A., Budanov, A. V., Ilyinskaya, G. V., Agapova, L.S., Kravchenko, J.E., Chumakov, P.M.: The antioxidant function of the p53 tumor suppressor. *Nat. Med.* (2005). <https://doi.org/10.1038/nm1320>
47. Cao, L., Xu, X., Cao, L.L., Wang, R.H., Coumoul, X., Kim, S.S., Deng, C.X.: Absence of full-length Brca1 sensitizes mice to oxidative stress and carcinogen-induced tumorigenesis in the esophagus and forestomach. *Carcinogenesis.* (2007). <https://doi.org/10.1093/carcin/bgm060>
48. Ogrunc, M., Di Micco, R., Liontos, M., Bombardelli, L., Mione, M., Fumagalli, M., Gorgoulis, V.G., D'Adda Di Fagagna, F.: Oncogene-induced reactive oxygen species fuel hyperproliferation and DNA damage response activation. *Cell Death Differ.* (2014). <https://doi.org/10.1038/cdd.2014.16>

49. Liu, P., Cheng, H., Roberts, T.M., Zhao, J.J.: Targeting the phosphoinositide 3-kinase pathway in cancer, (2009)
50. Roberts, P.J., Der, C.J.: Targeting the Raf-MEK-ERK mitogen-activated protein kinase cascade for the treatment of cancer, (2007)
51. Shaw, A.T., Winslow, M.M., Magendantz, M., Ouyang, C., Dowdle, J., Subramanian, A., Lewis, T.A., Maglathin, R.L., Tolliday, N., Jacks, T.: Selective killing of K-ras mutant cancer cells by small molecule inducers of oxidative stress. *Proc. Natl. Acad. Sci. U. S. A.* (2011). <https://doi.org/10.1073/pnas.1105941108>
52. Halama, A.: Metabolomics in cell culture — A strategy to study crucial metabolic pathways in cancer development and the response to treatment. *564*, 100–109 (2014)
53. Pauling, L., Robinson, a B., Teranishi, R., Cary, P.: Quantitative analysis of urine vapor and breath by gas-liquid partition chromatography. *Proc. Natl. Acad. Sci. U. S. A.* *68*, 2374–2376 (1971). <https://doi.org/10.1073/pnas.68.10.2374>
54. Lenz, E.M., Wilson, I.D.: Analytical strategies in metabolomics. *J. Proteome Res.* *6*, 443–458 (2007). <https://doi.org/10.1021/pr0605217>
55. Dunn, W.B., Broadhurst, D.I., Atherton, H.J., Goodacre, R., Griffin, J.L.: Systems level studies of mammalian metabolomes: The roles of mass spectrometry and nuclear magnetic resonance spectroscopy, (2011)
56. Heinzle, E., Yuan, Y., Kumar, S., Wittmann, C., Gehre, M., Richnow, H.-H., Wehrung, P., Adam, P., Albrecht, P.: Analysis of <sup>13</sup>C labeling enrichment in microbial culture applying metabolic tracer experiments using gas chromatography–combustion–isotope ratio mass spectrometry. *Anal. Biochem.* *380*, 202–210 (2008). <https://doi.org/10.1016/j.ab.2008.05.039>

57. Icard, P., Lincet, H.: A global view of the biochemical pathways involved in the regulation of the metabolism of cancer cells. *Biochim. Biophys. Acta - Rev. Cancer.* 1826, 423–433 (2012). <https://doi.org/10.1016/j.bbcan.2012.07.001>
58. Poisson, L.M., Munkarah, A., Madi, H., Datta, I., Hensley-Alford, S., Tebbe, C., Buekers, T., Giri, S., Rattan, R.: A metabolomic approach to identifying platinum resistance in ovarian cancer. *J. Ovarian Res.* (2015). <https://doi.org/10.1186/s13048-015-0140-8>
59. Denmeade, S.R., Lin, X.S., Isaacs, J.T.: Role of programmed (apoptotic) cell death during the progression and therapy for prostate cancer. *Prostate.* (1996). [https://doi.org/10.1002/\(SICI\)1097-0045\(199604\)28:4<251::AID-PROS6>3.0.CO;2-G](https://doi.org/10.1002/(SICI)1097-0045(199604)28:4<251::AID-PROS6>3.0.CO;2-G)
60. Denis, L.J., Griffiths, K.: *Endocrine treatment in prostate cancer*, (2000)
61. Harris, K.A., Reese, D.M.: *Treatment options in hormone-refractory prostate cancer: Current and future approaches*, (2001)
62. Harvey, C.J., Pilcher, J., Richenberg, J., Patel, U., Frauscher, F.: Applications of transrectal ultrasound in prostate cancer. *Br. J. Radiol.* (2012). <https://doi.org/10.1259/bjr/56357549>
63. Lee, J.T., Lehmann, B.D., Terrian, D.M., Chappell, W.H., Stivala, F., Libra, M., Martelli, A.M., Steelman, L.S., McCubrey, J.A.: Targeting prostate cancer based on signal transduction and cell cycle pathways. *Cell Cycle.* (2008). <https://doi.org/10.4161/cc.7.12.6166>
64. Chua, C.W., Lee, D.T.W., Ling, M.T., Zhou, C., Man, K., Ho, J., Chan, F.L., Wang, X., Wong, Y.C.: FTY720, a fungus metabolite, inhibits in vivo growth of androgen-independent prostate cancer. *Int. J. Cancer.* 117, 1039–1048 (2005). <https://doi.org/10.1002/ijc.21243>

65. Huggins, C., Hodges, C. V.: Studies on prostatic cancer i. the effect of castration, of estrogen and of androgen injection on serum phosphatases in metastatic carcinoma of the prostate. *Cancer Res.* (1941). <https://doi.org/10.1111/j.1743-6109.2009.01680.x>
66. Sridhar, S.S., Moore, M.J.: Chemotherapy in prostate cancer. *Urol. Cancers Clin. Pract.* 50–74 (2007). [https://doi.org/10.1007/978-1-84628-507-3\\_4](https://doi.org/10.1007/978-1-84628-507-3_4)
67. James, N.D., Spears, M.R., Clarke, N.W., Dearnaley, D.P., De Bono, J.S., Gale, J., Hetherington, J., Hoskin, P.J., Jones, R.J., Laing, R., Lester, J.F., McLaren, D., Parker, C.C., Parmar, M.K.B., Ritchie, A.W.S., Russell, J.M., Strebel, R.T., Thalmann, G.N., Mason, M.D., Sydes, M.R., Sweeney, C.J., Chen, Y.-H., Carducci, M., Liu, G., Jarrard, D.F., Eisenberger, M., Wong, Y.-N., Hahn, N., Kohli, M., Cooney, M.M., Dreicer, R., Vogelzang, N.J., Picus, J., Shevrin, D., Hussain, M., Garcia, J.A., DiPaola, R.S., Gravis, G., Fizazi, K., Joly, F., Oudard, S., Priou, F., Esterni, B., Latorzeff, I., Delva, R., Krakowski, I., Laguerre, B., Rolland, F., Théodore, C., Deplanque, G., Ferrero, J.M., Pouessel, D., Mourey, L., Beuzebec, P., Zanetta, S., Habibian, M., Berdahl, J.F., Dauba, J., Baciuchka, M., Platini, C., Linassier, C., Labourey, J.L., Machiels, J.P., El Kouri, C., Ravaud, A., Suc, E., Eymard, J.C., Hasbini, A., Bousquet, G., Soulie, M.: Androgen-deprivation therapy alone or with docetaxel in non-castrate metastatic prostate cancer (GETUG-AFU 15): A randomised, Open-label, Phase 3 trial. *Lancet Oncol.* 67, 149–158 (2015). <https://doi.org/10.1056/NEJMoa1503747>
68. Paugh, S.W., Paugh, B.S., Rahmani, M., Kapitonov, D., Almenara, J. a., Kordula, T., Milstien, S., Adams, J.K., Zipkin, R.E., Grant, S., Spiegel, S.: A selective sphingosine kinase 1 inhibitor integrates multiple molecular therapeutic targets in human leukemia. *Blood.* 112, 1382–1391 (2008). <https://doi.org/10.1182/blood-2008-02-138958>
69. Kapitonov, D., Allegood, J.C., Mitchell, C., Hait, N.C., Almenara, J. a, Adams, J.K., Zipkin, R.E., Dent, P., Kordula, T., Milstien, S., Spiegel, S.: Targeting



- sphingosine kinase 1 inhibits Akt signaling, induces apoptosis, and suppresses growth of human glioblastoma cells and xenografts. *Cancer Res.* 69, 6915–23 (2009). <https://doi.org/10.1158/0008-5472.CAN-09-0664>
70. French, K.J., Upson, J.J., Keller, S.N., Zhuang, Y., Yun, J.K., Smith, C.D.: Antitumor activity of sphingosine kinase inhibitors. *J. Pharmacol. Exp. Ther.* 318, 596–603 (2006). <https://doi.org/10.1124/jpet.106.101345>
71. French, K.J., Zhuang, Y., Maines, L.W., Gao, P., Wang, W., Beljanski, V., Upson, J.J., Green, C.L., Keller, S.N., Smith, C.D.: Pharmacology and antitumor activity of ABC294640, a selective inhibitor of sphingosine kinase-2. *J. Pharmacol. Exp. Ther.* 333, 129–139 (2010). <https://doi.org/10.1124/jpet.109.163444>
72. Beljanski, V., Knaak, C., Smith, C.D.: A novel sphingosine kinase inhibitor induces autophagy in tumor cells. *J. Pharmacol. Exp. Ther.* 333, 454–64 (2010). <https://doi.org/10.1124/jpet.109.163337>
73. Tonelli, F., Alossaimi, M., Natarajan, V., Gorshkova, I., Berdyshev, E., Bittman, R., Watson, D., Pyne, S., Pyne, N.: The Roles of Sphingosine Kinase 1 and 2 in Regulating the Metabolome and Survival of Prostate Cancer Cells. *Biomolecules.* 3, 316–333 (2013). <https://doi.org/10.3390/biom3020316>
74. Tonelli, F., Alossaimi, M., Williamson, L., Tate, R.J., Watson, D.G., Chan, E., Bittman, R., Pyne, N.J., Pyne, S.: The sphingosine kinase inhibitor 2-(phyoxyanilino)-4-(pchlorophenyl) thiazole reduces androgen receptor expression via an oxidative stress-dependent mechanism. *Br. J. Pharmacol.* (2013). <https://doi.org/10.1111/bph.12035>
75. Lim, K.G., Sun, C., Bittman, R., Pyne, N.J., Pyne, S.: (R)-FTY720 methyl ether is a specific sphingosine kinase 2 inhibitor: Effect on sphingosine kinase 2 expression in HEK 293 cells and actin rearrangement and survival of MCF-7 breast cancer cells. *Cell. Signal.* 23, 1590–1595 (2011).

<https://doi.org/10.1016/j.cellsig.2011.05.010>

76. Katajamaa, M., Orešič, M.: Data processing for mass spectrometry-based metabolomics, (2007)
77. Simmler, C., Napolitano, J.G., McAlpine, J.B., Chen, S.N., Pauli, G.F.: Universal quantitative NMR analysis of complex natural samples, (2014)
78. Watson, D.: *Pharmaceutical Analysis*. Elsevier , Edinburgh (2012)
79. Jandera, P.: Stationary phases for hydrophilic interaction chromatography, their characterization and implementation into multidimensional chromatography concepts, (2008)
80. Cubbon, S., Antonio, C., Wilson, J., Thomas-Oates, J.: Metabolomic applications of HILIC-LC-MS. *Mass Spectrom. Rev.* (2010).  
<https://doi.org/10.1002/mas.20252>
81. Zhang, R., Watson, D.G., Wang, L., Westrop, G.D., Coombs, G.H., Zhang, T.: Evaluation of mobile phase characteristics on three zwitterionic columns in hydrophilic interaction liquid chromatography mode for liquid chromatography-high resolution mass spectrometry based untargeted metabolite profiling of *Leishmania* parasites. *J. Chromatogr. A.* (2014).  
<https://doi.org/10.1016/j.chroma.2014.08.039>
82. Alpert, A.J.: Hydrophilic-interaction chromatography for the separation of peptides, nucleic acids and other polar compounds. *J. Chromatogr. A.* (1990).  
[https://doi.org/10.1016/S0021-9673\(00\)96972-3](https://doi.org/10.1016/S0021-9673(00)96972-3)
83. Jandera, P.: Stationary and mobile phases in hydrophilic interaction chromatography: A review, (2011)
84. Moldoveanu, S.C., David, V.: *Selection of the HPLC Method in Chemical Analysis*. (2016)

85. Nawrocki, J.: The silanol group and its role in liquid chromatography, (1997)
86. Botsoglou, N.A.: Encyclopedia of Chromatography. (2005)
87. Rojo, D., Barbas, C., Rupérez, F.J.: LC-MS metabolomics of polar compounds, (2012)
88. Alpert, A.J.: HILIC at 21: Reflections and perspective, (2011)
89. Donald L. Pavia, Gary M Lampman ; George S Kriz ; James R Vyvyan: Introduction to spectroscopy. Pacific Grove, Calif. : Brooks/Cole , Lodon (2008)
90. Cech, N.B., Enke, C.G.: Practical implications of some recent studies in electrospray ionization fundamentals. *Mass Spectrom. Rev.* (2001).  
<https://doi.org/10.1002/mas.10008>
91. Watson, J.T., Sparkman, O.D.: Introduction to Mass Spectrometry: Instrumentation, Applications and Strategies for Data Interpretation: Fourth Edition. (2008)
92. Michalski, A., Damoc, E., Hauschild, J.P., Lange, O., Wieghaus, A., Makarov, A., Nagaraj, N., Cox, J., Mann, M., Horning, S.: Mass spectrometry-based proteomics using Q exactive, a high-performance benchtop quadrupole orbitrap mass spectrometer. *Mol. Cell. Proteomics.* (2011).  
<https://doi.org/10.1074/mcp.M111.011015>
93. Perry, R.H., Cooks, R.G., Noll, R.J.: Orbitrap mass spectrometry: Instrumentation, ion motion and applications. *Mass Spectrom. Rev.* (2008).  
<https://doi.org/10.1002/mas.20186>
94. Glish, G.L., Burinsky, D.J.: Hybrid Mass Spectrometers for Tandem Mass Spectrometry. *J. Am. Soc. Mass Spectrom.* (2008).  
<https://doi.org/10.1016/j.jasms.2007.11.013>

95. Gibbons, H., O’Gorman, A., Brennan, L.: Metabolomics as a tool in nutritional research, (2015)
96. Smith, C.A., Want, E.J., O’Maille, G., Abagyan, R., Siuzdak, G.: XCMS: Processing mass spectrometry data for metabolite profiling using nonlinear peak alignment, matching, and identification. *Anal. Chem.* (2006).  
<https://doi.org/10.1021/ac051437y>
97. Pluskal, T., Castillo, S., Villar-Briones, A., Orešič, M.: MZmine 2: Modular framework for processing, visualizing, and analyzing mass spectrometry-based molecular profile data. *BMC Bioinformatics.* (2010).  
<https://doi.org/10.1186/1471-2105-11-395>
98. Xia, J., Wishart, D.S.: Using metaboanalyst 3.0 for comprehensive metabolomics data analysis. *Curr. Protoc. Bioinforma.* (2016). <https://doi.org/10.1002/cpbi.11>
99. Katajamaa, M., Miettinen, J., Oresic, M.: MZmine: toolbox for processing and visualization of mass spectrometry based molecular profile data. *Bioinformatics.* 22, 634–636 (2006). <https://doi.org/10.1093/bioinformatics/btk039>
100. Parsons, H.M., Ludwig, C., Günther, U.L., Viant, M.R.: Improved classification accuracy in 1- and 2-dimensional NMR metabolomics data using the variance stabilising generalised logarithm transformation. *BMC Bioinformatics.* (2007).  
<https://doi.org/10.1186/1471-2105-8-234>
101. Foti, A., Musumarra, G., Trovato-salinaro, A., Scire, S., Barresi, V., Fortuna, C.G., Strazzulla, G., Condorelli, D.F., Doria, V. a, Chimiche, S.: Identification of genes involved in radiation-induced G 1 arrest y. *J. Chemom.* 398–405 (2007).  
<https://doi.org/10.1002/cem>
102. Yamamoto, H., Yamaji, H., Abe, Y., Harada, K., Waluyo, D., Fukusaki, E., Kondo, A., Ohno, H., Fukuda, H.: Dimensionality reduction for metabolome data using PCA, PLS, OPLS, and RFDA with differential penalties to latent variables.

Chemom. Intell. Lab. Syst. (2009).  
<https://doi.org/10.1016/j.chemolab.2009.05.006>

103. Kirwan, G.M., Johansson, E., Kleemann, R., Verheij, E.R., Wheelock, Å.M., Goto, S., Trygg, J., Wheelock, C.E.: Building multivariate systems biology models. *Anal. Chem.* (2012). <https://doi.org/10.1021/ac301269r>
104. Pasikanti, K.K., Esuvaranathan, K., Ho, P.C., Mahendran, R., Kamaraj, R., Wu, Q.H., Chiong, E., Chan, E.C.Y.: Noninvasive urinary metabonomic diagnosis of human bladder cancer. *J. Proteome Res.* (2010).  
<https://doi.org/10.1021/pr901173v>
105. Westerhuis, J.A., Hoefsloot, H.C.J., Smit, S., Vis, D.J., Smilde, A.K., Velzen, E.J.J., Duijnhoven, J.P.M., Dorsten, F.A.: Assessment of PLS-DA cross validation. *Metabolomics.* (2008). <https://doi.org/10.1007/s11306-007-0099-6>
106. L. Eriksson, T. Byrne, E. Johansson, J.T. and C.V.: Response permutation and cross-validation. *Multi- and Megavariate Data Analysis: Basic Principles and Application.* , Sweden: MKS Umetrics (2013)
107. Bewick, V., Cheek, L., Ball, J.: Statistics review 13: Receiver operating characteristics curves, (2004)
108. Zou, K.H., Resnic, F.S., Talos, I.F., Goldberg-Zimring, D., Bhagwat, J.G., Haker, S.J., Kikinis, R., Jolesz, F.A., Ohno-Machado, L.: A global goodness-of-fit test for receiver operating characteristic curve analysis via the bootstrap method. *J. Biomed. Inform.* (2005). <https://doi.org/10.1016/j.jbi.2005.02.004>
109. Alamri, A., Burzangi, A.S., Coats, P., Watson, D.G.: Untargeted metabolic profiling cell-based approach of pulmonary artery smooth muscle cells in response to high glucose and the effect of the antioxidant vitamins d and e. *Metabolites.* (2018). <https://doi.org/10.3390/metabo8040087>

110. Dalle-Donne, I., Rossi, R., Colombo, G., Giustarini, D., Milzani, A.: Protein S-glutathionylation: a regulatory device from bacteria to humans, (2009)
111. Monostori, P., Wittmann, G., Karg, E., Túri, S.: Determination of glutathione and glutathione disulfide in biological samples: An in-depth review, (2009)
112. Dang, C. V., Le, A., Gao, P.: MYC-induced cancer cell energy metabolism and therapeutic opportunities. *Clin. Cancer Res.* (2009). <https://doi.org/10.1158/1078-0432.CCR-09-0889>
113. Miller, D.M., Thomas, S.D., Islam, A., Muench, D., Sedoris, K.: c-Myc and cancer metabolism, (2012)
114. Shim, H., Dolde, C., Lewis, B.C., Wu, C.S., Dang, G., Jungmann, R.A., Dalla-Favera, R., Dang, C. V.: c-Myc transactivation of LDH-A: Implications for tumor metabolism and growth. *Proc. Natl. Acad. Sci. U. S. A.* (1997). <https://doi.org/10.1073/pnas.94.13.6658>
115. Hawksworth, D., Ravindranath, L., Chen, Y., Furusato, B., Sesterhenn, I.A., Mcleod, D.G., Srivastava, S., Petrovics, G.: Overexpression of C-MYC oncogene in prostate cancer predicts biochemical recurrence. *Prostate Cancer Prostatic Dis.* (2010). <https://doi.org/10.1038/pcan.2010.31>
116. Nesbit, C.E., Tersak, J.M., Prochownik, E. V.: MYC oncogenes and human neoplastic disease, (1999)
117. Levine, A.J.: p53, the cellular gatekeeper for growth and division, (1997)
118. Atadja, P., Wong, H., Garkavtsev, I., Veillette, C., Riabowol, K.: Increased activity of p53 in senescing fibroblasts. *Proc. Natl. Acad. Sci. U. S. A.* (1995). <https://doi.org/10.1073/pnas.92.18.8348>
119. Lane, D.P.: p53, guardian of the genome, (1992)

120. Dameron, K.M., Volpert, O. V., Tainsky, M.A., Bouck, N.: Control of angiogenesis in fibroblasts by p53 regulation of thrombospondin-1. *Science* (80- ). (1994). <https://doi.org/10.1126/science.7521539>
121. Hollstein, M., Sidransky, D., Vogelstein, B., Harris, C.C.: p53 mutations in human cancers. *Science* (80- ). (1991). <https://doi.org/10.1126/science.1905840>
122. Wyss, M., Kaddurah-Daouk, R.: Creatine and creatinine metabolism. *Physiol. Rev.* 80, 1107–1213 (2000). <https://doi.org/10.1152/physrev.2000.80.3.1107>
123. McGarry, J.D., Brown, N.F.: The mitochondrial carnitine palmitoyltransferase system. From concept to molecular analysis, (1997)
124. Orr, A.L., Quinlan, C.L., Perevoshchikova, I. V., Brand, M.D.: A refined analysis of superoxide production by mitochondrial sn-glycerol 3-phosphate dehydrogenase. *J. Biol. Chem.* 287, 42921–42935 (2012). <https://doi.org/10.1074/jbc.M112.397828>
125. Antoniewicz, M.R.: Methods and advances in metabolic flux analysis: a mini-review. *J. Ind. Microbiol. Biotechnol.* 42, 317–325 (2015). <https://doi.org/10.1007/s10295-015-1585-x>
126. Huergo, L.F., Dixon, R.: The Emergence of 2-Oxoglutarate as a Master Regulator Metabolite. *Microbiol. Mol. Biol. Rev.* 79, 419–435 (2015). <https://doi.org/10.1128/mnbr.00038-15>
127. Berg JM, Tymoczko JL, S.L.: *Biochemistry*. In: *Biochemistry*. W H Freeman, New York (2002)
128. Demarquoy, J.: Crosstalk between mitochondria and peroxisomes. *World J. Biol. Chem.* 6, 301 (2015). <https://doi.org/10.4331/wjbc.v6.i4.301>
129. Kumari, S., Badana, A.K., G, M.M., G, S., Malla, R.: Reactive Oxygen Species: A Key Constituent in Cancer Survival. *Biomark. Insights.* (2018).

<https://doi.org/10.1177/1177271918755391>

130. Griendling, K.K., Minieri, C.A., Ollerenshaw, J.D., Alexander, R.W.: Angiotensin II stimulates NADH and NADPH oxidase activity in cultured vascular smooth muscle cells. *Circ Res.* 74, 1141–1148 (1994).  
<https://doi.org/10.1161/01.RES.74.6.1141>
131. McNaughton, M., Pitman, M., Pitson, S.M., Pyne, N.J., Pyne, S.: Proteasomal degradation of sphingosine kinase 1 and inhibition of dihydroceramide desaturase by the sphingosine kinase inhibitors, SKi or ABC294640, induces growth arrest in androgen-independent LNCaP-AI prostate cancer cells. *Oncotarget.* (2016).  
<https://doi.org/10.18632/oncotarget.7693>
132. Pyne, N.J., McNaughton, M., Boomkamp, S., MacRitchie, N., Evangelisti, C., Martelli, A.M., Jiang, H.R., Ubhi, S., Pyne, S.: Role of sphingosine 1-phosphate receptors, sphingosine kinases and sphingosine in cancer and inflammation. *Adv. Biol. Regul.* 60, 151–159 (2016). <https://doi.org/10.1016/j.jbior.2015.09.001>
133. Van Den Berg, H.: *Asparaginase revisited*, (2011)
134. Nguyen, B.T., Sadee, W.: Compartmentation of guanine nucleotide precursors for DNA synthesis. *Biochem. J.* 234, 263–269 (1986).  
<https://doi.org/10.1042/bj2340263>
135. Cherfils, J., Zeghouf, M.: *Regulation of small GTPases by GEFs, GAPs, and GDIs*, (2013)
136. Xu, D.D., Xu, C.B., Lam, H.M., Wong, F.L., Leung, A.W.N., Leong, M.M.L., Cho, W.C.S., Hoeven, R., Lv, Q., Rong, R.: Proteomic analysis reveals that pheophorbide a-mediated photodynamic treatment inhibits prostate cancer growth by hampering GDP-GTP exchange of ras-family proteins. *Photodiagnosis Photodyn. Ther.* (2018). <https://doi.org/10.1016/j.pdpdt.2018.05.014>



137. Bazhin, A. V., Philippov, P.P., Karakhanova, S.: *Reactive Oxygen Species in Cancer Biology and Anticancer Therapy*, (2016)
138. Gupta, S.C., Hevia, D., Patchva, S., Park, B., Koh, W., Aggarwal, B.B.: *Upsides and downsides of reactive oxygen species for Cancer: The roles of reactive oxygen species in tumorigenesis, prevention, and therapy*, (2012)
139. Liou, G.-Y., Storz, P.: Reactive oxygen species in cancer. *Free Radic. Res.* 44, 479–496 (2010). <https://doi.org/10.3109/10715761003667554>
140. Brenneisen, P., Reichert, A.S.: *Nanotherapy and reactive oxygen species (ROS) in cancer: A novel perspective. Antioxidants.* (2018). <https://doi.org/10.3390/antiox7020031>
141. Chung, L.Y., Cheung, T.C., Kong, S.K., Fung, K.P., Choy, Y.M., Chan, Z.Y., Kwok, T.T.: Induction of apoptosis by green tea catechins in human prostate cancer DU145 cells. *Life Sci.* 68, 1207–1214 (2001). [https://doi.org/10.1016/S0024-3205\(00\)01020-1](https://doi.org/10.1016/S0024-3205(00)01020-1)
142. Chai, Y.C., Ashraf, S.S., Rokutan, K., Johnston, R.B., Thomas, J.A.: S-thiolation of individual human neutrophil proteins including actin by stimulation of the respiratory burst: Evidence against a role for glutathione disulfide. *Arch. Biochem. Biophys.* (1994). <https://doi.org/10.1006/abbi.1994.1167>
143. Valko, M., Leibfritz, D., Moncol, J., Cronin, M.T.D., Mazur, M., Telser, J.: Free radicals and antioxidants in normal physiological functions and human disease. *Int. J. Biochem. Cell Biol.* 39, 44–84 (2007). <https://doi.org/10.1016/j.biocel.2006.07.001>
144. Vermeersch, K., Styczynski, M.: *Applications of metabolomics in cancer research. J. Carcinog.* (2013). <https://doi.org/10.4103/1477-3163.113622>
145. DeBerardinis, R.J., Lum, J.J., Hatzivassiliou, G., Thompson, C.B.: *The Biology*

- of Cancer: Metabolic Reprogramming Fuels Cell Growth and Proliferation. *Cell Metab.* 7, 11–20 (2008). <https://doi.org/10.1016/j.cmet.2007.10.002>
146. Collection, S.P.: Suppression of ceramide-mediated programmed cell death by sphingosine-1-phosphate. (1996)
147. Fernandis, A.Z., Wenk, M.R.: Lipid-based biomarkers for cancer. *J. Chromatogr. B Anal. Technol. Biomed. Life Sci.* 877, 2830–2835 (2009). <https://doi.org/10.1016/j.jchromb.2009.06.015>
148. Adibhatla, R.M., Hatcher, J.F., Dempsey, R.J.: Lipids and lipidomics in brain injury and diseases, (2006)
149. Ogretmen, B., Hannun, Y.A.: Biologically active sphingolipids in cancer pathogenesis and treatment, (2004)
150. Malavaud, B., Pchejetski, D., Mazerolles, C., De Paiva, G.R., Calvet, C., Doumerc, N., Pitson, S., Rischmann, P., Cuvillier, O.: Sphingosine kinase-1 activity and expression in human prostate cancer resection specimens. *Eur. J. Cancer.* (2010). <https://doi.org/10.1016/j.ejca.2010.07.053>
151. Duan, J., Merrill, A.H.: 1-deoxysphingolipids encountered exogenously and made de novo: Dangerous mysteries inside an enigma. *J. Biol. Chem.* (2015). <https://doi.org/10.1074/jbc.R115.658823>
152. Merrill, A.H., Nimkar, S., Menaldino, D., Hannun, Y.A., Loomis, C., Bell, R.M., Tyagi, S.R., Lambeth, J.D., Stevens, V.L., Hunter, R., Liotta, D.C.: Structural requirements for long-chain (sphingoid) base inhibition of protein kinase C in vitro and for the cellular effects of these compounds. *Biochemistry.* (1989). <https://doi.org/10.1021/bi00434a004>
153. Zitomer, N.C., Mitchell, T., Voss, K.A., Bondy, G.S., Pruett, S.T., Garnier-Amblard, E.C., Liebeskind, L.S., Park, H., Wang, E., Sulllards, M.C., Merrill,

- A.H., Riley, R.T.: Ceramide synthase inhibition by fumonisin B1 causes accumulation of 1-deoxysphinganine. A novel category of bioactive 1-deoxysphingoid bases and 1-deoxydihydroceramides biosynthesized by mammalian cell lines and animals. *J. Biol. Chem.* (2009).  
<https://doi.org/10.1074/jbc.M808798200>
154. Humpf, H.U., Schmelz, E.M., Meredith, F.I., Vesper, H., Vales, T.R., Wang, E., Menaldino, D.S., Liotta, D.C., Merrill, A.H.: Acylation of naturally occurring and synthetic 1-deoxysphinganines by ceramide synthase: Formation of N-palmitoyl-aminopentol produces a toxic metabolite of hydrolyzed fumonisin, AP1, and a new category of ceramide synthase inhibitor. *J. Biol. Chem.* (1998).  
<https://doi.org/10.1074/jbc.273.30.19060>
155. Desai, K., Sullards, M.C., Allegood, J., Wang, E., Schmelz, E.M., Hartl, M., Humpf, H.U., Liotta, D.C., Peng, Q., Merrill, A.H.: Fumonisin and fumonisin analogs as inhibitors of ceramide synthase and inducers of apoptosis, (2002)
156. Massard, C., Salazar, R., Armand, J.P., Majem, M., Deutsch, E., García, M., Oaknin, A., Fernández-García, E.M., Soto, A., Soria, J.C.: Phase I dose-escalating study of ES-285 given as a three-hour intravenous infusion every three weeks in patients with advanced malignant solid tumors. *Invest. New Drugs.* (2012).  
<https://doi.org/10.1007/s10637-011-9772-8>
157. Cells, A., Fendersons, B.: A Specific Enhancing effect of N,N dimethylsphingosine on Epidermal Growth Factor Receptor Autophosphorylation. *Biochemistry.* 265, 5365–5369 (1990)
158. Hajra AK, D.A.: Lipid biosynthesis in peroxisomes. *Ann N Y Acad Sci* (1996)
159. Bergan, J., Skotland, T., Sylvänne, T., Simolin, H., Ekroos, K., Sandvig, K.: The Ether Lipid Precursor Hexadecylglycerol Causes Major Changes in the Lipidome of HEp-2 Cells. *PLoS One.* (2013). <https://doi.org/10.1371/journal.pone.0075904>

160. Tonelli, F., Lim, K.G., Loveridge, C., Long, J., Pitson, S.M., Tigyi, G., Bittman, R., Pyne, S., Pyne, N.J.: FTY720 and (S)-FTY720 vinylphosphonate inhibit sphingosine kinase 1 and promote its proteasomal degradation in human pulmonary artery smooth muscle, breast cancer and androgen-independent prostate cancer cells. *Cell. Signal.* 22, 1536–1542 (2010).  
<https://doi.org/10.1016/j.cellsig.2010.05.022>
161. Lim, K.G., Tonelli, F., Berdyshev, E., Gorshkova, I., Leclercq, T., Pitson, S.M., Bittman, R., Pyne, S., Pyne, N.J.: Inhibition kinetics and regulation of sphingosine kinase 1 expression in prostate cancer cells: Functional differences between sphingosine kinase 1a and 1b. *Int. J. Biochem. Cell Biol.* (2012).  
<https://doi.org/10.1016/j.biocel.2012.05.012>
162. Zheng, L., T'Kind, R., Decuypere, S., von Freyend, S.J., Coombs, G.H., Watson, D.G.: Profiling of lipids in leishmania donovani using hydrophilic interaction chromatography in combination with fourier transform mass spectrometry. *Rapid Commun. Mass Spectrom.* (2010). <https://doi.org/10.1002/rcm.4618>
163. Han, X., Gross, R.W.: Shotgun lipidomics: Electrospray ionization mass spectrometric analysis and quantitation of cellular lipidomes directly from crude extracts of biological samples. *Mass Spectrom. Rev.* 24, 367–412 (2005).  
<https://doi.org/10.1002/mas.20023>
164. Welti, R., Wang, X.: Lipid species profiling: A high-throughput approach to identify lipid compositional changes and determine the function of genes involved in lipid metabolism and signaling, (2004)
165. Brizuela, L., Dayon, A., Doumerc, N., Ader, I., Golzio, M., Izard, J.C., Hara, Y., Malavaud, B., Cuvillier, O.: The sphingosine kinase-1 survival pathway is a molecular target for the tumor-suppressive tea and wine polyphenols in prostate cancer. *FASEB J.* (2010). <https://doi.org/10.1096/fj.10-160838>
166. Mao, C., Obeid, L.M.: Ceramidases: regulators of cellular responses mediated by

ceramide, sphingosine, and sphingosine-1-phosphate, (2008)

167. Wang, Y., Zhang, C., Jin, Y., Wang, S., He, Q., Liu, Z., Ai, Q., Lei, Y., Li, Y., Song, F., Bu, Y.: Alkaline ceramidase 2 is a novel direct target of p53 and induces autophagy and apoptosis through ROS generation. *Sci. Rep.* (2017).  
<https://doi.org/10.1038/srep44573>
168. Laviad, E.L., Albee, L., Pankova-Kholmyansky, I., Epstein, S., Park, H., Merrill, A.H., Futerman, A.H.: Characterization of ceramide synthase 2: Tissue distribution, substrate specificity, and inhibition by sphingosine 1-phosphate. *J. Biol. Chem.* (2008). <https://doi.org/10.1074/jbc.M707386200>
169. Miller, D.J., Jerga, A., Rock, C.O., White, S.W.: Analysis of the *Staphylococcus aureus* DgkB Structure Reveals a Common Catalytic Mechanism for the Soluble Diacylglycerol Kinases. *Structure.* (2008).  
<https://doi.org/10.1016/j.str.2008.03.019>
170. Im, D.S., Tomura, H., Tobe, M., Sato, K., Okajima, F.: Enhancement of sphingosine 1-phosphate-induced phospholipase C activation during G0-G1 transition in rat hepatocytes. *J. Pharmacol. Sci.* (2004).  
<https://doi.org/10.1254/jphs.FPJ04007X>
171. Wang, P., Yuan, Y., Lin, W., Zhong, H., Xu, K., Qi, X.: Roles of sphingosine-1-phosphate signaling in cancer. *Cancer Cell Int.* 19, 1–12 (2019).  
<https://doi.org/10.1186/s12935-019-1014-8>
172. Rhee, S.G.: Regulation of Phosphoinositide-Specific Phospholipase C. *Annu. Rev. Biochem.* (2001). <https://doi.org/10.1146/annurev.biochem.70.1.281>
173. Augert, G., Bocckino, S.B., Blackmore, P.F., Exton, J.H.: Hormonal stimulation of diacylglycerol formation in hepatocytes. Evidence for phosphatidylcholine breakdown. *J. Biol. Chem.* (1989)

174. Flores, I., Jones, D.R., Mérida, I.: Changes in the balance between mitogenic and antimitogenic lipid second messengers during proliferation, cell arrest, and apoptosis in T-lymphocytes. *FASEB J.* (2000). <https://doi.org/10.1096/fj.99-1066fje>
175. Hashizume, T., Nakao, M., Kageura, T., Sato, T.: Sphingosine enhances arachidonic acid liberation in response to U46619 through an increase in phospholipase A2 activity in rabbit platelets. *J. Biochem.* (1997). <https://doi.org/10.1093/oxfordjournals.jbchem.a021843>
176. Chang, M.C., Lee, J.J., Chen, Y.J., Lin, S.I., Lin, L.D., Liou, E.J.W., Huang, W.L., Chan, C.P., Huang, C.C., Jeng, J.H.: Lysophosphatidylcholine induces cytotoxicity/apoptosis and IL-8 production of human endothelial cells: Related mechanisms. *Oncotarget.* 8, 106177–106189 (2017). <https://doi.org/10.18632/oncotarget.22425>
177. Hollie, N.I., Cash, J.G., Matlib, M.A., Wortman, M., Basford, J.E., Abplanalp, W., Hui, D.Y.: Micromolar changes in lysophosphatidylcholine concentration cause minor effects on mitochondrial permeability but major alterations in function. *Biochim. Biophys. Acta - Mol. Cell Biol. Lipids.* (2014). <https://doi.org/10.1016/j.bbalip.2013.11.013>
178. Peter, C., Waibel, M., Radu, C.G., Yang, L. V., Witte, O.N., Schulze-Osthoff, K., Wesselborg, S., Lauber, K.: Migration to apoptotic “find-me” signals is mediated via the phagocyte receptor G2A. *J. Biol. Chem.* 283, 5296–5305 (2008). <https://doi.org/10.1074/jbc.M706586200>
179. Chandraprakash Reddy, K., Byun, H.S., Bittman, R.: Antitumor ether lipids: An improved synthesis of ilmofosine and an enantioselective synthesis of an ilmofosine analog. *Tetrahedron Lett.* (1994). [https://doi.org/10.1016/S0040-4039\(00\)77004-3](https://doi.org/10.1016/S0040-4039(00)77004-3)
180. Li, Z., Agellon, L.B., Allen, T.M., Umeda, M., Jewell, L., Mason, A., Vance,

- D.E.: The ratio of phosphatidylcholine to phosphatidylethanolamine influences membrane integrity and steatohepatitis. *Cell Metab.* (2006).  
<https://doi.org/10.1016/j.cmet.2006.03.007>
181. Yen, C.E., Mar, M., Zeisel, S.H.: Choline deficiency-induced apoptosis in PC12 cells is associated with diminished membrane phosphatidylcholine and sphingomyelin, accumulation of ceramide and diacylglycerol, and activation of a caspase. *FASEB J.* (1999). <https://doi.org/10.1096/fasebj.13.1.135>
182. Lin, Q., Zhang, D., Xia, Y.: Analysis of ether glycerophosphocholines at the level of CC locations from human plasma. *Analyst.* (2020).  
<https://doi.org/10.1039/c9an01515a>
183. Dean, J.M., Lodhi, I.J.: Structural and functional roles of ether lipids, (2018)
184. Wanders, R.J.A., Ferdinandusse, S., Brites, P., Kemp, S.: Peroxisomes, lipid metabolism and lipotoxicity, (2010)
185. Cancer Research UK, [https://www.cancerresearchuk.org/health-professional/cancer-statistics/statistics-by-cancer-type/prostate-cancer/mortality?\\_ga=2.162630526.370508025.1585879218-1744064071.1585879218](https://www.cancerresearchuk.org/health-professional/cancer-statistics/statistics-by-cancer-type/prostate-cancer/mortality?_ga=2.162630526.370508025.1585879218-1744064071.1585879218)
186. Perletti, G., Monti, E., Marras, E., Cleves, A., Magri, V., Trinchieri, A., Rennie, P.S.: Efficacy and safety of second-line agents for treatment of metastatic castration-resistant prostate cancer progressing after docetaxel. A systematic review and meta-analysis, (2015)
187. Gottesman, M.M., Fojo, T., Bates, S.E.: Multidrug resistance in cancer: Role of ATP-dependent transporters, (2002)
188. Gillet, J.P., Gottesman, M.M.: Mechanisms of multidrug resistance in cancer. *Methods Mol. Biol.* (2010). [https://doi.org/10.1007/978-1-60761-416-6\\_4](https://doi.org/10.1007/978-1-60761-416-6_4)

189. Hannun, Y.A., Obeid, L.M.: Principles of bioactive lipid signalling: Lessons from sphingolipids, (2008)
190. Okazaki, T., Bell, R.M., Hannun, Y.A.: Sphingomyelin turnover induced by vitamin D3 in HL-60 cells. Role in cell differentiation. *J. Biol. Chem.* (1989)
191. Hannun, Y.A., Bell, R.M.: Functions of sphingolipids and sphingolipid breakdown products in cellular regulation. *Science* (80- ). (1989).  
<https://doi.org/10.1126/science.2643164>
192. Pyne, S., Pyne, N.J.: Translational aspects of sphingosine 1-phosphate biology. *Trends Mol. Med.* 17, 463–472 (2011).  
<https://doi.org/10.1016/j.molmed.2011.03.002>
193. Pitson, S.M., D'Andrea, R.J., Vandeleur, L., Moretti, P.A.B., Xia, P., Gamble, J.R., Vadas, M.A., Wattenberg, B.W.: Human sphingosine kinase: Purification, molecular cloning and characterization of the native and recombinant enzymes. *Biochem. J.* (2000). <https://doi.org/10.1042/0264-6021:3500429>
194. Olivera, A., Kohama, T., Tu, Z., Milstien, S., Spiegel, S.: Purification and characterization of rat kidney sphingosine kinase. *J. Biol. Chem.* (1998).  
<https://doi.org/10.1074/jbc.273.20.12576>
195. Nava, V.E., Lacana', E., Poulton, S., Liu, H., Sugiura, M., Kono, K., Milstien, S., Kohama, T., Spiegel, S.: Functional characterization of human sphingosine kinase-1. *FEBS Lett.* (2000). [https://doi.org/10.1016/S0014-5793\(00\)01510-6](https://doi.org/10.1016/S0014-5793(00)01510-6)
196. Cao, M., Ji, C., Zhou, Y., Huang, W., Ni, W., Tong, X., Wei, J.F.: Sphingosine kinase inhibitors: A patent review, (2018)
197. Pitman, M.R., Powell, J.A., Coolen, C., Moretti, P.A.B., Zebol, J.R., Pham, D.H., Finnie, J.W., Don, A.S., Ebert, L.M., Bonder, C.S., Gliddon, B.L., Pitson, S.M.: A selective ATP-competitive sphingosine kinase inhibitor demonstrates anti-cancer



- properties. *Oncotarget*. (2015). <https://doi.org/10.18632/oncotarget.3178>
198. French, K.J., Schrecengost, R.S., Lee, B.D., Zhuang, Y., Smith, S.N., Eberly, J.L., Yun, J.K., Smith, C.D.: Discovery and evaluation of inhibitors of human sphingosine kinase. *Cancer Res*. (2003)
199. Ren, S., Xin, C., Pfeilschifter, J., Huwiler, A.: A novel mode of action of the putative sphingosine kinase inhibitor 2-(p-hydroxyanilino)-4-(p-chlorophenyl) thiazole (SKI II): Induction of lysosomal sphingosine kinase 1 degradation. *Cell. Physiol. Biochem*. (2010). <https://doi.org/10.1159/000315110>
200. Antoon, J.W., Meacham, W.D., Bratton, M.R., Slaughter, E.M., Rhodes, L. V., Ashe, H.B., Wiese, T.E., Burow, M.E., Beckman, B.S.: Pharmacological inhibition of sphingosine kinase isoforms alters estrogen receptor signaling in human breast cancer. *J. Mol. Endocrinol*. (2011). <https://doi.org/10.1530/JME-10-0116>
201. Gao, P., Peterson, Y.K., Smith, R.A., Smith, C.D.: Characterization of isoenzyme-selective inhibitors of human sphingosine kinases. *PLoS One*. (2012). <https://doi.org/10.1371/journal.pone.0044543>
202. Byun, H.S., Pyne, S., MacRitchie, N., Pyne, N.J., Bittman, R.: Novel sphingosine-containing analogues selectively inhibit sphingosine kinase (SK) isozymes, induce SK1 proteasomal degradation and reduce DNA synthesis in human pulmonary arterial smooth muscle cells. *Medchemcomm*. (2013). <https://doi.org/10.1039/c3md00201b>
203. Zammit, V.A., Ramsay, R.R., Bonomini, M., Arduini, A.: Carnitine, mitochondrial function and therapy, (2009)
204. Fraser, F., Corstorphine, C.G., Zammit, V.A.: Topology of carnitine palmitoyltransferase I in the mitochondrial outer membrane. *Biochem. J*. (1997). <https://doi.org/10.1042/bj3230711>

205. Paumen, M.B., Ishida, Y., Muramatsu, M., Yamamoto, M., Honjo, T.: Inhibition of carnitine palmitoyltransferase I augments sphingolipid synthesis and palmitate-induced apoptosis. *J. Biol. Chem.* (1997). <https://doi.org/10.1074/jbc.272.6.3324>
206. Knauss, T.C., Jaffer, F.E., Abboud, H.E.: Phosphatidic acid modulates DNA synthesis, phospholipase C, and platelet-derived growth factor mRNAs in cultured mesangial cells. Role of protein kinase C. *J. Biol. Chem.* (1990)
207. Van Corven, E.J., Van Rijswijk, A., Jalink, K., Van Der Bend, R.L., Van Blitterswijk, W.J., Moolenaar, W.H.: Mitogenic action of lysophosphatidic acid and phosphatidic acid on fibroblasts. Dependence on acyl-chain length and inhibition by suramin. *Biochem. J.* (1992). <https://doi.org/10.1042/bj2810163>
208. Sugiura, R., Sio, S.O., Shuntoh, H., Kuno, T.: Calcineurin phosphatase in signal transduction: Lessons from fission yeast, (2002)
209. Bensaad, K., Favaro, E., Lewis, C.A., Peck, B., Lord, S., Collins, J.M., Pinnick, K.E., Wigfield, S., Buffa, F.M., Li, J.L., Zhang, Q., Wakelam, M.J.O., Karpe, F., Schulze, A., Harris, A.L.: Fatty acid uptake and lipid storage induced by HIF-1 $\alpha$  contribute to cell growth and survival after hypoxia-reoxygenation. *Cell Rep.* (2014). <https://doi.org/10.1016/j.celrep.2014.08.056>
210. Zimmermann, R., Strauss, J.G., Haemmerle, G., Schoiswohl, G., Birner-Gruenberger, R., Riederer, M., Lass, A., Neuberger, G., Eisenhaber, F., Hermetter, A., Zechner, R.: Fat mobilization in adipose tissue is promoted by adipose triglyceride lipase. *Science* (80-. ). (2004). <https://doi.org/10.1126/science.11100747>
211. Menendez, J.A., Lupu, R.: Fatty acid synthase and the lipogenic phenotype in cancer pathogenesis, (2007)
212. Dettmer, K., Aronov, P.A., Hammock, B.D.: Mass spectrometry-based metabolomics, (2007)

